MODEL BASED ANALYSIS AND IDENTIFICATION OF UNBALANCE AND MISALIGNMENT IN ROTOR SYSTEMS LEVITATED BY ACTIVE MAGNETIC BEARINGS

A Thesis Submitted in
Partial Fulfilment of the Requirements
for the Degree of

DOCTOR OF PHILOSOPHY

by

PRABHAT KUMAR
(Roll No. 166103028)

DEPARTMENT OF MECHANICAL ENGINEERING
INDIAN INSTITUTE OF TECHNOLOGY GUWAHATI, GUWAHATI

FEBRUARY, 2021

CERTIFICATE

This is to certify that the thesis entitled "**Model based Analysis and Identification of Unbalance and Misalignment in Rotor Systems Levitated by Active Magnetic Bearings**", submitted by **Mr. Prabhat Kumar** (166103028), a PhD student in the Department of Mechanical Engineering, Indian Institute of Technology Guwahati, for the award of the degree of Doctor of Philosophy, is a record of an original research work carried out by him under my supervision and guidance. The thesis has fulfilled all requirements as per the regulations of the institute and in my opinion has reached the standard needed for submission. The results embodied in this thesis have not been submitted to any other University or Institute for the award of any degree or diploma.

Dr. Rajiv Tiwari
Professor
Department of Mechanical Engineering
Indian Institute of Technology Guwahati,
Guwahati-781039, Assam, India.

ACKNOWLEDGEMENTS

It is a great privilege for me to have an opportunity to acknowledge a feeling of grate gratitude to my thesis supervisor, Professor Rajiv Tiwari for his wonderful guidance, encouragement and strong support throughout my research work. Also, I really appreciate his patience and time that he spent with me to give advices and answers my questions that I had. I heartily thank him for introducing me into such an interesting and challenging area of research in the rotor dynamic field. It would be my privilege to correspond and learn from him in future as well.

I would like to thank Prof. Santosha Kumar Dwivedy, Dr. Atanu Banerjee and Prof. Harshal B. Nemade for being on my doctoral committee and reviewing my dissertation periodically. With their support and suggestions during annual progress evaluation, I have been gone more deep in the analysis of my research area.

I am also very much thankful to Dr. D. J. Bordoloi of Vibration and Acoustic Lab and my PhD colleagues Gyan Ranjan, Dr. Dipendra Kumar Roy, Nilakshi Sarmah and Gargi Majumder for their kind support and constant source of encouragement.

It's my fortune to greatly acknowledge my parents and sisters, for their patience and love which enable me to overcome obstacles and complete my research. My sincere thanks goes to my wife Saroj Kumari for her constant support and understanding during my pursuit of PhD degree that made the completion of thesis possible. I appreciate my baby, my little son Pransh Modi for abiding my ignorance and the patience he showed during my thesis writing. Last but not least, I am always thankful to almighty God for his constant shower of blessing upon me.

Prabhat Kumar

ABSTRACT

Rotating machineries are principally important and advantageous elements in various industrial plants. Rotating shaft in these rotor systems requires bearings for supporting purpose. Over the past years, conventional bearings have been utilized for supporting the rotor through the direct physical contact in rolling element bearings or fluid forces induced from lubricant in fluid-film bearings. However, the latest trend is towards using active magnetic bearings (AMBs) for mounting the rotating elements without physical contact. They can overcome most of the practical and limited constraints in conventional bearings. AMBs are the recent mechatronic adaptation to the rotor dynamic field. They offer clean and high-speed frictionless operations. The present work primarily focusses on two main aspects of the rotor-AMB system, i.e., the first is the dynamic analysis of a rotor system integrated with AMBs, whereas the second is the identification of faults in a magnetically levitated rotor model. The identification has been done based on the inverse problem approach through developed mathematical models.

Multiple malfunctions, such as the unbalance in rotor, misalignment, crack, shaft bow, bearing faults, sensor faults, etc. are quite inevitable in a rotating machinery. These faults can lead to high level of vibration and reduce the life span, efficiency and productivity of the machine. Hence, it is mandatory to understand the dynamic behaviour of a faulty rotor system and identify the faults. Among all faults, the rotor unbalance and misalignment are the most frequent faults that appear in a rotating machinery. Therefore, the entire work emphasises fully on the simultaneous identification of unbalance and misalignment faults as well as AMB stiffness parameters in a magnetically levitated rigid and flexible rotor system using an innovative trial misalignment approach. This approach is aligned with the similar concept of trial unbalance utilized in balancing of the rotor. In real practice, the known trial misalignment between the operating axis of the rotor and the axis of AMBs can be provided by two

approaches. The first is physical trial misalignment (PTM) approach and the second is virtual trial misalignment (VTM) approach.

At first, a simple rigid rotor levitated by two identical parallel-misaligned AMBs is considered for mathematically modelling. It is based on two transverse translational displacements at AMB locations. The linearized form of magnetic force due to misaligned AMBs for the case of residual and additional trial misalignments has been obtained. The second model consists of both parallel and angular misalignments in a rigid rotor with two offset discs supported on two different isotropic AMBs. It is relying on two translational and two rotational displacements at the rotor centre of gravity with consideration of gyroscopic effects. The third model is finite element method based for a magnetically levitated multi-disc flexible rotor system equipped with multiple (anisotropic and different) misaligned AMBs. The final model is an extension of third model with integration of misaligned sensors along with the parallel and angular misalignments in AMBs in a flexible rotor system. Moreover, the first three models are relying on physical trial misalignment approach for providing additional known trial misalignment in rotor-AMB system, whereas the last model is based on a virtual trial misalignment approach. For the stability and controlling performances of the rotor system, a PID controller has been used in AMBs.

Equations of motion of the different models are developed and numerically solved to get time domain displacements at various rotor positions and controlling current responses at AMB locations. Further, a fast Fourier Transform (FFT) technique is utilized to obtain frequency domain responses from time domain signals. The magnitude and corrected phase of the responses are computed to get the real and imaginary components of frequency based signals. These are given as input in the trial misalignment based identification methodology for quantitative estimation of unknown unbalance and AMB misalignment parameters in a rotor-AMB system.

The rotor unbalance parameters (disc eccentricities and phases), AMB residual misalignments and their force-displacement and force-current stiffness constants are the identified parameters from developed estimation methodology. Additionally, the residual offsets of sensors located at AMB locations are also identified using VTM approach in the final model. The identification algorithm has been tested against various levels of measurement noise and modelling errors and found to be robust.

The work performed in this dissertation is entirely distinct from the usual misalignment procedure followed in the misaligned rotor system. This work is focused on novel (physical and virtual) trial misalignment concept for identifying the misalignment of shaft quantitatively with respect to supported AMBs i.e., the estimation of the residual offset amount of the shaft. Identifying the amount of offset would be extremely helpful to perform the required corrections, modifications and proper assembling of various mechanical parts of the rotor-AMB-sensor system. Therefore, the discussed analysis and faults identification technique have a great scope in a rotor system integrated with AMBs and sensors in smart industries.

TABLE OF CONTENTS

LIST OF FIGURES

LIST OF TABLES

NOMENCLATURE

Variables

a	AMB residual misalignment (mm)
a_1, a_2	Distances of AMB1 and AMB2 from center of gravity of rotor (m)
A_{a1}, A_{a2}	Cross sectional areas of the magnetic pole of AMB1 and AMB2 (m^2)
$\mathbf{C}$	Shaft damping matrix
d	Diameter of shaft (mm)
e_i	Eccentricity of disc unbalance (μm)
f_c^{mis}	Constant force due to AMB misalignment
$\mathbf{G}$	Shaft gyroscopic matrix
i_{Txq}, i_{Tyq}	Additional trial (bias) currents at q^{th} AMB location in x and y directions (A)
i_0	Nominal bias current (A)
i_{x1}, i_{y1}	Controlling currents in x and y directions at AMB1 position (A)
i_{x2}, i_{y2}	Controlling currents in x and y directions at AMB2 position (A)
I_d	Diametral moment of inertia of the rotor (kg-m^2)
I_{p1}, I_{p2}	Polar moment of inertias of the disc1 and disc2 (kg-m^2)
k_s	AMB force-displacement stiffness constant (N/m)
k_s^{mis}	Force-displacement stiffness constant of misaligned AMB (N/m)
k_i	AMB force-current stiffness constant (N/A)
k_i^{mis}	Force-current stiffness constant of misaligned AMB (N/A)
k_P	Proportional factor of PID controller (A/m)

k_I	Integral factor of PID controller (A-s/m)
k_D	Derivative factor of PID controller (A/m-s)
K	Stiffness matrix
l, l_i	Total length of shaft and elemental length of shaft (m)
l_1, l_2	Distances of disc1 and disc2 from centre of gravity of the rotor (m)
m	Mass of the rotor (kg)
m_{d1}, m_{d2}	Mass of disc1 and disc2 (kg)
m_{di}	Disc mass (kg)
M	Mass matrix
N_1, N_2	Number of turning coils in AMB1 and AMB2
N_q	Number of turning coils in q^{th} AMB
s_0	Nominal air gap between rotor and AMBs (mm)
t	Time (s)
u_x, u_y	Displacements of rotor in x and y directions at centre of gravity position (m)
u_{x1}, u_{y1}	Displacements of rotor in x and y directions at AMB1 position (m)
u_{x2}, u_{y2}	Displacements of rotor in x and y directions at AMB2 position (m)

Greek letters

β_1, β_2	Phases of unbalance force due to disc1 and disc2
δ_{x1}, δ_{y1}	Residual misalignments between rotor and AMB1 in x and y directions (mm)
δ_{x2}, δ_{y2}	Residual misalignments between rotor and AMB2 in x and y directions (mm)
δ^a_{xq} , δ^a_{yq}	Residual misalignments of q^{th} AMB with rotor in x and y directions (mm)

δ_{xq}^{s} , δ_{yq}^{s}	Residual misalignments of sensors with rotor in *x* and *y* directions (mm)
Δ	Known trial misalignment provided to the actuator housing (mm)
Δ_{xq}^{r} , Δ_{yq}^{r}	Trial misalignments of rotor (virtual) at q^{th} AMB location in *x* and *y* directions (mm)
$d\Delta_{xq}$, $d\Delta_{yq}$	Additional air gap of sensors at q^{th} AMB location in *x* and *y* directions (mm)
Δ_{x2}, Δ_{y2}	Additional trial misalignments between rotor and AMB2 in *x* and *y* directions (mm)
φ_x, φ_y	Rotational displacements of the rigid rotor in the *y*-*z* and *x*-*z* planes
$\boldsymbol{\eta}$	Vibration induced rotor displacement vector
μ_0	Vacuum permeability of free space (H/m)
ω	Spin speed of rotor (rad/s)
ϕ_i, θ_i, ψ_i	Phases of reference, displacement and current signals of i^{th} harmonic

Superscripts

d	Dynamic condensed case
*m*1	Residual misalignment
*m*2	Additional trial misalignment
mis	Misalignment
Re	Real part
Im	Imaginary part
T	Transpose
x	Along the *x*-coordinate axis

y	Along the y-coordinate axis

Subscripts

m	Master degree-of-freedom
s	Slave degree-of-freedom

ABBREVIATIONS

$A_{1,2}$: Active Magnetic Bearing locations

$D_{1,2}$: Disc locations

G: Rotor center of gravity

AMB: Active Magnetic Bearing

DOF: Degree of Freedom

EOM: Equation of Motion

FEM: Finite Element Method

FFT: Fast Fourier Transform

PID: Proportional-Integral-Derivative

PTM: Physical Trial Misalignment

VTM: Virtual Trial Misalignment

Chapter 1

Introduction and Literature Review

1.1 Significance of the Study

High speed rotating machinery, such as pumps, compressors, gas turbines, etc., are extremely essential and crucial elements in modern manufacturing and production industries for diverse engineering applications. These applications include household accessories, transport vehicles, machine tools, ships, power stations, aircraft engines and marine propulsion systems. Rotors in these machines run at high speeds and appropriate bearings are needed to support these rotors. Nowadays vast research is being conducted on active magnetic bearings (AMBs) over conventional bearings due to their multiple performance restrictions, such as they are mostly suitable for moderate speed operations and light load conditions. They also use lubricant and there is a chance of wear coating issue and having short life span.

AMBs levitate a rotor in the air or vacuum without any physical contact due to electromagnetic forces induced in the rotating conductor. Moreover, in this bearing support, the rotor does not experience wear or frictional resistance during rotation. Thus, AMBs help in rotating the rotor at ultra-high speeds and increase the life span of the rotor system. The advantages of properly designed AMBs include the improvement of the stability as well as vibration controlling performances of the system, assisted by tunable stiffness and damping parameters of a controller. AMBs are also used as an element for the fault identification in the high speed turbomachinery, viz. centrifugal pumps and gas turbine engines (Aenis et al., 2002; Nordmann and Aenis, 2004).

Rotors in real machines may experience multiple faults simultaneously, including the unbalance, bow in the rotor, crack and misalignment, while in continuous operation or starting

from the manufacturing of the different components due to design errors or from assembling the rotor system set up. In this context, Isermann (1984) defined the fault as an unpermitted deviation of at least one characteristic property of a variable from an acceptable behaviour. Therefore, the fault is a state that may cause to enhance vibration amplitudes of machines, which may affect the efficiency of the machine and result in unavoidable health hazards to workers. Thus, for the smooth and efficient performance of rotating machines, it is immensely important to detect and identify these faults.

Unbalance and misalignment are the major faults in rotating system. The unbalance in rotor may be caused due to the existence of geometrical errors, non-uniformity of raw materials, and also due to wear as well as tear of the elemental parts and accumulation of unwanted mass in the form of dust, etc. However, the misalignment fault can occur when the axes of two coupled rotors are not aligned with each other or the rotor axis and supported bearings axis are not in alignment. Causes of this fault may be due to mechanical machining errors, improper installation and machine assembly (Hori and Uematsu, 1980; Longxiang, 2009) or as a consequence of thermal distortion due to the strain through continuous operations of the equipment, from thermal distortion of the supporting frame due to uneven thermal expansion, etc.

Sensor measurement errors may also cause misalignment of rotor with the supported active magnetic bearings. In a fully floated rotor-AMB system, the centre position of AMB in the vertical direction is located using the change in voltage detected from eddy current proximity sensor, by placing the core at the lower pole of AMB and then at upper pole of AMB. Similarly, the change in voltage perceived from sensor, by placing the core at the extreme backside pole of AMB and subsequently at the extreme front side pole of AMB, is used to detect the centre position of AMB in the horizontal direction. However, it is difficult to exactly locate the centre position of AMB in both the vertical and horizontal directions through the

non-contact sensor due to measurement error, arising from the defective positioning of displacement sensors. This inability in finding the exact location of AMB centre will lead to residual misalignment of the axes of AMBs with respect to the absolute reference of operating axis of rotor. This non-coincidence of the axes may influence the AMB performance due to uneven air gap distribution, which results in development of one extra force term other than the linearized forces associated with AMBs force-displacement and force-current stiffness coefficients for the perfectly aligned case. This extra force term may be the cause of high level of vibration, more power consumption as well as severe unstable levitation of AMB-rotor (Li et al., 2012).

Therefore, it is extremely important to study the dynamic influence of AMB misalignment on the rotor vibration performances and controlling current responses as well as quantitatively identifying the unbalance in rotor and residual misalignment of AMBs with a unique approach. In the following sections, literature reviews are elaborately presented. The literature review section is mainly organised in four parts, which includes reviews on condition monitoring of rotating machinery, research performed in unbalance, misalignment and combined multiple faults, reviews on condensation schemes and lastly on AMBs and their applications in a rotor system.

1.2 Review on Condition Monitoring of Rotating Machinery

Condition based monitoring of rotating machinery is an effective tool for the detection and diagnosis of various faults as well as maintaining production continuity in manufacturing industries. Condition monitoring is of great support to predictive maintenance and found to be much better way than corrective and preventive maintenance. The use of condition monitoring allows regular maintenance of the rotor-bearing system so that the maintenance personnel gets

alerted to avoid costly downtime and expensive emergency repairs. Thus, the condition-based maintenance (CBM) shows exactly when a machine needs replacement or is in need of maintenance and ensures optimal use of machines during their lifespan (Randall, 2011).

Condition-based maintenance (CBM) has been discretized into mainly three steps (Jardine et al., 2006) (shown in Figure 1.1), in which the first is data acquisition, the second is data processing and lastly is maintenance decision-making. Data acquisition part collects the information related to data or signals for health conditioning of the system. After that, this data is sent to the data processing domain for handling, analysing and interpreting the data. Finally, the maintenance decision part builds the steps for recommending the efficient maintenance policies. There are two prime facets in CBM program.

(a) *Diagnostics*: This aspect deals with the detection, isolation and identification of faults when they occur, in which fault detection is a task to indicate whether something is going wrong in the monitored system; fault isolation is a task to locate the component that is faulty; whereas fault identification is a task to determine the nature of the fault when it is detected.

(b) *Prognostics*: This aspect deals with the prediction of fault before its occurring in the machine. The fault prediction is an activity which decides the time for complete failure of system components due to impending fault. It also estimates the remaining useful life of the system. This is a prior event analysis and much more efficient than diagnostics to achieve zero-downtime performance.

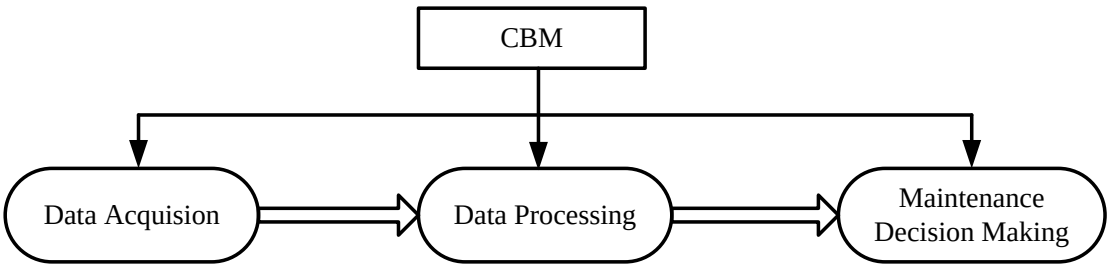

Figure 1.1 The three main aspects of condition-based maintenance.

Condition of a rotating equipment can be judged by collecting and visualizing the signals originating from the machine during its operation. In signal based condition monitoring technique, the vibration and current signatures are captured from the faulty machine and compared with the reference signature of healthy machine. This technique can be improved and give more as well as depth information and characteristics of various faults utilizing spectral analysis, i.e., frequency response function (FRF) such as Nyquist plot and Bode plot, fast Fourier Transform (FFT) and full spectrum techniques (to show both forward and backward whirls) as well as time-frequency analysis methods (i.e., wavelet transform, short-time Fourier transform), etc.

Model based condition monitoring strategy (Isermann and Balle, 1997; Isermann, 2005) rely on developing the explicit mathematical models of the monitored system. The models are numerically simulated to generate the vibration signals which are indicator of fault present in the machine. Usually, the different approaches, like Kalman filter, system parameters estimation, state observers and output observers as well as parity equations, etc. are used to generate residuals, which are further analysed for detecting, isolating and identifying the rotor-bearing-motor faults. Due to its capability of simultaneously identifying multiple faults in machine components, the model based approaches are usually utilized in rotor dynamic fields.

Based on natural frequency and mode shape approaches, Adams et al. (1978) and Cawley and Adams (1979) proposed that the damage location can be determined by the ratio

of change in the frequency in the two corresponding modes. The position of probable damage sites was obtained by the measurement of one pair of natural frequencies. Moreover, the actual damage site had been found out by the intersection of the curves for several pairs of modes. This developed method was favourably applied in various laboratories, using the axial resonances of the beams, for moderate levels of damage in structure. Later, Banks et al. (1996) developed a technique using parameterized partial differential equations and Galerkin approximation approaches for the identification of damage location in a structure. They demonstrated that the natural frequencies get affected not only due to the location and severity of the damage, but also from the geometry of the damage.

As condition monitoring systems for fault identification became popular and elaborated, the analysis of vibration data yielded by these systems also becomes more-in depth and involved. Hill and Baines (1988) described the design of an expert system for the purpose of analysis of the measured vibrational data. A computer program was considered as an expert system which processes and analyses the input signals to perform the diagnosis of a fault. This requires knowledgeable and experienced traditional human experts in the field, such as rotating machinery operators, professional engineers, and maintenance managers. They came to the conclusion that an expert system approach linked with vibration monitoring would be quite beneficial, as long as care is taken in the thorough design of the rotating system.

Further, on the basis of change in natural frequency to a numerical model of a beam mounted on a simple support, cantilever support, and also on an elastic foundation (i.e., under different boundary conditions), Choy et al. (1995) developed a novel damage identification technique based on vibration theory in a beam of either uniform or non-uniform cross section. In this technique, the damage and elastic foundation were modelled using reduction in the modulus of elasticity of a beam element and change in stiffness and damping of a Winkler

spring approach. This developed scheme was capable of identifying both location and severity of the structural damage of faulted elements for single fault and multiple faults.

Relying upon vibration based condition monitoring, Rytter (1993) has given various levels for damage identification in a structural system. These levels include (i) detection (ii) localization (iii) sizing (iv) prognosis. In the first level, the damage which is present in the structural system can be identified. Then, the geometric location of the damage can be determined in the second step. The quantification for the severity of the damage is to be done in the next level. Lastly, the remaining service life of the monitored structure can be predicted in the prognosis process. These steps for identification was observed to be excellent for researchers working in the field of structural damage.

Doebling et al. (1998) have emphasized the four levels of damage identification given by Rytter (1993). They also provided a survey on methods for detecting, locating and characterizing the fault or damage in structural as well as mechanical systems assisted with the change in the measured vibration responses. Vibration based monitoring was done with the variations in modal parameters such as modal frequencies, modal shapes, and modal damping values of the structural system. These modal parameters were obtained from the system physical parameters (i.e., mass, stiffness, and damping coefficients). The methods were explained along with their suitable applications in actual engineering systems for the recent and future scopes. They also summarized the possible difficulties that would appear while their implantation and their fidelity.

A review on condition monitoring of rotating machinery for fault detection and diagnosis methods has been given by Edwards et al. (1998). The faults, such as rotor unbalance, crack and bow in shafts were mostly studied and explained in his review paper. They mainly focussed on the modelling and diagnosis techniques for identification of those faults. They

concluded that model based monitoring methods are quite robust and effective as compared to other identification techniques. These methods can fulfil the demand of present scenario in the field of condition monitoring in rotor dynamic analysis. Later, a review paper was published in a specific manner on the crack detection and the estimation of severity of the crack in shafts (Sabnavis et al., 2004). The types and causes of rotor cracks and basics of their initiation as well as propagation were elaborately described. This review was based on primarily three methods for crack identification, i.e. vibration based methods, modal testing methods (utilize change in the mode shapes and natural frequencies) and non-traditional methods (include neural networks, fuzzy logic, and sophisticated signal processing techniques, e.g. wavelet and Wigner-Ville transforms, etc.).

Sinha (2002) presented a research concerned with health monitoring techniques for rotating machinery, such as turbogenerator sets in the power industry. His research was mainly on three main parts of rotating machine, i.e. flexible rotor, supported fluid-film bearings and flexible foundation. He provided reliable modelling for the system foundation and the mathematical modelling of the rotor (based on finite element method) and the fluid bearings. The identification technique used measured vibration response at bearing pedestals during run-down of the machine and estimated rotor unbalance and stiffness as well as damping coefficients of the flexible foundation. The method was experimentally validated and found to be robust. It was also demonstrated that the developed condition monitoring technique can estimate reliably two major faults such as rotor unbalance and the misalignment in the rotor.

Heng et al. (2009) reviewed the detection and diagnosis techniques for monitoring the health condition of rotating machineries. In this article, the merits and demerits of present fault diagnosis techniques were elaborately discussed. To predict failures in a rotating machinery, they classified the existing methods into mainly three approaches in which the first approach

is traditional reliability approach, i.e. the event data based prediction, the second approach is prognostics approach which is based on the condition data based prediction, whereas the last way is integrated approach i.e., the prediction based on combination of both the event and condition data.

Bogue (2013) provided a detailed review on sensors and other instruments technology along with their advantageous applications in condition monitoring of rotating machinery. He concluded that the rotor system health monitoring techniques are reliant on various range of sensors based mostly on eddy current, piezoelectric, inductive, electrodynamic, magnetic and thermal technologies. Lei et al. (2013) in his review paper completely focussed on empirical mode decomposition (EMD) method for diagnosis of faults in rotating machinery. They briefly introduced the EMD method and illustrated its benefit and usefulness. The problems in applying EMD technique for diagnosis purpose were also discussed together with their optimum solutions. Then, the applications of EMD method to multiple faults diagnosis of machine in industries were overviewed in the elements of rotating system, such as rolling element bearings, gears and rotors. Later, Lu et al. (2015) combined EMD method with the modified genetic algorithm and receiver operating characteristics (ROC) to develop a hybrid kind of scheme for the purpose of fault diagnosis. They demonstrated that the proposed fault diagnosis model can achieve improvements in identification accuracy with lower feature dimensionality.

Zhang (2018) presented a review of condition monitoring techniques for gas turbines. It was done with the motive that the efficiency and reliability of gas turbines can be monitored effectively. They described that the condition monitoring for these turbines includes the following steps:

(a) Vibration data collection and pre-processing;

(b) Sensor validation (which also included signal reconstruction in the case of sensor fault);

(c) Separation of steady-state and transient operations;

(d) Novelty detection and fault diagnostics in different operational regimes; and

(e) Decision-making and fault report.

Further, the discussed methodologies were classified as knowledge-based rules, signal processing-based techniques and model-based approaches. Among them, model-based approaches were observed to be more effective and robust. The advantages and disadvantages of the methods were also discussed along with the scope of future work in the research area of condition monitoring.

For the sake of solving the problem of fault feature extraction for rotating machinery in a strong impulse noise environment, Miao et al. (2020) proposed a fault separation method based on vibration signals measured by multiple sensors. This method combined both algorithms of the median filter (MF) and an improved joint approximate diagonalization of eigenmatrices (JADE). Through the numerical simulation and experimental investigation of the vibration signal separation of a hybrid rotor, they concluded that the median filtering method can eliminate adequately the signal of impulse noise, improve the signal-to-noise ratio, and provide precondition for the accurate realization of blind separation. But, the combined method (MF-JADE) would provide a good platform for the separation of aliased signals in strong impulse noise environments.

Among studying various literature in the different types of fault detection and diagnosis techniques, it can be concluded that the quantitative model based approach is much better and preferred than qualitative signal based approach to identify the underlying fault. Model based identification method has the advantage of estimating the fault or damage parameters. These

parameters can be further used for the quantification and prognosis. The accuracy of results in mathematical model based techniques is highly sensitive to the model accuracy.

1.3 Literature Review on Faults in Rotating Machinery

In this section, the literature survey on the detection and diagnosis of the rotor faults, such as unbalance in rotor and rotor misalignment as well as combination of multiple faults along with estimation of bearing and foundations dynamic parameters has been presented.

1.3.1 Unbalance in Rotor

Rotor unbalance is the most common reason in machine vibration. Unbalance fault in rotor system causes more vibration and generates excessive forces in the bearing areas and reduces the life span of a machine. A perfectly balanced rotating system does not have any kind of vibration as the centre of gravity of the rotor coincides with its centre of rotation. But, in actuality it is very difficult to construct a perfectly balanced rotating machinery, because of presence of geometrical errors during manufacturing process, non-homogeneity of raw materials and thermal distortion of the components. These reasons lead to deviate the centre of gravity of the rotor from the centre of rotation. During operation of the rotor system, unbalance may vary in magnitude due to wear and tear of the rotor system, abrasion, and accumulation of unwanted mass in the form of dust, etc. At a very high speed of the rotor (or near critical speeds), this unbalance fault can cause vibration of excessive amplitudes in the rotor system, which may be undesirable and results in failure of rotating machines (e.g. spindles, turbines and aircraft propellers). Therefore, the effect of unbalance fault along with its various identification and balancing techniques have been investigated by several researchers since a long time ago.

There are mainly two methods for balancing of the flexible rotor i.e., modal balancing method and influence coefficient method. The first balancing method was developed by (Bishop and Gladwell, 1959; Gnielka, 1983), that requires the accurate knowledge of the modal parameters of the machine; however, the second method (developed by Drechslen (1980)) utilizes the vibration amplitude and phase measurement for the calculation of balance correction masses. At first, the unbalance response is determined at the rotor measuring planes at a given speed without any correction masses. Afterwards, a trial mass is given in one of the balancing planes and the rotor response is obtained for all of the measuring planes. This process is repeated for all of the balancing planes and from this data the influence coefficient matrix is obtained. The required correction masses can be calculated by multiplying the inverse of the influence coefficient matrix with the original unbalance response vector. The obtained trial masses will be helpful in the rotor balancing. Hence, the second method requires less a priori knowledge of the system model parameters.

A modal balancing method was proposed by Morton (1985) to balance a flexible shaft without the use of trial weights and a knowledge of the support bearings characteristics. The shaft gyroscopic effect and rotating damping of shaft were ignored for modelling of the rotor system. He concluded from numerical results that developed balancing technique can be utilized together with any other technique and is quite suitable for balancing of flexible shafts in the multiple range of critical speeds. Later, Krodkiewski et al. (1994) presented a method for identification of the plane of the rotor with the changes in residual unbalance responses. They developed non-linear mathematical model of the rotor-bearing system and further numerically illustrated in a system consisting of flexible rotor (modelled using Timoshenko beam finite elements with four degrees-of-freedom at each node), four identical three-sleeve journal bearings and a rigid concrete foundation. The method was also tested with the addition of white noise in the signals and found to be accurate in identification.

A theoretical model was proposed by Lees and Friswell (1997) to estimate the unbalance distributions of flexible shafts and eccentricities of rigid disks supported on flexible bearings. This method was based on finite element method (FEM) for analysing the steady-state responses of rotor-bearing system. Each bearing was modelled with eight number of linearized coefficients, i.e. four stiffness and four damping parameters. The identification technique used simulated measured response data (measured at one free end in the shaft) in frequency domain and least-squares fitting approach for estimation of the unbalance fault parameters. Further, Shih and Lee (1997) used measured pedestal vibration to determine the imbalance condition of a rotating machinery. For this purpose, they modelled rotor, bearings and the supporting structure in a consistent manner. The method was found to be insensitive to measurement noise in determining the imbalance fault parameters although the stiffness and mass terms showed moderate sensitivity to uncertainties.

Edwards et al. (2000) validated experimentally the proposed algorithm of Lees and Friswell (1997) to investigate the state of unbalance in rotating machinery by utilizing single run-down machine data. Along with the excitation due to unbalance fault, the excitation coming from bow in shaft was taken into consideration for the result analysis. The parameters related to elastic support structure (i.e., flexible foundation) of machine was also identified along with the unbalance parameters. The values of measured and estimated fault parameters were almost matching which signifies the accuracy of the proposed method. One of the most important observations was made from this experimental exploration that this single-shot balancing technique could reduce approximately 92% of the vibration after balancing the flexible rotor.

Zhou and Shi (2001) reviewed on dynamic analysis, different techniques for active balancing and active vibration control of the rotating system. To present his review in a completeness manner, they also presented the mathematical model for both the simple rigid rotor and complex flexible rotor model, separately. The complicated rotor system was

discretized into various elements, such as flexible shaft model, rigid disc model, linearized bearing model, coupling model, etc. Further, the system equations were obtained by assembling the equations of motion for each of those components. They concluded that the active balancing method can suppress the induced vibrational response of the unbalanced system. Moreover, the active balancing of rotor can enhance quality of the product in industries and increase machine fatigue life and reduce overall cost of the system.

A new method was proposed by De Queiroz (2009) for identification of the unknown unbalance parameters of a simple Jeffcott-like rotor by exploiting a dynamic robust control mechanism. He used unbalance disturbance forces by active feedback control mechanism to identify the unbalance-related parameters. He also demonstrated the effectiveness of the proposed identification strategy using numerical simulation.

Sudhakar and Sekhar (2011) developed three different approaches, i.e. equivalent loads minimization method, equivalent loads minimization method with modified theoretical fault model and vibration minimization method for the identification of unbalance fault in a rotor system. These approaches are the types of model based fault identification technique. In modified theoretical fault model, the effect of modal expansion gets nullified or reduced in the difference operation of least-squares minimization, which results in reduction of errors in the fault parameters identified. In vibration minimization method, the difference between measured and calculated vibrations is minimized using least-squares algorithm by varying fault parameters and this method does not depend on the number of measured degree of freedom. They compared all three methods and found that error gets reduced in modified theoretical fault model as compared to equivalent loads minimization method without modification. They also found that equivalent loads minimization method with modified theoretical fault model and vibration minimization methods are equally effective in identifying unbalance fault with

reduced error even in case of measured degree of freedom as low as two. Unbalance fault was identified using proposed methods by measuring transverse vibrations at only one location.

An identification scheme was presented by Menshikov (2013) for identifying the characteristics of the unbalance fault in a rotor supported on two flexible supports. They developed the mathematical model of the system and used vibrational response of the rotor in the two transverse directions as the main information in the developed identification scheme. Afterwards, they used inverse problem to estimate the unbalance and bearing support parameters. Pennacchi et al. (2013) proposed an estimation methodology for identification of the unbalance in a large rotor system. All components of the system, such as flexible rotor, bearings, flexible foundation, were accurately modelled and analysed before using in the identification method. The frequency domain data of displacement responses were utilized in the identification algorithm to identify the fault location and its severity along the shaft line. They also performed an experimental work on a large size steam turbine (about 1.3 GW) and validated the numerical simulated results.

Chatzisavvas and Dohnal (2015) explored the concept of equivalent load approach as discussed in (Markert et al., 2001) and used for identification of single and double unbalance in a simple rotor-bearing system. They also applied the assumption of a sparse equivalent force vector to improve the unbalance identification without a priori information of the number of faults. The identification of fault parameters was done using both the time domain and frequency domain displacement signals. The proposed method provided effective and satisfying results even in the ill-conditioned problem arising due to an inadequate number of measuring locations and machine running at a constant speed.

For the identification and optimisation of unbalance parameters in a rotating machinery, the two different approaches were proposed by Yao et al. (2018). The first approach was based

on modal expansion method along with the concept of optimization algorithms, while the second approach was related to the combined use of modal expansion method, the inverse problem and optimization procedure. To overcome the practical issue of measuring responses at every locations of the shaft, the modal expansion technique was utilized. The first approach was illustrated in a single disc rotor-bearing system for the identification of unbalance fault, whereas the second approach was applied for the unbalance identification in a rotor system consisting of two discs. Both the numerical simulations and experimental works were conducted based on the two approaches of identification method. The method was capable of identifying the unbalance fault, not only their locations but also their magnitudes and severities.

Recently, a joint-input state and Kalman filter based input estimation techniques were utilized to identify unbalance force in a rigid rotor-conventional bearings system. The proposed techniques were a model-based method, which required a mathematical model of the rotor system along with response measurements. Accelerations were measured at bearing pedestals and used for unbalance parameters estimation. Bearing stiffnesses were also estimated using a frequency domain parameter estimation technique with measured unbalance responses. Sensitivity analysis of the proposed method was also performed by changing the values of these estimated stiffnesses. The results for distinct spin speeds of shaft and measurement noise signal levels were found stably and validated experimentally in a single disc rotor-bearing system (Shrivastava and Mohanty, 2019; Shrivastava and Mohanty, 2020).

The literature presented in this section discussed about the effect of severe unbalance fault in a rotor system. The research performed in the balancing techniques including modal balancing method and influence coefficient method has been well described. For identification of rotor unbalance fault, the model based methods along with the measured vibrational response have gained more importance in the rotor dynamic field as these techniques can identify both location and severity of the fault.

1.3.2 Rotor Misalignment

Misalignment is also a common fault in rotating machinery, which is one of the prime reason for machine vibration. This may reduce the fatigue life and stability of the stationary as well as rotating components of a system. Misalignment in rotor system can occur when the axes of the two shafts are not coinciding with each other or the axis of the bearing and the rotor axis are not collinear or the axes of the bearings supporting a common shaft are not collinear. There are mainly three types of misalignment in rotor, which can be better understood from shaft-to-shaft misalignment at coupling location.

a) *Parallel misalignment*: - In this kind of misalignment, the axes of both the coupled shafts are parallel to each other, but not collinear at the coupling location. There is both shear force and bending moment at the coupled end of each shaft. Parallel misalignment may be horizontal or vertical or both, depending upon the direction of misaligned axis with respect to the collinear axes of shafts. This misalignment is shown in Figure 1.2(a).

b) *Angular misalignment*: - The axes of both the coupled shafts are neither parallel nor collinear, but make an angle with each other (follow Figure 1.2(b)).

c) *Combined misalignment*: - It includes both parallel (presence of parallel offset) and angular misalignment together. This misalignment is represented in Figure 1.2(c).

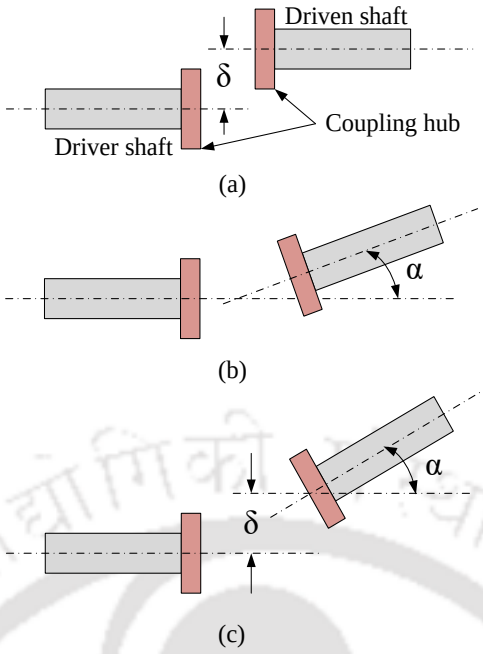

Figure 1.2 Types of misalignment (a) parallel misalignment (b) angular misalignment (c) combined misalignment.

Coupling is a device which is used to connect the driver and driven shafts together for transmitting power and to permit some degree of misalignment at their end positions. The mechanical coupling has been basically classified into two main categories:

(a) *Rigid coupling*: This type of coupling has no flexibility or resilience, hence it is used to rigidly connect two shafts when they are precisely in the same line and close alignment. If somehow they are not aligned, then a slight misalignment may cause important damages in the components such as shafts, bearings, etc. due to an excessive load. Therefore, it is necessary for the coupled shafts to have good alignment, both laterally and angularly. This coupling cannot absorb vibrations and require lubrication in many times.

(b) *Flexible coupling*: This coupling is mostly used in engineering practices and utilized to connect two shafts having some amount of misalignment. This allows the fluctuation

of torsional moment and angular speed. The flexible coupling contains an elastic element which enables it to absorb shocks, vibrations and misalignment. One of the advantages of this coupling is that it also compensates for temperature changes in the couplings and shafts.

Apart from coupling misalignment, there may be misalignment between the shaft and the bearing. The misalignment in conventional bearing and active magnetic bearing is shown in Figure 1.3.

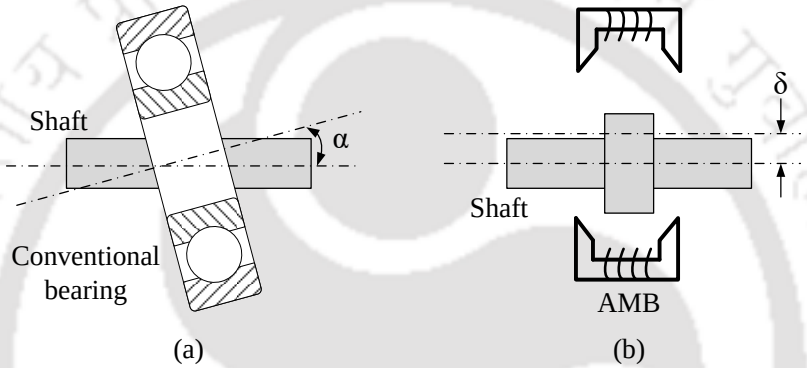

Figure 1.3 Misalignment in bearing (a) conventional bearing (angular misalignment) (b) active magnetic bearing (parallel misalignment).

The major causes of misalignment fault are as follows (i) asymmetric bearing loading; (ii) elastic deflection of shaft, under an imposed under load or its own weight; (iii) thermal distortion of the shaft; (iv) distortions caused by bearing housing supports; (v) manufacturing tolerances (due to inaccurate machining, casting and forging); and (vi) errors due to installation and assembly defects. Therefore, the detection and diagnosis of misaligned rotor systems has gained importance in recent times. The detailed literature survey on modelling, analysis and identification of misalignment fault, such as coupling misalignment, bearing misalignment, etc. has been presented here.

Gibbons (1976) gave mathematical expressions for the reaction forces and moments developed due to misalignment at the coupling location. He analysed the effects of misalignment forces and moments in different types of flexible couplings, such as gear coupling, multi-disc diaphragm coupling with constant thickness, and diaphragm coupling with contoured thickness and flat mid-plane. From this analysis, it was concluded that all the torsionally loaded misaligned couplings have restoring moments which causes bending the rotating shaft. With an increase in the rotor spin speed, the severity due to rotor bow and correspondingly machine vibration were found to be increased. Hori and Uematsu (1980) presented the stability analysis of a multi-rotor system under the influence of misalignment of supported journal bearings. They elucidated that the initial setting errors during rotor model set up and the distortion of the supporting frame arising from uneven thermal expansion are the main causes of bearing misalignment. The considered model was consisting of two rigidly coupled rotor mounted on four journal bearings. Both the horizontal and vertical misalignments were included in the model. To analyse the numerical simulation, the transfer matrix method (TMM) was used. The quasi-catenary alignment was used for aligning the rotor system. Quasi-catenary alignment is the case in which neither shearing force nor bending moment appears at the coupling location. The Newton-Raphson method was utilized to solve the frequency domain equation obtained from TMM. The stability of the rotor system was checked by the real part of its root. Finally, they concluded that the best stability was observed for the case of zero amount of misalignment and the two rotors were the same. However, when both the rotors were different, the stability was acquired at a certain amount of misalignment.

Dewell and Mitchell (1984) used the vibration frequency analysis technique to detect an abnormally misaligned metallic-disc-type coupling in a rotor system with the help of a real-time spectrum analyser. Parallel and angular misalignments were imposed on the disc coupling. An experiment was also performed to validate the theoretical model. They found that vibration

frequency of one and two times the shaft speed gets produced due to misaligned disc-metallic-type coupling. A theoretical model based on the component mode synthesis method was developed by Xu and Marangoni (1994a) to investigate the dynamic effect due to unbalance in the rotor and shaft-flexible-coupling misalignment faults. To consider the misalignment effect into the system account, a universal joint coupling effect was included in the model. The finite element method (FEM) was used to obtain the generalised equations of motion of the complete rotor-coupling-bearing system by taking six degrees of freedom (DOFs) at each node. Later, the developed theoretical model was verified experimentally by using two types of couplings, i.e. self-made flexible coupling and a commercial helical coupling. For the validation of the simulated results, the same conditions of unbalance and misalignment faults were considered. From the analysis, they noticed that the unbalance and coupling misalignment can be mainly characterized, respectively, by 1 × and 2 × shaft running speed. One of the observations was also made that the natural frequency of the system may get shifted due to a change in the flexible coupling. The change in coupling may increase or decrease the vibration response, but the signature of frequency domain vibration pattern remains the same (Xu and Marangoni, 1994b).

Sekhar and Prabhu (1995) presented the effects of coupling misalignment including both parallel and angular misalignment on vibrations of rotating machinery. A higher-order finite element method was used for modelling of rotor-bearing-disc system. They also included gyroscopic effects into the system. They incorporated the reaction forces and moments due to coupling misalignments into the finite element model. They did modelling of the rotor system having coupling misalignment by considering deflection, slope, shear force, bending moment with eight DOFs per node. The result analysis showed the frequency of vibration responses having two times the shaft speed. This represents the presence of misaligned shafts in the rotor system. Rao and Sekhar (1996) presented the consequences of misalignment in rotating

machinery. They presented a theoretical model for a rotor-coupling-bearing system. Finite element method has been used to model this system for both the parallel and angular misalignment including the flexible coupling. They carried out vibration analyses, such as eigenvalue analysis and unbalance response for the rotor system with misaligned shaft. They concluded with the analysis of results that the 2×vibration response clearly shoots up with misalignment.

A dynamic model was proposed by Lee and Lee (1999) for the rotor system supported on ball bearings and integrated with misaligned coupling. For deriving the model, they considered the reaction loads and deformations at the bearing and coupling locations as the misalignment effect. They used an axisymmetric rubber coupling as the coupling element, which was more flexible than the shaft. The investigation on the effect of misalignment was done based on the three kinds of misalignment, i.e. parallel, angular and combination of both misalignments. They explored the whirling orbits, frequency responses and parameter sensitivities for the dynamic features of misalignment fault. Experimental work was also conducted by them and its results showed that as the value of angular misalignment increases, the whirling orbit tends to flat in shape and becomes a straight line. The natural frequency of the system was also found to be higher at the high level of angular misalignment due to an increase in the effective moment stiffness of the supported bearings. However, the whirling orbit and natural frequency were not affected due to a change in the value of parallel misalignment. Prabhakar et al. (2001) did the transient analysis of a rotor-coupling-bearing system passing through the critical speed by using the finite element method for flexural vibrations. They modelled the coupling (both parallel and angular misalignment) by taking two possibilities, i.e. a frictionless joint and a joint with stiffness and damping. They used continuous wavelet transform (CWT) as a tool for significant feature extraction from the time response of the misaligned rotor-coupling-bearing system and found the subcritical speeds at

one-half, one-third and one-fourth the critical speed during this analysis. They also observed that the critical speed of the rotor-bearing system having a coupling with a frictionless joint is higher than that of a joint with stiffness and damping as well as the variations in CWT coefficients at critical as well as subcritical speeds with misalignment are linear.

Al-Hussain and Redmond (2002) investigated the effect of parallel misalignment on the lateral and torsional responses of a combined two Jeffcott rotors. The rotors were connected by rigid coupling. Derivation of the dimensionless equations of motion was presented, which revealed that parallel misalignment couples the translation and angular deflections through the stiffness matrix and the force vector. Solutions of EOMs were obtained using a combination of Newmark and Newton Raphson methods, which gave dimensionless frequency and transient responses in terms of misalignment magnitude. It was observed that due to the presence of only parallel misalignment, the system natural frequencies were excited at transient condition. However, 1× vibration response was available in both the translational and angular directions in a steady-state condition. This showed that parallel misalignment can be a source of both torsional and lateral excitations. Later, Al-Hussain (2003) considered the pure angular misalignment between the two rigid rotors with one disc at each rotor and explored the dynamic nature of the system. The two rotors were tied through a flexible coupling and supported on two hydrodynamic bearings for each rotor. The modelling of the bearings was done with the linearized direct and cross-coupled stiffness and damping coefficients. They derived the energy expressions for the rigid rotor-coupling-bearing system and obtained the stability criteria from Liapunov's direct method. They concluded that the model stability region increases with an increase in angular misalignment and mechanical coupling stiffness terms.

Sinha et al. (2004) proposed a method that can estimate both unbalance and misalignment from measured vibration during a single machine run-down. This method was presented for the case of a flexibly and rigidly coupled rotor system and demonstrated using

experimental data from a machine with two journal bearings and a flexible coupling connected with the motor shaft. Actually, in a real machine, accurate models of the rotor and fluid bearings may not be available, so they carried out a sensitivity analysis with perturbation errors in the rotor and bearing models to confirm the robustness of the proposed method. They observed that the estimation method was far less sensitive to errors in the fluid bearing modelling compared to the rotor modelling error, and rotor systems having fluid bearings were also less sensitive to modelling errors, compared to systems having rigid bearings.

Two different fault diagnostic techniques were proposed by Pennacchi and Vania (2005) to identify the most severe faults in rotating machinery. These approaches include the orbit shape analysis as the first approach and mathematical model based identification technique in the frequency domain as the second approach. They illustrated the developed techniques experimentally in a real gas turbine-generator unit of a small power plant for estimating the angular misalignment in a flexible coupling. The fault type was identified using the orbit shape analysis, further they identified the equivalent bending moments with the help of second approach, which enabled the 1× vibrations caused by the angular misalignment to be simulated. They also performed the experiments within a large range of rotational speed and validated the obtained results. Lees (2007) developed the simplest possible model for two shafts, which are rigidly coupled together by means of number of bolts having finite stiffness mounted on idealized linear bearings. Excitation at twice synchronous speed for this misalignment case was developed and an expression for the magnitude and phase of the response was derived. He presented the resulting motion analysis of the model both analytically and numerically, and observed that the linear model generates responses at harmonics of shaft speed and these harmonics were caused by an interaction of torsional and flexural effects. Patel and Darpe (2009) did experimental investigation of the vibration response of the rotor system included misaligned coupled rotors supported on rolling element bearings by using full

spectrum analysis (i.e. forward and backward whirl both) having unique vibration features and resulting orbit plots for diagnosis of misalignment fault. They also obtained lateral vibration response at integer fraction of the first critical speed of the system for both types of misalignments (parallel and angular misalignment).

Bouaziz et al. (2011) presented three simplified theoretical models based on the number of electromagnets, i.e. four, six and eight in current biased radial magnetic bearings to analyse the dynamic behaviour of a misaligned rotor with two degrees-of-freedom, mounted in two identical AMBs. They developed the equations of motion for the rotor-bearing system and simulated with Newmark method. They observed that the 2× and 4× running speed components were predominant in case of the angular misalignment and their magnitudes varied linearly with number of electromagnets in the bearing and with the air gap between the stator and the shaft and also found that the vibration in the system due to the misalignment effect can be attenuated by increasing the number of electromagnets. Messaoud et al. (2011) proposed a theoretical model of the system consisting of a rotor supported on two identical active magnetic bearings to investigate the dynamic behaviour of the rotor while having an angular misalignment. They also described the effect of the air gap distance between the stator and rotor as well as the rotor speed on the dynamic behaviour of rotor and observed that the intensity of electromagnetic forces is inversely proportional to the air gap, but it remains unresponsive with respect to the magnitude of the rotor speed.

Lal and Tiwari (2012) considered a simple turbo-generator model consisting of two rigid rotors, each supported to two flexible bearings and connected by a misaligned flexible coupling. They derived the equations of motion of the rotor-train system using Lagrange's equation. The misaligned coupling was modelled by considering coupling stiffness and damping coefficients along with the rotor displacements at bearing locations. They proposed an identification algorithm based on frequency domain responses and determined the disc

unbalance parameters, flexible bearings dynamic parameters, and stiffness and damping constants of coupling. During the parameters estimation procedure, they faced the issues of ill-conditioning of regression matrix, in which the number of equations was less than the number of unknowns. Therefore, to overcome this condition of regression matrix, they have taken the response measurements at another spin speed and also by rotating the rotor in the clockwise and anti-clock wise directions for both speeds. They also calculated the misalignment forces and moments from forced-responses of the rotor system. Later, Lal and Tiwari (2013) considered the flexible shafts instead of rigid rotors and explored the analysis and identification using finite element method (FEM) based modelled turbo-generator system. They proposed a conventional dynamic condensation scheme in the development of identification algorithm to tackle a practical difficulties of limited response measurements. The bearings as well as coupling dynamic parameters as well as residual unbalances at predefined planes were estimated using run-down machine vibration data. The proposed algorithm was found to be robust in estimating system and fault parameters with the addition of various levels of noise signal and modelling errors. Further, they performed an experimental work and validated the numerically simulated results. They also considered the different levels of misalignment between the coupled shafts and studied their effect on estimated parameters. It was observed that the theoretical responses were in good agreement with experiment responses (Lal and Tiwari, 2018).

Verma et al. (2014) investigated the effect of different types of misalignment (parallel, angular, and combination of both lateral and angular misalignments) on the rotor vibration signal and stator current signature, in a misaligned coupled rotor mounted on fluid film bearings (the whole rotor system was driven by an induction motor). The orbital response and Fourier transform of both vibration and current were also effectively utilized along with the vibration and current waveforms, in identifying the unique characteristics of misalignment fault. They

concluded that the performed experiments had contributed towards great improvement in diagnosis of misalignment fault, in which the stator current signature alone can predict the misalignment effect without use of vibration signal. They also noticed that the vibration levels in horizontal direction were slightly more than the vertical direction of vibrations. It was due to the increased preload effect of rotor along vertical direction. The misalignment preload increases the stiffness of rotor along the misalignment direction, and as consequence, the response level in misalignment direction would be less.

A literature review of misalignment of journal bearings was presented by Jang and Khonsari (2015). They also presented the basic theory for the misalignment and some results for the circular journal bearing under the influence of misalignment. Later, they investigated the influence of misalignment on a dynamically-loaded engine bearing using a mass-conserving cavitation algorithm (Jang and Khonsari, 2019). Wang and Jiang (2018) explored the dynamic analysis of unbalance and coupling misalignment faults in a dual-rotor system equipped with inter-shaft bearing using both the numerical analysis and experiments. This system includes a low pressure rotor (inner rotor) and a high pressure rotor (outer rotor). The low pressure and high pressure rotors rotate at lower and higher spin speeds, respectively. The differential equations of the considered rotor system were derived with the help of modern nonlinear dynamics and dual-rotor dynamics principles, and numerically solved using the Runge-Kutta method. They analysed the complicated vibration responses under the influence of different rotational speeds, mass eccentricity, misalignment angle and parallel misalignment by the cascade and waterfall plots, time waveform and frequency spectrum. The beat vibration was observed in the responses when the excitation frequencies of the high pressure rotor and low pressure rotor were close to each other. Sawalhi et al. (2019) proposed an experimental methodology and signal processing algorithm, which was illustrated in a physics-based dynamic model of a misaligned rotor-coupling-bearing system. They used FEM modelling for

deriving the overall equations of motion of the system with the consideration of mass, stiffness and damping matrices of the rotor-bearing system. The EOMs of the model with residual unbalance and bearing nonlinear excitations were formulated and solved with the help of a variable-step solver. The interpolated stiffness values of coupling and displacements at the motor as well as rotor sides of the coupling were utilized to determine the misalignment forces. Further, the coupling misalignment forces were fed to the system as excitation forces. The coupling stiffness was interpolated as a function of the shaft spin speed and the misalignment level (i.e., level of pure parallel misalignment). They compared the numerically simulated results with experimentally measured data and found that both the results showed an increase in low and higher response harmonics with speed fluctuations.

Lal (2020) developed an identification algorithm for multi degrees-of-freedom turbine-generator system for estimating speed-dependent bearing parameters and coupling misalignment fault parameters and speed independent unbalance parameters, both numerically and experimentally. The global EOMs of the dynamic rotor-coupling-bearing system was derived using finite element method. The frequency domain identification method was solved using least-squares fitting technique to determine the fault characteristic parameters of the turbine-generator system. An additive noise of different levels of 1%, 2% and 5% were added in the numerically generated response signal to check the robustness of the algorithm. He observed that the algorithm performed even in the presence of noisy response. Moreover, he captured three sets of forced responses at four supported bearing positions, at randomly selected spin speeds in the experimental analysis. Further, the responses were given as input in the developed algorithm and system as well as fault parameters were identified experimentally.

The present literature review covers the dynamic influence of misalignment in a rotor system. Most of the literature were found to be studied in coupling misalignment between two rotating shafts and some includes bearing misalignment in hydrodynamic journal bearing.

Large number of research has been performed considering three kinds of misalignment (parallel, angular and combined parallel and angular misalignments) in coupling misalignment. Estimation of coupling misalignment parameters especially in rotor-train, i.e. turbo-generator system and dual rotor system (which is used in aero-engines) has been done well with model based identification techniques and experimental works. Moreover, the study on the analysis of supported bearing misalignment (especially active magnetic bearings, which have multiple advantages over conventional bearings) in a rotor system needs to be explored more, which may cause high level of vibration and instability in the rotor system.

1.3.3 Multiple Faults in Rotating Machinery

A rotor system may get affected simultaneously from several kinds of faults. It is very essential and crucial task to detect and monitor these faults for safety and efficient operations of rotating machinery. Generally, the vibrational signal of rotor is employed for fault diagnosis; however, the identification process becomes more challenging when multiple faults manifest similar symptoms in the vibration response. Therefore, this section discusses the different kinds of fault identification techniques for identifying the various faults and the related fault parameters.

Flack et al. (1982) studied the dynamic nature of a simple Jeffcott rotor with combined faults of unbalance, shaft bow (a function of rotational speed of rotor) and shaft runout. Equations of motion of the faulty rotor system were derived and numerically simulated. The displacement responses of rotor with same amounts of bow or runout were observed to be significantly distinct in both Bode and Nyquist plots. They also developed a small test rig and tested the simulated responses experimentally with various values of bow. From experimental investigation, it was found that the radius of the response in Nyquist form is strongly dependent on the bow vector. A flexible rotor-coupling-bearing system was examined by Sekhar and

Sreenivasa Rao (1996) with two main faults, such as crack and shaft-to-shaft misalignment at flexible coupling location. They separately presented the mathematical modelling of transverse crack, flexible coupling and coupling misalignment and further investigated the dynamic vibrational responses. Observations made from this analysis that they were able to distinguish the crack fault from misalignment fault using 1× and 2× component of rotor displacement responses. The increment rate of 2× vibration component was found to be higher in coupling misalignment as compared to crack in the shaft.

A model based method was developed by Markert et al. (2001) for on-line identification of multiple faults occurring in rotating machinery. The type of faults and the fault parameters, i.e. the position and magnitude were evaluated based on minimizing the difference between equivalent loads calculated from measured vibrations and equivalent loads from mathematical fault model. This minimization was done using least-squares fitting technique in time domain. They presented two types of probability measures based on correlation functions i.e. coherence and intensity, which were used to estimate the probability of the different identified faults. This model based identification method was tested experimentally on two different test rigs. They investigated three faults, i.e. unbalance, coupling misalignment and rubbing based on this identification method. They also observed that the accuracy of this method is proportional to the number of measured locations. Prabhakar et al. (2002) investigated the combined faults of transverse crack and coupling misalignment in a finite element modelled based flexible rotor system in transient conditions. They concluded that although the symptom of the coupling misalignment and crack faults in terms of vibration pattern look similar. But, the misalignment amount in small quantity is found to be sensitive in comparison to the crack fault with little depth using the continuous wavelet transform (CWT) method. Modelling of the coupling misalignment fault was based on the number of harmonics of forces and moments developed at the coupling location.

Sinha et al. (2002) developed a model based identification methodology for estimating the rotor unbalance (amplitude and phase) and foundation dynamic (stiffness and damping) parameters of a flexible rotating machinery, i.e. turbogenerator. For developing the identification technique, they used the measured rotor vibration data from run-down condition of machine. Further, the whole frequency range of run-down was not taken as a single band, but those were divided into various frequency bands for the reliable estimation of parameters. The division in frequency range was done to overcome the issue of occurrence of many modes in a single band machine run-down, which had given inaccuracy in identification. The method was also tested experimentally and found to be trustworthy even with addition of modelling and noise errors. Bachschmid et al. (2002) presented a model-based identification method for multiple faults in a rotor system. Models of various components, such as the rotor, the bearings and the foundation as well as models of the faults (represented by harmonic components of equivalent forces or moments systems) were required for the purpose of identification of faults. The least-squares fitting approach in the frequency domain was used for evaluating fault parameters on the basis of minimizing the multi-dimensional residual between the measured vibrations and the calculated vibrations using mathematical models of the acting faults. The procedures of this method using some numerical examples were described briefly for identification of simultaneous faults, such as unbalance fault model, bow and rigid coupling misalignment fault models, transverse crack and axial asymmetry fault models, etc. This method was tested and validated using some experimental responses obtained on a test-rig.

Later, a model based identification technique was proposed by Bachschmid and Pennacchi (2003) for estimating the multiple faults in a rotor system, such as the residual unbalance, thermal bow, fatigue crack and the lateral as well as angular coupling misalignment faults. The presented novel method was able to even locate the actual fault and determine their severities, and discriminate the faults, which had almost same kind of vibration patterns. Using

developed method, the experiments were conducted on an actual machine and also on a laboratory test rig set up. To examine the reliability and accuracy of the method, the residual unbalance was evaluated experimentally. Vania and Pennacchi (2004) developed various methods for measuring the accuracy of the results obtained from model-based fault identification method in a rotating machinery. They discussed the reasons for poor accuracy of the results of the fault identification that may be due to a wrong selection of the type of the fault, due to poor adequacy of the model of the fully assembled machine and may be because of the presence of noise in the vibration signals. The potentiality and effectiveness of these developed methods were tested with the help of two techniques, i.e. machine response simulated with mathematical models and experimental data on a real machine.

Jain and Kundra (2004) developed a model based technique for diagnosis and identification of faults, such as unbalance and transverse crack (taken as breathing crack) in a shaft separately. They applied these techniques while the rotor system was on working condition. Equivalent load minimization method (one of the model based technique) was used for identification of the location and severity of faults. Modal expansion method was used to approximate vibration response at unmeasured DOFs on the basis of mode shape. Theoretical equivalent loads were compared with those from measured data via curve fitting algorithm (i.e. least-squares fitting method) to identify the faults parameters. They considered different cases based on the number of measured vibrations for identification of unbalance and crack faults. They found that the error gets reduced greatly with increase in measured degrees of freedom (DOFs). Crack was identified successfully using this technique when measured vibrations were assumed to be available at all DOFs. Experimental validation of this technique was also done using the test rig set up at Darmstadt University of Technology, Germany. Tiwari (2005) presented an identification algorithm for simultaneous estimation of the residual unbalance and bearing dynamic parameters in multiple DOFs rotor-bearing systems. In this paper, he found

ill-conditioning of the regression matrix while simultaneously estimating them. Therefore, he proposed three methods to change ill-conditioning into well conditioning of regression matrix. Those methods involve firstly by putting multiple trial masses, secondly by rotating the rotor in opposite directions and lastly by an auxiliary balance unit. This identification algorithm was also tested against the measurement noise and found to be robust.

Pennacchi et al. (2006a) and Pennacchi et al. (2006b) presented a method of using a modal foundation for modelling the supporting structure of a rotor system, to be used to identify a fault with the help of the least-squares fitting technique in frequency domain. This modal representation of supporting structures was required for increasing the accuracy of the identification method. They considered two ways of representing this modal foundation, the first one was considering as rigid foundation and the other by pedestals, i.e. two DOFs mass-spring-damper systems. They also discussed mathematical modelling for identification of various faults. Moreover, the developed model-based technique was utilized for identification of transverse cracks present in industrial machines. The identified results were validated with experimental results obtained from a large test rig developed for examining the dynamic behaviour of the horizontal cracked rotors. Three different types of cracks were considered, i.e. crack having a slot of 34% depth, partially breathing crack having depth of 14% of the diameter and a deep crack having depth of 47% of the diameter. The presented method was found to be effective, robust and reliable with good accuracy for identifying position and location of different cracks. It was concluded that this method was suitable for large industry field applications, as only measurements in the bearings, or close to the bearings were required for this identification procedure. Patel and Darpe (2008) developed dynamic vibration analysis of a cracked rotor under steady-state condition at the instant when there was rub fault between rotor and stator, and presence of unbalance fault. They developed the equation of motion of the rotor system including faults, such as transverse crack, rubbing and unbalance. Runge-Kutta

fourth-order numerical integration scheme with a small time step to ensure a stable solution was used for the solution of the non-linear equation. Full spectrum analysis was used to eliminate discrepancies raised in these rotor faults. They found that the results coming from experimental investigations were similar to the theoretical results. They also observed that backward whirl nature of 2× frequency component as well as that of higher harmonics at corresponding subharmonic resonances are used for diagnosis of rotor rub in cracked rotor system.

Moreover, an overview on machine fault signature analysis, especially focussed on vibrational analysis, was presented by Jayaswal et al. (2008) for the identification of different types of faults, such as gear fault, electrical machine fault, faults in rolling contact bearing and journal bearing, and flexible coupling faults. However, the main intention of the paper was concentrated on the rolling element bearing faults identification from vibration signature analysis. The authors provided two prime objectives of machine fault identification: (i) avoidance of future failure incidents (ii) assurance of safety, reliability, and maintainability of machineries. Afterwards, Jing and Meng (2009) developed a novel method for the diagnosis of multiple faults, such as impact rub between rotor and stator, traverse crack in shaft and oil whirl in a rotating machinery utilizing blind source separation (BSS) technique. This technique was used for segregating the vibrational characteristics generated by those faults. They tested the proposed statistic variable-based algorithm by performing both the numerical simulation and experiments. From the experimental work, they came to a conclusion that the BSS technique was quite feasible and useful in diagnosing the multiple faults in a rotor system. Jalan and Mohanty (2009) described model based technique for identification of faults in rotor-bearing system. They used this technique for diagnosis of faults, such as misalignment in shaft and unbalance in rotor under steady-state condition. Residual vibrations were generated from experimental results for the rotor bearing system subject to misalignment (both parallel and

angular) and unbalance using the residual generation technique. Then, the residual forces due to presence of faults were calculated and compared with the equivalent theoretical forces due to faults. Experimental validation of the model based fault identification method was also done using comparison between numerical results and experimental results.

Li et al. (2009) proposed a model based approach to estimate simultaneously the degrees of unbalance and misalignment in a flexible rotor-coupling system. Using this approach, the degrees of unbalance and coupling misalignment faults were estimated, respectively, by examing the components of the equivalent external loads of which the frequencies are equal to one and two times shaft angular frequency. Lees et al. (2009) presented an overview of the recent developments in the model-based identification method used for determining types of faults and the fault parameters, accurately. This identification technique was based on quantitative basis rather than qualitative basis, which required mathematical modelling of a system and methods related to multiple faults. They explained briefly the procedure for the estimation of the foundation parameters from the measured vibration responses. Some research done in the field of rotor balancing methods, estimation of rotor bow fault, rotor misalignment fault, identification of crack fault in rotor and estimation of bearing parameters are also discussed in this paper. An identification algorithm on the basis of the forced-response information was proposed by Lal and Tiwari (2012) for simultaneous estimation of bearing dynamic parameters, residual unbalance, and the forces and moments caused by coupling misalignment in a turbine-generator system model. They considered a discrete model system consisting of two rotors, each of them supported on two flexible bearings and connected by a flexible coupling for the development of the methodology. The equations of motion of the considered system were derived by using Lagrange's equation. Least-squares fitting approach was incorporated into the identification algorithm for evaluating the unknown parameters. They observed that this identification method was used for estimation of the bearing dynamic and residual unbalance parameters as

well as for the estimation of misalignment forces and moments. The identified results were tested and validated with experimental results and found to be robust against the measurement noise.

Jalan and Mohanty (2013) developed a model based method for on-line identification of unbalance and misalignment faults occurring simultaneously in the rotor system. They used residual generation technique for calculating the residual forces emanating from residual vibrations (measured experimentally). Then, the difference between the residual forces and the equivalent forces calculated from mathematical model of the system in presence of these faults was minimized using optimization technique, i.e. the least squares fitting approach to get the location and severity of the faults. Mogal and Lalwani (2015) proposed an order analysis technique based on vibration analysis for diagnosing the rotor unbalance fault from misalignment fault. Both the amplitude and phase of the vibrational response were obtained using order analysis which was further utilized to identify the type and location of fault. They also validated the proposed technique by performing experiments, which was found to be quite effective for fault diagnosis.

Tahir et al. (2016) utilized multi-axis time domain (TD) vibration signals (radial and axial vibrations) to detect simultaneously the unbalance and misalignment faults in a rotor system. It was observed that the proposed multi-axis TD features provided extremely precise result using Support Vector Machine (SVM) classifier. Later, K-Nearest Neighbor (KNN) analysis technique was presented by Nejadpak and Yang (2017) for detection as well as classification of unbalance and misalignment faults together. For this purpose, they used measured vibration data coming from four industrial accelerometers situated at both bearing housings along radial (vertical and horizontal) directions while the system was in operating condition. From testing data, the KNN analysis method was found to be reliable in the detection of these faults during operation. A finite element method based numerical simulations and

experimental investigations were performed by El-Mongy and Younes (2017) in order to distinguish the crack in shaft from the other faults such as the rotor unbalance and coupling misalignment. They analysed the transient vibrational response of the faulty rotor system with the consideration of sub-critical limit speed, the crack and unbalance parameters as well as severity of misalignment. From the result analysis, they observed that crack can be successfully detected from the sub-critical response. In this case, a sub-critical resonance was found to be emerged in the transient response and increased with propagation of the crack. As the crack deepened, more sub-resonances was observed to have emerged but in lower amplitudes. Meanwhile, misalignment was found to show up in the transient response as a series of sub-resonances that were relatively equal in amplitude. The increase in misalignment amount showed a corresponding noticeable increase in the sub-resonance amplitudes. The presence of these sub-resonances in the transient response was mainly attributed to misalignment presence. Therefore, this feature was useful in distinguishing both faults from each other using the transient sub-critical responses.

To overcome the issue of differentiating various faults using fast Fourier transform (FFT) technique as the faults may have similar type of signatures, Shari et al. (2019) combined FFT technique and independent component analysis (ICA). They measured the vibration of the multi-fault rotor system through multichannel vibration data acquisition system. Afterwards, the signals were analysed using ICA and finally, FFT was applied on ICA components. The extracted features provided the best signature to identify each fault from others. They applied the combined fault detection technique to detect general faults, such as bearing fault, unbalance, misalignment, shaft fatigue occurring in the rotating machines. Wang and Gong (2019) investigated the vibrational analysis of a flexible coupled rotor in the presence of coupling misalignment and rotor unbalance faults. In order to better understand the misalignment faults, a coupled rotor-flexible bearing system was established by six degrees of

freedom based on finite element modelling. Both the parallel and angular misalignment model were used to simulate fault characteristics. Further, the response characteristics were analyzed to reveal the mechanism of the effect of misalignments with respect to forces (torques) and response.

Kumar and Kumar (2020) proposed an innovative Linear Discriminant Analysis (LDA) based indicator for the simultaneous detection of unbalance and misalignment at multiple spin speeds of the shaft. The features were extracted from the resampled signal and its spectrum. The LDA of original features was carried to form numerical indicator to identify three shaft conditions such as defect free, unbalance and misalignment. A fault diagnosis method based on multi-input convolutional neural network (MI-CNN) was proposed by Zhao et al. (2020) for distinguishing the shaft misalignment and crack in a rotor system. They observed that the method was very effective and had better accuracy as compared to the other intelligent algorithms. Recently, a model based identification algorithm was developed by Roy and Tiwari (2019a) and (2020a) for the simultaneous identification of unbalance, crack and internal as well as external damping in a rotor system with one disc at middle and also at offset position supported on rigid bearings. They performed full spectrum analysis and used the frequency domain forward and backward whirl responses in the proposed methodology for estimating the multiple fault parameters. The modelling of transverse crack was done using switching crack concept. The algorithm was tested using noisy vibration signal responses and rotor modelling errors in system parameters. Later, they also explored this full spectrum based identification scheme experimentally on an assembled fatigue cracked rotor test rig setup and validated the numerical simulation results (Roy and Tiwari, 2019b; Roy and Tiwari, 2020b).

In continuation of this, Sarmah and Tiwari (2019) incorporated an AMB near the crack and disc position in the above considered rotor model. AMB was provided in order to control the vibration responses and stability of the cracked rotor system. They also proposed a model

based identification algorithm for the estimation of multiple fault parameters, such as the external and internal damping, translational as well as rotational additive crack stiffness, disc eccentricity and its phase and AMB parameters. The same identification technique was successfully employed to identify the additive and multiplicative parameters in a more complex multi-fault cracked-bowed-unbalanced rotor system integrated with an auxiliary active magnetic bearing (Sarmah and Tiwari, 2020).

On the basis of literature review presented in this section, it is observed that the simultaneous identification of multiple faults in a rotating machinery is a very challenging issue in the rotor dynamic field. This becomes more difficult when the symptoms of one fault match with other faults. The multiple faults also increase the number of unknown parameters and complexity in modelling of the dynamic system. Therefore, it can be concluded from the reviewed papers that a model based identification technique (i.e., quantitative approach) is an excellent approach and much better than signal based identification technique (i.e., qualitative approach) in identifying the faults with their different parameters in faulty multi-rotor system.

1.4 Review on Condensation Schemes

The investigation on the dynamic analysis of a large rotor system is very difficult due to high complexity. The complexity arises from the presence of multiple numbers of degrees-of-freedom (DOFs) in the system. It becomes a tedious task to measure all DOFs, especially the rotational ones, due to difficulties in accessing certain locations on the rotor and limitations in the availability of number of displacement sensors. Moreover, taking measurements at all DOFs would be more expensive and consume more time. Therefore, the researchers have proposed various approaches, which can reduce the large size of the complex rotor model involved in the mathematic formulation.

Usually, there are two different methods used for the reduction of degrees-of-freedom. One of the method is static reduction method, whereas the other method is dynamic reduction method. Out of both the methods, the static reduction method is simpler and popular. In earlier times, the formal method has been developed by Guyan (1965). The degrees of freedom eliminated in the reduction process are called slave DOFs and those retained for the analysis are called master DOFs. The limitation of this method is that it is suitable for zero frequency or low range of frequency and the inertia terms are assumed to be negligible as compared to the stiffness term. Moreover, this method cannot produce the accurate eigen solutions. Therefore, to overcome these concerns, Paz (1984) proposed a dynamic condensation method. The proposed method provided exact eigenvalues and eigenvectors for all the modes considered in the reduced eigenproblem of a structural system. He concluded that the method is quite suitable from the fundamental mode to any desired number of higher modes. O'Callahan (1989) improved the static reduction method with the help of improved reduction system method (IRS), which was approximated up to the first order of a binomial series expansion in the transformation of slave DOFs. Further, an improved dynamic condensation method based on iterative approach was proposed to calculate the accurate values of a large structural system eigen properties, i.e. natural frequencies and modes of vibration of systems (Singh and Suarez, 1992).

Friswell et al. (1995) extended an improved reduction system (IRS) method using two approaches, in order to obtain more accurate reduction in degrees-of-freedom. The first approach was using the equivalent transformation based on dynamic reduction instead of static reduction, whereas the second approach was based on introducing an iterative scheme in which the corrective term was generated iteratively. They also investigated the convergence of the natural frequencies of the reduced model to those of the full model. Later, they have developed a model reduction method for a damped and gyroscopic coupled systems. They also compared

its reduction results with reduction process for no damping in the systems and found that the reduction transformations generated from the undamped model contained more errors (Friswell et al., 2001). Xia and Lin (2004) proposed an iterative reduction order (IRO) method to improve the computational efficiency and estimated accurately the eigenvalues and eigenvectors of a large structural systems. They have also demonstrated the novel reduction technique practically in a plate structure with large DOFs and observed that the developed iterative based approach was very efficient. Jung et al. (2004) developed an iterative dynamic condensation scheme for the finite element model reduction in a structural system. They concluded that the proposed scheme was more advantageous than the other iterative schemes. The convergence was found to be faster especially at the condition when the eigen properties of reduced model was close to that of the full model.

A high-frequency and hybrid reduction schemes were proposed by Dharmaraju et al. (2005) and Tiwari and Dharmaraju (2006) to reduce the number of measurement responses in their developed identification algorithm. They eliminated transverse rotational DOFs and identified beam crack flexibility coefficients and crack depth. They extended the hybrid reduction method for damping in the rotor system (Karthikeyan and Tiwari, 2010). Choi et al. (2008) presented an iterated improved reduced system (IIRS) method combined with substructuring scheme for both undamped and damped structures. The method provided highly accurate eigenproperties without consuming expensive computational cost. Numerical simulations were performed to validate the proposed method and to evaluate the computational efficiency. Prasad and Tiwari (2018) proposed a gyroscopic dynamic reduction method to reduce rotational DOFs in a finite element modelled flexible rotor-AMB system. The transformation matrix in the condensation method also included the gyroscopic matrix along with the mass and stiffness matrices. The dynamic condensation scheme was also utilized by several authors (Lal and Tiwari, 2013; Singh and Tiwari, 2016; Singh and Tiwari, 2018; Kuppa

and Lal, 2019; Kuppa and Lal, 2020; Srinivas R et al., 2020) for utilizing the reduced response measurements in their identification algorithm to estimate system and multiple faults such as unbalance, crack and coupling misalignment parameters as well as bearing dynamic parameters in a rotor system.

Upon carrying out various literature survey in this section, it can be stated that research has been performed well in the condensation schemes, especially in dynamic reduction method due to its advantage over static reduction method. Moreover, still the researchers depend on the dynamic condensation method for eliminating the rotational DOFs in the analytical model. This is done to compare the measured experimental data and numerically generated data with complete information during model updating.

1.5 Review on AMB and its Applications in Rotor System

Active Magnetic Bearing (AMB) is a type of bearing, which generates forces on the rotor system through electromagnetic field rather than forces due to mechanical contact in rolling element bearings or induced fluid forces in lubricant film in hydrodynamic journal bearings. AMB provides stable levitation to the rotor by continuously providing the magnetic field between the stationary magnetic poles and rotor. As there is no contact between rotor and stator, so there is no need of lubrication and no chance of wear; hence, the rotor can be rotated at higher speeds during operation and in the wide range of temperature. AMB technology can also enrich the life span of the several components of the rotor system. One of the most advantages of AMB is that its stiffness and damping parameters are tunable, which allows the stable operation of a rotor at different rotor system parameters and higher spin speeds.

An active (electro) magnetic bearing (AMB) can only produce attractive forces. Therefore, a closed loop controller with additional hardware components is required to

maintain stable operation. Figure 1.4 depicts the schematic diagram for working principle of an AMB along with its main components, which includes actuator, proximity sensor, controller and amplifier. Firstly, a stationary rotor is lifted up in air by providing bias current, such that the force due to this constant current balances the weight of rotor. Then, the motor drive is used for rotating the rotor at desired speed. When the rotor changes its position due to faults while rotation, this non-contact proximity sensor measures the displacement signal in voltage form (by maintaining a constant air gap from rotor) and sends it to the controller. The controller sends the correction signal to the power amplifier, which then sends appropriate current correction to the coils of magnetic actuator. The electromagnet creates magnetic flux, which attracts the rotor and brings it to its equilibrium position. This process continues, which causes levitation of rotor in air during operation.

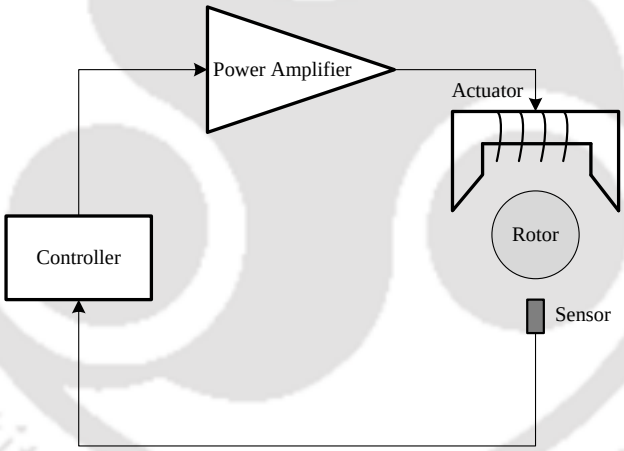

Figure 1.4 Schematic diagram for working principle of an AMB.

Usually, AMB is used for three purposes in the field of rotor dynamics, in which the first is to utilize AMB as a bearing for supporting the spinning rotor. The second is using AMB as an active control for controlling the vibrational response. Lastly, AMB is also used as an exciter to provide a known dynamic force (constant magnitude) to the rotor system with the help of control currents based on user's choice. In recent times, there are also enormous applications

of AMB for fault identification in rotating machinery. The literature survey done in AMB technology for vibration control, fault identification, supporting purpose, used as an exciter is briefly presented here.

Brunet (1989) discussed the working performance of active magnetic bearing in various applications, such as the cryogenic turbo expander, centrifugal compressor, blower, steam turbine and very high speed milling machine, etc. He observed that less maintenance is required in these machines and vibration is highly reduced with the use of AMBs. Nonami (1989) utilized magnetic bearings primarily for two purposes, i.e. for main support to the rotor and for active vibration control. He employed FEM for modelling of flexible rotor and executed experimental work in a laboratory test rig setup (shown in Figure 1.5) for validating the numerical results. One of the conclusions was made that it becomes necessary to add new active control loops for the higher flexible modes even in the case of collocation.

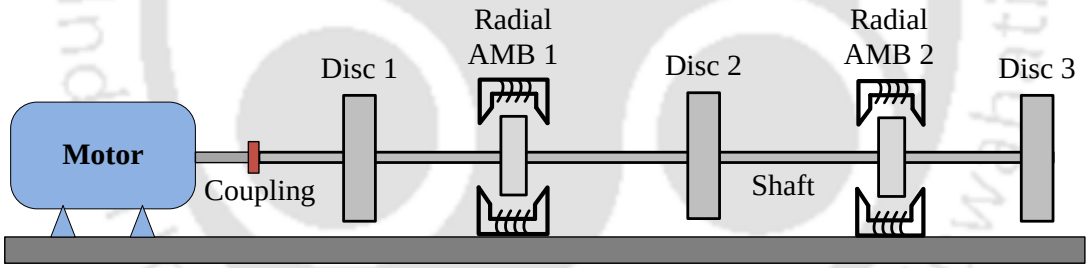

Figure 1.5 Test rig schematic developed by Nonami (1989).

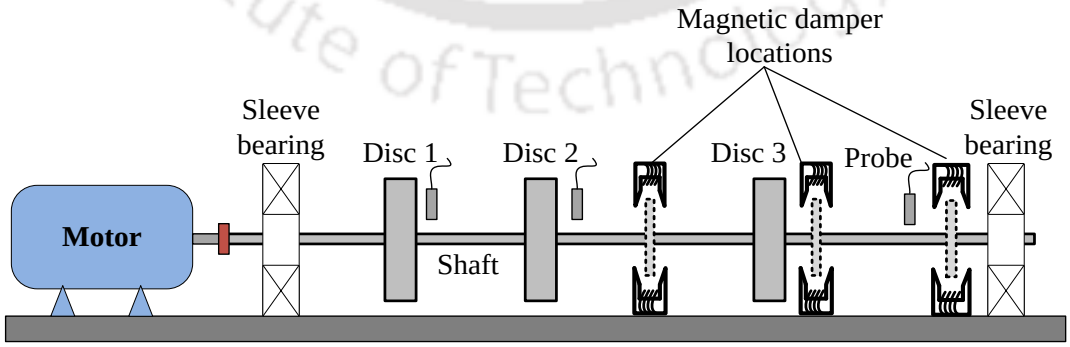

Figure 1.6 Schematic diagram of laboratory test rig set up developed by (Kasarda et al., 1990)

Kasarda et al. (1990) considered a magnetic damper consisting of four electromagnets located radially around the rotor shaft. They utilized the damper for reducing vibration in a long thin shaft connected with several discs and supported by sleeve bearings at both ends (follow Figure 1.6). The vibration analysis was investigated with three conditions based on placing magnetic damper at different locations. The location of damper was chosen first at the mid span, then near the end disc and lastly close to the bearing. They observed from the experimental results that the mid span location reduced the first mode vibration by 82%, the disc location reduced it by 75%, and the bearing location achieved 74% vibration reduction.

Nordmann and Aenis (2004) used AMB for rotor supporting purpose and controlling vibration of the system due to unbalance fault by performing experiments. They used a combination of feedback control and the adaptive open-loop control algorithms for the vibration control. Kasarda (2000) and Schweitzer (2002) reviewed the working principles of active magnetic bearings and their applications in large scale turbomachinery and high-speed flywheels for the purpose of energy storage. Later, an overview of the advantages of AMB over other traditional mechanical bearings in gas turbine engines in the aerospace industry was presented by Clark et al. (2004). Aenis et al. (2002) and Nordmann and Aenis (2004) utilized AMB technology for fault detection and diagnosis technique in turbomachinery, such as centrifugal pump. An AMB was used by Kim and Lee (2003) as an exciter for identification of the dynamic characteristics of an oil-lubricated short squeeze film damper (SFD). They observed that AMB was a perfect and ideal device for experimental tests in SFDs. Lee et al. (2006) designed a radial AMB system based on the analysis of differential magnet actuator, in order to support a high-speed rotating massive rotor in turbo-machinery induction motor. They used proportional-derivative (PD) feedback controller to make the closed loop AMB system stable.

Das et al. (2008) proposed an active vibration control scheme using AMB to minimise the transverse vibration of an unbalanced rotor. AMB technology was incorporated with a proportional-derivative (PD) controller to supply suitable control current for generating the electromagnetic force. Even at higher speeds, a high level of stability was achieved in the rotor-AMB system. Further, a fault identification algorithm was developed by Tsai et al. (2009) to analyse malfunctions in actuators along with sensors in a rotor system integrated with AMB. They found that the proposed method performs well against the conducted experiments.

Beltran-Carbajal et al. (2013) proposed an algebraic identification scheme for on-line estimation of the system parameters, such as rotor mass, unbalance magnitude, damping and disturbance signals in three DOFs Jeffcott rotor mounted on AMB and conventional bearing at one and another ends (depicted in Figure 1.7). AMB was used to generate electromagnetic radial forces for the active vibration control as well as balancing of the rotor. This technique was found to be fast, effective and robust. A multidisc flexible rotor model supported on multiple AMBs was considered by Tiwari and Chougale (2014) in developing an identification algorithm for simultaneously estimating the residual unbalance parameters and AMBs dynamic coefficients (i.e., force-displacement and force-current stiffness constants).

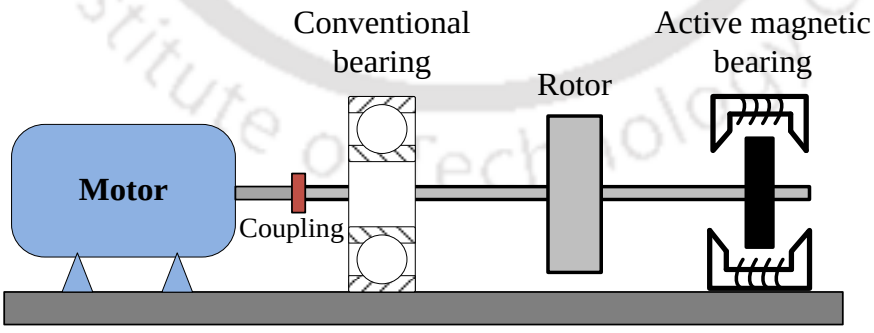

Figure 1.7 A Jeffcott-like rotor-bearing system supported on a conventional bearing and an AMB (Beltran-Carbajal et al., 2013).

Singh and Tiwari (2015) included an AMB in a transverse cracked rotor-bearing system for suppressing the vibration response induced from availability of breathing crack and rotor unbalance faults. They also identified AMB displacement and current stiffness parameters along with parameters associated with unbalance and crack additive stiffness by developing a model based identification algorithm. An AMB was used as an exciter by Xu et al. (2016) for detection of the outer race defect in rolling element bearings. They considered a rotor system supported on rolling element bearings and an AMB was placed at the middle of the shaft to provide electromagnetic forces to the system. Later, they used multiple AMBs (two thrust and two radial AMBs at front and rear positions) for supporting the rotor and identified the stiffness and damping coefficients of AMBs with the help of experimentally measured unbalanced response (Xu et al., 2017). A non-contact electromagnetic exciter was designed by Wang et al. (2017) to identify the dynamic coefficients of journal bearings in a high-speed grinding spindle system.

Srinivas et al. (2018) reviewed the hardware elements of AMB and discussed the prime objectives as well as fundamental aspects in developing an experimental test bench for flexible rotor-AMB system. Further, they have also used an AMB for controlling the vibration in a misaligned rotor-train system and additionally the frequency domain displacement and controlling current responses were utilized in a model based identification scheme for estimation of unbalance, AMB and coupling misalignment (parallel and angular) parameters. The coupling misalignment fault was modelled using a steering function with multiple harmonics (Srinivas et al., 2019; Srinivas R et al., 2020). Further, the two number of AMBs were utilized by Kuppa and Lal (2020) for active vibration controls in a flexible coupled misaligned rotor system (modelled with finite element method). They also developed an identification algorithm based on vibrational response and AMBs current response as input and

estimated imbalance and coupling stiffness and damping coefficients along with AMBs stiffness parameters.

Ranjan and Tiwari (2019) incorporated AMB as a controller in a flexible rotor-conventional bearing system. AMB was able to minimise the vibration even at high spin speeds and further the suppressed rotor responses as well as controlling force were utilized to estimate the residual unbalances in the system. Later, AMB was utilized as a suppression actuator and an excitation actuator. A virtual trial unbalance concept based identification algorithm was proposed by them, which was used in high-speed balancing of rotor. The virtual trial unbalances were introduced from additional magnetic force generated through AMB (Ranjan and Tiwari, 2020).

It is quite evident from the above literature that an enormous quantity of work has been executed in the field of presenting an overview of working principles, hardware components and applications of AMB in turbomachines, and gas turbines. Several kinds of research have also been conducted in utilizing AMB as a bearing support, an active vibration control and as an exciter and still the research is being conducted on these areas. In the recent days, researchers are also focussing on using AMB technology for multiple faults identification and active balancing of rotor in a rotating machinery.

1.6 Outcomes of the Literature Review

In the starting of the literature review, the different types of condition monitoring techniques for fault detection and diagnosis in rotating machinery have been presented. This included basically the signal based methods and model based methods. Subsequently, the special emphasis was given on reviewing the dynamic analysis and fault identification techniques for identifying the most common faults, such as rotor unbalance and misalignment. The spinning

rotor and the associated system components can have multiple faults simultaneously, which increases the high amplitude of vibrations and complexity in the system. Therefore, a review on identifications of multiple faults is also discussed. Finally, the research papers published on condensation schemes and applications of AMB in the field of rotor dynamics is presented in a concise manner. The general observations made from executing the literature survey are as follows:

- In condition monitoring techniques, the model based methods are found to be more favourable for identification of faults in a rotating system. The main advantage of these methods is that they are able to quantify the faults along with their locations and to some extent the prognosis. Identification of a single fault (unbalance, misalignment, crack, etc.) through model based identification is well developed. But, still vast research works are needed for simultaneous identification of multiple faults, especially for those who are showing same vibrational signatures. For example, the simultaneous identification of faults such as misalignment, bow, crack and rub still require a comprehensive research.
- One of the limitations of model based methods is that they require a very accurate analytical model and model properties. Moreover, if the system structure or parameters are not precisely known and diagnosis has to be based primarily on heuristic information, no quantitative model can be set up. In this case, a qualitative approach to fault diagnosis is necessary. So, it is necessary to conduct more research in qualitative based approach.
- There is a need for reducing the dependence of the monitoring methods on the input measurements, such as the force excitation. The external input sources make the methods impractical for industrial applications as they demand additional attachments

and measurements. Moreover, the early fault detection and robustness of the monitoring methods are also required for better condition monitoring of rotating machinery.

- Most of the available literature is based on using AMB as an active vibration control and exciter. Little research has been performed in utilizing AMB as bearing. Therefore, the recent trend also requires AMB technology for the rotor supporting purpose in high speed practical machines, such as gas turbines, steam turbines, aircraft engines, etc. to overcome the performance restrictions of conventional bearings.
- Research is found to be mostly conducted in the field of examining the dynamic behaviour and faults identification in a rigid and flexible coupled rotor system, coupled rotor-train-traditional bearing system without and with AMB, basically associated with coupling misalignment fault. Here, AMB has been used an active vibration control, not for rotor levitation purpose.
- Study on the analysis of rotor supported on conventional bearing having misalignment is also very limited.
- The concept of trial unbalance for balancing of the rotor has been developed. But, the trial misalignment approach for identifying the misalignment amounts and then aligning the system has not been approached yet. Identification of misalignment quantitatively (i.e., knowing the offset amounts) would be extremely helpful for modern industries due to safety and reliable operations of rotating machinery.
- Analysing the combined effect of coupling misalignment, AMBs misalignment and crack in shaft in a dual rotor system fully levitated on active magnetic bearings would be really a challenging work in the rotor dynamic field.
- Misalignment in proximity sensors and supported AMBs in a smart rotor dynamic system has not been investigated.

1.7 Objectives of the Present Work

The main objectives of the present work are as follows

- Modelling, analysis and identification of unbalance parameters and AMBs residual (parallel) misalignment in a simple rigid rotor system levitated by two (isotropic and identical nature) AMBs.
- Modelling, analysis and identification of unbalance parameters and AMBs residual (parallel and angular) misalignments in a rigid rotor system having gyroscopic effects and levitated by two (isotropic and different nature) AMBs.
- Modelling, analysis and identification of unbalance parameters, AMBs residual (parallel and angular) misalignments and their stiffness constants in a multidisc flexible rotor system levitated by multiple (anisotropic and different nature) AMBs.
- Modelling, analysis and identification of unbalance parameters, AMBs and sensors residual (parallel and angular) misalignments as well as AMBs stiffness constants in a multidisc flexible rotor system levitated by multiple (anisotropic and different nature) AMBs and integrated with multiple offset sensors.

1.8 Organisation of the Thesis

The present thesis work is organized into six chapters. The introduction and literature review are presented in Chapter 1. The modelling, analysis and identification (unbalance and misaligned AMB parameters) based on a novel trial misalignment approach (physical trial misalignment) for a 2 DOFs unbalanced rigid rotor system supported on two misaligned AMBs are explored in Chapter 2. It also includes the derivation of linearized form of misaligned AMB force for the residual and additional trial misalignments. The same procedure has been extended for rigid rotor with two offset discs in Chapter 3. The combination of parallel and

angular misalignments as well as disc gyroscopic effects are considered in the analysis. Chapter 4 discusses the development of mathematical model (FEM based model flexible shaft, rigid discs, misaligned AMBs) and identification algorithm for multidisc flexible rotor system misaligned with multiple supported AMBs at different locations. Finally, Chapter 5 is an extension of Chapter 4, in which the misalignment has also been considered in non-contact displacement sensors along with misaligned AMBs. Chapter 5 also includes a novel concept of virtual trial misalignment (VTM) given to the rotor for creating additional misalignments in sensors and AMBs. The identification algorithm derived from the VTM strategy is developed and utilized in estimating unbalance parameters, AMBs residual misalignments and their stiffness constants. The VTM approach has been employed in identifying the offset amounts of sensors located at AMB locations. Conclusions, limitations and future scopes from the present work are presented in Chapter 6.

Chapter 2

Modelling and Identification in a Simple Misaligned Rigid Rotor-AMB System

2.1 Introduction

In the present chapter, a model based identification algorithm is developed to estimate the unbalance and AMB misalignment in a rotor system levitated with active magnetic bearings (AMBs). For this, a simple discrete model of the rotor-AMB system has been developed with assumption of an unbalanced rigid rotor with a disc at the middle of shaft levitated by two misaligned active magnetic bearings. This model is capable of describing the vibration resulting from the rotor unbalance and AMB misalignment (parallel misalignment) faults.

The shaft in this chapter has been considered rigid in nature due to some of advantages over the flexible shaft in experimentation. In comparison to the rigid rotor system, more number of eddy current proximity sensors are required to measure transverse displacement responses at different locations of flexible shaft. There is a difficulty in measuring the rotational displacements of the flexible shaft. Balancing of the flexible rotor is more complex than rigid rotor balancing. The flexible rotor continuously changes its elastic configuration as more critical speeds are encountered. Since it is recognized that rotor-bending operating deflections modify the resulting forces from residual unbalance, flexible rotor need to be balanced at high speed. Moreover, at higher speeds of the rotor, the aligning of supported AMBs may be difficult due to large amplitude of vibration. Thus, it is better to first align the system at low speeds (where the shaft is considered rigid) by identifying the residual misalignment amount. After aligning, the system can cross its critical speeds with less vibration (i.e., for the case of flexible rotor).

Two cases of the misalignment depending upon the amount of radial offset between the rigid rotor and AMB axes have been examined for the investigation. In the first case (i.e., residual misalignment), an unknown misalignment is considered that is to be estimated. In the second case (i.e., additional trial misalignment), a trial misalignment is added in addition to the residual misalignment. This is a novel concept proposed in line with the trial unbalance in rotor dynamic balancing. The linearized form of force due to misaligned AMB is also innovatively derived for residual and additional trial misalignment cases. It is found that this force consists an additional constant force along with the modified displacement and current stiffnesses of AMB.

With inclusion of inertia force, unbalance force and force due to misaligned AMBs, the equations of motion of the rigid rotor-misaligned AMB system are derived and numerically simulated to generate the time domain rotor displacement and controlling current responses, which are further converted into frequency domain signals assisted by the fast Fourier transform (FFT) analysis. These responses have been utilized in the identification algorithm to estimate the unbalance and stiffnesses of misaligned AMBs as well as the misalignment amount between the rotor and AMBs. Estimations of unbalance and AMB misalignment parameters have also been carried out against various levels of measurement signal noise and modelling errors.

2.2 System Configuration and Basic Assumptions

In the present section, the system modelling configuration and basic assumptions considered for exploring the dynamic vibrational analysis of the rotor-AMB system and illustrating the proposed identification methodology have been stated. A rigid rotor with a rigid disc at middle position, supported by two misaligned AMBs, has been considered as shown in Figure 2.1. The

motion of rigid rotor is taken in two transverse directions, i.e. the vertical (x) and horizontal (y) directions, for the analysis purpose.

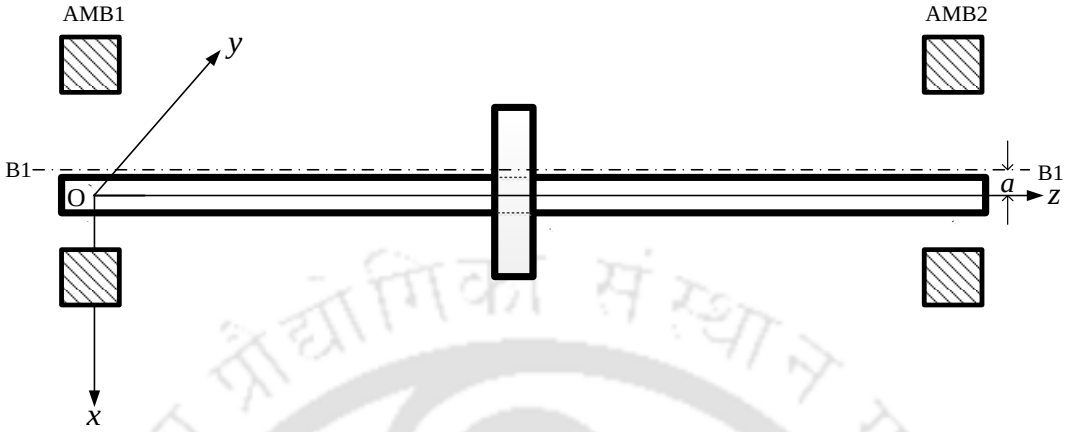

Figure 2.1 Schematic diagram of a rigid rotor with a disc at middle position supported on two misaligned AMBs.

Here, B1B1 is the central axis of both AMBs, Oz is the rotor operating axis and the radial distance 'a' is the misalignment between axes of the rotor and the AMB that is to be estimated. It is assumed that the misalignment between the rotor and AMB axes in the x and y directions are same. It is also assumed that both AMBs are parallel misaligned with the same amount 'a' as shown in Figure 2.1. Both AMBs are also assumed to be identical with the same force-displacement and force-current stiffnesses. Moreover, the eight-pole AMB actuators are treated as isotropic, thus AMB constants along the two orthogonal directions would be same.

2.3 Mathematical Modelling and Equations of Motion of the Rotor-AMB System

In this section, the mathematical modelling for the above considered rigid rotor-AMB system has been developed with consideration of unbalance force model and misaligned AMB force model for residual and additional trial misalignment cases. Equations of motion of the system in the two transverse translational directions are also derived with inclusion of inertia force and force due to unbalance as well as misaligned AMBs for both the cases of misalignment.

2.3.1 Unbalance Force Model

The unbalance force exciting on the rigid rotor, in the *x*- and *y*-directions, can be written as

$$f_{unbx} = m_d e\omega^2 \cos(\omega t + \beta); \qquad f_{unby} = m_d e\omega^2 \sin(\omega t + \beta) \tag{2.1}$$

where, m_d is the disc mass, and the magnitude and phase of disc unbalance are represented by e and β, respectively. The spin speed of the rotor is denoted by ω.

2.3.2 Force due to Active Magnetic Bearing on the System

Figure 2.2(a) presents an actuator model when there is no misalignment between the rotor and the active magnetic bearing (i.e., there is an equal air gap in the lower and upper poles of AMB). The polarity of poles in the actuator model is kept N-S-S-N-N-S-S-N to avoid the loss of magnetic flux. In this Figure, BR represents aligned axis of the actuator and the rotor.

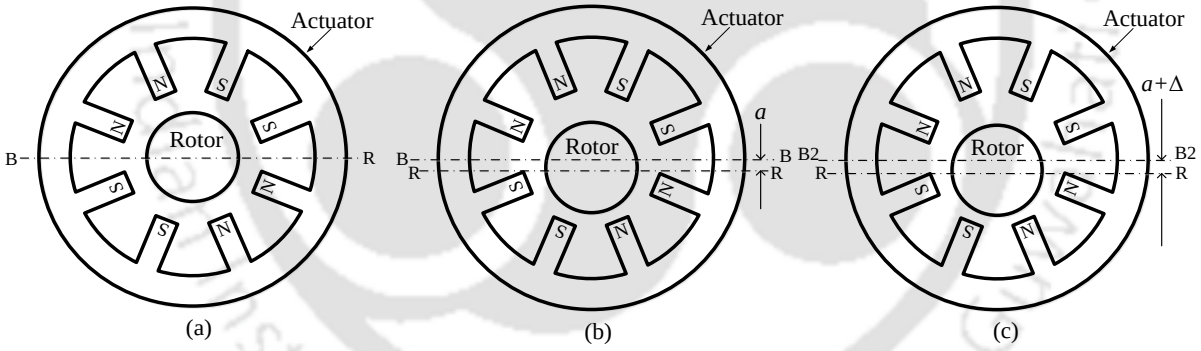

Figure 2.2 Side view of a heteropolar eight-pole actuator with rotor (a) perfectly aligned (b) misaligned with residual '*a*' amount (c) misaligned with additional trial '*a*+Δ' amount.

In the perfectly aligned case (Schweitzer and Maslen, 2009), the force acting on the rotor due to AMB in *x*-direction, can be expressed as

$$f_x = k\left\{\frac{(i_0 + i_x)^2}{(s_0 - u_x)^2} - \frac{(i_0 - i_x)^2}{(s_0 + u_x)^2}\right\} \tag{2.2}$$

with $$k = \frac{1}{4}\mu_0 N^2 A_a \cos\frac{\alpha}{2} \tag{2.3}$$

where μ_0 is the permeability in vacuum and equal to $4\pi\times10^{-7}$ H/m, N is the number of coil turns, A_a is the cross sectional area of magnetic pole, α is the angle between two adjacent magnetic poles, i_0 and i_x are the bias and controlling currents, respectively. The air gap between rotor and AMB is denoted by s_0 and u_x is the vibration induced displacement in x-direction. Now, simplifying Equation (2.2) and then linearizing with the assumption of $u_x \ll s_0$, it gives

$$f_x = k_s u_x + k_i i_x \tag{2.4}$$

where, the force-displacement (k_s) and force-current stiffness (k_i) parameters are

$$k_s = \frac{4ki_0^2}{s_0^3}; \qquad k_i = \frac{4ki_0}{s_0^2} \tag{2.5}$$

Similarly, the force acting on the rotor due to AMB in y-direction, in perfectly aligned case, can be expressed as

$$f_y = k_s u_y + k_i i_y \tag{2.6}$$

where, u_y and i_y are the vibration induced displacement of rotor and the controlling current in the y-direction, respectively, when the rotor is perfectly aligned with AMB axis. A feedback control loop system is required to ensure stability in the rotor-AMB system in which the controlling current output directly depends upon the vibration induced displacements. In this regard, a PID controller has been utilized to provide the current in the coil at both AMB locations. Controlling current output at both AMB locations (Schweitzer and Maslen, 2009), in x- and y-directions, in perfectly aligned case can be written as

$$i_x = -\left(k_P u_x + k_I \int u_x dt + k_D \dot{u}_x\right); \qquad i_y = -\left(k_P u_y + k_I \int u_y dt + k_D \dot{u}_y\right) \tag{2.7}$$

where the proportional, integral and derivative gain factors of the PID controller are represented by k_P, k_I and k_D, respectively.

The following section describes how the forces due to AMBs on rotor gets transformed when there is an offset between the axis of rotor and AMBs. In this connection two cases of misalignment, i.e. the residual and additional trial misalignments have been considered. The residual misalignment is the unknown misalignment that needs to be identified. The additional trial misalignment is related to an additional known misalignment together with the unknown one. The prime objective of providing additional misalignment to AMBs and illustrating the second case is to estimate the unknown amount of AMB misalignment from the developed identification methodology.

2.3.2.1 AMB Force Model for Residual Misalignment

In actual practices, it is extremely difficult to perfectly align the rotor-AMB system due to mechanical machining and rotor system assembling errors (Longxiang, 2009) as well as sensor measurement error while locating the centre of AMB. In a full floated rotor-AMB system, the centre locations of AMB in the vertical and horizontal directions are detected using the change in voltage perceived from proximity sensors, by settling the AMB core consecutively at the lower and upper poles as well as at the extreme backside and front side poles of AMB, respectively. However, the exact detection of AMB centre using non-contact eddy current sensors is a challenging task due to sensor measurement errors, arising from their defective positioning. This inability in finding the correct location of AMB centre will lead to residual misalignment of the AMBs axis with respect to the absolute reference of the rotor operating axis. This non-coincidence of the axes may influence the AMB performance due to uneven air gap distribution, which results in development of one extra force term other than the linearized forces associated with modified AMBs force-displacement and force-current stiffness

coefficients for the perfectly aligned case. This extra force term may be the cause of high level of vibration, more power consumption as well as severe unstable levitation of AMB-rotor. Hence, in this section, the linearized form of force due to misaligned AMB in the *x*- and *y*-directions are derived. The residual misalignment '*a*' of AMB with the rotor is shown in Figure 2.2(b). Here, BB represents the axis of actuator and RR for the rotor operating axis. It is assumed that this misalignment is same in both the *x*- and *y*-directions for brevity and simplicity to examine and illustrate the developing identification method. Later, in the next three chapters, the misalignment has been assumed different in the *x* and *y* directions at both AMBs locations to increase the complexity in the system. Thus, the air gap of AMB gets changed in both directions due to this radial offset. The lower air gap and upper air gap of AMB are (s_0-a) and (s_0+a), respectively. Based on this consideration, the force on the rotor due to misaligned AMB in the *x* direction can be expressed as

$$f_x^{m1} = k\left\{\frac{\left(i_0 + i_x^{m1}\right)^2}{\left(s_0 - a - u_x^{m1}\right)^2} - \frac{\left(i_0 - i_x^{m1}\right)^2}{\left(s_0 + a + u_x^{m1}\right)^2}\right\} \tag{2.8}$$

where, the superscript $m1$ denotes the residual misalignment case. u_x^{m1} and i_x^{m1} are the *x*-directional rotor vibrational displacement and controller current output at AMB location for the present case of misalignment. Further, on simplifying Equation (2.8) and neglecting the higher order terms of $\left(u_x^{m1}\right)^2$ with the assumption of less vibration induced displacement in comparison to the lower and upper air gaps between the rotor and AMB stator i.e., $u_x^{m1} \ll (s_0$-$a)$ and $u_x^{m1} \ll (s_0$+$a)$, we get

$$f_x^{m1} = k\left\{\frac{4s_0 i_0^2 u_x^{m1}}{\left(s_0-a\right)^2\left(s_0+a\right)^2} + \frac{4i_0\left(s_0^2+a^2\right)i_x^{m1}}{\left(s_0-a\right)^2\left(s_0+a\right)^2} + \frac{4s_0 a\left(i_x^{m1}\right)^2 + 4s_0 u_x^{m1}\left(i_x^{m1}\right)^2 + 4i_0 a i_x^{m1} u_x^{m1} + 4s_0 a i_0^2}{\left(s_0-a\right)^2\left(s_0+a\right)^2}\right\} \quad (2.9)$$

On neglecting the higher order terms, i.e., $\left(i_x^{m1}\right)^2$, $u_x^{m1}\left(i_x^{m1}\right)^2$ and $i_x^{m1}\,u_x^{m1}$, Equation (2.9) can be expressed in a linearized form as

$$f_x^{m1} = k\left\{\frac{4s_0 i_0^2 u_x^{m1}}{\left(s_0-a\right)^2\left(s_0+a\right)^2} + \frac{4i_0\left(s_0^2+a^2\right)i_x^{m1}}{\left(s_0-a\right)^2\left(s_0+a\right)^2} + \frac{4s_0 a i_0^2}{\left(s_0-a\right)^2\left(s_0+a\right)^2}\right\} \quad (2.10)$$

On substituting Equation (2.5) into Equation (2.10), it gives

$$f_x^{m1} = \frac{k_s}{\left(1-a_1^2\right)^2}u_x^{m1} + \frac{k_i\left(1+a_1^2\right)}{\left(1-a_1^2\right)^2}i_x^{m1} + \frac{f_a a_1}{\left(1-a_1^2\right)^2} \quad (2.11)$$

with $$f_a = \frac{4ki_0^2}{s_0^2}; \qquad a_1 = \frac{a}{s_0}$$

Finally, the force on the rigid rotor due to misaligned AMB with radial offset '*a*' in *x*-direction can be written as

$$f_x^{m1} = k_s^{m1}u_x^{m1} + k_i^{m1}i_x^{m1} + f_c^{m1} \quad (2.12)$$

with $$k_s^{m1} = \frac{k_s}{\left(1-a_1^2\right)^2}; \qquad k_i^{m1} = \frac{k_i\left(1+a_1^2\right)}{\left(1-a_1^2\right)^2}; \qquad f_c^{m1} = \frac{f_a a_1}{\left(1-a_1^2\right)^2} \quad (2.13)$$

Similarly, the force on the rotor due to misaligned AMB in *y*-direction can be written as

$$f_y^{m1} = k_s^{m1}u_y^{m1} + k_i^{m1}i_y^{m1} + f_c^{m1} \quad (2.14)$$

Herein, in Equation (2.14), it can be seen that the misaligned AMB stiffness constants (k_s^{m1}, k_i^{m1}) and constant force (f_c^{m1}) arising from misalignment are same in the *x* and *y* directions. This is due to isotropic nature of AMB and equal amounts of *x*- and *y*-directional AMB offset

(i.e., the amount '*a*') with the rotor. The vibration induced displacements (u_x^{m1}, u_y^{m1}) arising due to unbalance and AMB misalignment faults have been taken about the equilibrium position of AMB. So, the same amount of rotor displacement will be used to generate the controlling current in the case of actuator misalignment also. Controlling current output of PID controller for the case of residual misalignment will follow Equation (2.7), with the replacement of (u_x, u_y) by (u_x^{m1}, u_y^{m1}) and (i_x, i_y) by (i_x^{m1}, i_y^{m1}).

2.3.2.2 AMB Force Model for Additional Trial Misalignment

Similarly, for the case of additional trial misalignment as shown in Figure 2.2(c), the force due to misaligned AMB in the *x*- and *y*-directions can be obtained in the linearized form. In this misalignment case, an additional amount of misalignment 'Δ' is provided between the axis of rotor and AMBs in both the vertical and horizontal directions. This novel concept of providing known trial misalignment will be helpful to identify the unknown residual misalignment using the developed identification algorithm. Thus, the new offset between the axis of rotor and both actuators in the *x*- and *y*-directions becomes (*a*+Δ) as shown in Figure 2.2(c), where, B2B2 and RR represent the axes of actuator and rotor, respectively.

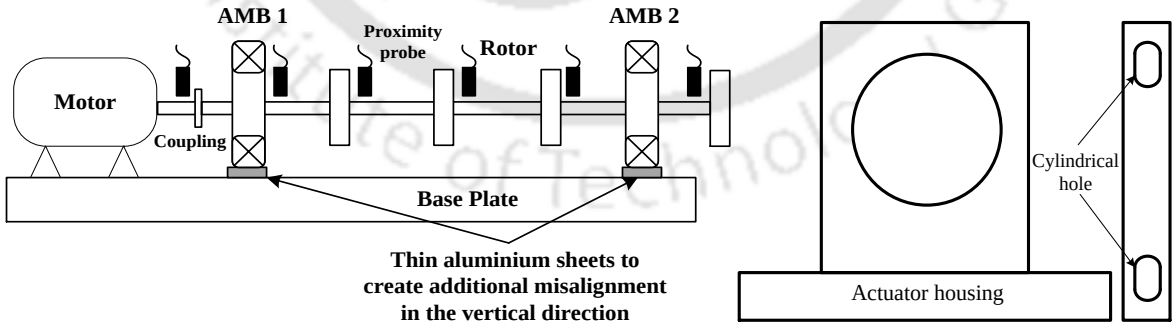

(a) (b)

Figure 2.3 Method to provide additional (trial) misalignment in the rotor-AMB system (a) vertical direction (b) horizontal direction.

In real practice, the additional (trial) known misalignment in the vertical direction (Δ) can be created by elevating the housings of AMBs actuators by putting thin aluminium shim plates (or by providing fine threaded screw/bolts arrangement) between the housings and base plate, as shown in Figure 2.3(a). In the horizontal direction, the known trial misalignments between rotor and AMBs (Δ) can be given by shifting the bolts of the actuator housings with fixed amount. Figure 2.3(b) shows the actuator housing and its top view with the cylindrical holes for bolts fitting with the base plate. The holes are made cylindrical, so that the user can shift the housing as per requirement for the horizontal trial misalignment. Moreover, the trial misalignment in the horizontal direction can also be provided through movable housing by screw or screw-jack arrangement. This method to provide additional (known) misalignment to the actuator housings can be termed as physical trial method (PTM). The limitation of PTM is that it is time consuming and needs more number of test runs as well as a precise model of the rotor-bearing system.

Therefore, to avoid number of test runs in the above discussed physical trial misalignment (PTM) method, the additional (trial) misalignment can also be created virtually in both the vertical (x) and horizontal (y) directions. This can be done by shifting the rotor with respect to AMBs current position, through additional bias current supplied to AMBs along with the controlling current. In this virtual trial misalignment approach, the rotor will be given additional offset with the same amount (Δ) in both the transverse directions using the bias current. This virtual method for providing the trial misalignment to the rotor is more reliable and effective than the physical trial misalignment, which will be discussed in Section 5.3.1.

Using the concept of AMB force model for the residual misalignment case as elaborated in previous section, the force on the rotor due to 'a+Δ' amount misaligned AMB in the x- and y-directions can be written as

$$f_x^{m2} = k_s^{m2} u_x^{m2} + k_i^{m2} i_x^{m2} + f_c^{m2}; \qquad f_y^{m2} = k_s^{m2} u_y^{m2} + k_i^{m2} i_y^{m2} + f_c^{m2} \tag{2.15}$$

with

$$k_s^{m2} = \frac{k_s}{\left(1-b_1^2\right)^2}; \quad k_i^{m2} = \frac{k_i\left(1+b_1^2\right)}{\left(1-b_1^2\right)^2}; \quad f_c^{m2} = \frac{f_a b_1}{\left(1-b_1^2\right)^2}; \quad b_1 = a_1 + \Delta_1; \quad \Delta_1 = \frac{\Delta}{s_0} \tag{2.16}$$

Here, the superscript *m*2 represents for the additional trial misalignment. Controlling current outputs for this misalignment case, in the *x*- and *y*-directions will be similar to Equation (2.7), only the variables (u_x, u_y) and (i_x, i_y) are to be replaced by (u_x^{m2}, u_y^{m2}) and (i_x^{m2}, i_y^{m2}), respectively.

2.3.3 Equations of Motion of the Unbalanced and Misaligned Rotor-AMB Model

With inclusion of the inertia force, unbalance force, and force on rotor due to misaligned AMBs, the equations of motion of the rigid rotor-misaligned AMB system (as shown in Figure 2.1), in *x*- and *y*-directions, for the residual and additional trial misalignment cases can be written as

$$m\ddot{u}_x^{m1} = f_{unbx} + 2f_x^{m1}; \qquad m\ddot{u}_y^{m1} = f_{unby} + 2f_y^{m1} \tag{2.17}$$

$$m\ddot{u}_x^{m2} = f_{unbx} + 2f_x^{m2}; \qquad m\ddot{u}_y^{m2} = f_{unby} + 2f_y^{m2} \tag{2.18}$$

where *m* is the rotor mass. Equations (2.17) and (2.18) represent for residual misalignment and additional trial misalignment, respectively. It is to be noted that in a real rotor system, the stationary rotor is lifted in the air by providing a bias current, such that the force due to this constant current balances the weight of the rotor. Then, the rotor is operated at the desired speed. Hence, the vibration-induced displacements arising due to unbalance and AMB misalignment faults while the rotation has been considered about the equilibrium position of AMB. Therefore, these equations of motion (i.e., equations (2.17) and (2.18)) of the rotor-AMB system do not include the gravity effect.

Further, on using Equations (2.1), (2.12), (2.14) and (2.15), Equations (2.17) and (2.18) can be written in the complex form, as

$$m\ddot{r}^{m1} = m_d e\omega^2 e^{\mathrm{j}(\omega t+\beta)} + 2\left\{k_s^{m1} r^{m1} + k_i^{m1} i_c^{m1} + f_c^{m1}(1+\mathrm{j})\right\} \tag{2.19}$$

$$m\ddot{r}^{m2} = m_d e\omega^2 e^{\mathrm{j}(\omega t+\beta)} + 2\left\{k_s^{m2} r^{m2} + k_i^{m2} i_c^{m2} + f_c^{m2}(1+\mathrm{j})\right\} \tag{2.20}$$

where, j denotes for a complex number equal to $\sqrt{-1}$, the complex rotor displacement and controlling current responses for both misalignment cases are

$$r^{m1} = u_x^{m1} + \mathrm{j}u_y^{m1}; \qquad i_c^{m1} = i_x^{m1} + \mathrm{j}i_y^{m1} \tag{2.21}$$

$$r^{m2} = u_x^{m2} + \mathrm{j}u_y^{m2}; \qquad i_c^{m2} = i_x^{m2} + \mathrm{j}i_y^{m2} \tag{2.22}$$

Complex rotor displacement response $\{R_i^{m1}(t),\ R_i^{m2}(t)\}$ and controlling current response $\{I_i^{m1}(t),\ I_i^{m2}(t)\}$ in time domain can be assumed as $\{R_i^{m1}(\omega)e^{\mathrm{j}i\omega t},\ R_i^{m2}(\omega)e^{\mathrm{j}i\omega t}\}$ and $\{I_i^{m1}(\omega)e^{\mathrm{j}i\omega t},\ I_i^{m2}(\omega)e^{\mathrm{j}i\omega t}\}$ respectively, for (i = 0 and 1), for both the misalignment cases. Here, (i = 0) is due to presence of constant force (f_c^{m1}, f_c^{m2}) in AMB misalignment force, followed in Equations (2.12) and (2.15). Similarly, (i = 1) is due to the disc unbalance force. Further, the second derivative of complex rotor displacement for the residual and additional trial misalignments can be expressed, respectively, as

$$\ddot{R}_i^{m1}(t) = -i^2\omega^2 R_i^{m1}(\omega)e^{\mathrm{j}i\omega t} \tag{2.23}$$

and

$$\ddot{R}_i^{m2}(t) = -i^2\omega^2 R_i^{m2}(\omega)e^{\mathrm{j}i\omega t} \tag{2.24}$$

2.4 Development of Unbalance and AMB Misalignment Identification Algorithm

A model based identification algorithm has been developed based on utilizing frequency domain rigid rotor displacement and current responses at both AMB locations. The prime objective of developing the identification methodology is to estimate unbalance parameters (*e*, *β*) along with misaligned AMB force-displacement constants (k_s^{m1}, k_s^{m2}), force-current constant (k_i^{m1}, k_i^{m2}) and additional constant force (f_c^{m1}, f_c^{m2}) for both residual and additional trial misalignment cases. Further, these identified misaligned AMB constants for both cases of misalignment are evaluated to estimate the amount of radial offset (*a*) between the rigid rotor and AMB axes as shown in Fig 2.1.

2.4.1 Fast Fourier Transform based Response Generation

It is well known that a fast Fourier Transform (FFT) technique is the most powerful tool in converting time domain responses to frequency domain signals for all practical purposes. This is due to its fastness property in conversion process and high computational efficiency. Therefore, FFT function of MATLAB^{TM} is utilized to convert the time domain rigid rotor displacement and controlling current responses into frequency domain responses. A complex number includes both the amplitude and phase of responses in the output of FFT analysis. Due to linearity nature of FFT, the amplitude of the response remains same but the phase changes during transformation of the time domain analysis into frequency domain analysis. Thus, the correct phase is obtained by taking the difference of phase of measured response signal and phase of a reference signal (follow Appendix C). For this purpose, a reference signal is included with FFT analysed signal, which is measured by attaching an eddy current proximity sensor near the motor shaft. This yields a reference for measuring phases of the displacement and current signals at AMB locations with respect to a fixed orientation mark present at the shaft. The procedure for phase correction method during FFT analysis is explained in Appendix C.

2.4.2 Procedure for Estimation of Unbalance and Misalignment Parameters

The FFT processed rigid rotor displacement and current responses (for residual and additional trial misalignments) as well as unbalance force can be segregated into the real and imaginary parts, as follows

$$\left.\begin{aligned} R_i^{m1}(\omega) &= R_{i,\mathrm{Re}}^{m1}(\omega) + \mathrm{j}R_{i,\mathrm{Im}}^{m1}(\omega) \\ I_i^{m1}(\omega) &= I_{i,\mathrm{Re}}^{m1}(\omega) + \mathrm{j}I_{i,\mathrm{Im}}^{m1}(\omega) \end{aligned}\right\} \tag{2.25}$$

$$\left.\begin{aligned} R_i^{m2}(\omega) &= R_{i,\mathrm{Re}}^{m2}(\omega) + \mathrm{j}R_{i,\mathrm{Im}}^{m2}(\omega) \\ I_i^{m2}(\omega) &= I_{i,\mathrm{Re}}^{m2}(\omega) + \mathrm{j}I_{i,\mathrm{Im}}^{m2}(\omega) \end{aligned}\right\} \tag{2.26}$$

$$m_d e\omega^2 e^{j\beta} = m_d\omega^2\left(e\cos\beta + je\sin\beta\right) = m_d\omega^2\left(e_{\mathrm{Re}} + je_{\mathrm{Im}}\right) \tag{2.27}$$

On substituting Equations (2.25), (2.26) and (2.27) into Equations (2.19) and (2.20), for both cases of misalignments, we get

$$\begin{aligned} -mi^2\omega^2\left\{R_{i,\mathrm{Re}}^{m1}(\omega) + \mathrm{j}R_{i,\mathrm{Im}}^{m1}(\omega)\right\}e^{\mathrm{j}i\omega t} &= m_d\omega^2\left(e_{\mathrm{Re}} + \mathrm{j}e_{\mathrm{Im}}\right) + 2k_s^{m1}\left\{R_{i,\mathrm{Re}}^{m1}(\omega) + \mathrm{j}R_{i,\mathrm{Im}}^{m1}(\omega)\right\}e^{\mathrm{j}i\omega t} \\ &\quad + 2k_i^{m1}\left\{I_{i,\mathrm{Re}}^{m1}(\omega) + \mathrm{j}I_{i,\mathrm{Im}}^{m1}(\omega)\right\}e^{\mathrm{j}i\omega t} + 2f_c^{m1}(1+\mathrm{j}) \end{aligned} \tag{2.28}$$

$$\begin{aligned} -mi^2\omega^2\left\{R_{i,\mathrm{Re}}^{m2}(\omega) + \mathrm{j}R_{i,\mathrm{Im}}^{m2}(\omega)\right\}e^{\mathrm{j}i\omega t} &= m_d\omega^2\left(e_{\mathrm{Re}} + \mathrm{j}e_{\mathrm{Im}}\right) + 2k_s^{m2}\left\{R_{i,\mathrm{Re}}^{m2}(\omega) + \mathrm{j}R_{i,\mathrm{Im}}^{m2}(\omega)\right\}e^{\mathrm{j}i\omega t} \\ &\quad + 2k_i^{m2}\left\{I_{i,\mathrm{Re}}^{m2}(\omega) + \mathrm{j}I_{i,\mathrm{Im}}^{m2}(\omega)\right\}e^{\mathrm{j}i\omega t} + 2f_c^{m2}(1+\mathrm{j}) \end{aligned} \tag{2.29}$$

The real and imaginary components of Equations (2.28) and (2.29) for (i = 0) and (i = 1) can be written separately and then rearranged in such a way that the known parameters related terms are in the right hand side and all the terms accompanied with the identifiable parameters that has to be estimated (i.e., e_{Re}, e_{Im}, k_s^{m1}, k_i^{m1} and f_c^{m1} for residual misalignment and e_{Re}, e_{Im}, k_s^{m2}, k_i^{m2} and f_c^{m2} for additional trial misalignment) are on the left hand side of the equations. For the purpose of performing linear regression analysis, all the equations for both

cases associated with the real and imaginary parts for (i = 0) and (i = 1) can be expressed in matrix form, as

$$\mathbf{A}^{m1}(\omega)\mathbf{x}^{m1} = \mathbf{b}^{m1}(\omega) \tag{2.30}$$

with

$$\mathbf{A}^{m1}(\omega) = \begin{bmatrix} 0 & 0 & -2R_{0,\mathrm{Re}}^{m1} & -2I_{0,\mathrm{Re}}^{m1} & -2 \\ 0 & 0 & -2R_{0,\mathrm{Im}}^{m1} & -2I_{0,\mathrm{Im}}^{m1} & -2 \\ -m_d\omega^2 & 0 & -2R_{1,\mathrm{Re}}^{m1} & -2I_{1,\mathrm{Re}}^{m1} & 0 \\ 0 & -m_d\omega^2 & -2R_{1,\mathrm{Im}}^{m1} & -2I_{1,\mathrm{Im}}^{m1} & 0 \end{bmatrix};\ \mathbf{x}^{m1} = \begin{Bmatrix} e_{\mathrm{Re}} \\ e_{\mathrm{Im}} \\ k_s^{m1} \\ k_i^{m1} \\ f_c^{m1} \end{Bmatrix};\ \mathbf{b}^{m1}(\omega) = \begin{Bmatrix} 0 \\ 0 \\ m\omega^2 R_{1,\mathrm{Re}}^{m1} \\ m\omega^2 R_{1,\mathrm{Im}}^{m1} \end{Bmatrix}$$

$$\mathbf{A}^{m2}(\omega)\mathbf{x}^{m2} = \mathbf{b}^{m2}(\omega) \tag{2.31}$$

with

$$\mathbf{A}^{m2}(\omega) = \begin{bmatrix} 0 & 0 & -2R_{0,\mathrm{Re}}^{m2} & -2I_{0,\mathrm{Re}}^{m2} & -2 \\ 0 & 0 & -2R_{0,\mathrm{Im}}^{m2} & -2I_{0,\mathrm{Im}}^{m2} & -2 \\ -m_d\omega^2 & 0 & -2R_{1,\mathrm{Re}}^{m2} & -2I_{1,\mathrm{Re}}^{m2} & 0 \\ 0 & -m_d\omega^2 & -2R_{1,\mathrm{Im}}^{m2} & -2I_{1,\mathrm{Im}}^{m2} & 0 \end{bmatrix};\ \mathbf{x}^{m2} = \begin{Bmatrix} e_{\mathrm{Re}} \\ e_{\mathrm{Im}} \\ k_s^{m2} \\ k_i^{m2} \\ f_c^{m2} \end{Bmatrix}\ \mathbf{b}^{m2}(\omega) = \begin{Bmatrix} 0 \\ 0 \\ m\omega^2 R_{1,\mathrm{Re}}^{m2}(\omega) \\ m\omega^2 R_{1,\mathrm{Im}}^{m2}(\omega) \end{Bmatrix}$$

where the regression matrices and vectors containing the known parameters (basically frequency related terms and responses) for the residual and additional trial misalignments are represented by $\left(\mathbf{A}^{m1}(\omega),\ \mathbf{A}^{m2}(\omega)\right)$ and $\left(\mathbf{b}^{m1}(\omega),\ \mathbf{b}^{m2}(\omega)\right)$, respectively. The vectors carrying the unknown identifiable parameters for residual and additional trial misalignments are, respectively, shown by $\mathbf{x}^{m1}$ and $\mathbf{x}^{m2}$. It can be noticed from regression equations (i.e., Equations (2.30) and (2.31)) that the number of equations (i.e., four) are less than the number of unknowns (i.e., five), so it is a class of underdetermined system of equations. This is the ill-conditioning of regression equations for both misalignment cases. Moreover, the determination

of all the unknowns is only possible when the number of equations equal to or more than the number of unknowns.

It is also observable that the real and imaginary values of disc eccentricity (e_{Re}, e_{Im}) are available in both the unknown vectors $\mathbf{x}^{m1}$ and $\mathbf{x}^{m2}$. Therefore, for obtaining the unique values of these unbalance parameters, Equations (2.30) and (2.31) can be combined together. The combined form of identification equation can be expressed as

$$\mathbf{A}(\omega)\mathbf{x} = \mathbf{b}(\omega) \tag{2.32}$$

$$\mathbf{A}(\omega) = \begin{bmatrix} 0 & 0 & -2R_{0,\mathrm{Re}}^{m1} & -2I_{0,\mathrm{Re}}^{m1} & -2 & 0 & 0 & 0 \\ 0 & 0 & -2R_{0,\mathrm{Im}}^{m1} & -2I_{0,\mathrm{Im}}^{m1} & -2 & 0 & 0 & 0 \\ -m_d\omega^2 & 0 & -2R_{1,\mathrm{Re}}^{m1} & -2I_{1,\mathrm{Re}}^{m1} & 0 & 0 & 0 & 0 \\ 0 & -m_d\omega^2 & -2R_{1,\mathrm{Im}}^{m1} & -2I_{1,\mathrm{Re}}^{m1} & 0 & 0 & 0 & 0 \\ 0 & 0 & 0 & 0 & 0 & -2R_{0,\mathrm{Re}}^{m2} & -2I_{0,\mathrm{Re}}^{m2} & -2 \\ 0 & 0 & 0 & 0 & 0 & -2R_{0,\mathrm{Im}}^{m2} & -2I_{0,\mathrm{Im}}^{m2} & -2 \\ -m_d\omega^2 & 0 & 0 & 0 & 0 & -2R_{1,\mathrm{Re}}^{m2} & -2I_{1,\mathrm{Re}}^{m2} & 0 \\ 0 & -m_d\omega^2 & 0 & 0 & 0 & -2R_{1,\mathrm{Im}}^{m2} & -2I_{1,\mathrm{Im}}^{m2} & 0 \end{bmatrix}; \quad \mathbf{x} = \begin{Bmatrix} e_{\mathrm{Re}} \\ e_{\mathrm{Im}} \\ k_s^{m1} \\ k_i^{m1} \\ f_c^{m1} \\ k_s^{m2} \\ k_i^{m2} \\ f_c^{m2} \end{Bmatrix};$$

$$\mathbf{b}(\omega) = \begin{Bmatrix} 0 & 0 & m\omega^2 R_{1,\mathrm{Re}}^{m1} & m\omega^2 R_{1,\mathrm{Im}}^{m1} & 0 & 0 & m\omega^2 R_{1,\mathrm{Re}}^{m2} & m\omega^2 R_{1,\mathrm{Im}}^{m2} \end{Bmatrix}^T$$

Equation (2.32) will give the unique values of disc unbalance eccentricity (e_{Re}, e_{Im}) along with misaligned AMB parameters (i.e., k_s^{m1}, k_i^{m1}, f_c^{m1}, k_s^{m2}, k_i^{m2} and f_c^{m2}). This equation has also overcome the ill-condition of the regression matrices and increases the number of equations to eight. The size of regression matrix **A** is (8×8) and the size of unknown vector **x** and known vector **b** are also (8×1). So, it becomes possible to solve Equation (2.32) to estimate eight number unknowns.

Further, the displacement and current responses for (i = 0, 1), for the range of multiple number of rotor spin speeds are also taken to check the performance of estimation procedure with the

help of developed identification algorithm. This range of spin speeds may accommodate more information from the rotor system. The regression equation (i.e., Equation (2.32)) for '*n*' number of range of different spin speeds can be expressed as

$$\begin{pmatrix} \mathbf{A}_{(\omega_1)} \\ \mathbf{A}_{(\omega_2)} \\ \vdots \\ \mathbf{A}_{(\omega_n)} \end{pmatrix} \mathbf{x} = \begin{pmatrix} \mathbf{B}_{(\omega_1)} \\ \mathbf{B}_{(\omega_2)} \\ \vdots \\ \mathbf{B}_{(\omega_n)} \end{pmatrix} \tag{2.33}$$

Equation (2.33) is an overdetermined system of linear equations. It is due to increase in the number of rows in the regression matrix A and the known vector B from the responses collected at different and combined spin speeds. Therefore, the Moore-Penrose inverse has been utilized to solve Equation (2.33), as

$$\mathbf{x} = \left(\mathbf{A}^T\mathbf{A}\right)^{-1}\mathbf{A}^T\mathbf{b} \tag{2.34}$$

In addition to that, the identified values of misaligned AMB stiffness parameters will be certainly helpful in estimating the radial offset '*a*' between the rotor and AMB axes using Equations (2.13) and (2.16). For example, the ratio of k_s^{m1} and k_s^{m2} can be written as

$$\frac{k_s^{m1}}{k_s^{m2}} = \frac{\left(1-b_1^2\right)^2}{\left(1-a_1^2\right)^2} = \frac{\left\{1-\left(a_1+\Delta_1\right)^2\right\}^2}{\left(1-a_1^2\right)^2} \;;\; a_1 = \frac{a}{s_0};\; \Delta_1 = \frac{\Delta}{s_0} \tag{2.35}$$

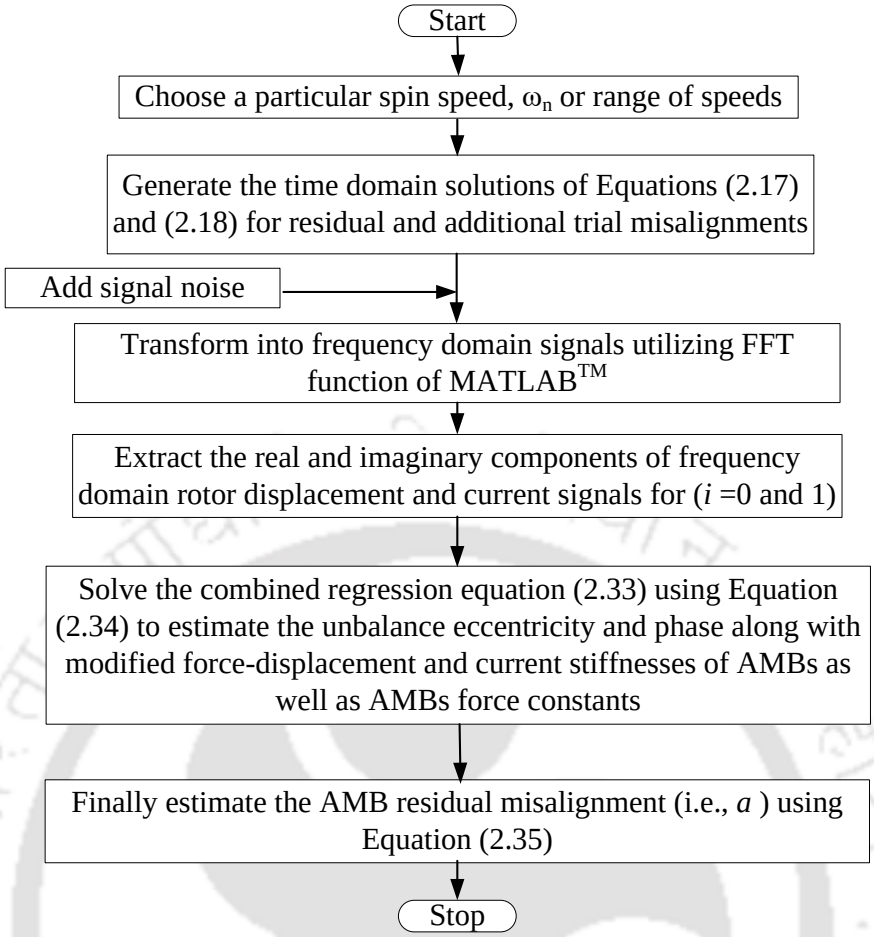

Figure 2.4 Flow chart for a novel identification algorithm.

Equation (2.35) is able to estimate the amount of radial offset 'a' following Fig 2.1, with the known values of k_s^{m1}, k_s^{m2} and the manually added (physical trial) misalignment 'Δ'. Similarly, the ratios of k_i^{m1} and k_i^{m2} as well as f_c^{m1} and f_c^{m2} also give the same value of amount of misalignment 'a'. Figure 2.4 presents the flow chart of mathematically model based identification algorithm for the simultaneous estimation of unbalance and AMB misalignment faults in a rotor-AMB system to ensure their safe, smooth and sustained operation and functioning. In the next section, the numerical simulation and identification have been performed on the considered rigid rotor-AMBs system to test the developed estimation methodology derived from PTM approach.

2.5 Numerical Response Generation and Identification

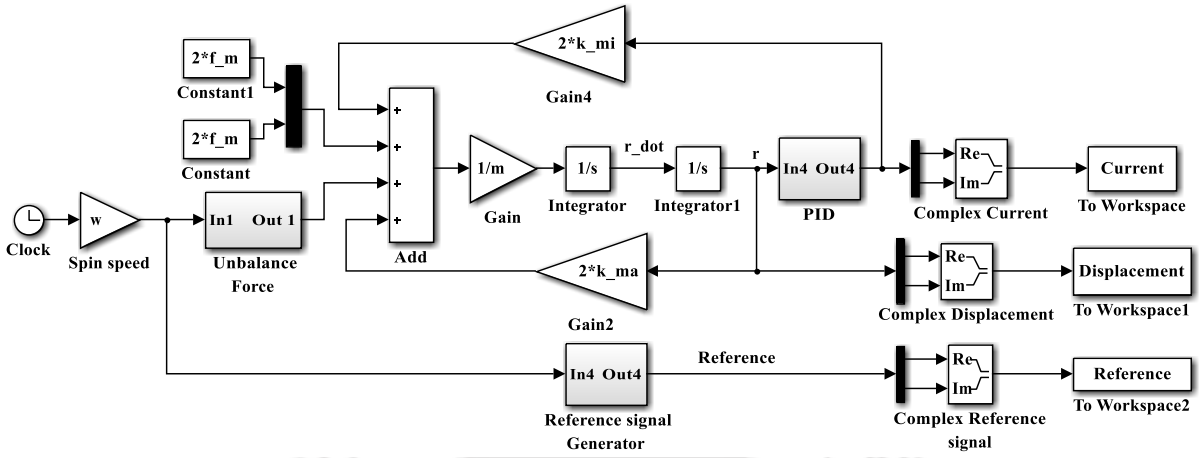

Figure 2.5 SIMULINK model of the rigid rotor-misaligned AMB system.

Equations of motion, i.e. Equations (2.17) and (2.18), of the rigid rotor-misaligned AMB system for residual and additional trial misalignments have been solved by building a SIMULINK^{TM} model as shown in Figure 2.5. Multiple blocks in this model carried out various functions to generate the rotor displacement and controlling current responses at both AMB locations in the *x*- and *y*-directions, in time domain.

The simulation time required for generating these responses is executed by the *clock*. The *gain* block in triangular shape is useful for the purpose of multiplication of a number and parameter. The spin speed of the rotor is considered in gain block, multiplied with the clock gives the output, i.e. ωt, which is further input to the unbalance force. Summation of various forces due to unbalance force, and force due to misaligned AMBs-are performed by the *add* block. The acceleration response of the rigid rotor system is acquired by multiplying the mass inverse to the add block. Further, the velocity and the displacement responses are achieved with the help of *integrator* blocks. First integrator block gives the velocity as output and the second delivers the displacement response. One of the most important block is the *PID*, which contains the proportional, derivative and integrative gain factors together with *integrator and derivative* blocks to give the controlling current as an output utilising the displacement response

as an input. To obtain the correct phase in FFT processed responses, a *reference signal* is included in the model. The complex data of responses are preserved by the *workspace* block. The model can also generate the response of the rotor system in the individual or simultaneous presence of unbalance force, AMB force without or with misalignment.

Table 2.1 Rigid rotor-misaligned AMB system data for the numerical simulation.

Rotor and Controller parameters	**Assumed Values**	**AMB parameters**	**Assumed Values**
Mass density of shaft and disc material, ρ	7850 kg/m^3	Number of poles	8
Shaft diameter, d	15.6 mm	Number of turning coils, N	100
shaft length, l	600 mm	Angle between two adjacent poles, α	45 deg.
Disc diameter, D	150 mm	Area of a pole-shoe, A_a	2.4 cm^2
Disc thickness, t	15.2 mm	Bias current, i_0	2 A
Rotor mass (m)	3 kg	Misaligned AMB force displacement constant1 (k_s^{m1})	237,550 N/m
Disc mass (m_d)	2.1 kg	Misaligned AMB force current constant1 (k_i^{m1})	54.19 N/A
Disc eccentricity (e)	100 μm	Misaligned constant force1 (f_c^{m1})	35.63 N
Unbalance phase (β)	30 deg.	Misaligned AMB force displacement constant2 (k_s^{m2})	472,450 N/m
Proportional gain of PID controller (k_P)	6000 A/m	Misaligned AMB force current constant2 (k_i^{m2})	131.40 N/A
Derivative gain of PID controller (k_D)	3 A-s/m	Misaligned constant force2 (f_c^{m2})	118.11 N
Integral gain of PID controller (k_I)	5000 A/m-s	Amount of radial offset of AMBs (a)	0.15 mm
Air gap between rotor and AMB (s_0)	0.40 mm	Amount of manually given offset in AMBs (Δ)	0.10 mm

Table 2.1 summarizes the numerical data utilised for the simulation purpose to generate responses of the system at both AMB locations. The assumed values of unbalance eccentricity in the range of 10^{-4} m has been taken from Singh and Tiwari (2015). Similarly, the values of

initial radial offset (a) and manually added misalignment (Δ) between the rotor and AMB axes are assumed depending upon the condition that these values are less than AMB air gap, s_0. This condition is essentially required to have stable levitation of the rotor in air. The values of proportional, integral and derivative factors of PID controller (k_P, k_I and k_D) in Table 2.1 have been chosen based on tuning from Routh-Hurwitz criterion (refer Appendix D), to have stable rotor displacement and controlling current responses of the considered unbalanced and misaligned rotor-AMB system.

The dynamic influence of misalignment at AMBs on the rotor performance has been studied using numerical simulation. It can be noticed from Figures 2.6(a) and 2.6(b) that the misalignment fault causes to enhance the orbital plot of displacement responses of the rotor system at AMB locations. The size of the displacement orbit also increases as the misalignment level at both AMB locations increases. The values of lower and higher levels of AMB misalignment are 0.15 mm and 0.25 mm. The magnitude of the displacement response in the x and y directions at an angular frequency of 25 Hz (i.e., the spin speed of 157.08 rad/s) is only 3.35×10^{-5} m in an unbalanced rotor system levitated by active magnetic bearings when the axes of the rigid rotor and AMBs are perfectly aligned. But the magnitude is increased to 4.65×10^{-5} m and 7.31×10^{-5} m for the lower and higher misalignment values, respectively. These increments in response due to lower and higher levels of misalignment are about 38.80% and 118.20% respectively, with respect to the perfectly aligned case. Thus, it is tremendously needed to identify quantitatively the misalignment fault together with unbalance in a rotor system.

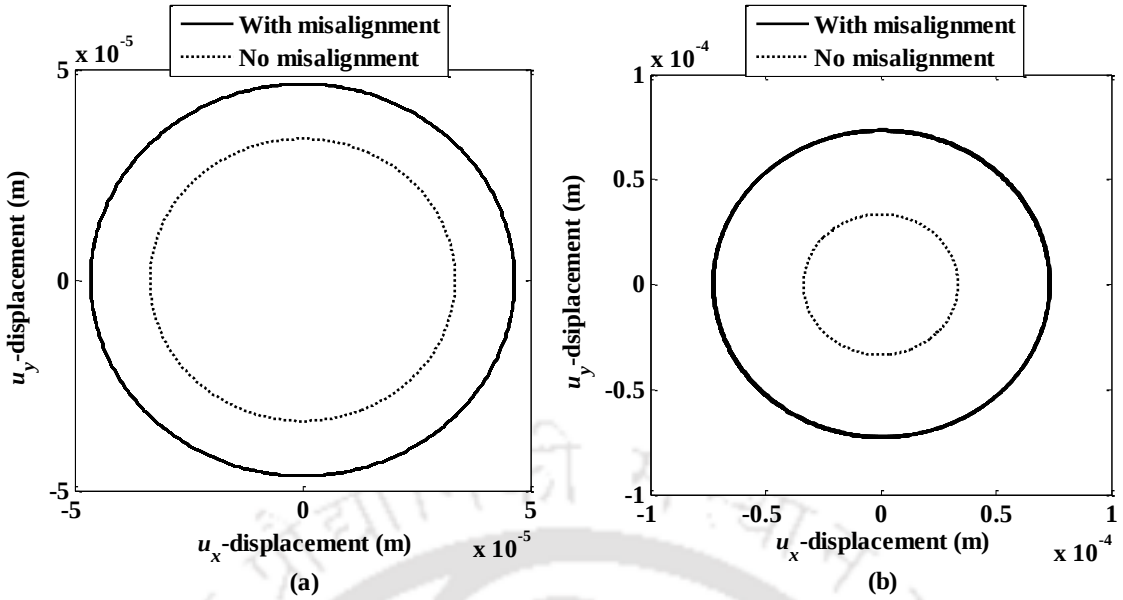

Figure 2.6 Orbit plot for rotor displacement response to show the effect of AMB misalignment (a) lower level of misalignment (b) higher level of misalignment at 25 Hz angular frequency.

In accordance with Equation (2.17) for residual misalignment, the rotor displacement and current responses of the system in *x*- and *y*-directions at an angular frequency of 25 Hz are depicted in Figure 2.7. This speed is arbitrarily chosen below the critical speed (38.4 Hz) of the rigid rotor-AMB system. This is essentially required for exhibiting rigid rotor behaviour during operation. Observation can be made from Figure 2.7 that the displacement responses (u_x^{m1} and u_y^{m1}) as well as controlling current responses (i_x^{m1} and i_y^{m1}) are symmetrical in *x*- and *y*-directions. This symmetry in responses arises due to consideration of certain assumptions such as symmetrical radial offset along the rotor length and identical as well as isotropic nature of both AMBs (as discussed in Section 2.2) while developing the mathematical model of the considered rotor-AMB system.

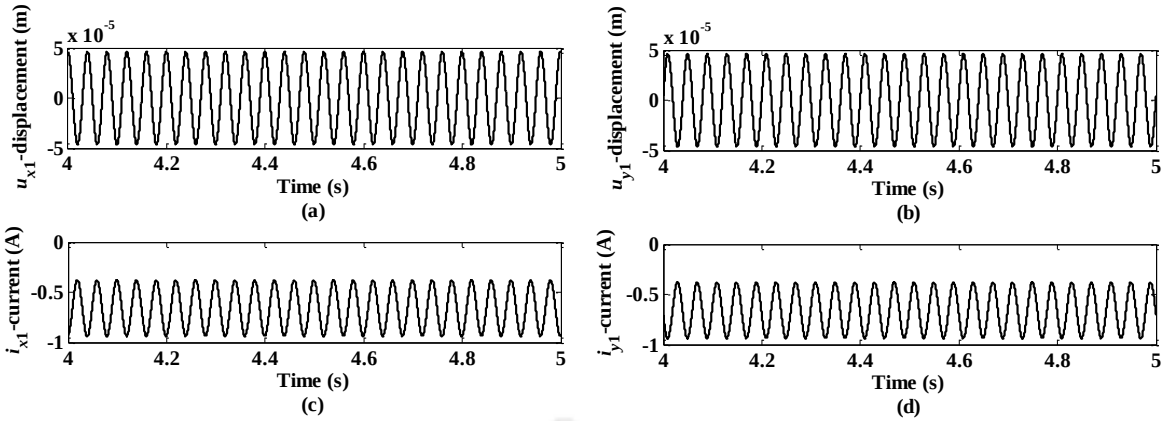

Figure 2.7 Rigid rotor system responses: (a) displacement in *x* direction (b) displacement in *y* direction (c) current in *x* direction (d) current in *y* direction (e) Rotor displacement orbit (f) AMB current orbit at 25 Hz angular frequency.

2.5.1 Quantitative Estimation of Unbalance and AMB Misalignment Parameters

The simulation for the rigid rotor-misaligned AMB system was executed for 5 s utilizing Table 2.1 assumed parameters. For further exploring the dynamic vibrational analysis, the responses associated with the time domain displacement and current generated in the system for the time duration from 4 to 5 s (i.e. 1 s time length) was considered. The fast Fourier Transform analysis (Tiwari, 2017) has been done to achieve frequency domain responses related to the solution of Equations (2.17) and (2.18) for both residual and additional trial misalignments. FFT plots of the rotor displacement and controlling current signals at AMB locations with their amplitude and phase at an angular frequency of 25 Hz for residual misalignment are presented in Figure 2.8.

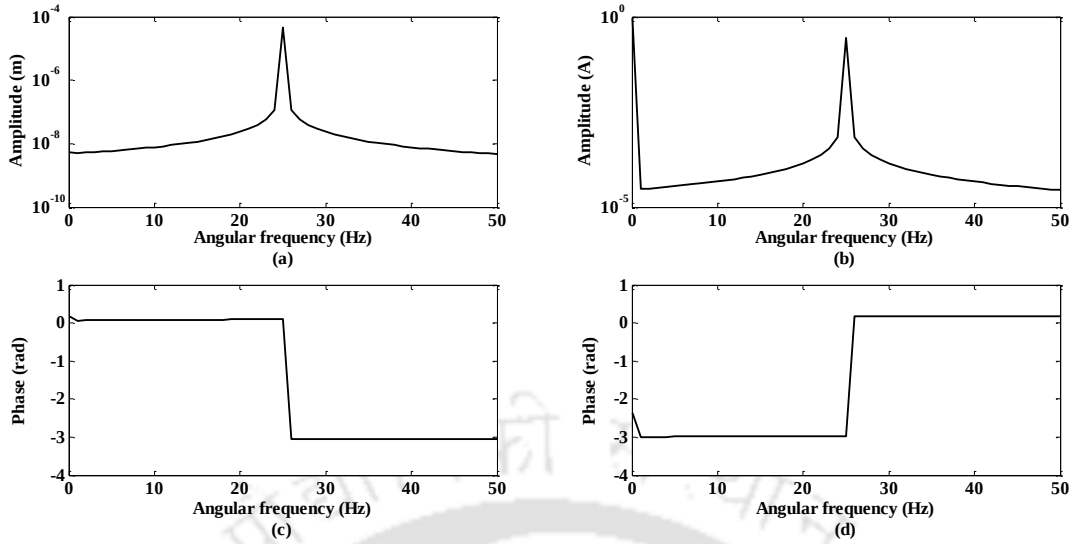

Figure 2.8 FFT analysed responses for residual misalignment: (a) Rotor displacement amplitude (b) Controlling current amplitude (c) Rotor displacement phase with compensation (d) Controlling current phase with compensation at 25 Hz angular frequency.

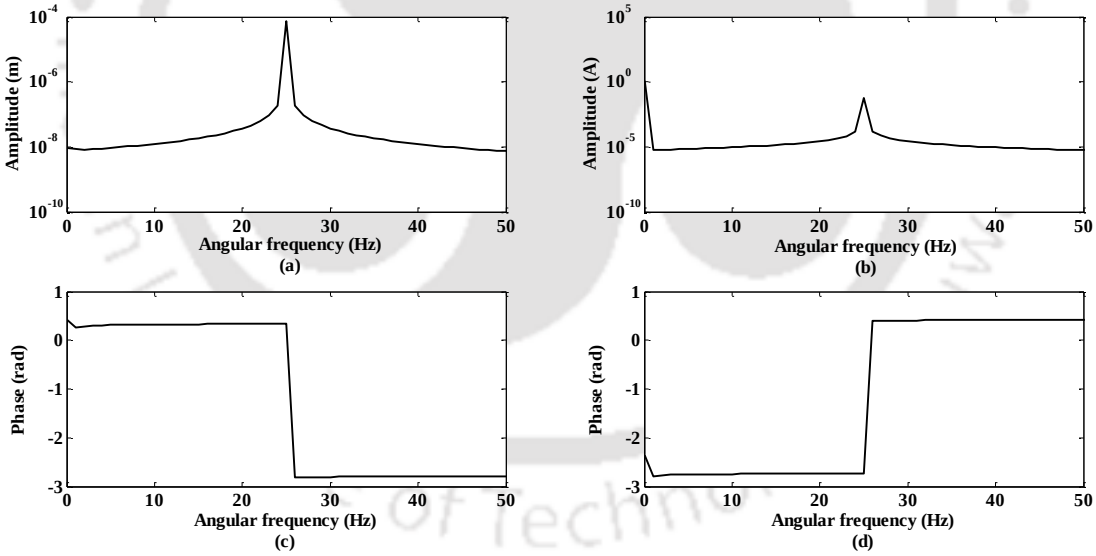

Figure 2.9 FFT processed responses for additional trial misalignment: (a) Rotor displacement amplitude (b) Controlling current amplitude (c) Rotor displacement phase with compensation (d) Controlling current phase with compensation at 25 Hz angular frequency.

Similarly, FFT processed frequency domain responses for additional trial misalignment are shown in Figure 2.9. The phase diagrams for both response signals have been plotted in

accordance with phase correction method (follow Appendix C) utilizing reference signal in Figure 2.5. The amplitude and phase of FFT processed frequency domain displacement and current of the system for (i = 0 and 1) assisted with both cases of misalignment are depicted in Table 2.2. It is noticeable from Table 2.2 that the peak values of the rotor displacement and current responses for the residual misalignment are found to be 4.65×10^{-5} m and 0.93 A, respectively, at an angular frequency of 25 Hz. Similarly, the peak values of responses at both AMB locations for the additional trial misalignment are 7.31×10^{-5} m and 1.27 A.

Table 2.2 Rotor displacement and controlling current responses at both AMB locations obtained in the frequency domain at 25 Hz angular frequency.

Misalignment		Displacement (R_i)		Current (I_i)	
	(i)	Amplitude (m)	Phase (deg.)	Amplitude (A)	Phase (deg.)
Residual misalignment	0	5.21×10^{-9}	9.81	9.30×10^{-1}	-134.99
	1	4.65×10^{-5}	5.25	2.80×10^{-1}	-171.72
Additional trial misalignment	0	9.09×10^{-9}	24.20	12.71×10^{-1}	-134.99
	1	7.31×10^{-5}	19.26	5.50×10^{-1}	156.76

It can also be depicted from Table 2.2 that the displacement level for the additional trial misalignment is higher than residual misalignment for (i = 0 and 1). Similarly, the more controlling current is required for the second case as compared to the first case of AMB misalignment for both (i = 0) and (i = 1). The real and imaginary components of complex displacement and controlling current responses in frequency domain for (i = 0 and 1), for both cases of rotor-AMB misalignment can be adopted from the magnitudes and phases presented in Table 2.2. Based on assumptions that the misalignment amounts (a and Δ) as well as AMB parameters (k_s and k_i) are same for both AMBs, the values of displacement and current

harmonics will also be same at both AMB locations, as displayed in Table 2.2. Further, the real and imaginary components of displacement and current responses for (i = 0 and 1) captured from FFT analysed signals have been given as input in the developed identification equation (2.32) for the estimation purpose. The parameters to be estimated from novel trial misalignment based identification scheme are e_{Re}, e_{Im}, k_s^{m1}, k_i^{m1}, f_c^{m1}, k_s^{m2}, k_i^{m2} and f_c^{m2}.

Usually, an actual measurement of response taken in a real rotor system is always associated with various noise signals derived from the nearby environment or from the undesired vibrations from the system itself. There are number of type of noise used in the signal processing such as random Gaussian noise, Poisson noise, and multiplicative noise, shot noise, phase noise, etc. Out of these noise, Gaussian noise is the most common and usually used in the signal processing. Gaussian noise is a statistical noise having a probability density function equal to that of the normal distribution or Gaussian distribution. The probability density function contains the mean, standard deviation and variance of the real-valued random variables which follows normal distribution. This noise is created by activities in the environment, people working nearby area, operation of other machines, instrumentation and data acquisition errors. Hence, to simulate the actual measurement conditions and account for the effect of possible presence of instrumentation and data acquisition errors in the system responses, random Gaussian noise of 1%, 2% and 5% (mean at zero, with ± 0.5%, ± 1% and ± 2.5% on either side) are added to the rotor displacement and current signals generated from the numerical simulation. Further, the estimation of several system and fault parameters assisted with noise added signals has been done for both the cases of misalignment. The randn function of MATLAB is used to add random Gaussian noise to the rotor response and AMB current signal. The mathematical model used for development of the random Gaussian noise added signal is explained in Appendix E. Although the added percentage (1%, 2% and 5%) of noise

in signal is much less demanding than the broadband noise signal. However, it is not realistic, but this has been done to illustrate the important features of the identification methodology.

Moreover, as compared to a real system, the present model may also suffer from modelling or bias errors owing to multiple operational constraints and measurement of model parameters of the system. Due to certain simplifying assumptions used in development of the mathematical model of the rotor-AMB system like rigid shaft with a disc at the middle position and its motion in translational directions only, the rotor mass is observed to be more uncertain than the uncertainties due to other model parameters such as disc moment of inertia, shaft stiffness, Young's modulus, intact shaft deflection, etc. Hence, only variation in mass (i.e., density of the shaft and disc material) is considered for the modelling error. The effectiveness of the developed methodology is also checked against modelling error (up to 5% variation in rotor mass). So, the modelling (or bias) errors of 1%, 2% and 5% are added to the rotor mass parameter, and then the responses are generated using these parameters. The modified responses have been utilized for the estimation purpose.

Tables 2.3 outlines the assumed values and sensitivity of estimated disc unbalance parameters (eccentricity, *e* and phase, β), misaligned AMBs parameters (k_s^{m1}, k_i^{m1}, f_c^{m1}, k_s^{m2}, k_i^{m2} and f_c^{m2}) and AMBs residual misalignment (*a*) for clean signal along with the addition of various levels of noise and modelling errors. The identified values shown in Table 2.3 are in the percentage form calculated with respect to assumed values for the speed range of 18 Hz to 25 Hz in the step of 1 Hz angular frequency. The identified values are obtained using the identification equation (i.e., Equation (2.33)) solved by the Moore-Penrose inverse (i.e., Equation (2.34)). The value of residual misalignment (*a*) in Table 2.3 is identified using the estimated misaligned AMBs stiffness parameters and Equation (2.35). It can be observed from Table 2.3 that among all the estimated parameters, the least affected parameter is phase (β) of

the disc unbalance. Even under the influence of highest percentage deviation i.e., 5% noise and modelling errors, the maximum percentage error for phase lies within the range of -0.01% to -0.58%. Parameters associated with misaligned AMBs for the first misalignment case, such as the stiffness constants of AMBs and the constant force term (k_s^{m1} , k_i^{m1} and f_c^{m1}) are found to be very sensitive with error percentage of -11.11%, -10.19% and -9.90%, respectively, at 5% signal noise addition. Similarly, the system parameters associated with misaligned AMBs (i.e., k_s^{m2} , k_i^{m2} and f_c^{m2}) for the second misalignment condition are affected with -11.84%, -10.93% and -10.65% errors at 5% noise addition. Although these misaligned AMBs parameters are affected severely for the noisy responses. But, the identified value of residual misalignment calculated from them (follow Equation (2.35)) is also one of the good estimates. The maximum percentage error for AMBs radial offset '*a*' is only -0.94% at the highest level of noise addition.

Table 2.3 Sensitivity of estimated unbalance and AMB misalignment parameters with addition of noise and modelling errors for the speed range of 18 Hz to 25 Hz.

Parameters	Assumed values	Error percentage in identified values with addition of noise and modelling or bias errors						
		Clean signal	1% noise	2% noise	5% noise	1% bias	2% bias	5% bias
e (μm)	100	-0.19%	-3.57%	-6.72%	-9.65%	-0.19%	-0.19%	-0.19%
β (deg)	30	-0.01%	-0.20%	-0.39%	-0.58%	-0.01%	-0.01%	-0.01%
k_s^{m1} (N/m)	237,550	-0.21%	-4.11%	-7.73%	-11.11%	-0.21%	-0.21%	-0.21%
k_i^{m1} (N/A)	54.19	-0.20%	-3.77%	-7.10%	-10.19%	-0.20%	-0.20%	-0.20%
f_c^{m1} (N)	35.63	-0.20%	-3.67%	-6.90%	-9.90%	-0.20%	-0.20%	-0.20%
k_s^{m2} (N/m)	472,450	-0.22%	-4.39%	-8.25%	-11.84%	-0.22%	-0.22%	-0.22%
k_i^{m2} (N/A)	131.40	-0.22%	-4.06%	-7.62%	-10.93%	-0.22%	-0.22%	-0.22%
f_c^{m2} (N)	118.11	-0.22%	-3.95%	-7.42%	-10.65%	-0.22%	-0.22%	-0.22%
a (mm)	0.15	-0.02%	-0.33%	-0.63%	-0.94%	-0.02%	-0.02%	-0.02%

The identification algorithm for the purpose of parameters estimation is also found to be exhibiting outstanding results when the rotor parameter is added with modelling errors of 1%, 2% and 5% serially. It can be observed from Table 2.3 that the modelling errors do not severely affect the estimated parameters. Absolute estimation error percentage associated with the unbalance phase is found to be very less, i.e. 0.01%. Maximum errors for the unbalance eccentricity is only -0.19%. Similarly, the variations in the errors for the force-displacement, force-current parameters and constant force terms for both cases of misalignment are in the range of -0.20% to -0.22%. The residual misalignment of AMBs is also identified with maximum percentage error of -0.02%.

Moreover, the percentage errors in the parameters estimation are found to be more with the addition of increasing levels of random Gaussian noise as compared to the estimated parameters from clean signal. Since only mass parameter is considered to be erroneous in the modelling error, so the deviation of estimated parameters from the assumed parameters is less at every levels (i.e., 1%, 2% and 5%) of bias errors irrespective of large deviation with addition of each level of noise error. Overall, the error percentage corresponding to the estimated rotor system parameters with addition of noise signal and modelling errors are within acceptable range.

The numerically simulated results such as rotor dynamic analysis and the effectiveness as well as robustness of the developed identification algorithm proves the stability and accuracy of the proposed methodology in the present work. It is well known that for higher level of misalignment, more deviation should take place. This point can be validated from Figure 2.6 and Table 2.2, in which it is clearly shown that how the AMB misalignment affect the displacement response and enhance its magnitude and increase the displacement orbit size. With slight increase in radial offset between the axes of rotor and AMBs, the amplitude of vibration response also increases. The displacement and AMB controlling current levels for

additional trial misalignment is higher than residual misalignment both for (i = 0) and (i = 1). Similarly, Tables 2.3 reveals that the assumed system and fault parameters in Table 2.1 has been excellently estimated in the clean vibration and current signals and even with addition up to 5% level of random Gaussian noise and modelling errors in the combined speed case. These results show the robustness and effectiveness of the developed methodology for the considered two degrees-of-freedom rotor-AMB system. It is also to be noted that in the present rotor system, the excitation frequency is taken low for the result analysis so the resistance generated by the electrical circuit will be less. Moreover, with current-mode control present in the amplifier, the amplitude and phase change generated due to electrical load is compensated. Therefore, the frequency dependency of the electrical circuit is neglected while consideration of response data at several frequencies in the identification process.

2.6 Summary

In this chapter, an unbalanced 2 DOF rigid rotor misaligned with two active magnetic bearings is mathematically modelled and the dynamic vibrational analysis of the misaligned rotor system is studied considering two cases of AMB misalignments (residual and additional trial misalignments). The rotor is assumed to be in parallel misalignment with AMBs. The misalignment cases are based on the amount of radial offset between the rotor and active magnetic bearing axes. The linearized form of misaligned AMB force has been innovatively derived for both misalignment conditions.

A *novel trial misalignment approach* in line with trial unbalance in rotor balancing technique has been utilized to identify the misalignment amount between rotor and supported AMBs. The physical trial misalignment (PTM) concept to provide additional known misalignment through actuator housings in the vertical and horizontal directions is also described. The equations of motion are derived and numerically simulated to generate the time

domain rotor displacement and controlling current responses of the system at AMB locations for both cases of misalignments.

The dynamic influence of the AMB misalignment on the rotor performance is also investigated. More deviations were observed in the rotor displacement signal for the higher level of AMB misalignment. The FFT technique is applied to obtain frequency domain responses, which have been further utilized in the developed identification algorithm to estimate unbalance and misalignment parameters of the rotor-misaligned AMB system. The algorithm is found to be quite robust and effective against the various levels of measurement signal noise and modelling errors in the range of multiple rotor spin speeds.

The present chapter provides a framework for the development of misaligned AMB force and identification equation (derived from novel trial misalignment approach) for the estimation of system and fault parameters in a rotor system levitated by AMBs. However, the proposed technique can be applied to a more realistic model, where the disc present at centre position can be replaced with offset discs. The tilting motion of discs available at offset positions in the shaft will give rise to gyroscopic effects in addition to other effects considered in this chapter. Thus, there is a need for analysing more complex 4-DOF model. Moreover, in practical aspects, it is also not necessary that both AMBs would be identical in nature and offset by same amounts in the vertical and horizontal directions.

To overcome these shortcomings in the present chapter, the modelling, analysis and identification in a rigid rotor with two offset discs supported by two (isotropic and different in nature) misaligned AMBs has been presented in the next chapter. The misalignment between rotor and AMBs are considered to be combination of parallel and angular misalignments.

Chapter 3

Modelling and Identification in a Misaligned Rigid Rotor-AMB system with Gyroscopic Effects

3.1 Introduction

The mathematical model and equations of motion of a simple rigid rotor with a disc middle and supported on two misaligned active magnetic bearings were presented in the previous chapter. The time domain and frequency domain responses were obtained and utilized in the identification of disc unbalance and AMB misalignment parameters from an identification algorithm based on novel trial misalignment approach. However, this chapter explores the possibility of applications of novel identification methodology proposed in Chapter 2, to a magnetically levitated rigid rotor system with two offset discs. This configuration of rotor system increases the complexity in the analysis with consideration of gyroscopic effects due to tilting of the discs. Moreover, this rotor model will be four degrees-of-freedom (DOFs) instead of 2 DOFs in the previous chapter. Both AMBs will have different force-displacement and force-current stiffness parameters. The misalignment between rotor and AMBs will be combination of parallel and angular misalignments (due to different amount of offsets in the vertical and horizontal directions between rotor and AMBs).

In the present chapter, a dynamic model of a four-degree-of-freedom unbalanced and misaligned rigid rotor with two offset discs levitated by two active magnetic bearings has been mathematically developed. The offset discs result in the gyroscopic effect at high rotor speeds. Equations of motion of the system have been derived using moment equilibrium method. A novel trial misalignment concept has been proposed for developing an identification algorithm (the procedures will be followed from Chapter 2) based on utilizing the frequency domain displacement and AMBs current responses at both AMB locations. This would estimate the

both discs unbalance parameters, misaligned AMBs parameters for residual and additional trial misalignments and finally, the misalignment amounts between rotor and both AMBs. Testing of the algorithm has also been done at multiple discrete spin speeds against measurement signal noise in rotor responses and bias errors in rotor system parameters to check its effectiveness and robustness.

3.2 System Configuration and Mathematical Modelling of Rotor-AMB System

A rigid rotor system has been considered to develop a mathematical model for execution of the identification technique, for the simultaneous estimation of unbalance and misalignment fault parameters in a rotating machinery integrated with AMBs. Figure 3.1 depicts a rotor system consisting of an unbalanced and misaligned rigid rotor with two offset rigid discs, supported by two active magnetic bearings (AMBs) in the *x*-*z* plane, where *z* is the rotor spinning axis, B1B1 and B2B2 are axes of AMB1 and AMB2, respectively.

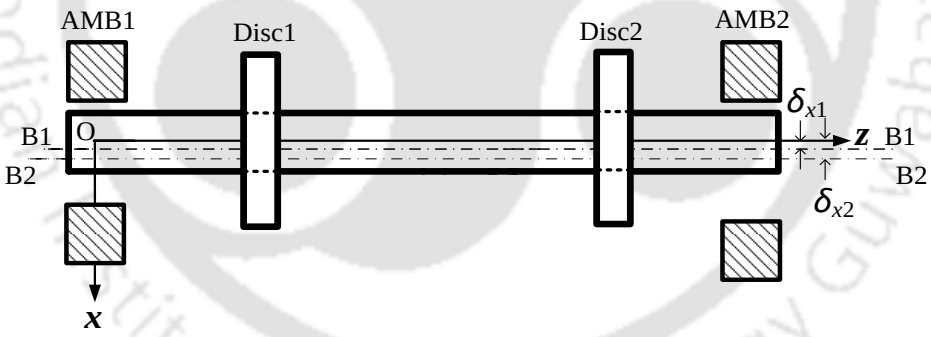

Figure 3.1 A rigid rotor system with two offset discs levitated by two active magnetic bearings when the rotor is in the *x*-*z* plane.

The residual misalignments between rotor and AMB1 as well as AMB2 axes in the *x*-direction are represented by δ_{x1} and δ_{x2}. Similarly, δ_{y1} and δ_{y2} are the residual misalignments between rotor and AMB1 as well as AMB2 axes in the *y*-direction. Both AMBs are misaligned with the rotor rotating axis (O*z*) differently in the *x*- and *y*-directions, thus this misalignment is

the combination of parallel and angular misalignments. The gyroscopic couple effect due to the offset discs at high spin speeds is also considered in the analysis. Rigid discs in the system model are equivalent to rotating mechanical components such as the rotary vane of air compressors, clutch discs, impellers of the gas turbine as well as centrifugal pumps and flywheels, etc. Both AMBs are assumed to be isotropic in nature, but having different values of force-displacement and force-current stiffness coefficients.

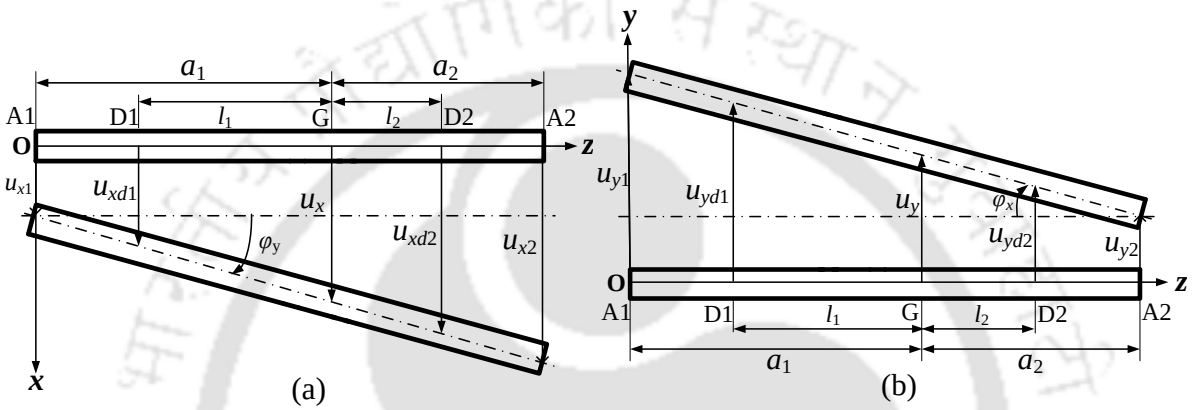

Figure 3.2 Translational and rotational displacements of the rigid rotor at different positions in (a) *x-z* plane (b) *y-z* plane.

Figure 3.2 shows the displacement of the rigid rotor in the *x-z* and *y-z* planes, which have been considered for deriving equations of motion of the misaligned rotor-AMB system. Here, A1 and A2 are active magnetic bearing locations, G is the rotor center of gravity, and D1 and D2 are the disc locations, a_1 and a_2 are the distances of AMB1 and AMB2 from the center of gravity of the rigid rotor, and l_1 and l_2 are the distance of the disc1 and disc2 from the center of gravity of the rigid rotor, respectively. Vibration induced displacements of the rigid rotor at the center of gravity in terms of displacement at the active magnetic bearing locations can be written, using Figures 3.2(a) and 3.2(b), as

$$u_x = \bar{a}_2 u_{x1} + \bar{a}_1 u_{x2};\quad u_y = \bar{a}_2 u_{y1} + \bar{a}_1 u_{y2};\quad \varphi_y = \left(-u_{x1} + u_{x2}\right)/l;\quad \varphi_x = \left(u_{y1} - u_{y2}\right)/l \qquad (3.1)$$

with $$\bar{a}_1 = \frac{a_1}{l}; \quad \bar{a}_2 = \frac{a_2}{l}$$

where u_x and u_y are the translational displacement at the rotor center of gravity position in the x and y directions. φ_x and φ_y are the rotational displacements of the rigid rotor in the y-z and x-z planes. The vibrational induced displacements at AMB1 and AMB2 locations in the x and y directions are represented by $\{u_{x1}(t), u_{y1}(t)\}$ and $\{u_{x2}(t), u_{y2}(t)\}$.

3.2.1 Unbalance Force Model

The unbalance force due to disc1 and disc2 on the rotor, in the x and y directions, can be written as

$$\begin{cases} f_{unbx1} = m_{d1} e_1 \omega^2 \cos(\omega t + \beta_1); \; f_{unby1} = m_{d1} e_1 \omega^2 \sin(\omega t + \beta_1) \\ f_{unbx2} = m_{d2} e_2 \omega^2 \cos(\omega t + \beta_2); \; f_{unby2} = m_{d2} e_2 \omega^2 \sin(\omega t + \beta_2) \end{cases} \tag{3.2}$$

where m_{d1} and m_{d2} are the mass of disc1 and disc2, e_1 and e_2 denote the eccentricity of the disc1 and disc2 as well as β_1 and β_2 are their phase, respectively. The spin speed of the rotor is shown by, ω. This equation is consistent with Equation (2.1).

3.2.2 Modelling of AMB Force for Residual and Additional Trial Misalignments

The force modelling for perfectly aligned AMB with the rotor is already discussed in Section 2.3.2. The same section also presented the innovative derivation for the linearized form of AMB force for the case of residual misalignment and additional trial misalignment. In the Chapter 2, the force-displacement (k_s) and force-current (k_i) stiffness of both AMBs were assumed to be same as well as the parallel misalignment between rotor and AMBs was considered. However, this is not always the case in a real rotor-AMB system, the stiffness constants (force-displacement and force-current) may be different for both AMBs and there

can be a combination of parallel and angular misalignments. In these conditions, the expression for AMBs force for perfect alignment state and for the residual and additional trial misalignment cases will be modified.

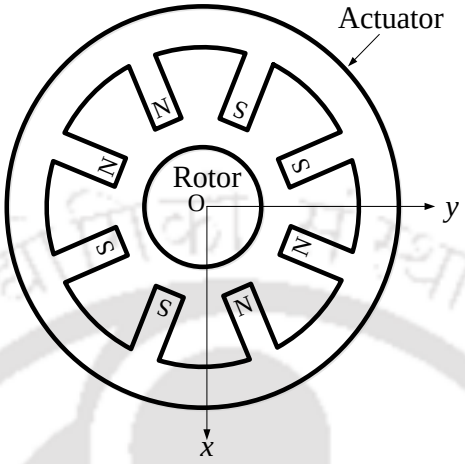

Figure 3.3 Side view of a hetero-polar eight pole actuator in *x-y* plane when the rotor is perfectly aligned with both actuators.

In the perfect alignment state as shown in Figure 3.3, the force due to AMB1 on the rigid rotor in the *x* and *y* directions can be written as

$$f_{x1} = k_{s1}u_{x1} + k_{i1}i_{x1}; \qquad f_{y1} = k_{s1}u_{y1} + k_{i1}i_{y1} \tag{3.3}$$

with

$$k_{s1} = \frac{4k_1 i_0^2}{s_0^3}; \quad k_{i1} = \frac{4k_1 i_0}{s_0^2}; \quad k_1 = \frac{1}{4}\mu_0 N_1^2 A_{a1}\cos\frac{\alpha}{2} \tag{3.4}$$

Similarly, the force due to AMB2 on the rigid rotor in *x* and *y* directions can be expressed as

$$f_{x2} = k_{s2}u_{x2} + k_{i2}i_{x2}; \qquad f_{y2} = k_{s2}u_{y2} + k_{i2}i_{y2} \tag{3.5}$$

with

$$k_{s2}=\frac{4k_2i_0^2}{s_0^3};\quad k_{i2}=\frac{4k_2i_0}{s_0^2};\quad k_2=\frac{1}{4}\mu_0 N_2{}^2 A_{a2}\cos\frac{\alpha}{2} \tag{3.6}$$

where N_1 and N_2 are the number of coils in AMB1 and AMB2, respectively; A_{a1} and A_{a2} are the areas of the magnetic pole of AMB1 and AMB2, respectively; k_{s1} and k_{i1} are, respectively, the force-displacement and force-current constants of AMB1, and k_{s2} and k_{i2} are, respectively, the force-displacement and force-current constants of AMB2. The controlling current in the x and y directions at AMB1 and AMB2 locations are represented by $\{i_{x1}(t),\ i_{y1}(t)\}$ and $\{i_{x2}(t),\ i_{y2}(t)\}$, respectively. Following Equation (2.7), the expressions for controlling current in the x and y directions at the AMB1 and AMB2 locations can be expressed as

$$\begin{aligned} i_{x1}&=-\left(k_P u_{x1}+k_I\int u_{x1}dt+k_D\dot{u}_{x1}\right);\quad i_{y1}=-\left(k_P u_{y1}+k_I\int u_{y1}dt+k_D\dot{u}_{y1}\right)\\ i_{x2}&=-\left(k_P u_{x2}+k_I\int u_{x2}dt+k_D\dot{u}_{x2}\right);\quad i_{y2}=-\left(k_P u_{y2}+k_I\int u_{y2}dt+k_D\dot{u}_{y2}\right)\end{aligned} \tag{3.7}$$

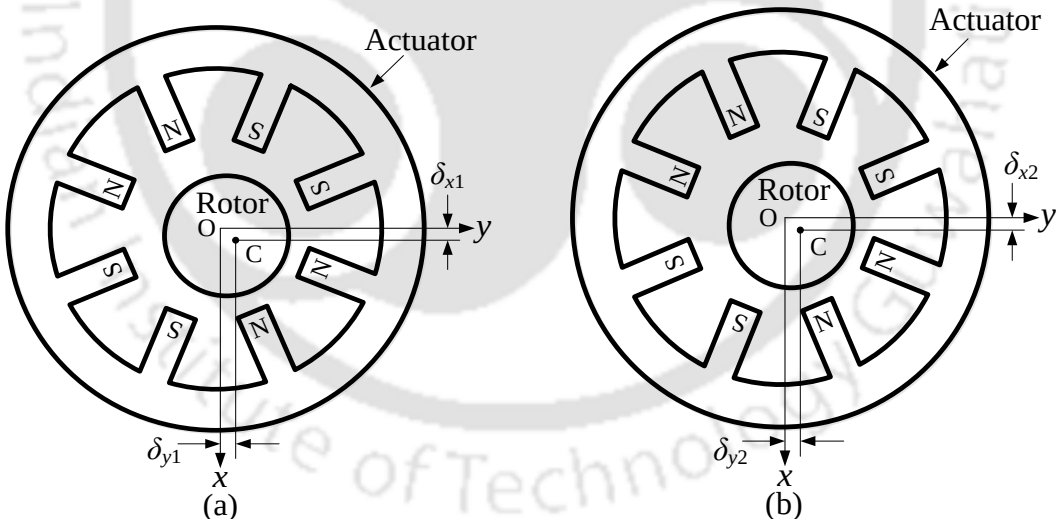

Figure 3.4 Misalignment of the rotor in the x-y plane with (a) AMB1 by δ_{x1} and δ_{y1} amounts (b) AMB2 by δ_{x2} and δ_{y2} amounts.

Similarly, for the residual misalignment case of AMBs as shown in Figure 3.4(a) (with the concept discussed in Section 2.3.2.1), the linearized force equations at AMB1 location in the x and y directions can be expressed as

$$f_{x1}^{m1} = k_{s1}^{m1} u_{x1}^{m1} + k_{i1}^{m1} i_{x1}^{m1} + f_1^{m1}; \qquad f_{y1}^{m1} = k_{s2}^{m1} u_{y1}^{m1} + k_{i2}^{m1} i_{y1}^{m1} + f_2^{m1} \tag{3.8}$$

with

$$\begin{aligned} k_{s1}^{m1} &= \frac{k_{a1}}{\left(1-\delta_1^2\right)^2}; \quad k_{i1}^{m1} = \frac{k_{i1}\left(1+\delta_1^2\right)}{\left(1-\delta_1^2\right)^2}; \quad f_1^{m1} = \frac{f_{a1}\delta_1}{\left(1-\delta_1^2\right)^2}; \quad f_{a1} = \frac{4k_1 i_0^2}{s_0^2}; \quad \delta_1 = \frac{\delta_{x1}}{s_0} \\ k_{s2}^{m1} &= \frac{k_{a1}}{\left(1-\delta_2^2\right)^2}; \quad k_{i2}^{m1} = \frac{k_{i1}\left(1+\delta_2^2\right)}{\left(1-\delta_2^2\right)^2}; \quad f_2^{m1} = \frac{f_{a1}\delta_2}{\left(1-\delta_2^2\right)^2}; \quad \delta_2 = \frac{\delta_{y1}}{s_0} \end{aligned} \tag{3.9}$$

where $(u_{x1}^{m1}, u_{y1}^{m1})$ and $(i_{x1}^{m1}, i_{y1}^{m1})$ are, respectively, the *x*- and *y*-directional displacement of the rotor and the controlling current at AMB1 location, and $(k_{s1}^{m1}, k_{i1}^{m1})$ and $(k_{s2}^{m1}, k_{i2}^{m1})$ is the modified force-displacement and force-current stiffness constants of AMB1 in the *x* and *y* directions, respectively. The new constant force terms arise due to AMB1 misalignment in the *x* and *y* directions are represented by f_1^{m1} and f_2^{m1}, respectively. Similarly, the AMB2 force on the rotor, in the *x* and *y* directions, when there is a misalignment of δ_{x2} and δ_{y2} amounts as shown in Figure 3.4(b), can be written, respectively, as

$$f_{x2}^{m1} = k_{s3}^{m1} u_{x2}^{m1} + k_{i3}^{m1} i_{x2}^{m1} + f_3^{m1}; \qquad f_{y2}^{m2} = k_{s4}^{m2} u_{y2}^{m2} + k_{i4}^{m2} i_{y2}^{m2} + f_4^{m2} \tag{3.10}$$

with

$$\begin{aligned} k_{s3}^{m1} &= \frac{k_{a2}}{\left(1-\delta_3^2\right)^2}; \quad k_{i3}^{m1} = \frac{k_{i2}\left(1+\delta_3^2\right)}{\left(1-\delta_3^2\right)^2}; \quad f_3^{m1} = \frac{f_{a2}\delta_3}{\left(1-\delta_3^2\right)^2}; \quad f_{a2} = \frac{4k_2 i_0^2}{s_0^2}; \quad \delta_3 = \frac{\delta_{x2}}{s_0} \\ k_{s4}^{m1} &= \frac{k_{a2}}{\left(1-\delta_4^2\right)^2}; \quad k_{i4}^{m1} = \frac{k_{i2}\left(1+\delta_4^2\right)}{\left(1-\delta_4^2\right)^2}; \quad f_4^{m1} = \frac{f_{a2}\delta_4}{\left(1-\delta_4^2\right)^2}; \quad \delta_4 = \frac{\delta_{y2}}{s_0} \end{aligned} \tag{3.11}$$

where $(u_{x2}^{m1}, u_{y2}^{m1})$ and $(i_{x2}^{m1}, i_{y2}^{m1})$ are, respectively, the displacements of the rotor and the controlling currents in the *x* and *y* directions at AMB2 location, and $(k_{s3}^{m1}, k_{i3}^{m1})$ and $(k_{s4}^{m1}, k_{i4}^{m1})$ are the modified force-displacement and force-current stiffness constants of AMB2 in the *x*

and *y* directions, respectively. The constant force terms appearing due to AMB2 misalignment in the *x* and *y* directions are denoted by f_3^{m1} and f_4^{m1}, respectively.

One of the prime objectives of this chapter is to obtain the four unknown residual misalignments, i.e. δ_{x1}, δ_{y1}, δ_{x2} and δ_{y2} from the proposed model-based identification algorithm derived from novel trial misalignment approach. For the estimation of these parameters, the known trial misalignments in addition to the unknown residual misalignments are provided at the AMB1 and AMB2 locations. These trial misalignments between the rotor and supported AMBs in the vertical and horizontal directions can be created by using the physical trial misalignment (PTM) concept, as discussed in Section 2.3.2.2. The combination of trial and residual misalignments can be termed as additional trial misalignment. Figure 3.5 represents for additional trial misalignment (residual plus trial) between the axes of the rotor and AMBs.

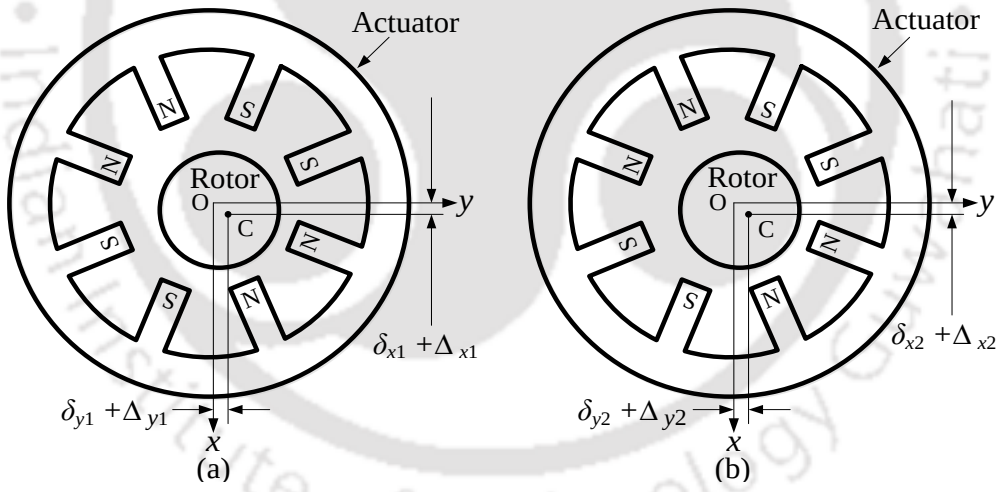

Figure 3.5 Misalignment of the rotor in *x*-*y* plane with (a) AMB1 by ($\delta_{x1} + \Delta_{x1}$) and ($\delta_{y1} + \Delta_{y1}$) amounts (b) AMB2 by ($\delta_{x2} + \Delta_{x2}$) and ($\delta_{y2} + \Delta_{y2}$) amounts.

Here, C is the rotor center, Δ_{x1} and Δ_{y1} are the trial misalignments in the vertical (*x*) and horizontal (*y*) directions at the AMB1 position. Trial misalignments in the vertical and horizontal directions at AMB2 location are represented by Δ_{x2} and Δ_{y2}, respectively. This case will be beneficial to determine the unknown residual misalignment. After the application of

trial misalignment, Δ_{x1}, the new misalignment between the rotor and AMB1 axis is (δ_{x1}+Δ_{x1}) in the *x*-direction. For the present case, the force on the rigid rotor due to AMB1 misaligned by ($\delta_{x1}+\Delta_{x1}$) and ($\delta_{y1}+\Delta_{y1}$), in the *x* and *y* directions, respectively, can be expressed as

$$f_{x1}^{m2}=k_{s1}^{m2}u_{x1}^{m2}+k_{i1}^{m2}i_{x1}^{m2}+f_1^{m2};\qquad f_{y1}^{m2}=k_{s2}^{m2}u_{y1}^{m2}+k_{i2}^{m2}i_{y1}^{m2}+f_2^{m2} \tag{3.12}$$

with

$$\begin{aligned} k_{s1}^{m2}&=\frac{k_{s1}}{\left(1-p_1^2\right)^2};\ k_{i1}^{m2}=\frac{k_{i1}\left(1+p_1^2\right)}{\left(1-p_1^2\right)^2};\ f_1^{m2}=\frac{f_{a1}p_1}{\left(1-p_1^2\right)^2};\ p_1=\delta_1+\Delta_1;\ \Delta_1=\frac{\Delta_{x1}}{s_0}\\ k_{s2}^{m2}&=\frac{k_{s1}}{\left(1-p_2^2\right)^2};\ k_{i2}^{m2}=\frac{k_{i1}\left(1+p_2^2\right)}{\left(1-p_2^2\right)^2};\ f_2^{m2}=\frac{f_{a1}p_2}{\left(1-p_2^2\right)^2};\ p_2=\delta_2+\Delta_2;\ \Delta_2=\frac{\Delta_{y1}}{s_0} \end{aligned} \tag{3.13}$$

Similarly, the force on the rotor due to AMB2 misaligned by ($\delta_{x2}+\Delta_{x2}$) and ($\delta_{y2}+\Delta_{y2}$), in the *x* and *y* directions, respectively, can be written as

$$f_{x2}^{m2}=k_{s3}^{m2}u_{x2}^{m2}+k_{i3}^{m2}i_{x2}^{m2}+f_3^{m2};\qquad f_{y2}^{m2}=k_{s4}^{m2}u_{y2}^{m2}+k_{i4}^{m2}i_{y2}^{m2}+f_4^{m2} \tag{3.14}$$

with

$$\begin{aligned} k_{s3}^{m2}&=\frac{k_{s2}}{\left(1-p_3^2\right)^2};\ k_{i3}^{m2}=\frac{k_{i2}\left(1+p_3^2\right)}{\left(1-p_3^2\right)^2};\ f_3^{m2}=\frac{f_{a2}p_3}{\left(1-p_3^2\right)^2};\ p_3=\delta_3+\Delta_3;\ \Delta_3=\frac{\Delta_{x2}}{s_0}\\ k_{s4}^{m2}&=\frac{k_{s2}}{\left(1-p_4^2\right)^2};\ k_{i4}^{m2}=\frac{k_{i2}\left(1+p_4^2\right)}{\left(1-p_4^2\right)^2};\ f_4^{m2}=\frac{f_{a2}p_4}{\left(1-p_4^2\right)^2};\ p_4=\delta_4+\Delta_4;\ \Delta_4=\frac{\Delta_{y2}}{s_0} \end{aligned} \tag{3.15}$$

where ($u_{x1}^{m2}, u_{y1}^{m2}, u_{x2}^{m2}$ and u_{y2}^{m2}) and ($i_{x1}^{m2}, i_{y1}^{m2}, i_{x2}^{m2}$ and i_{y2}^{m2}) are the displacements of the rigid rotor and the controlling current in the *x* and *y* directions, respectively, at AMB1 and AMB2 locations; (k_{s1}^{m2}, k_{i1}^{m2}), (k_{s2}^{m2}, k_{i2}^{m2}), (k_{s3}^{m2}, k_{i3}^{m2}) and (k_{s4}^{m2}, k_{i4}^{m2}) are the modified force-displacement and force-current stiffness constants of AMB1 and AMB2 in the *x* and *y* directions for additional trial misalignment, respectively. The constant force terms appearing

due to AMB1 and AMB2 misalignment in the *x* and *y* directions for the present misalignment case are denoted by f_1^{m2}, f_2^{m2}, f_3^{m2} and f_4^{m2}, respectively.

3.3 Equations of Motion of the Misaligned Rotor System considering Gyroscopic Effects

In this section, the equations of motion of the misaligned rigid rotor-AMB system have been derived for both residual and additional trial misalignment cases. For the purpose of derivation, the moment equilibrium of various forces about the centre of both active magnetic bearings in (*x*-*z*) and (*y*-*z*) planes are considered. For both the residual and additional trial misalignments, taking the moment equilibrium of forces due to misaligned AMB1, unbalance forces due to both discs, inertia force, and the inertia moment as well as gyroscopic moment due to both discs in the *x*-*z* and *y*-*z* planes about the AMB2 center and equating to zero, and further division by length 'l' on both sides it gives

$$m\ddot{u}_x^{mis}\frac{a_2}{l}-\frac{I_d}{l}\ddot{\varphi}_y^{mis}+\left(\frac{I_{p1}+I_{p2}}{l}\right)\dot{\varphi}_x^{mis}\omega-\left\{f_{unbx1}\left(\frac{a_2}{l}+\frac{l_1}{l}\right)+f_{unbx2}\left(\frac{a_2}{l}-\frac{l_2}{l}\right)\right\}-f_{x1}^{mis}=0 \qquad (3.16)$$

$$m\ddot{u}_y^{mis}\frac{a_2}{l}+\frac{I_d}{l}\ddot{\varphi}_x^{mis}-\left(\frac{I_{p1}+I_{p2}}{l}\right)\dot{\varphi}_y^{mis}\omega-\left\{f_{unby1}\left(\frac{a_2}{l}+\frac{l_1}{l}\right)+f_{unby2}\left(\frac{a_2}{l}-\frac{l_2}{l}\right)\right\}-f_{y1}^{mis}=0 \qquad (3.17)$$

Similarly, with the consideration of moment equilibrium of forces due to the AMB2, unbalance forces and inertia forces, the inertia moment and gyroscopic moments in the *x*-*z* and *y*-*z* planes about the AMB1 center and equating to zero, and then division by length 'l' on both sides it gives

$$m\ddot{u}_x^{mis}\frac{a_1}{l}+\frac{I_d}{l}\ddot{\varphi}_y^{mis}-\left(\frac{I_{p1}+I_{p2}}{l}\right)\dot{\varphi}_x^{mis}\omega-\left\{f_{unbx1}\left(\frac{a_1}{l}-\frac{l_1}{l}\right)+f_{unbx2}\left(\frac{a_1}{l}+\frac{l_2}{l}\right)\right\}-f_{x2}^{mis}=0 \qquad (3.18)$$

$$m\ddot{u}_y^{mis}\frac{a_1}{l}-\frac{I_d}{l}\ddot{\varphi}_x^{mis}+\left(\frac{I_{p1}+I_{p2}}{l}\right)\dot{\varphi}_y^{mis}\omega-\left\{f_{unby1}\left(\frac{a_1}{l}-\frac{l_1}{l}\right)+f_{unby2}\left(\frac{a_1}{l}+\frac{l_2}{l}\right)\right\}-f_{y2}^{mis}=0 \tag{3.19}$$

with

$$\begin{aligned} u_x^{mis}&=\bar{a}_2u_{x1}^{mis}+\bar{a}_1u_{x2}^{mis}; \qquad u_y^{mis}=\bar{a}_2u_{y1}^{mis}+\bar{a}_1u_{y2}^{mis}\\ \varphi_y^{mis}&=\left(-u_{x1}^{mis}+u_{x2}^{mis}\right)/l; \qquad \varphi_x^{m1}=\left(u_{y1}^{mis}-u_{y2}^{mis}\right)/l \end{aligned} \tag{3.20}$$

where the superscript *mis* represents for both the misalignment cases, i.e., *m*1 for the residual misalignment and *m*2 for the additional trial misalignment. u_x^{mis} and u_y^{mis} are the translational displacements of the rigid rotor at the centre of gravity in the *x* and *y* directions. φ_y^{mis} and φ_x^{mis} are the rotational displacements of the rotor in the *x*-*z* and *y*-*z* planes, respectively. I_d is the diametral mass moment of inertia of the rigid rotor (shaft and both discs) system, I_{p1} and I_{p2} are the polar mass moment of inertia of the disc1 and disc2. On substituting Equations (3.2) and (3.20) into Equations (3.16), (3.17), (3.18) and (3.19), we get the matrix form of the equations of motion, as

$$\mathbf{M}\Delta\ddot{\mathbf{q}}^{mis}(t)-\omega\mathbf{G}\Delta\dot{\mathbf{q}}^{mis}(t)=\mathbf{f}_{unb}+\mathbf{f}_{AMB}^{mis} \tag{3.21}$$

where the mass matrix **M** and the gyroscopic matrix **G** are

$$\mathbf{M}=\begin{bmatrix} \left(m\bar{a}_2^2+i_d\right) & 0 & \left(m\bar{a}_1\bar{a}_2-i_d\right) & 0\\ 0 & \left(m\bar{a}_2^2+i_d\right) & 0 & \left(m\bar{a}_1\bar{a}_2-i_d\right)\\ \left(m\bar{a}_1\bar{a}_2-i_d\right) & 0 & \left(m\bar{a}_1^2+i_d\right) & 0\\ 0 & \left(m\bar{a}_1\bar{a}_2-i_d\right) & 0 & \left(m\bar{a}_1^2+i_d\right) \end{bmatrix};\quad \mathbf{G}=\begin{bmatrix} 0 & i_p & 0 & -i_p\\ i_p & 0 & -i_p & 0\\ 0 & -i_p & 0 & i_p\\ -i_p & 0 & i_p & 0 \end{bmatrix};$$

$$i_d=\frac{I_d}{l^2};\quad i_P=\left(\frac{I_{P1}+I_{P2}}{l^2}\right);\quad \bar{l}_1=\frac{l_1}{l};\quad \bar{l}_2=\frac{l_2}{l}$$

The vibration induced displacement vector of the rigid rotor at both AMB locations is given by

$$\Delta\mathbf{q}^{mis}(t)=\left\{u_{x1}^{mis}\quad u_{y1}^{mis}\quad u_{x2}^{mis}\quad u_{y2}^{mis}\right\}^{T} \tag{3.22}$$

The unbalance force vector is

$$\mathbf{f}_{unb}=\begin{Bmatrix} m_{d1}e_1\omega^2\cos(\omega t+\beta_1)(\bar{a}_2+\bar{l}_1)+m_{d2}e_2\omega^2\cos(\omega t+\beta_2)(\bar{a}_2-\bar{l}_2)\\ m_{d1}e_1\omega^2\sin(\omega t+\beta_1)(\bar{a}_2+\bar{l}_1)+m_{d2}e_2\omega^2\sin(\omega t+\beta_2)(\bar{a}_2-\bar{l}_2)\\ m_{d1}e_1\omega^2\cos(\omega t+\beta_1)(\bar{a}_1-\bar{l}_1)+m_{d2}e_2\omega^2\cos(\omega t+\beta_2)(\bar{a}_1+\bar{l}_2)\\ m_{d1}e_1\omega^2\sin(\omega t+\beta_1)(\bar{a}_1-\bar{l}_1)+m_{d2}e_2\omega^2\sin(\omega t+\beta_2)(\bar{a}_1+\bar{l}_2) \end{Bmatrix} \tag{3.23}$$

The force vector due to misaligned AMBs is

$$\mathbf{f}_{AMB}^{mis}=\left\{f_{x1}^{mis}\quad f_{y1}^{mis}\quad f_{x2}^{mis}\quad f_{y2}^{mis}\right\}^{T} \tag{3.24}$$

On substituting the misaligned AMB forces (for both residual and additional trial misalignment cases) presented in Sections 3.2.2 into Equation (3.24), we get the vector form of the force due to both AMBs, as

$$\mathbf{f}_{AMB}^{mis}=\mathbf{K}_s^{mis}\Delta\mathbf{q}^{mis}(t)+\mathbf{K}_i^{mis}\mathbf{i}^{mis}(t)+\mathbf{f}_c^{mis} \tag{3.25}$$

where the controlling current vector is

$$\mathbf{i}^{mis}(t)=-\left\{k_P\Delta\mathbf{q}^{mis}(t)+k_I\int\Delta\mathbf{q}^{mis}(t)dt+k_D\Delta\dot{\mathbf{q}}^{mis}(t)\right\} \tag{3.26}$$

$$\mathbf{i}^{mis}(t)=\left\{i_{x1}^{mis}\quad i_{y1}^{mis}\quad i_{x2}^{mis}\quad i_{y2}^{mis}\right\}^{T} \tag{3.27}$$

with

$$\mathbf{K}_s^{mis}=\begin{bmatrix} k_{s1}^{mis} & 0 & 0 & 0\\ 0 & k_{s2}^{mis} & 0 & 0\\ 0 & 0 & k_{s3}^{mis} & 0\\ 0 & 0 & 0 & k_{s4}^{mis} \end{bmatrix};\quad \mathbf{K}_i^{mis}=\begin{bmatrix} k_{i1}^{mis} & 0 & 0 & 0\\ 0 & k_{i2}^{mis} & 0 & 0\\ 0 & 0 & k_{i3}^{mis} & 0\\ 0 & 0 & 0 & k_{i4}^{mis} \end{bmatrix};$$

Here, the controlling current vector (i.e., Equation (3.27)) will follow Equation (3.7) depending

upon misalignment cases. Now, Equation (3.21) representing for the residual and additional trial misalignments, respectively, can be solved using the SIMULINK^{TM} to generate the displacement and current responses of the system in the time domain, at both AMB locations. For measuring the displacement of shaft in the transverse directions, the sensors need to be located close to AMB positions in a practical rotor system. Further, the equation of motion (3.21) can be expressed in complex form by multiplying a complex number $\mathrm{j}=\sqrt{-1}$ with the second row and adding to the first row of Equation (3.21), it gives

$$\begin{aligned}&\left(m\bar{a}_2^2+i_d\right)\ddot{r}_1^{mis}+\left(m\bar{a}_1\bar{a}_2-i_d\right)\ddot{r}_2^{mis}-\omega i_p\left\{\left(\dot{u}_{y1}^{mis}-\dot{u}_{y2}^{mis}\right)+\mathrm{j}\left(\dot{u}_{x1}^{mis}-\dot{u}_{x2}^{mis}\right)\right\}\\&\quad=m_{d1}e_1\omega^2\left(\bar{a}_2+\bar{l}_1\right)e^{\mathrm{j}(\omega t+\beta_1)}+m_{d2}e_2\omega^2\left(\bar{a}_2-\bar{l}_2\right)e^{\mathrm{j}(\omega t+\beta_2)}\\&\quad+\left(k_{s1}^{mis}u_{x1}^{mis}+\mathrm{j}k_{s2}^{mis}u_{y1}^{mis}\right)+\left(k_{i1}^{mis}i_{x1}^{mis}+\mathrm{j}k_{i2}^{mis}i_{y1}^{mis}\right)+\left(f_1^{mis}+\mathrm{j}f_2^{mis}\right)\end{aligned}\tag{3.28}$$

And on multiplying $\mathrm{j}=\sqrt{-1}$ with the fourth row and adding to the third row of Equation (3.21), it gives

$$\begin{aligned}&\left(m\bar{a}_1\bar{a}_2-i_d\right)\ddot{r}_1^{mis}+\left(m\bar{a}_1^2+i_d\right)\ddot{r}_2^{mis}+\omega i_p\left\{\left(\dot{u}_{y1}^{mis}-\dot{u}_{y2}^{mis}\right)+\mathrm{j}\left(\dot{u}_{x1}^{mis}-\dot{u}_{x2}^{mis}\right)\right\}\\&\quad=m_{d1}e_1\omega^2\left(\bar{a}_1-\bar{l}_1\right)e^{j(\omega t+\beta_1)}+m_{d2}e_2\omega^2\left(\bar{a}_1+\bar{l}_2\right)e^{j(\omega t+\beta_2)}\\&\quad+\left(k_{s3}^{mis}u_{x2}^{mis}+\mathrm{j}k_{s4}^{mis}u_{y2}^{mis}\right)+\left(k_{i3}^{mis}i_{x2}^{mis}+\mathrm{j}k_{i4}^{mis}i_{y2}^{mis}\right)+\left(f_3^{mis}+\mathrm{j}f_4^{mis}\right)\end{aligned}\tag{3.29}$$

where the complex vibrational displacements at AMB1 and AMB2 for misaligned case are

$$r_1^{mis}(t)=u_{x1}^{mis}(t)+\mathrm{j}u_{y1}^{mis}(t);\quad r_2^{mis}(t)=u_{x2}^{mis}(t)+\mathrm{j}u_{y2}^{mis}(t)\tag{3.30}$$

Similarly, the current at AMBs in *x* and *y* directions can be expressed in complex form as

$$i_{c1}^{mis}(t)=i_{x1}^{mis}(t)+\mathrm{j}i_{y1}^{mis}(t);\quad i_{c2}^{mis}(t)=i_{x2}^{mis}(t)+\mathrm{j}i_{y2}^{mis}(t)\tag{3.31}$$

Complex displacements $\{r_{i1}^{mis}(t),r_{i2}^{mis}(t)\}$ and controlling currents $\{i_{i1}^{mis}(t),i_{i2}^{mis}(t)\}$ in the time domain can be assumed in a particular harmonic form, as

$$\begin{aligned} r_{i1}^{mis}(t) &= R_{i1}^{mis}(\omega)e^{\mathrm{j}i\omega t} \\ r_{i2}^{mis}(t) &= R_{i2}^{mis}(\omega)e^{\mathrm{j}i\omega t} \end{aligned} \quad \text{and} \quad \begin{aligned} i_{i1}^{mis}(t) &= I_{i1}^{mis}(\omega)e^{\mathrm{j}i\omega t} \\ i_{i2}^{mis}(t) &= I_{i2}^{mis}(\omega)e^{\mathrm{j}i\omega t} \end{aligned} \tag{3.32}$$

The subscript 'i' denotes the number of harmonics present in the responses. The first and second derivatives of the displacement responses can be expressed as

$$\begin{cases} \dot{r}_{i1}^{mis}(t) = \mathrm{j}i\omega R_{i1}^{mis}(\omega)e^{\mathrm{j}i\omega t}; \quad \dot{r}_{i2}^{mis}(t) = \mathrm{j}i\omega R_{i2}^{mis}(\omega)e^{\mathrm{j}i\omega t} \\ \ddot{r}_{i1}^{mis}(t) = -i^2\omega^2 R_{i1}^{mis}(\omega)e^{\mathrm{j}i\omega t}; \quad \ddot{r}_{i2}^{mis}(t) = -i^2\omega^2 R_{i2}^{mis}(\omega)e^{\mathrm{j}i\omega t} \end{cases} \tag{3.33}$$

The real and imaginary parts of the complex frequency domain rotor displacement and current responses at both AMBs, for without and with trial misalignment, will be further utilized in the identification algorithm. The algorithm required for estimating the various system and faults parameters is explained in the next section.

3.4 Development of Identification Algorithm

An identification algorithm based on the described mathematical model of the rotor-AMB system has been developed in this section. This algorithm is helpful for estimating the unbalance eccentricities (e_1 and e_2), the unbalance phases (β_1 and β_2), the modified force-displacement coefficients of AMB (k_{s1}^{m1}, k_{s2}^{m1}, k_{s3}^{m1} and k_{s4}^{m1}), the modified force-current coefficients of AMB (k_{i1}^{m1}, k_{i2}^{m1}, k_{i3}^{m1} and k_{i4}^{m1}), as well as the constant force terms of AMB (f_1^{m1}, f_2^{m1}, f_3^{m1} and f_4^{m1}) with residual misalignment. Similarly, the force-displacement stiffness coefficients of AMB (k_{s1}^{m2}, k_{s2}^{m2}, k_{s3}^{m2} and k_{s4}^{m2}), the force-current stiffness coefficients of AMB (k_{i1}^{m2}, k_{i2}^{m2}, k_{i3}^{m2} and k_{i4}^{m2}), as well as the constant force terms of AMB (f_1^{m2}, f_2^{m2}, f_3^{m2} and f_4^{m2}) related to the additional trial misalignment can also be estimated from the developing algorithm. Afterwards, the estimated values of modified AMB's parameters and force constants

of AMBs for without and with trial misalignment will be computed to determine the values of the unknown residual misalignments, i.e. δ_{x1}, δ_{y1}, δ_{x2} and δ_{y2} of AMB1 and AMB2.

For the conversion of the time domain responses into the frequency domain, the fast Fourier transform (FFT) technique (as discussed in Section 2.4.1 and Appendix C) has been employed, because this technique is numerically fast and efficient as well as reduces the computation time significantly during the transformation task. Afterwards, the frequency domain complex displacements $\{R_{i1}^{mis}(\omega), R_{i2}^{mis}(\omega)\}$ and complex currents $\{I_{i1}^{mis}(\omega), I_{i2}^{mis}(\omega)\}$ are captured from FFT analysed responses of the system. The complex form of these rotor displacements and AMB current responses for without and with trial misalignment (represented by the superscript *mis* in the combined form) as well as complex unbalance force due to disc1 and disc2 can be separated into the real and imaginary components, as follows

$$\begin{cases} R_{i1}^{mis}(\omega) = R_{i1,\mathrm{Re}}^{mis}(\omega) + \mathrm{j}R_{i1,\mathrm{Im}}^{mis}(\omega); & R_{i2}^{mis}(\omega) = R_{i2,\mathrm{Re}}^{mis}(\omega) + \mathrm{j}R_{i2,\mathrm{Im}}^{mis}(\omega) \\ I_{i1}^{mis}(\omega) = I_{i1,\mathrm{Re}}^{mis}(\omega) + \mathrm{j}I_{i1,\mathrm{Im}}^{mis}(\omega); & I_{i2}^{mis}(\omega) = I_{i2,\mathrm{Re}}^{mis}(\omega) + \mathrm{j}I_{i2,\mathrm{Im}}^{mis}(\omega) \end{cases} \tag{3.34}$$

$$\begin{cases} m_{d1}e_1\omega^2 e^{\mathrm{j}\beta_1} = m_{d_1}\omega^2(e_1\cos\beta_1 + \mathrm{j}e_1\sin\beta_1) = m_{d1}\omega^2(e_{\mathrm{Re}1} + \mathrm{j}e_{\mathrm{Im}1}) \\ m_{d2}e_2\omega^2 e^{\mathrm{j}\beta_2} = m_{d_2}\omega^2(e_2\cos\beta_2 + \mathrm{j}e_2\sin\beta_2) = m_{d2}\omega^2(e_{\mathrm{Re}2} + \mathrm{j}e_{\mathrm{Im}2}) \end{cases} \tag{3.35}$$

The real and imaginary components of Equations (3.34) and (3.35) are substituted into Equations (3.28) and (3.29), and further, the real and imaginary parts for residual misalignment and additional trial misalignments are written separately, for harmonic numbers (i = 0) and (i = 1). Afterwards, the equations for (i = 0, 1) harmonics are arranged in such a way that all identifiable parameters, i.e. the disc eccentricities ($e_{\mathrm{Re}1}$, $e_{\mathrm{Re}2}$, $e_{\mathrm{Im}1}$ and $e_{\mathrm{Im}2}$), the modified stiffness coefficients of AMBs ($k_{s1}^{m1}, k_{s2}^{m1}, k_{s3}^{m1}$ and k_{s4}^{m1}, $k_{i1}^{m1}, k_{i2}^{m1}, k_{i3}^{m1}$ and k_{i4}^{m1}), and the AMBs constant force (f_1^{m1}, f_2^{m1}, f_3^{m1} and f_4^{m1}) associated terms for residual misalignment as well as the parameters ($e_{\mathrm{Re}1}$, $e_{\mathrm{Re}2}$, $e_{\mathrm{Im}1}$, $e_{\mathrm{Im}2}$, $k_{s1}^{m2}, k_{s2}^{m2}, k_{s3}^{m2}, k_{s4}^{m2}, k_{i1}^{m2}, k_{i2}^{m2}, k_{i3}^{m2}$ and k_{i4}^{m2}, f_1^{m2},

f_2^{m2}, f_3^{m2} and f_4^{m2}) related terms for additional trial misalignment case are present in the left-hand side and the known parameters (m, i_d, i_p) associated terms are on the right-hand side. The compact form of a matrix containing all equations corresponding to the real and imaginary parts for (i = 0, 1) harmonics for without and with trial misalignments, respectively, gives

$$\mathbf{A}_1(\omega)\mathbf{x}_1 = \mathbf{b}_1(\omega) \tag{3.36}$$

with

$$\mathbf{x}_1 = \left\{ e_{\mathrm{Re}1} \quad e_{\mathrm{Re}2} \quad e_{\mathrm{Im}1} \quad e_{\mathrm{Im}2} \quad k_{s1}^{m1} \quad k_{s2}^{m1} \quad k_{s3}^{m1} \quad k_{s4}^{m1} \right.$$
$$\left. k_{i1}^{m1} \quad k_{i2}^{m1} \quad k_{i3}^{m1} \quad k_{i4}^{m1} \quad f_1^{m1} \quad f_2^{m1} \quad f_3^{m1} \quad f_4^{m1} \right\}^T$$

and

$$\mathbf{A}_2(\omega)\mathbf{x}_2 = \mathbf{b}_2(\omega) \tag{3.37}$$

with

$$\mathbf{x}_2 = \left\{ e_{\mathrm{Re}1} \quad e_{\mathrm{Re}2} \quad e_{\mathrm{Im}1} \quad e_{\mathrm{Im}2} \quad k_{s1}^{m2} \quad k_{s2}^{m2} \quad k_{s3}^{m2} \quad k_{s4}^{m2} \right.$$
$$\left. k_{i1}^{m2} \quad k_{i2}^{m2} \quad k_{i3}^{m2} \quad k_{i4}^{m2} \quad f_1^{m2} \quad f_2^{m2} \quad f_3^{m2} \quad f_4^{m2} \right\}^T$$

Since the real and imaginary components of eccentricity of the discs are common in Equations (3.36) and (3.37) for residual and additional trial misalignment cases, so both the equations can be combined to have unique values of eccentricity parameters. The combined form of identification equation can be expressed as

$$\mathbf{A}(\omega)\mathbf{x} = \mathbf{b}(\omega) \tag{3.38}$$

with

$$\mathbf{x} = \left\{ e_{\mathrm{Re}1} \quad e_{\mathrm{Re}2} \quad e_{\mathrm{Im}1} \quad e_{\mathrm{Im}2} \quad k_{s1}^{m1} \quad k_{s2}^{m1} \quad k_{s3}^{m1} \quad k_{s4}^{m1} \quad k_{i1}^{m1} \quad k_{i2}^{m1} \quad k_{i3}^{m1} \quad k_{i4}^{m1} \quad f_1^{m1} \quad f_2^{m1} \right.$$
$$\left. f_3^{m1} \quad f_4^{m1} \quad k_{s1}^{m2} \quad k_{s2}^{m2} \quad k_{s3}^{m2} \quad k_{s4}^{m2} \quad k_{i1}^{m2} \quad k_{i2}^{m2} \quad k_{i3}^{m2} \quad k_{i4}^{m2} \quad f_1^{m2} \quad f_2^{m2} \quad f_3^{m2} \quad f_4^{m2} \right\}^T$$

where $\mathbf{A}(\omega)$ is the regression matrix of dimension (16×28), $\mathbf{x}$ is the vector containing identifiable parameters of dimension (28×1) and $\mathbf{b}(\omega)$ is the vector containing known parameters of dimension (16×1). The rows of regression matrix $\mathbf{A}(\omega)$ as well as of the vector $\mathbf{b}(\omega)$ are elaborately stated in Appendix F. It can be observed from Equation (3.38) that there are 16 equations and 28 unknowns, i.e. number of equations are less than number of unknowns, so it is a class of underdetermined system of linear simultaneous equations. To determine the exact or optimal solutions of Equation (3.38), the number of equations should be equal to or more than the unknowns. Therefore, the rotor-AMB system need to operate with at least two different speeds (ω_1 and ω_2), which increases the number of equations to 32 and the unknowns remain 28 in number. This will make the linear equations overdetermined type, which can be solved by utilizing the Moore-Penrose inverse technique. Equation (3.38) at two different speeds can be written as

$$\begin{bmatrix} \mathbf{A}(\omega_1) \\ \mathbf{A}(\omega_2) \end{bmatrix} \mathbf{x} = \begin{Bmatrix} \mathbf{b}(\omega_1) \\ \mathbf{b}(\omega_2) \end{Bmatrix} \tag{3.39}$$

To estimate all the identifiable parameters using the Moore-Penrose inverse, Equation (3.39) can be expressed in the matrix form as

$$\mathbf{x} = \left(\mathbf{A}^T \mathbf{A} \right)^{-1} \mathbf{A}^T \mathbf{b} \tag{3.40}$$

More number of equations for harmonics (i = 0, 1), for multiple sets of two different spin speeds of rigid rotor are also taken to show the betterment of identifiable parameters estimation with the help of developed identification algorithm. Equation (3.39) for 'n' number of two different speeds can be expressed as

$$\begin{pmatrix} \mathbf{A}_{(\omega_{11})} \\ \mathbf{A}_{(\omega_{21})} \\ \vdots \\ \mathbf{A}_{(\omega_{1n})} \\ \mathbf{A}_{(\omega_{2n})} \end{pmatrix} \mathbf{x} = \begin{pmatrix} \mathbf{b}_{(\omega_{11})} \\ \mathbf{b}_{(\omega_{21})} \\ \vdots \\ \mathbf{b}_{(\omega_{1n})} \\ \mathbf{b}_{(\omega_{2n})} \end{pmatrix} \tag{3.41}$$

Here, ω_{1n} and ω_{2n} represent two different speeds for 'n' number of times. The identified values of stiffness as well as force constants of misaligned AMBs (i.e., $k_{s1}^{m1}, k_{s2}^{m1}, k_{s3}^{m1}, k_{s4}^{m1}, k_{i1}^{m1}, k_{i2}^{m1}, k_{i3}^{m1}, k_{i4}^{m1}, f_1^{m1}, f_2^{m1}, f_3^{m1}$ and f_4^{m1}) for the first level of misalignment as well as ($k_{s1}^{m2}, k_{s2}^{m2}, k_{s3}^{m2}, k_{s4}^{m2}, k_{i1}^{m2}, k_{i2}^{m2}, k_{i3}^{m2}, k_{i4}^{m2}, f_1^{m2}, f_2^{m2}, f_3^{m2}$ and f_4^{m2}) for the second misalignment level) contained in the vector **x** can be further utilized for evaluating the essential values of the amount of misalignment (δ_{x1}, δ_{y1}, δ_{x2} and δ_{y2}). The amount of misalignment (δ_{x1}) between the rotor and AMB1 in the x-direction can be determined through the ratios of force-displacement stiffness coefficients, force-current stiffness coefficients and constant forces of Equations (3.9) and (3.13). As an illustration, the ratio of force-displacement constants can be expressed as

$$\begin{aligned} \frac{k_{s1}^{m1}}{k_{s1}^{m2}} &= \frac{\left(1-p_1^2\right)^2}{\left(1-\delta_1^2\right)^2} = \frac{\left\{1-\left(\delta_1+\Delta_1\right)^2\right\}^2}{\left(1-\delta_1^2\right)^2};\ \delta_1 = \frac{\delta_{x1}}{s_0};\ \Delta_1 = \frac{\Delta_{x1}}{s_0} \\ \frac{k_{s2}^{m1}}{k_{s2}^{m2}} &= \frac{\left(1-p_2^2\right)^2}{\left(1-\delta_2^2\right)^2} = \frac{\left\{1-\left(\delta_2+\Delta_2\right)^2\right\}^2}{\left(1-\delta_2^2\right)^2};\ \delta_2 = \frac{\delta_{y1}}{s_0};\ \Delta_2 = \frac{\Delta_{y1}}{s_0} \end{aligned} \tag{3.42}$$

Utilizing Equation (3.42), the residual misalignments δ_{x1} and δ_{y1} can be obtained with the identified values of AMB parameters (k_{s1}^{m1}, k_{s1}^{m2}, k_{s2}^{m1}, k_{s2}^{m2}), the known values of nominal air gap, s_0, and the manually added misalignments (Δ_{x1}, Δ_{y1}). Following the same procedure, the values of the misalignments δ_{x2} and δ_{y2} between the rotor and AMB2, in the x and y directions, can be determined with the ratio of Equations (3.11) and (3.15). The ratios of these equations can be expressed as

$$\frac{k_{s3}^{m1}}{k_{s3}^{m2}}=\frac{\left(1-p_3^2\right)^2}{\left(1-\delta_3^2\right)^2}=\frac{\left\{1-\left(\delta_3+\Delta_3\right)^2\right\}^2}{\left(1-\delta_3^2\right)^2};\ \delta_3=\frac{\delta_{x2}}{s_0};\ \Delta_3=\frac{\Delta_{x2}}{s_0}$$
$$\frac{k_{s4}^{m1}}{k_{s4}^{m2}}=\frac{\left(1-p_4^2\right)^2}{\left(1-\delta_4^2\right)^2}=\frac{\left\{1-\left(\delta_4+\Delta_4\right)^2\right\}^2}{\left(1-\delta_4^2\right)^2};\ \delta_4=\frac{\delta_{y2}}{s_0};\ \Delta_4=\frac{\Delta_{y2}}{s_0} \quad (3.43)$$

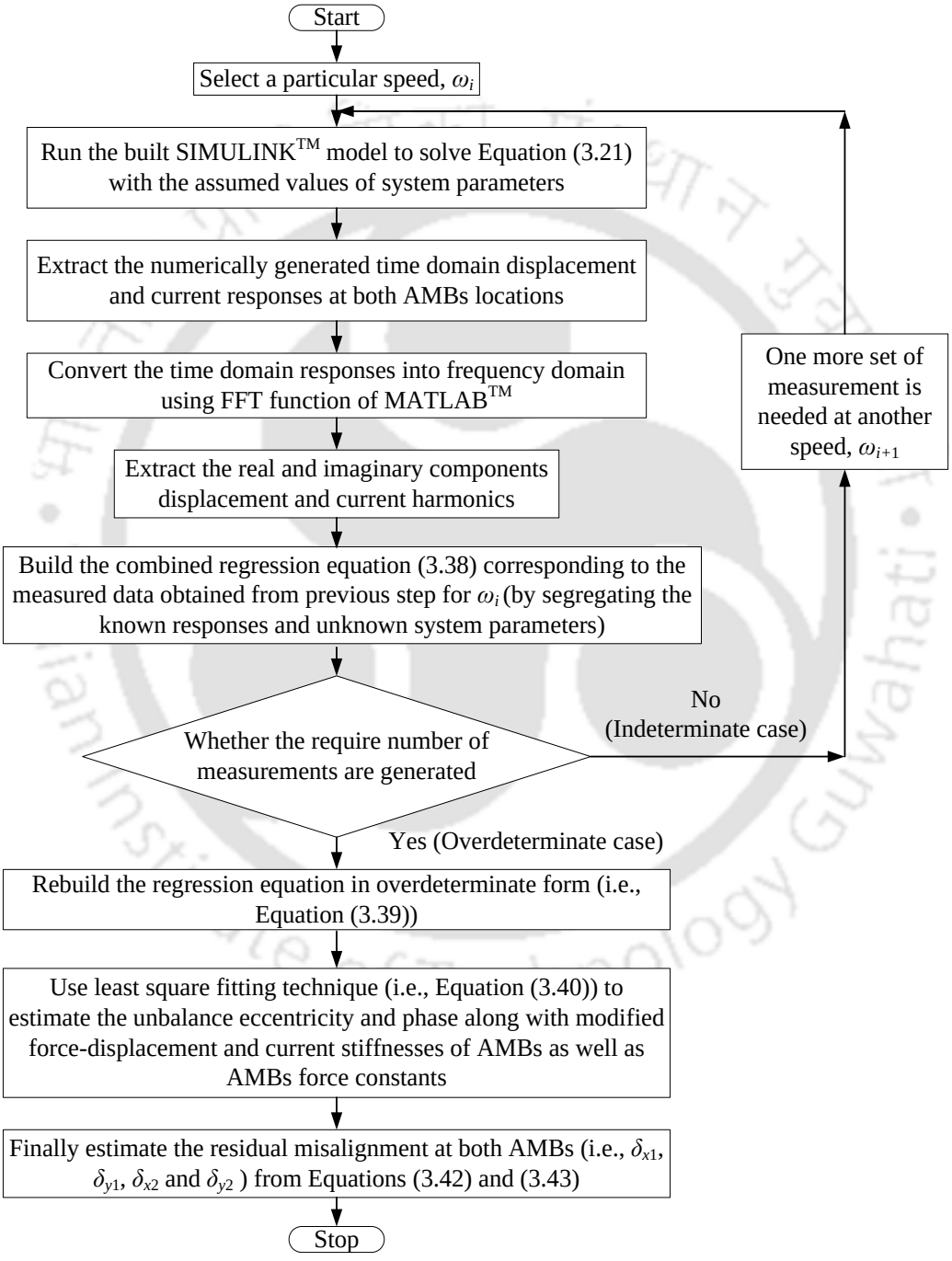

Figure 3.6 Flow chart of the unbalance and misalignment faults identification algorithm.

Thus, the developed identification algorithm for both residual and additional trial misalignment cases in combination form can be utilized to estimate quantitatively the disc unbalances and the residual misalignments between the rigid rotor and supported AMBs, which will fulfil the prime objective of the present work. Figure 3.6 demonstrates a flow chart describing the procedure of the identification algorithm, for simultaneous estimation of unbalance and misalignment faults in the rotor-AMB system. The results and discussion have been presented in the next section to verify the developed identification algorithm.

3.5 Generation of Simulated Responses and Parameters Estimation

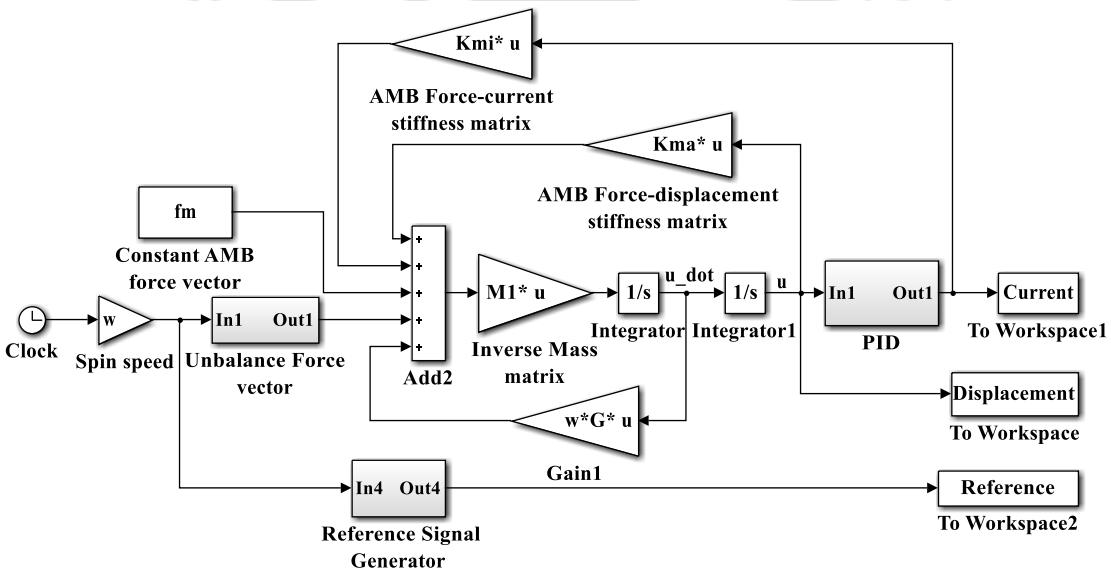

Figure 3.7 Schematic diagram of the SIMULINK model.

This section deals with generating the displacement and current responses of the unbalanced and misaligned rotor-AMB system. A SIMULINK^{TM} model has been developed to solve the equation of motion for the residual and additional trial misalignments, i.e., Equation (3.21) to obtain the responses. Figure 3.7 displays the schematic diagram of the model used for determining the rotor displacement as well as controlling current responses at AMB1 and AMB2 in the time domain.

Table 3.1 The misaligned rotor-AMB assumed data for the simulation purpose.

Parameters	Assumed Values	Parameters	Assumed Values
Rotor mass, m	3.910 kg	Proportional, k_P	5500 A/m
Disc 1 and 2 mass: m_{d1}, m_{d2}	1.065 and 2.081 kg	Derivative, k_D	3 A-s/m
Disc 1 and 2 eccentricity: e_1, e_2	80 and 100 μm	Integral, k_I	8000 A/m-s
Disc 1 eccentricity phase: β_1, β_2	20 and 30 deg	Length of the rotor, l	0.400 m
Diametral moment of inertia of the rotor, I_d	0.0455 kg-m^2	Distance of AMB 1 from centre of gravity of rotor, a_1	0.226 m
Polar moment of inertia of the disc 1 and disc 2: I_{P1} and I_{P2}	0.0019 and 0.0059 kg-m^2	Distance of AMB 2 from centre of gravity of rotor, a_2	0.174 m
Air gap between rotor and AMB 1	0.400 mm	Distance of disc 1 from centre of gravity of rotor, l_1	0.126 m
Air gap between rotor and AMB 2	0.400 mm	Distance of disc 2 from centre of gravity of rotor, l_2	0.074 m
AMB 1 force-displacement stiffness, k_{s1}	174, 150 N/m	AMB 1 force-current stiffness, k_{i1}	34.83 N/A
AMB 2 force-displacement stiffness, k_{s2}	365,710 N/m	AMB 2 force-current stiffness, k_{i2}	73.14 N/A
Residual misalignment between rotor and AMB 1 in x-direction, δ_{x1}	0.140 mm	Trial misalignment between rotor and AMB 1 in x-direction, Δ_{x1}	0.100 mm
Residual misalignment between rotor and AMB 1 in y-direction, δ_{y1}	0.160 mm	Trial misalignment between rotor and AMB 1 in y-direction, Δ_{y1}	0.130 mm
Residual misalignment between rotor and AMB 2 in x-direction, δ_{x2}	0.150 mm	Trial misalignment between rotor and AMB 2 in x-direction, Δ_{x2}	0.120 mm
Residual misalignment between rotor and AMB 2 in x-direction, δ_{y2}	0.145 mm	Trial misalignment between rotor and AMB 2 in y-direction, Δ_{y2}	0.110 mm

The rotor-AMB system data along with the assumed amounts of misalignment between rotor and AMB, utilized for the simulation purpose to generate the system responses are displayed in Table 3.1. From Table 3.1, it is observable that the assumed AMBs force-displacement and force-current coefficients (i.e., k_{s1}, k_{i1}, k_{s2} and k_{i2}) are the speed-independent parameters because from Equation (2.5), it can be seen that they are mainly dependent on the bias current i_0 and the other constant structural parameters of actuator (i.e., number of turning coils N, vacuum permeability μ_0, magnetic pole cross-sectional area A_a, air gap s_0, bias current i_0 and the angle between two adjacent magnetic poles α). These AMBs parameters are not dependent on spin speed of the rotor. Moreover, in the case of AMB, when the rotational speed of rotor changes, the magnetic force or magnetic field originating from AMB does not get changed. Here, only the shaft will vibrate about the fixed equilibrium position that the user has set through the bias current as well as the controlling current will get changed to suppress the small vibration. However, the bias current will be constant throughout the operation of the rotor. Thus, the AMB's parameters (i.e., k_{s1}, k_{i1}, k_{s2} and k_{i2}) are considered to be constant parameters. There is a significant amount of literature (Tiwari and Chougale, 2014; Singh and Tiwari, 2016; Srinivas et al., 2019; Sarmah and Tiwari, 2020) available, in which the speed-independent AMB parameters have been employed for their research purpose. For the assumed values of system parameters, the four critical speeds of the present rigid rotor system are found to be 243.71 rad/s, 258.11 rad/s, 465.64 rad/s and 475.69 rad/s, respectively. The corresponding mode shapes would be rigid body modes, meaning that the rotor is not bending, just bouncing in its bearings. A fourth-order Runge-Kutta ordinary differential equation solver with a fixed step size of 0.0001 s is used for generating the rotor displacement and controlling current responses at both AMB positions.

3.5.1 Dynamic Influence of AMB Residual Misalignment on the Rotor Performance

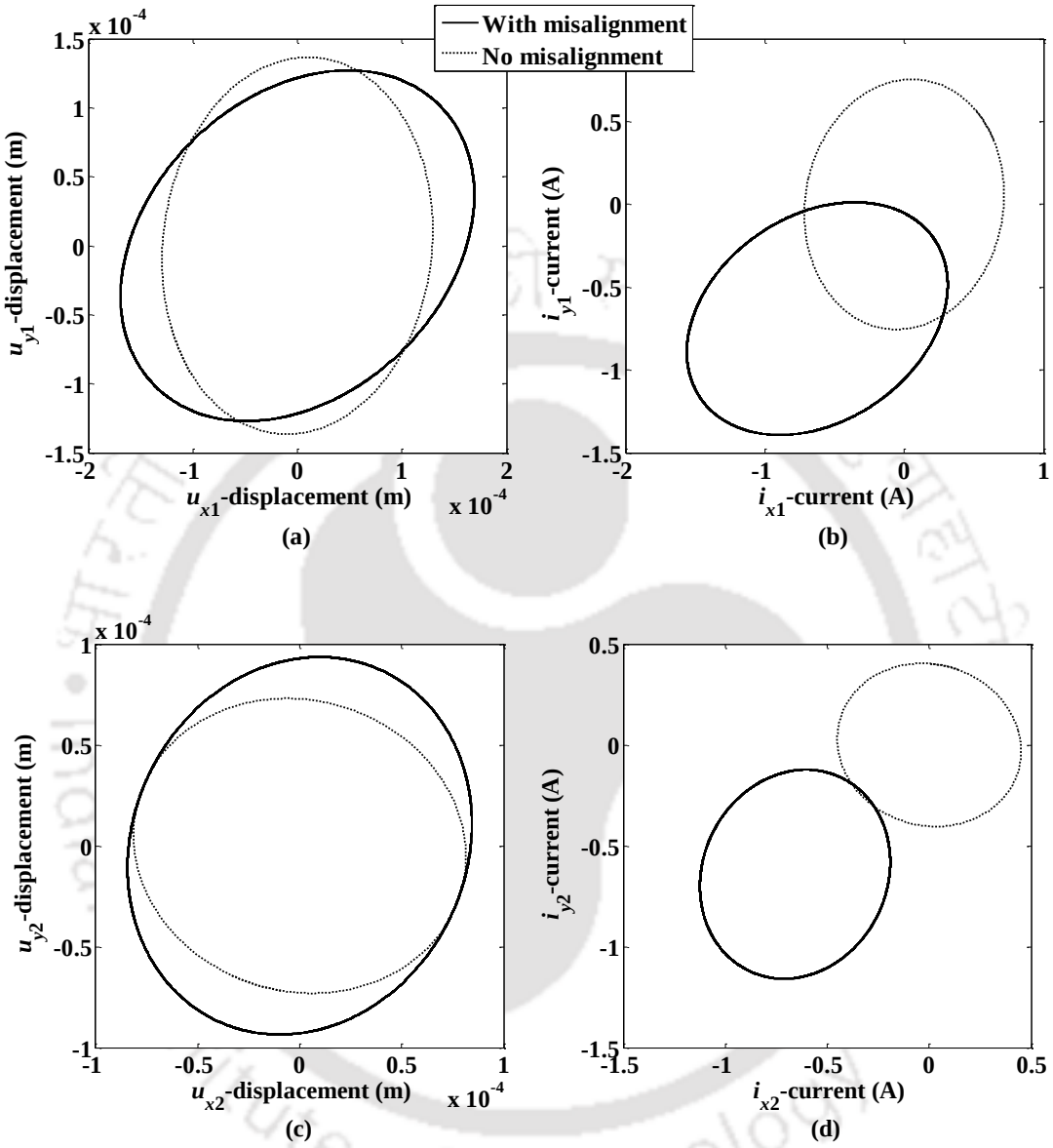

Figure 3.8 Orbital response representing the influence of AMB residual misalignment (a) displacement at AMB1 (b) current at AMB1 (c) displacement at AMB2 (d) current at AMB2 at an angular frequency of 30 Hz.

The rotor performance gets affected due to the residual misalignment fault between the rotor and AMBs. This fault causes to enhance the displacement response and more consumption of current in the rotor system at both AMB's locations. Figures 3.8 and 3.9 present

the orbital plots of rotor displacement and current at both AMB locations with and without misalignment at angular frequencies of 30 Hz (i.e., the spin speed of 188.50 rad/s) and 35 Hz (i.e. spin speed of 219.91 rad/s) respectively, to understand the dynamic effect of the residual misalignment. Theses speeds are selected below the first critical speed (243.71 rad/s) of the system to have rigid behaviour of rotor during its operation.

Following Figures 3.8 and 3.9, Table 3.2 summarizes the percentage increase in the time domain displacement and current responses due to residual misalignment along with their maximum amplitudes with and without misalignment, at AMB1 and AMB2 locations for shaft angular frequencies of 30 Hz and 35 Hz. It can be observed from Table 3.2 that the maximum displacement and current responses of the rotor system at both AMB locations for without and with misalignment are higher at 35 Hz frequency than 30 Hz. It is due to the dynamic effect of unbalance force present in the rotor system which directly depends upon the square of the angular frequency of the shaft, thus at higher speed, the response is found to be higher as compared to at the low speed. At an angular frequency of 30 Hz, the maximum amplitude of the displacement and current responses at AMB1 position for an unbalanced rigid rotor in the perfectly aligned case with AMB are observed to be only 1.095×10^{-4} m and 0.601 A, respectively, but the amplitudes are raised to 1.691×10^{-4} m and 1.559 A due to the residual misalignment. The increase in displacement response is about 54.43% of the perfectly aligned case. Similarly, the current consumption required in the rotor-AMB system has been increased by 159.40%. At AMB2 position, the maximum amplitude of the rotor displacement and controlling current raises to 9.356×10^{-5} m and 1.124 A, respectively from 7.304×10^{-5} m and 0.472 A. These increments are 28.10% and 141.43% of the aligned state. At AMB1 location, the maximum amplitude of displacement and current responses, at 35 Hz frequency are found to be increased by 73.57% and 173.86% due to AMB misalignment, as compared to the aligned position of the rigid rotor and AMB axes. Similarly, the misalignment causes to increase the

amplitude of the responses by 55.33% and 142.60% at AMB2 location. From Table 3.2, one of the remarkable observation is that the percentage increase in the responses due to AMB residual misalignment at 35 Hz is higher than at 30 Hz angular frequency of the shaft. This enhancement of the rotor response and more current or power consumption due to AMB misalignment inspires to identify this fault quantitatively together with unbalance parameters.

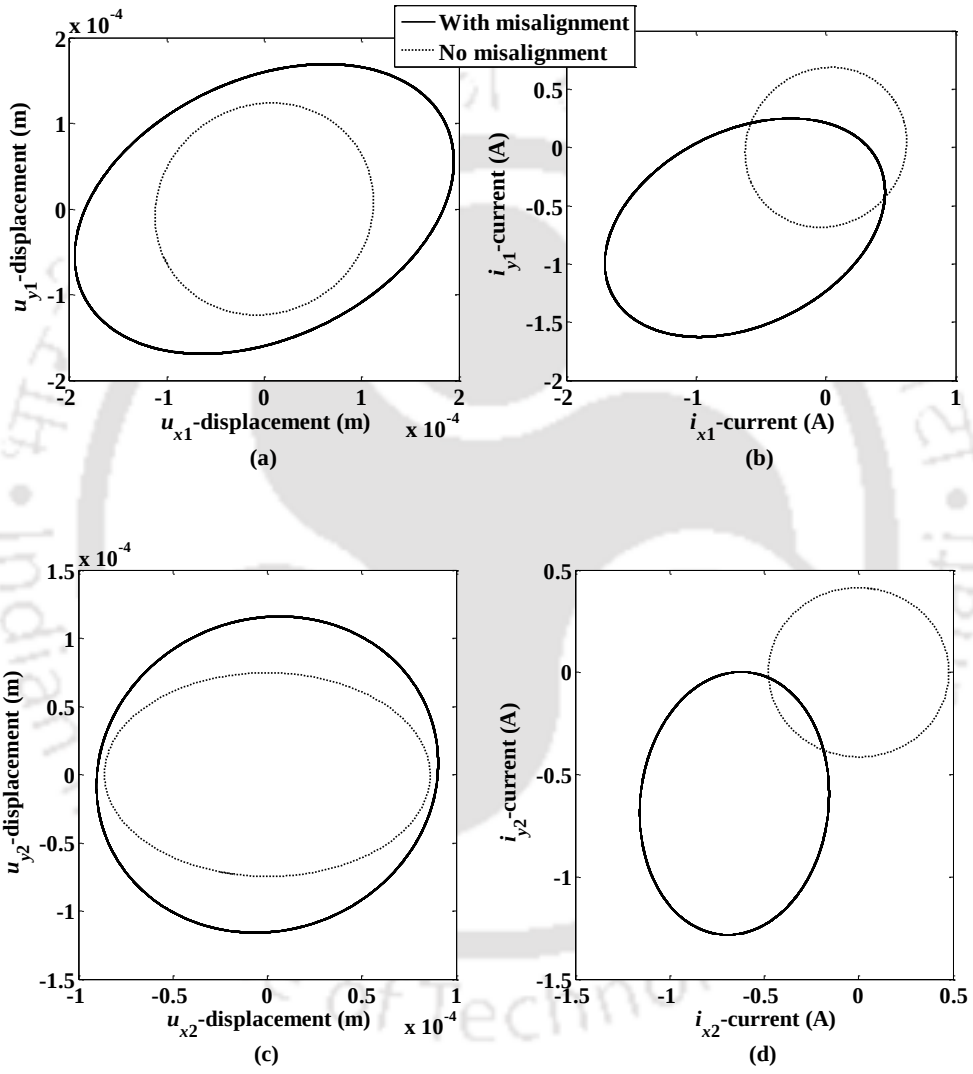

Figure 3.9 Orbital response representing the influence of AMB residual misalignment (a) displacement at AMB1 (b) current at AMB1 (c) displacement at AMB2 (d) current at AMB2 at an angular frequency of 35 Hz.

It is observable from Figures 3.8 and 3.9 that the current orbit plots are having non-zero mean. It is due to the constant forces, (f_1^{m1}, f_2^{m1}, f_3^{m1} and f_4^{m1}) available in misaligned AMB forces (i.e., Equations (3.8) and (3.10)) in the *x* and *y* directions. The constant forces cause to shift the displacement signals, but these signals get compensated due to the integral factor of PID controller. The factor (k_I) bring them to the mean position by generating a biased controlling currents, having a non-zero mean. It is worth mentioning that the neglected higher order terms $(i_{x1}^{m1})^2$, $u_{x1}^{m1}(i_{x1}^{m1})^2$ and $i_{x1}^{m1}u_{x1}^{m1}$ in the misaligned AMB force are the time dependent terms only (i.e., the terms related to vibration induced displacement and controlling current and their multiplications), there is no constant term here. Moreover, the vibration induced displacement and controlling current are the vibratory parts so they will oscillate about the mean position. Thus, the neglected higher terms will not affect the mean position of the rotor system.

Table 3.2 Percentage increase in the time domain displacement and current responses due to residual misalignment at AMB1 and AMB2 locations for shaft angular frequencies of 30 Hz and 35 Hz.

Angular frequency	Shaft location	Maximum amplitude in the time domain	No misalignment	Misalignment	Percentage increase (%)
30 Hz	AMB1	Displacement (m)	1.095×10^{-4}	1.691×10^{-4}	54.43
		Current (A)	0.716	1.559	117.69
	AMB2	Displacement (m)	7.304×10^{-5}	9.356×10^{-5}	28.10
		Current (A)	0.451	1.124	149.49
35 Hz	AMB1	Displacement (m)	1.122×10^{-4}	1.947×10^{-4}	73.57
		Current (A)	0.622	1.703	173.86
	AMB2	Displacement (m)	7.463×10^{-5}	1.159×10^{-4}	55.33
		Current (A)	0.478	1.159	142.6

One of the salient remarks can also be adopted from Figure 3.8 and 3.9, the orbit responses in the displacement and current plots are found to be stable although there is some variation with the mean position. Because if a rotor behaves in an unstable manner then the size of the shaft displacement and current orbits will increase with time, without apparent limit (Sarmah and Tiwari, 2019). However, this is not the case for the orbit plots in these figures. The amplitude of vibration, as well as the size of the orbits, remains constant with time. Moreover, the PID controller parameters have been tuned based on the Routh-Hurwitz criterion.

3.5.2 Estimation of Unbalance and AMB Misalignment Parameters

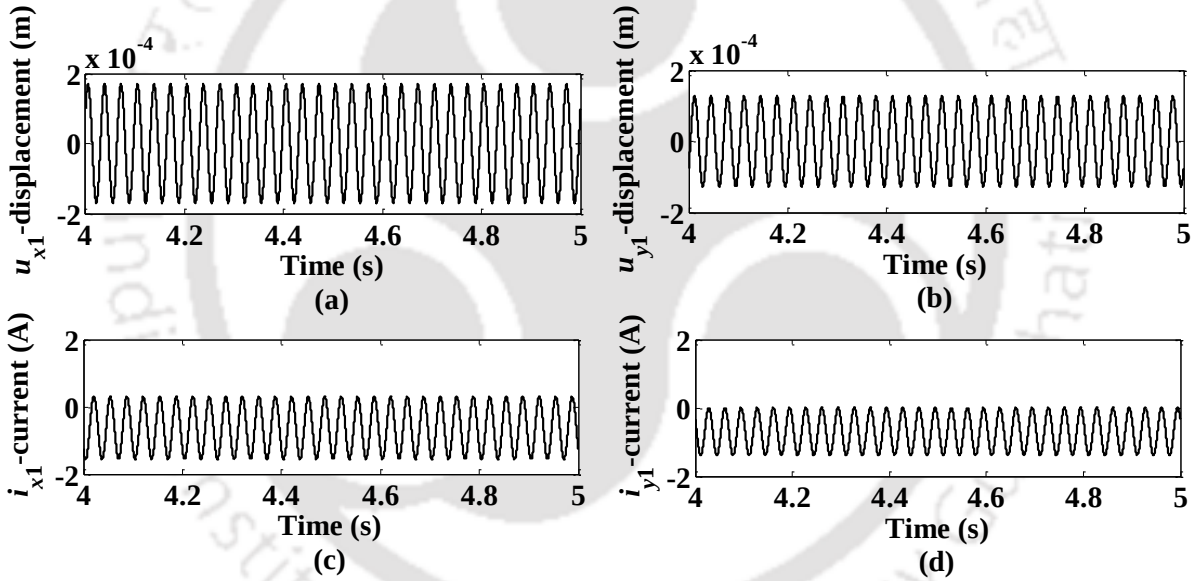

Figure 3.10 System responses at AMB1 location: (a) *x*-direction displacement (b) *y*-direction displacement (c) *x*-direction current (d) *y*-direction current.

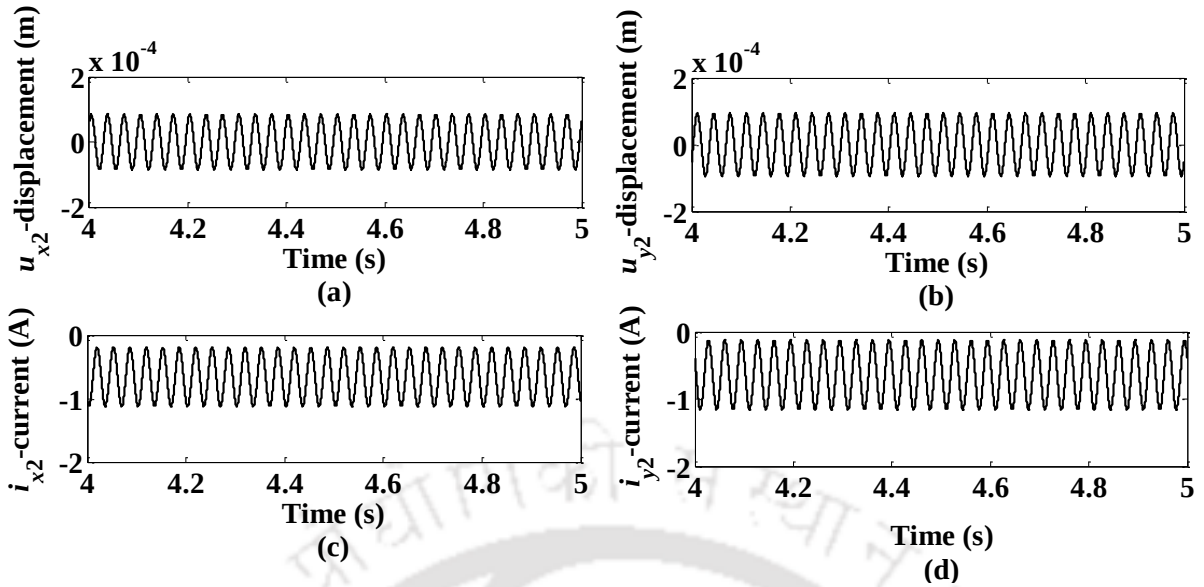

Figure 3.11 System responses at AMB2 location: (a) *x*-direction displacement (b) *y*-direction displacement (c) *x*-direction current (d) *y*-direction current.

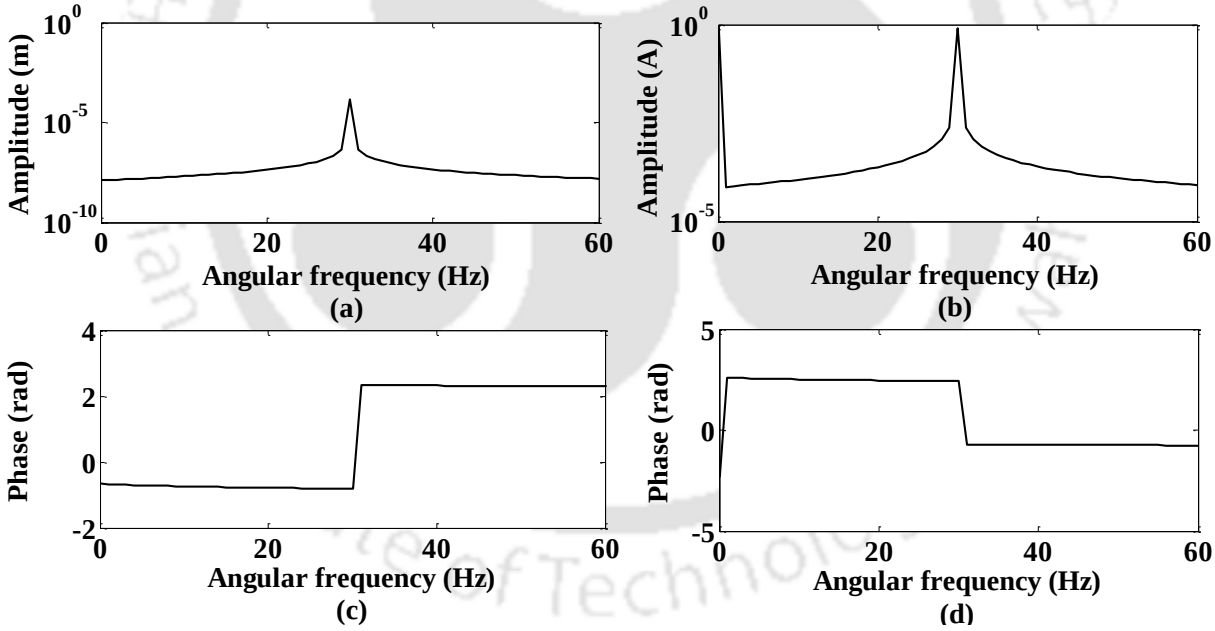

Figure 3.12 FFT of rotor system responses for residual misalignment at AMB1 location (a) displacement amplitude (b) current amplitude (c) displacement phase with compensation (d) current phase with compensation.

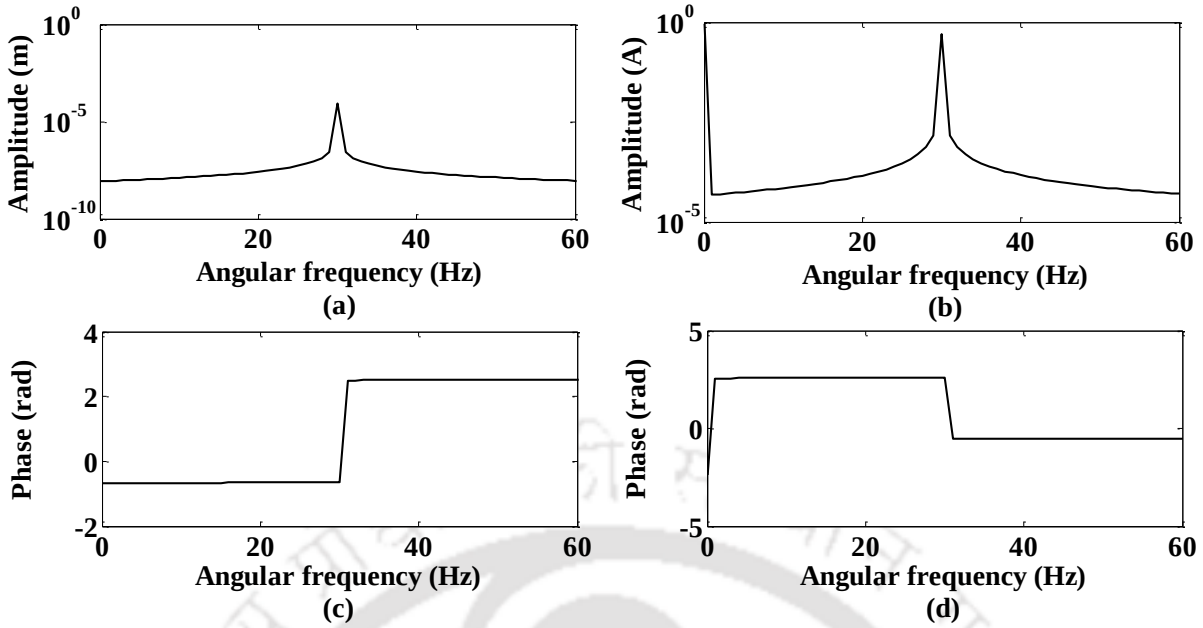

Figure 3.13 FFT of rotor system responses for residual misalignment at AMB2 location (a) displacement amplitude (b) current amplitude (c) displacement phase with compensation (d) current phase with compensation.

Table 3.3 Displacement and current harmonics captured from FFT technique at AMB1 and AMB2 locations for both residual and additional trial misalignment cases.

			Displacement (R_i)		Current (I_i)	
Misalignment	AMB location	Harmonics (i)	Amplitude (m)	Phase (deg)	Amplitude (A)	Phase (deg)
Residual misalignment	AMB1	0	1.26×10^{-8}	-37.73	9.30×10^{-1}	-132.12
		1	1.47×10^{-4}	-46.27	8.10×10^{-1}	139.17
	AMB2	0	8.27×10^{-9}	-39.54	9.20×10^{-1}	-135.73
		1	8.88×10^{-5}	-36.87	4.91×10^{-1}	148.57
Additional trial misalignment	AMB1	0	2.61×10^{-8}	5.02	13.00×10^{-1}	-132.87
		1	1.79×10^{-4}	6.60	9.90×10^{-1}	-168.00
	AMB2	0	1.00×10^{-8}	14.70	13.00×10^{-1}	-135.68
		1	1.12×10^{-4}	12.12	6.18×10^{-1}	-162.43

The simulation for the rotor model was run for 5 s using data given in Table 3.1. For the considered misaligned rigid rotor-AMB system, the rotor displacement and current responses at AMB1 and AMB2 locations in the *x* and *y* directions at an angular frequency of 30 Hz (i.e., the spin speed of 188.50 rad/s) for residual misalignment are shown in Figures 3.10 and 3.11, respectively. The displacement and current responses in time domain for the duration from 4 s to 5 s (i.e., 1 s time length) was considered for further investigation purpose. Fast Fourier transform analysis of the time domain responses was done using inbuilt FFT algorithm of MATLAB™. The complex or quadrature response signals in accordance with Equations (3.30) and (3.31) for misaligned AMB cases were input to the FFT function to generate the response in frequency domain. FFT plots of quadrature displacement and quadrature current signals at AMB1 and AMB2 locations with their amplitude and phase at an angular frequency of 30 Hz, for the first misalignment case, are presented in Figures 3.12 and 3.13, respectively. Similarly, for the additional trial misalignment, the FFT analyzed frequency domain plots of displacement and current responses at AMB1 and AMB2 are depicted in Figures 3.14 and 3.15 respectively. The phase diagram for frequency domain displacement and current signals at both AMBs for the residual and additional trial misalignments are plotted based on the phase correction method using a reference signal as already discussed in Appendix C.

Table 3.3 summarizes the magnitude and phase values of rotor displacement harmonics (R_{i1}^{m1}, R_{i2}^{m1}, R_{i1}^{m2} and R_{i2}^{m2}) and current harmonics (I_{i1}^{m1}, I_{i2}^{m1}, I_{i1}^{m2} and I_{i2}^{m2}) in the frequency domain at both AMB locations, for both residual and additional trial misalignment cases for harmonics numbers (i = 0, 1) captured from the FFT analysis. It can be observed from Table 3.3 that the peak values of the rotor displacement and current responses in the frequency domain at AMB1 location, for residual misalignment are found to be 1.47×10^{-4} m and 0.93 A, respectively, at an angular frequency of 30 Hz. Similarly, the maximum values of the rotor displacement and current in frequency domain, at AMB2 at the same angular frequency are

8.88×10^{-5} m and 0.92 A, respectively. For additional trial misalignment, in frequency domain, the peak values of the displacement and current responses at AMB1 are observed to 1.79×10^{-4} m and 1.30 A and at AMB2, the values are 1.12×10^{-4} m and 1.30 A, respectively. From Table 3.3, it can also be followed that the displacement level for additional trial misalignment is higher than residual misalignment for (i = 0 and 1). Similarly, the more controlling current is required for trial misalignment as compared to residual misalignment for both (i = 0) and (i = 1). Therefore, the main conclusion perceived from this observation is that the higher level of misalignment between the rotor and AMB axes causes to deviate the rotor displacement more from the equilibrium position. Similarly, the power consumption for driving the actuators and levitating the rotor as well as stabilizing it throughout the motion is more in case of increased misalignment amount.

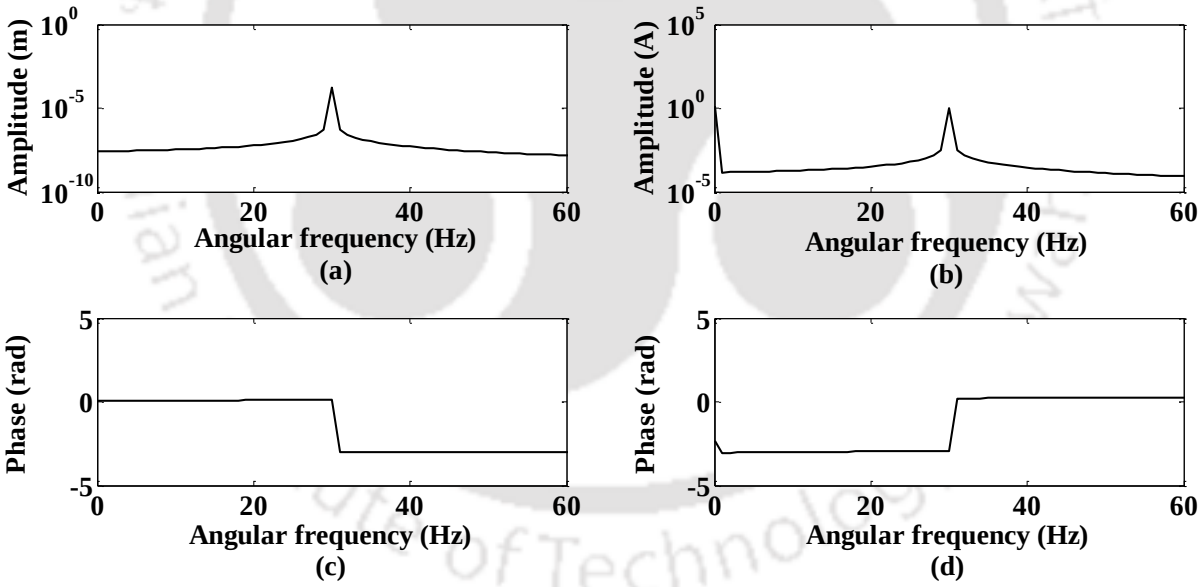

Figure 3.14 FFT of rotor system responses for additional trial misalignment at AMB1 location (a) displacement amplitude (b) current amplitude (c) displacement phase with compensation (d) current phase with compensation.

For both residual and additional trial misalignment cases, the real and imaginary values of complex rotor displacement and controlling current harmonics at both AMBs are procured

using magnitudes and phases of Tables 3.3. Further, these values have been utilized in the identification equation (3.38) to estimate several faults and AMB parameters. It is well explained in Section 3.4 that these equations are found to be under-determinate with 16 number of equations and 28 number of unknowns. To overcome this issue, the rotor has been operated at another angular frequency 35 Hz (i.e. spin speed of 219.91 rad/s), which raises the number of equations to 32. This is sufficient to determine all the unknowns based on regression technique (i.e., Equation (3.40)). Estimation of the unbalance and AMB parameters for residual and trial misalignment cases contained in the vector **x** has been done from Equation (3.40), by means of the real and imaginary parts of rotor displacement and current harmonics, gathered from the FFT processed signal at the angular frequencies of 30 Hz and 35 Hz.

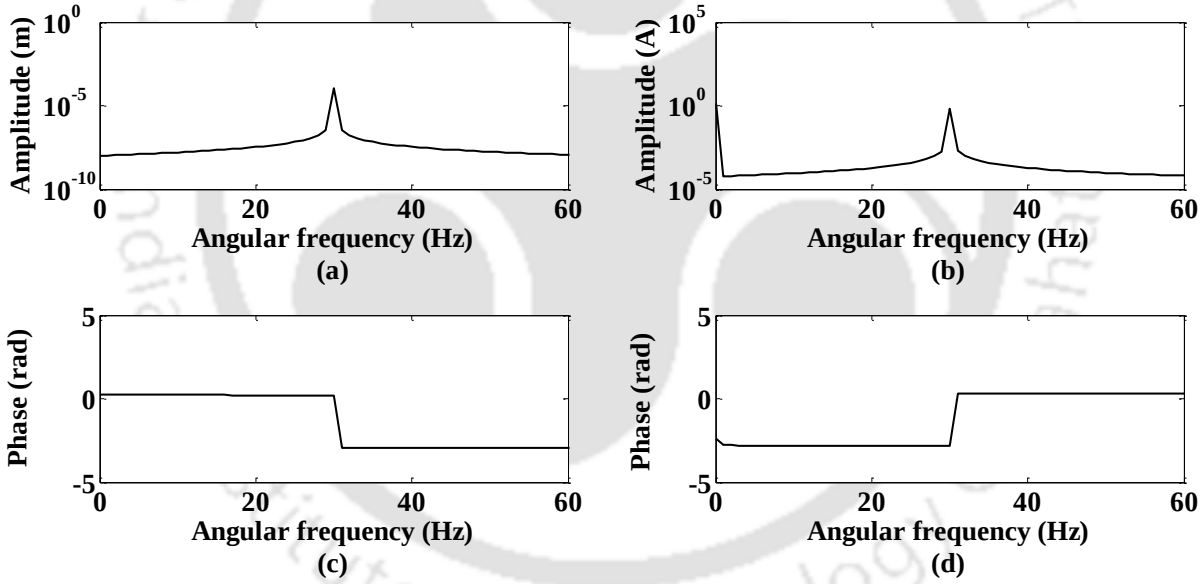

Figure 3.15 FFT of rotor system responses for additional trial misalignment at AMB2 location (a) displacement amplitude (b) current amplitude (c) displacement phase with compensation (d) current phase with compensation.

The actual measurement of response in a real rotor system is associated with various noise originated from rotating machines itself or from nearby environment (the more details on noise are given in Section 2.5.1). So, random noise of 1%, 2% or 5% is added to numerically

generated displacement responses and current responses for simulating the real measurement conditions, for both residual and additional trial misalignment cases. Tables 3.4 summarizes the error percentage of the estimated unbalance fault and misaligned AMBs parameters (for both residual and additional trial misalignments) relative to the assumed ones with noisy signals, at the combined angular frequencies of 30 Hz and 35 Hz. It can be observed that the identification of rotor-AMB system parameters is robust and effective against measurement noise signal. The identified values of disc unbalance eccentricities, e_1 and e_2 and their phases, β_1 and β_2, for the clean and noisy signals are well matching with the assumed values, which can be observed from Table 3.4. Furthermore, the results of unbalance eccentricities from the identification equation (i.e., Equation (3.40)) are observed to be more affected as compared to the estimated phases of unbalance for both the discs. The absolute error percentage of estimated eccentricities with respect to assumed ones vary only from 0.46% to 5.62%. Similarly, the absolute error related to phases are in the range of 0.10% to 3.95%. Absolute error percentage of identified AMB force-displacement stiffnesses ($k_{s1}^{m1}, k_{s2}^{m1}, k_{s3}^{m1}$ and k_{s4}^{m1}) for residual misalignment vary only from 0.44% to 6.31%.

Similarly, the absolute error for identified AMB force-current stiffnesses (k_{i1}^{m1}, k_{i2}^{m1}, k_{i3}^{m1} and k_{i4}^{m1}) are in the range of 0.21% to 9.43%. Among all the force-current stiffnesses of AMBs, k_{i1}^{m1} is the most affected with -9.43% error at 5% noise addition. The percentage deviation for error in the estimated AMB force constants (f_1^{m1}, f_2^{m1}, f_3^{m1} and f_4^{m1}) lies within 0.78% to 9.904%.

Table 3.4 Percentage deviations in the unbalance fault and misaligned AMBs parameters with noise error sensitivity at the combined angular frequencies of 30 Hz and 35 Hz.

Parameters	Assumed values	Identified values in percentage form with noise error sensitivity			
		0% noise	1% noise	2% noise	5% noise
e_1 (μm)	80	-0.85%	1.98%	3.43%	5.14%
e_2 (μm)	100	-0.46%	1.04%	2.87%	5.62%
β_1 (deg)	20	0.25%	-0.55%	-1.85%	-3.95%
β_2 (deg)	30	0.10%	-0.17%	-0.97%	-1.60%
k_{s1}^{m1} (N/m)	226,160	-0.55%	0.44%	2.09%	5.79%
k_{s2}^{m1} (N/m)	246,810	-0.98%	1.38%	3.77%	6.31%
k_{s3}^{m1} (N/m)	495,190	-0.61%	1.36%	3.32%	5.18%
k_{s4}^{m1} (N/m)	484,730	-0.95%	0.88%	3.62%	6.15%
k_{i1}^{m1} (N/A)	50.774	2.08%	-5.25%	-6.76%	-9.43%
k_{i2}^{m1} (N/A)	57.259	-2.11%	-4.36%	3.25%	8.59%
k_{i3}^{m1} (N/A)	112.964	0.21%	-1.83%	-4.12%	-6.45%
k_{i4}^{m1} (N/A)	109.686	1.49%	-3.19%	-4.27%	-6.81%
f_1^{m1} (N)	31.663	0.78%	-3.35%	5.42%	9.90%
f_2^{m1} (N)	39.489	1.35%	-2.39%	-4.68%	-8.27%
f_3^{m1} (N)	74.278	-1.50%	2.62%	5.55%	9.56%
f_4^{m1} (N)	70.286	-1.83%	1.56%	6.65%	9.17%
k_{s1}^{m2} (N/m)	425,160	-0.42%	0.89%	2.41%	5.16%
k_{s2}^{m2} (N/m)	773,880	-0.61%	2.39%	3.52%	6.03%
k_{s3}^{m2} (N/m)	1234,100	-1.79%	-2.08%	3.20%	7.07%
k_{s4}^{m2} (N/m)	1037,900	-1.60%	3.54%	5.15%	6.99%
k_{i1}^{m2} (N/A)	115.645	0.50%	-0.91%	-3.15%	-5.09%
k_{i2}^{m2} (N/A)	236.130	1.21%	-1.58%	-2.80%	6.27%
k_{i3}^{m2} (N/A)	359.268	-1.91%	2.21%	4.43%	6.06%
k_{i4}^{m2} (N/A)	291.943	0.21%	-1.87%	-3.28%	-4.94%
f_1^{m2} (N)	102.039	0.80%	-3.59%	-5.24%	-9.15%
f_2^{m2} (N)	224.425	1.31%	0.89%	2.41%	5.16%
f_3^{m2} (N)	333.199	-0.92%	2.39%	3.52%	6.00%
f_4^{m2} (N)	264.665	-1.37%	-2.08%	3.20%	7.07%

Table 3.5 Percentage deviations in the unbalance fault and misaligned AMBs parameters with modelling error sensitivity at the combined angular frequencies of 30 Hz and 35 Hz.

Parameters	Assumed values	Identified values in percentage form with modelling or bias error sensitivity			
		0% bias	1% bias	2% bias	5% bias
e_1 (μm)	80	-0.85%	1.25%	2.11%	4.25%
e_2 (μm)	100	-0.46%	0.32%	1.14%	6.32%
β_1 (deg)	20	0.25%	-0.30%	-2.25%	-3.45%
β_2 (deg)	30	0.10%	-0.17%	-0.80%	-1.87%
k_{s1}^{m1} (N/m)	226,160	-0.55%	-0.55%	0.93%	1.39%
k_{s2}^{m1} (N/m)	246,810	-0.98%	-0.98%	0.60%	2.75%
k_{s3}^{m1} (N/m)	495,190	-0.61%	-0.61%	0.94%	1.86%
k_{s4}^{m1} (N/m)	484,730	-0.95%	1.33%	4.45%	5.15%
k_{i1}^{m1} (N/A)	50.774	2.08%	-1.47%	-2.88%	-5.82%
k_{i2}^{m1} (N/A)	57.259	-2.11%	-2.83%	-5.19%	-7.30%
k_{i3}^{m1} (N/A)	112.964	0.21%	-3.20%	-4.43%	-7.91%
k_{i4}^{m1} (N/A)	109.686	1.49%	0.29%	-2.09%	-4.38%
f_1^{m1} (N)	31.663	0.78%	2.36%	6.28%	7.44%
f_2^{m1} (N)	39.489	1.35%	-0.86%	-3.77%	-6.99%
f_3^{m1} (N)	74.278	-1.50%	2.33%	3.71%	7.92%
f_4^{m1} (N)	70.286	-1.83%	2.25%	3.02%	8.00%
k_{s1}^{m2} (N/m)	425,160	-0.42%	0.56%	3.90%	7.53%
k_{s2}^{m2} (N/m)	773,880	-0.61%	0.59%	2.82%	5.35%
k_{s3}^{m2} (N/m)	1234,100	-1.79%	2.38%	3.84%	5.89%
k_{s4}^{m2} (N/m)	1037,900	-1.60%	3.08%	4.70%	6.91%
k_{i1}^{m2} (N/A)	115.645	0.50%	2.15%	2.88%	5.93%
k_{i2}^{m2} (N/A)	236.130	1.21%	-2.57%	-3.81%	-5.32%
k_{i3}^{m2} (N/A)	359.268	-1.91%	1.40%	5.22%	7.44%
k_{i4}^{m2} (N/A)	291.943	0.21%	1.08%	3.46%	5.22%
f_1^{m2} (N)	102.039	0.80%	-0.03%	3.78%	9.40%
f_2^{m2} (N)	224.425	1.31%	-1.76%	-3.80%	-7.08%
f_3^{m2} (N)	333.199	-0.92%	1.95%	5.63%	8.58%
f_4^{m2} (N)	264.665	-1.37%	-2.01%	2.73%	8.11%

Errors may also be associated with the measurements of rotor model parameters, such as the mass of rotor and diametral as well as polar moment of inertia of disc, and material density of shaft and disc due to various reasons. Development of this simplified mathematical model is based on certain assumptions, which may lead to establishing errors in the identification process. Combination of all such errors is termed as modeling errors or bias errors.

Effectiveness and robustness of the developed identification algorithm have also been tested by introducing random modelling errors of 1%, 2% and 5% to the rotor mass and moment of inertia of disc. Tables 3.5 outlines the error percentage of unbalance fault and misaligned AMB parameters for various levels of modelling errors, at the frequencies of 30 Hz and 35 Hz. All the force-displacement stiffnesses of AMBs for without trial misalignment (k_{s1}^{m1}, k_{s2}^{m1}, k_{s3}^{m1} and k_{s4}^{m1}) are found to be not severely affected as compared to the additional trial misalignment (k_{s1}^{m2}, k_{s2}^{m2}, k_{s3}^{m2} and k_{s4}^{m2}) in the presence of modelling errors. Among them, k_{s1}^{m1} have been identified with the best accuracy with 3.90% error even in the presence of 5% modelling errors. Estimation of the force-current stiffnesses (k_{i1}^{m1}, k_{i2}^{m1}, k_{i3}^{m1}, k_{i4}^{m1} and k_{i1}^{m2}, k_{i2}^{m2}, k_{i3}^{m2}, k_{i4}^{m2}) are also found to be stable with minimum and maximum error percentage of 0.287% and -7.91%, respectively. In the presence of modelling errors, AMB force constants (f_1^{m1}, f_2^{m1}, f_3^{m1}, f_4^{m1} and f_1^{m2}, f_2^{m2}, f_3^{m2}, f_4^{m2}) are found to be the most affected parameters. The error percentage for these parameters with the addition of 5% modelling errors lie in the range of -6.99% to 9.40%.

Table 3.6 Assumed and identified values of residual misalignment between rotor and AMBs with noise error sensitivity at the combined angular frequencies of 30 Hz and 35 Hz.

Parameters	Assumed values	Identified values with noise error sensitivity			
		0%	1%	2%	5%
δ_{x1} (mm)	0.140	0.1398	0.1409	0.1444	0.1462
	% *error*	-0.143	0.643	3.143	4.428
δ_{y1} (mm)	0.160	0.1604	0.1610	0.1598	0.1592
	% *error*	0.25	0.625	-0.125	-0.500
δ_{x2} (mm)	0.150	0.1496	0.1456	0.1499	0.1522
	% *error*	-0.267	-2.933	-0.067	1.467
δ_{y2} (mm)	0.145	0.1440	0.1489	0.1472	0.1468
	% *error*	-0.689	2.689	1.517	1.241

Table 3.7 Assumed and identified values of residual misalignment between rotor and AMBs with modelling error sensitivity at the combined angular frequencies of 30 Hz and 35 Hz.

Parameters	Assumed values	Identified values with modelling error sensitivity			
		0%	1%	2%	5%
δ_{x1} (mm)	0.140	0.1398	0.1393	0.1443	0.1464
	% *error*	-0.143	-0.5	3.071	4.571
δ_{y1} (mm)	0.160	0.1604	0.1596	0.1607	0.1610
	% *error*	0.25	-0.25	0.438	0.625
δ_{x2} (mm)	0.150	0.1496	0.1518	0.1524	0.1521
	% *error*	-0.267	1.200	1.600	1.400
δ_{y2} (mm)	0.145	0.1440	0.1476	0.1453	0.1475
	% *error*	-0.689	1.793	0.207	1.724

The identified values of misaligned AMBs stiffnesses and force constants with the addition of noise and modelling error sensitivity can be further employed in Equations (3.42) and (3.43) for estimating the residual misalignments (δ_{x1}, δ_{y1}, δ_{x2} and δ_{y2}) between the rotor and AMBs. Tables 3.10 and 3.11 concentrate on the assumed and identified values with error analysis of AMB misalignment amounts for clean and noise signals as well as modelling errors. The absolute error percentage in conjunction with the amounts of misalignment for various

levels of noise errors lie within the range of -0.067% to 4.428%. With the addition of modelling errors, the variation of percentage errors is only from -0.143% to 4.571%. The misalignment amount, δ_{x1} is found to be most affected parameter at 2% and 5% noise as well as modelling errors. However, overall variations in the estimated unbalance and misalignment fault parameters for noise and modelling errors are within acceptable limits.

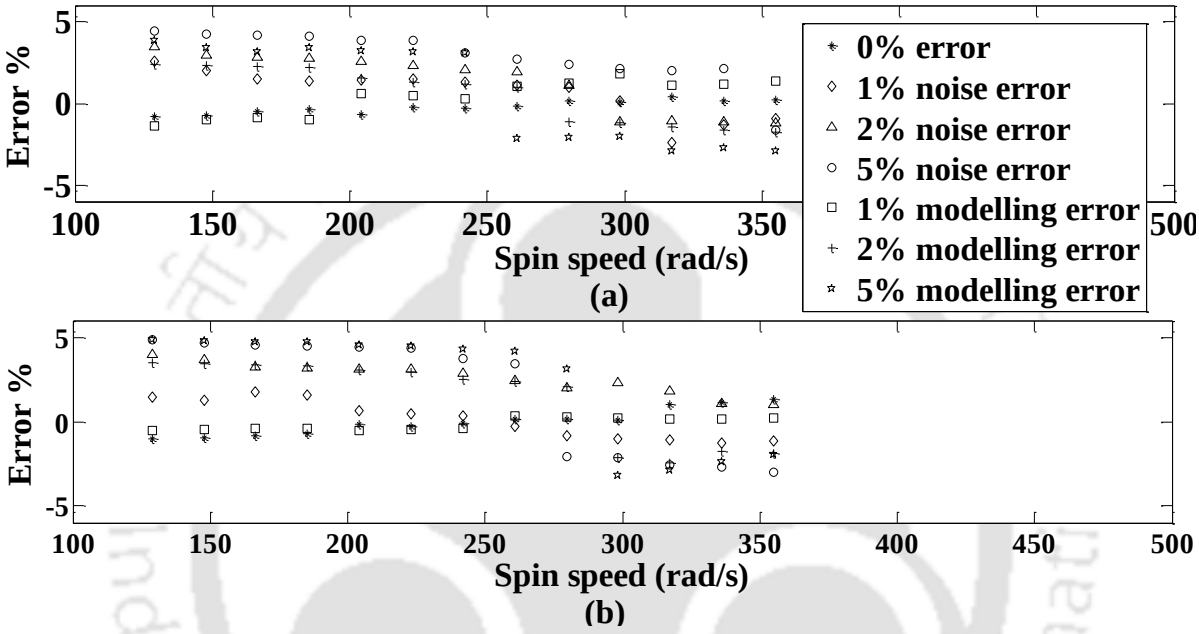

Figure 3.16 Error percentage in estimation of fault parameters with addition of noise and modelling errors at multiple spin speeds range (a) Unbalance eccentricity, e_1 (b) Misalignment amount, δ_{x1}.

Estimation of the most severe unbalance and misalignment faults in a rotor system integrated with active magnetic bearings has also been done with multiple sets of two different spin speeds of the rotor. This has been executed for testing the effectiveness and performance of the developed identification methodology. For the analysis purpose, the range of the first speed chosen is 113.10 rad/s to 339.29 rad/s, and the second speed range is 144.51 rad/s to 370.71 rad/s in discrete steps of 6π rad/s. The percentage error for estimation of one of the unbalance eccentricity and misalignment (i.e., e_1 and δ_{x1}) at multiple mean spin speeds range

with the addition of various levels of signal noise and modelling errors are depicted in Figure 3.16. From Figure 3.16, it is concluded that the developed algorithm is also exhibiting an outstanding outcome in simultaneous estimation of disc unbalance and AMB misalignment fault parameters at multiple spin speeds of the rigid rotor.

Results show that the novel trial misalignment approach associated with the developed model based identification algorithm gives the excellent estimates even with the addition of noise and modelling errors. Simultaneous estimation of several parameters related to unbalance fault, AMB force-displacement and force-current coefficients, misaligned AMB constant forces as well as different misalignment amounts between the rotor and AMB axes have been done successfully using this approach itself.

3.6 Summary

The rotor-AMB model presented in this chapter was found to be more complex than Chapter 2 model. Analysis was based on different values of stiffness constants of both AMBs, combination of parallel and angular misalignments as well as consideration of disc gyroscopic effects. Due to this complexity, the number of identifiable parameters was also noticed to be more than the model in the previous chapter. To overcome the ill-conditioning of the regression matrix, the responses (rotor displacement and AMBs current) were generated at two different speeds and combined together in the developed regression equation. This equation was successfully employed in estimating unbalance and AMB misalignment parameters for without and with trial misalignments along with misalignment amounts between the rotor and AMBs axes.

For illustration of the identification methodology derived from novel trial misalignment concept, an unbalanced and misaligned rigid rotor with two offset discs supported by two active magnetic bearings was mathematically modelled and analyzed in this chapter. Equations of

motion of the system were derived and simulated to generate the displacement and current responses at both AMB positions. The dynamic influence of AMBs residual misalignment on the rotor performance was also explored. It was found that the increase in misalignment level increases the displacement and current signals. The frequency domain responses were utilized in the novel trial misalignment based identification scheme for estimation of various system and faults parameters. The algorithm was also observed to be robust and effective against both noisy signal and modelling errors at multiple rotor spin speeds.

Although complexity is more in the present chapter as compared to the previous chapter due to consideration of disc gyroscopic effects, but the shaft is assumed to be rigid in nature. The analysis has been explored by operating the rotor below the first flexible mode critical speed of the system. However, in a practical system, the rotor has to operate above the first flexible mode critical speed for various applications. Therefore, the next chapter deals with the finite element modelling based flexible rotor system levitated by multiple misaligned AMBs. The shaft gyroscopic effects will be considered in addition to gyroscopic effects due to discs. Moreover, apart from different nature of each AMB, AMB will be also considered anisotropic in nature (i.e., the stiffness constants in the two orthogonal directions will be different).

Chapter 4

Finite Element Modelling and Identification in a Misaligned Flexible Rotor-AMB System

4.1 Introduction

This chapter is an extension of work performed in the previous two chapters, which discusses about more realistic magnetically levitated rotor model with multiple number of discs and active magnetic bearings. Herein, the rotor will be considered as flexible instead of rigid nature in Chapter 2 and Chapter 3. The modelling of the flexible shaft will be done using finite element method (based on Timoshenko beam elements) with consideration of shaft stiffness, shaft damping and its gyroscopic effect. Moreover, the rotor will be operated above the first flexible critical speed for analysing its dynamic behaviour as well as identification of system and faults parameters. Along with the different values of stiffness (displacement and current) parameters for each AMB, AMBs are also considered to be anisotropic in nature. The misalignment between rotor and AMBs axes is taken as a combination of parallel and angular misalignments.

The rotational displacements in Chapter 3 were as function of translational displacements at AMB locations due to rigid behaviour of rotor (follow Equation (3.1)). So, there was no requirement of dynamic condensation scheme for eliminating them. However, the dynamic condensation method will be used in this chapter to eliminate rotational DOFs. Number of sensors required for measurement of displacements will also be less and the rotational displacements will be derived intrinsically from the measurable translational displacements utilizing dynamic reduction scheme.

A novel trial misalignment approach based frequency domain identification algorithm will be developed for an unbalanced flexible shaft fastened with multiple discs and supported by multiple misaligned AMBs. The procedures for obtaining identification equation for this

complex rotor-AMB system will be followed from the previous two chapters, with different elements in regression matrix, known and unknown vectors. The Moore-Penrose inverse technique will be utilized to determine the optimum solution of identification equation. The solution would provide the disc unbalance parameters (eccentricities and phases) as well as misaligned AMBs parameters for residual and additional trial misalignments. The identified values of misaligned AMB stiffness constants for both cases of misalignments are further evaluated to estimate the misalignment amounts between rotor and multiple AMBs. Additionally, the actual force-displacement and force-current stiffness coefficients of AMBs (for perfect alignment state) will also be identified. These parameters were not estimated in the previous chapters.

4.2 Modelling Configuration of the Flexible Rotor System and Assumptions

A multi-disc flexible rotor system levitated by multiple AMBs at different locations, as shown in Figure 4.1, has been considered for analysis and identification formulation. Here, the elastic line RR represents for the axis of flexible shaft, whereas the operating axis of rotor is shown by Oz. There are p number of rigid discs and r number of AMBs in the considered rotor system. Each AMB is misaligned with the rotor both in the x- and y-directions by different amounts, which has been discussed in more details in Section 4.3.3. The rigid discs are connected with the flexible shaft either by the shrink fit or other mechanical mean. In practical applications, a rigid disc model represents turbine blades, flywheels, cranks, impellers, disc brakes, rotary wings, etc. Discrete unbalances are assumed to be present in each disc. To drive the flexible rotor, a flexible coupling has been used for connecting with the motor shaft.

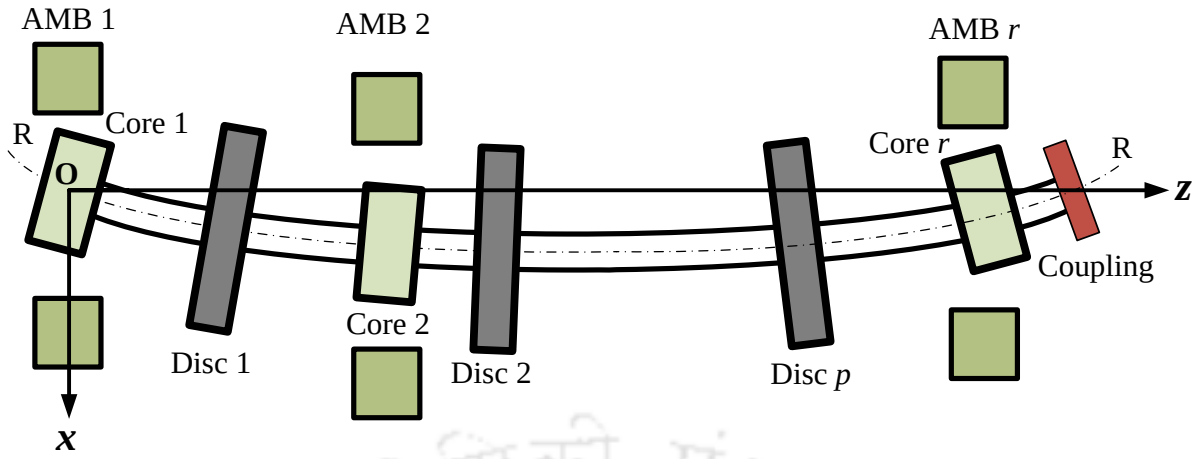

Figure 4.1 Schematic diagram of a multidisc flexible rotor system levitated on multiple active magnetic bearings.

For the finite element modelling of considered misaligned rotor-AMB model, the *Timoshenko beam theory* with the inclusion of *gyroscopic effects* has been utilized (Tiwari and Chakravarthy, 2006). *Shaft damping* is also considered using the proportional damping concept (Tiwari, 2017). In this concept, the damping of the shaft is calculated with the help of shaft mass, shaft stiffness and Rayleigh damping factors. AMBs are assumed to have the linearized force-displacement and force-current stiffnesses in two orthogonal transverse directions. For the stability and controlling performances of the rotor system, a PID controller has been used in AMBs.

4.3 Finite Element Formulation of Misaligned Rotor-AMB Model

Finite element method (FEM) is a well-established method and quite helpful for the design and analysis of complex practical rotors in rotating machineries. This method involves the discretization of the continuous rotor structure into finite number of elements for the study and investigation purpose. The rotor system, shown in Figure 4.1, is comprised of a flexible shaft, multiple rigid discs and multiple misaligned AMBs (parallel and angular). Thus, this whole rotor model is subdivided into various sub-models, i.e. flexible shaft sub-model, rigid disc-sub

model and misaligned AMB force sub-model, for derivation of the equations of motion individually. Further, these equations have been combined together to form global equations of motion, utilized for generating responses at each node and controlling current responses at AMB locations.

4.3.1 Flexible Shaft sub-model

The flexible shaft is divided into a finite number of linear elements for derivation of equations of motion. Each element is supposed to have two nodes and two translational as well as two rotational DOFs at each node, as shown in Figure 4.2. The equation of motion for each shaft element can be written as

$$\mathbf{M}^{(e)}\ddot{\boldsymbol{\eta}}^{(ne)} - \left(C^{(e)} - \omega\mathbf{G}^{(e)}\right)\dot{\boldsymbol{\eta}}^{(ne)} + \mathbf{K}^{(e)}\boldsymbol{\eta}^{(ne)} = \mathbf{f}^{(ne)} \tag{4.1}$$

with the displacement vector of j^{th} element (i.e., j^{th} and $j+1^{th}$ nodes) is

$$\boldsymbol{\eta}^{(ne)} = \left\{u_{x_j} \quad u_{y_j} \quad \varphi_{y_j} \quad \varphi_{x_j} \quad u_{x_{j+1}} \quad u_{y_{j+1}} \quad \varphi_{y_{j+1}} \quad \varphi_{x_{j+1}}\right\}^T \tag{4.2}$$

Here, $\mathbf{f}^{(ne)}$ is the elemental nodal force vector. The transverse translational displacements of each node in the vertical (x-direction) and horizontal (y-direction) are shown by u_x and u_y, respectively. Similarly, φ_y and φ_x are the x-z and y-z planes rotational displacements at each node. $\mathbf{M}^{(e)}$, $\mathbf{K}^{(e)}$, $\mathbf{G}^{(e)}$ and $\mathbf{C}^{(e)}$ are the elemental mass, stiffness, gyroscopic and damping matrices of shaft, respectively. Details of the shaft elemental mass, stiffness and gyroscopic matrices along with the concept of proportional damping matrix are given in Appendix A. The proportional damping concept for obtaining the damping matrix of shaft element is explained in Appendix B.

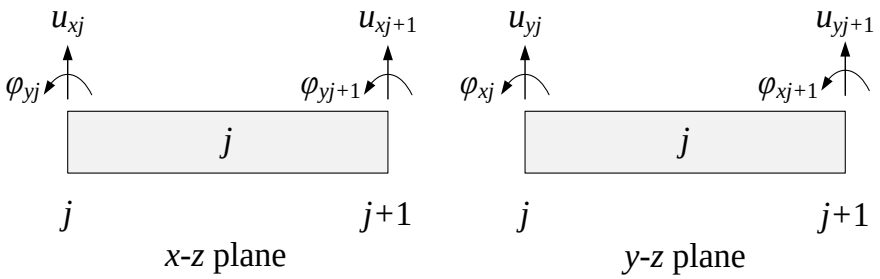

Figure 4.2 The j^{th} finite element with node points and degrees of freedoms.

4.3.2 Rigid Disc sub-model

The rigid discs have been modelled using the mass and diametral mass moment of inertia terms of each disc at the respective nodes. Equation of motion of the rigid disc can be expressed as

$$\mathbf{M}_d \ddot{\boldsymbol{\eta}}_d - \omega \mathbf{G}_d \dot{\boldsymbol{\eta}}_d = \mathbf{f}_d \tag{4.3}$$

where, $\boldsymbol{\eta}_d$ and $\mathbf{f}_d$ are the displacement and force vectors at a disc location. The disc mass and gyroscopic matrices are represented by $\mathbf{M}_d$ and $\mathbf{G}_d$, respectively (the details of these matrices are given in Appendix A).

4.3.3 AMB Force sub-model for Residual and Additional trial misalignments

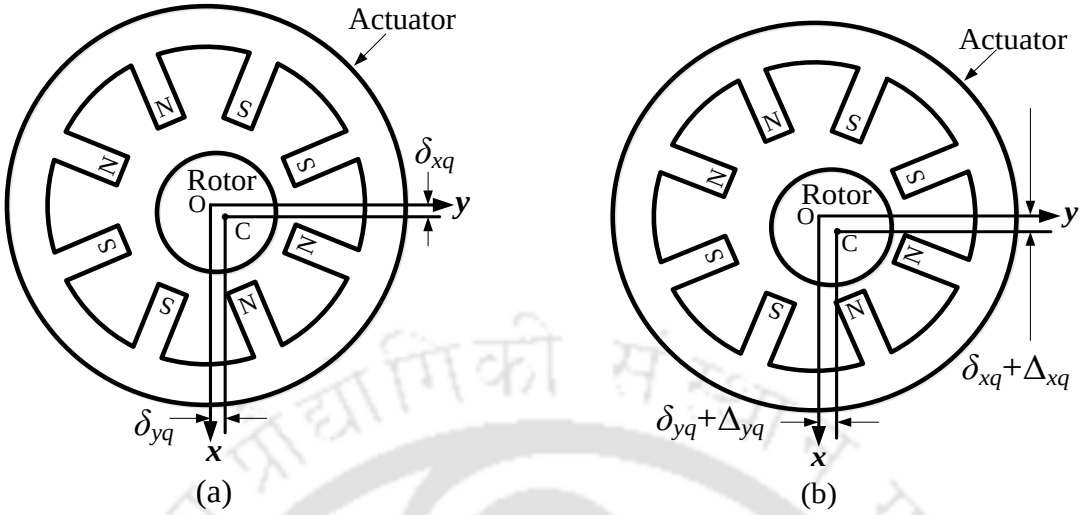

Figure 4.3 The *x*-*y* plane of rotor and eight pole q^{th} AMB (with q = 1, 2, …, r) actuator (a) the rotor is misaligned by δ_{xq} and δ_{yq} residual amounts (b) the rotor is misaligned by (δ_{xq} + Δ_{xq}) and (δ_{yq} + Δ_{yq}) residual and trial amounts.

In this chapter, all AMBs are considered to be anisotropic in nature with different force-displacement and current stiffness coefficients for each AMB. Therefore, the misaligned AMB force for the residual and additional trial misalignments will be slightly modified as presented in Chapters 2 and 3. The *x*- directional q^{th} AMB force (with q = 1, 2, …, r in Figure 4.1) when the flexible rotor is residually misaligned by the amounts of δ_{xq} and δ_{yq} (refer Figure 4.3(a)) using the concept of Equation (2.8) can be written as

$$f_{xq}^{m1} = k_{sxq}^{m1} u_{xq}^{m1} + k_{ixq}^{m1} i_{xq}^{m1} + f_{1q}^{m1} \tag{4.4}$$

with

$$k_{sxq}^{m1} = \frac{k_{sxq}}{\left(1-\delta_{1q}^2\right)^2}; \quad k_{ixq}^{m1} = \frac{k_{ixq}\left(1+\delta_{1q}^2\right)}{\left(1-\delta_{1q}^2\right)^2}; \quad f_{1q}^{m1} = \frac{f_q \delta_{1q}}{\left(1-\delta_{1q}^2\right)^2}; \quad f_q = \frac{4k_q i_0^2}{s_0^2}; \quad \delta_{1q} = \frac{\delta_{xq}}{s_0} \tag{4.5}$$

where the superscript $m1$ represents for the residual misalignment. k_{sxq}^{m1}, k_{ixq}^{m1} and f_{1q}^{m1} are, respectively, the *x*-directional displacement and current stiffness constants as well as newly

developed constant force of the misaligned q^{th} AMB. For the present case, the x-directional current output from PID controller (Schweitzer and Maslen, 2009), at q^{th} AMB location, can be given as

$$i_{xq}^{m1} = -\left(k_P u_{xq}^{m1} + k_I \int u_{xq}^{m1} dt + k_D \dot{u}_{xq}^{m1}\right) \tag{4.6}$$

where k_P, k_I and k_D are the proportional gain, integral gain and derivative gain factors of the controller, respectively. The expression for y-directional force due to residual misaligned q^{th} AMB and the controlling current output would follow Equations (4.4) and (4.6) by replacing x with y.

On providing the x-directional trial misalignment, Δ_{xq}, the updated misalignment level between the rotor axis and q^{th} AMB axis would be (δ_{xq}+Δ_{xq}) (refer Figure 4.3(b)), thus the force acting on the rotor due to additionally misaligned q^{th} AMB, can be expressed as

$$f_{xq}^{m2} = k_{sxq}^{m2} u_{xq}^{m2} + k_{ixq}^{m2} i_{xq}^{m2} + f_{1q}^{m2} \tag{4.7}$$

with

$$k_{sxq}^{m2} = \frac{k_{sxq}}{\left(1 - p_{1q}^2\right)^2};\ k_{ixq}^{m2} = \frac{k_{ixq}\left(1 + p_{1q}^2\right)}{\left(1 - p_{1q}^2\right)^2};\ f_{1q}^{m2} = \frac{f_q p_{1q}}{\left(1 - p_{1q}^2\right)^2};\ p_{1q} = \delta_{1q} + \Delta_{1q};\ \Delta_{1q} = \frac{\Delta_{xq}}{s_0} \tag{4.8}$$

where the superscript $m2$ denotes additional trial misalignment. The y-directional AMB force for additional trial misalignment can be written similar to Equation (4.7) with the replacement of subscript x by y. For this misalignment case, the x- and y-directional current output of the PID controller would follow Equation (4.6), by replacing $m1$ with $m2$ and x with y. The known trial misalignments can be provided in the rotor-AMB system using the concept of physical trial misalignment (PTM) or virtual trial misalignment (VTM). The procedure for PTM is already described in Section 2.3.2.2, whereas the VTM approach (virtual misalignment is created by moving rotor using AMB additional force) will be discussed in Section 5.3.1.

In the vector and combined form, the misaligned AMB force for the residual and additional trial misalignments can be expressed as

$$\mathbf{f}_{AMB}^{mis}(t)=\mathbf{K}_{s}^{mis}\boldsymbol{\eta}_{AMB}^{mis}(t)+\mathbf{K}_{i}^{mis}\mathbf{i}_{c}^{mis}(t)+\mathbf{f}_{c}^{mis} \tag{4.9}$$

with

$$\mathbf{K}_{s}^{mis}=\begin{bmatrix} k_{sxq}^{mis} & 0 \\ 0 & k_{syq}^{mis} \end{bmatrix};\ \mathbf{K}_{i}^{mis}=\begin{bmatrix} k_{ixq}^{mis} & 0 \\ 0 & k_{iyq}^{mis} \end{bmatrix};\ \mathbf{f}_{c}^{mis}=\begin{Bmatrix} f_{1q}^{mis} \\ f_{2q}^{mis} \end{Bmatrix} \tag{4.10}$$

The controlling current vector for the PID controller in the misaligned case can be expressed as

$$\mathbf{i}_{c}^{mis}(t)=-\begin{bmatrix} k_P & 0 & k_I & 0 & k_D & 0 \\ 0 & k_P & 0 & k_I & 0 & k_D \end{bmatrix}\left\{u_x^{mis} \quad u_y^{mis} \quad \int u_x^{mis}\mathrm{d}t \quad \int u_y^{mis}\mathrm{d}t \quad \dot{u}_x^{mis} \quad \dot{u}_y^{mis}\right\}^{T} \tag{4.11}$$

where the superscript *mis* represents for both the misalignment cases, i.e., *m*1 for the residual misalignment and *m*2 for the additional trial misalignment. $\mathbf{K}_{s}^{mis}$, $\mathbf{K}_{i}^{mis}$ and $\mathbf{f}_{c}^{mis}$ are the modified AMB force-displacement stiffness matrix, force-current stiffness matrix and constant force vector for the misaligned q^{th} AMB, respectively. The displacement and current vectors at the AMB location are represented by $\boldsymbol{\eta}_{AMB}^{mis}$ and $\mathbf{i}_{c}^{mis}$, respectively. The superscript *T* in Equation (4.11) represents for the transpose of the displacement vector.

4.3.4 Global Equations of Motion of the Misaligned Flexible Rotor System

Further, for both the cases of misalignment, the elemental equations of motion for the flexible shaft model, rigid disc model, residual unbalance force model (Ranjan and Tiwari, 2019) and misaligned AMB force model have been assembled together to form a global equation of motion. The assembled equations of motion of the unbalanced and misaligned rotor-AMB system for the residual and additional trial misalignments can be written as

$$\mathbf{M}\ddot{\boldsymbol{\eta}}^{mis} + \left(\mathbf{C} - \omega\mathbf{G}\right)\dot{\boldsymbol{\eta}}^{mis} + \mathbf{K}\boldsymbol{\eta}^{mis} = \mathbf{f}_{unb} + \mathbf{f}_{AMB}^{mis} \tag{4.12}$$

where **M, K, C** and **G** are the global mass, stiffness, damping and gyroscopic matrices, respectively. The vectors of global unbalance force and misaligned AMB force are represented by $\mathbf{f}_{unb}$ and $\mathbf{f}_{AMB}^{mis}$, respectively. The global rotor displacement vector is represented by $\boldsymbol{\eta}^{mis}$. The Equation (4.12) can be solved after the application of boundary conditions, to generate the displacement at each node and current at the nodes where AMBs are located.

4.3.5 Gyroscopic Dynamic Condensation Method

Generally, the accuracy of the results obtained from FEM based analysis improves with increase in number of elements used for discretisation of the system. The increase in elements number also increases the number of DOFs accompanied with FEM analysis. This poses practical difficulty of measurement of a large number of response on the physical system, being modelled with FEM. Certain DOFs may register responses so small that they might be physically limiting for measurements, like the rotational ones (Rao, 1996) , in case of a practical rotor. Certain locations on the rotor may be difficult to access, and mounting and availability of a large number of sensor may also be a limitation. Under such circumstances, the translational displacements are normally measurable with eddy current proximity probes and the rotational displacements are derived from them. In this context, the gyroscopic dynamic condensation method has been utilized to eliminate certain rotational DOFs. This method relies on the basis of assumption of neglecting damping term and no external force or moment at slave DOFs. The assumption is based on the fact that the natural frequencies do not get affected appreciably with damping term (Friswell and Mottershead, 1995). The *transformation vector* used for converting the full DOFs equations of motion into the reduced DOFs equations (in which unwanted DOFs have been removed), for both the misalignment cases, is given as

$$\boldsymbol{\eta}^{mis} = \begin{Bmatrix} \boldsymbol{\eta}_m^{mis} \\ \boldsymbol{\eta}_s^{mis} \end{Bmatrix} = \mathbf{T}^d \boldsymbol{\eta}_m^{mis} \tag{4.13}$$

with

$$\mathbf{T}^d = \begin{bmatrix} \mathbf{I} \\ -\left(\mathbf{K}_{ss} - ij\omega^2 \mathbf{G}_{ss} - (i\omega)^2 \mathbf{M}_{ss}\right)^{-1} \left(\mathbf{K}_{sm} - ij\omega^2 \mathbf{G}_{sm} - (i\omega)^2 \mathbf{M}_{sm}\right) \end{bmatrix} \tag{4.14}$$

where the transformation matrix related to the gyroscopic dynamic condensation method is represented by $\mathbf{T}^d$. The subscripts *m* and *s* denote the master and slave DOFs, respectively. Further, on substituting Equation (4.13) into Equation (4.12), then pre-multiplying both sides by $(\mathbf{T}^d)^T$, we get the reduced form of equation of motion for both the cases of misalignment, as

$$\mathbf{M}^d \ddot{\boldsymbol{\eta}}_m^{mis}(t) + \left(\mathbf{C}^d - \omega \mathbf{G}^d\right) \dot{\boldsymbol{\eta}}_m^{mis}(t) + \mathbf{K}^d \boldsymbol{\eta}_m^{mis}(t) = \mathbf{f}_{unb}^d + \mathbf{f}_{AMB}^{misd} \tag{4.15}$$

with

$$\mathbf{M}^d = \left(\mathbf{T}^d\right)^T \mathbf{M}\mathbf{T}^d;\ \ \mathbf{C}^d = \left(\mathbf{T}^d\right)^T \mathbf{C}\mathbf{T}^d;\ \ \mathbf{G}^d = \left(\mathbf{T}^d\right)^T \mathbf{G}\mathbf{T}^d;\ \ \mathbf{K}^d = \left(\mathbf{T}^d\right)^T \mathbf{K}\mathbf{T}^d;$$
$$\mathbf{f}_{unb}^d = \left(\mathbf{T}^d\right)^T \mathbf{f}_{unb};\ \ \mathbf{f}_{AMB}^{misd} = \left(\mathbf{T}^d\right)^T \mathbf{f}_{AMB}^{mis}$$

where $\mathbf{M}^d$, $\mathbf{C}^d$, $\mathbf{G}^d$ and $\mathbf{K}^d$ are the condensed mass, damping, gyroscopic and stiffness matrices of the rotor system. The condensed force vectors due to the disc unbalance and misaligned AMB are denoted by $\mathbf{f}_{unb}^d$ and $\mathbf{f}_{AMB}^{misd}$, respectively. The rotor induced displacement vector (master DOFs) in time domain, for both the misalignment cases is represented by $\boldsymbol{\eta}_m^{mis}$. The newly developed equation of motion (i.e., Equation (4.15)), has been solved to generate the steady-state rotor displacement and AMB current responses in the master DOFs. These have been further used in the developed model based identification algorithm for the system and fault parameters estimation purpose. The procedures for developing the identification algorithm based on frequency domain responses are discussed in the next section. The concept described here is consistent with Sections 2.4 and 3.4.

4.4 Identification Scheme for Estimation of the Unbalance, Misalignment and AMB Parameters

This section explains the mathematical procedures followed to develop the identification algorithm for estimation of the unknown unbalance and misalignment faults as well as constant parameters of AMBs, employing Equation (4.15). In this equation, the external force vectors on the right hand side (RHS) contain the unbalance force $\mathbf{f}_{unb}^{d}$, and misaligned AMB force $\mathbf{f}_{AMB}^{misd}$, respectively. Here, *d* superscript represents for the dynamic condensed force vector. This misaligned AMB force vector is assumed to have the harmonic form of $\mathbf{f}_{AMB}^{misd} = \mathbf{F}_{AMB}^{mis} e^{\mathrm{j}i\omega t}$. Similarly, the residual unbalance force vector is written in the harmonic form as $\mathbf{f}_{unb}^{d} = \mathbf{F}_{unb} e^{\mathrm{j}\omega t}$. Consecutively, the displacement and controlling current responses depending upon the nature of exciting force terms, can be expressed as

$$\boldsymbol{\eta}_{m}^{mis}(t) = \mathbf{N}_{m}^{mis}(\omega) e^{\mathrm{j}i\omega t}; \quad \mathbf{i}_{c}^{mis}(t) = \mathbf{I}_{c}^{mis}(\omega) e^{\mathrm{j}i\omega t} \tag{4.16}$$

where the information associated with the magnitude and phase of the rotor displacements, controlling currents and the external forces for the residual and additional trial misalignment cases are indicated by the complex vectors $\mathbf{N}_{m}^{mis}$, $\mathbf{I}_{m}^{mis}$ and $\left(\mathbf{F}_{unb}, \mathbf{F}_{AMB}^{mis}\right)$, respectively. The superscript *i* in Equation (4.16) will have the numerical values of 0 and 1 only. The value '0' is due to the developed constant force from AMB misalignment $\mathbf{F}_{c}^{mis}$, following Equation (4.9), whereas the value '1' is corresponding to the presence of the rotor unbalance force. Moreover, the frequency domain complex displacements and controlling current vectors of Equation (4.16) are extracted from the magnitude and corrected phase (elaborated in Appendix C) of FFT processed responses of the system.

Following the concept of Section 2.4.2, the equation of motion (i.e., Equation (4.15)) can be written in frequency domain as

$$\left\{-(i\omega)^2\mathbf{M}^d + \mathrm{j}(i\omega)\left(\mathbf{C}^d - \omega\mathbf{G}^d\right) + \mathbf{K}^d\right\}\mathbf{N}_m^{mis} = \mathbf{F}_{unb} + \mathbf{F}_{AMB}^{mis} \tag{4.17}$$

where, the force due to misaligned AMB, $\mathbf{F}_{AMB}^{mis}$ can be written in terms of the summation of force due to AMB modified stiffness (which includes forces from both the displacement and current stiffness coefficients), $\mathbf{F}_{AMB,s}^{mis}$ and constant AMB force, $\mathbf{F}_c^{mis}$ (follow Equation (4.9)), as

$$\mathbf{F}_{AMB}^{mis} = \mathbf{F}_{AMB,s}^{mis} + \mathbf{F}_c^{mis} \tag{4.18}$$

For (i = 0) and (i = 1) respectively, Equations (4.17) and (4.18) for both the misalignment cases can be expressed as

$$\mathbf{K}^d\mathbf{N}_m^{mis} = \mathbf{F}_{AMB,s}^{mis} + \mathbf{F}_c^{mis} \tag{4.19}$$

$$\left\{-\omega^2\mathbf{M}^d + \mathrm{j}\omega\left(\mathbf{C}^d - \omega\mathbf{G}^d\right) + \mathbf{K}^d\right\}\mathbf{N}_m^{mis} = \mathbf{F}_{unb} + \mathbf{F}_{AMB,s}^{mis} \tag{4.20}$$

It can be noticed that the left-hand side (LHS) of Equations (4.19) and (4.20) contains all known terms (i.e., mass, stiffness, damping and gyroscopic matrices) explicitly while right-hand side (RHS) has unknown terms (i.e., unbalance fault parameters, the modified AMB force-displacement and force-current stiffness parameters as well as constant AMB forces due to misalignment) in the form of unbalance force and misaligned AMB force. Hence, for estimation purpose, the above equations can be suitably manipulated such that all the unknown terms are in a vector in the left-hand side. Thus, by taking the terms relating to the unbalance and modified AMB parameters and AMB constant forces on LHS, Equations (4.19) and (4.20) can be given as

$$\mathbf{F}_{AMB,s}^{mis} + \mathbf{F}_c^{mis} = \mathbf{K}^d\mathbf{N}_m^{mis} \tag{4.21}$$

$$\mathbf{F}_{unb}+\mathbf{F}_{AMB,s}^{mis}=\left\{-\omega^2\mathbf{M}^d+\mathrm{j}\omega\left(\mathbf{C}^d-\omega\mathbf{G}^d\right)+\mathbf{K}^d\right\}\mathbf{N}_m^{mis} \tag{4.22}$$

Further, the force vectors (includes both the unbalance and misaligned AMB forces) on the LHS can be transformed in such a way that all the known terms (i.e. rotor design parameters, generated rotor displacement and AMB current information) are in the regression matrix in the left hand side. Here, the right-hand side vector itself includes all known quantities. Thus, the transformation for the residual and additional trial misalignments for (i = 0 and 1) can be expressed as

$$\mathbf{A}_{1,0}^{mis}\mathbf{k}_s^{mis}+\mathbf{A}_{2,0}^{mis}\mathbf{k}_i^{mis}+\mathbf{F}_c^{mis}=\mathbf{B}_{1,0}^{mis} \tag{4.23}$$

$$\mathbf{A}_{3,1}\mathbf{e}+\mathbf{A}_{1,1}^{mis}\mathbf{k}_s^{mis}+\mathbf{A}_{2,1}^{mis}\mathbf{k}_i^{mis}=\mathbf{B}_{1,1}^{mis} \tag{4.24}$$

with

$$\mathbf{e}=\begin{Bmatrix}e_1\\e_2\\\vdots\end{Bmatrix};\quad \mathbf{k}_s^{mis}=\begin{Bmatrix}k_{sx1}^{mis}\\k_{sy1}^{mis}\\k_{sx2}^{mis}\\k_{sy2}^{mis}\\\vdots\end{Bmatrix};\quad \mathbf{k}_i^{mis}=\begin{Bmatrix}k_{ix1}^{mis}\\k_{iy1}^{mis}\\k_{ix2}^{mis}\\k_{iy2}^{mis}\\\vdots\end{Bmatrix};\quad \mathbf{F}_c^{mis}=\begin{Bmatrix}f_{11}^{mis}\\f_{21}^{mis}\\f_{12}^{mis}\\f_{22}^{mis}\\\vdots\end{Bmatrix}$$
$$\mathbf{B}_{1,i}^{mis}=\left\{-(i\omega)^2\mathbf{M}^d+\mathrm{j}(i\omega)\left(\mathbf{C}^d-\omega\mathbf{G}^d\right)+\mathbf{K}^d\right\}\mathbf{N}_m^{mis};\quad \text{for } (i=0,1) \tag{4.25}$$

Further, Equations (4.23) and (4.24) for both the cases of misalignment can be rearranged in matrix form as

$$\mathbf{A}_1^{mis}\mathbf{x}_1^{mis}=\mathbf{B}_1^{mis} \tag{4.26}$$

with

$$\mathbf{A}_1^{mis}=\begin{bmatrix}0 & \mathbf{A}_{1,0}^{mis} & \mathbf{A}_{2,0}^{mis} & \mathbf{I}\\ \mathbf{A}_{3,1} & \mathbf{A}_{1,1}^{mis} & \mathbf{A}_{2,1}^{mis} & 0\end{bmatrix};\quad \mathbf{x}_1^{mis}=\begin{Bmatrix}\mathbf{e}\\\mathbf{k}_s^{mis}\\\mathbf{k}_i^{mis}\\\mathbf{F}_c^{mis}\end{Bmatrix};\quad \mathbf{B}_1^{mis}=\begin{Bmatrix}\mathbf{B}_{1,0}^{mis}\\\mathbf{B}_{1,1}^{mis}\end{Bmatrix} \tag{4.27}$$

Equation (4.26) is observed to have the common vector of unbalance parameters **e**, in the unknown vector $\mathbf{x}_1^{mis}$ of both cases of misalignment. Hence, Equation (4.26) for the residual and additional trial misalignments, i.e., the superscript *mis* replaced with *m*1 and *m*2, respectively, can be combined together to estimate unique value of parameters associated with the unbalance fault in the rotor system. Hence, the above equation can be written in combined and condensed matrix form as

$$\mathbf{A}_2(\omega)_{(a\times b)}\,\mathbf{x}_{2(b\times 1)} = \mathbf{B}_2(\omega)_{(a\times 1)} \tag{4.28}$$

with

$$\mathbf{A}_2(\omega) = \begin{bmatrix} 0 & \mathbf{A}_{1,0}^{m1} & \mathbf{A}_{2,0}^{m1} & \mathbf{I} & 0 & 0 & 0 \\ \mathbf{A}_{3,1} & \mathbf{A}_{1,1}^{m1} & \mathbf{A}_{2,1}^{m1} & 0 & 0 & 0 & 0 \\ 0 & 0 & 0 & 0 & \mathbf{A}_{1,0}^{m2} & \mathbf{A}_{2,0}^{m2} & \mathbf{I} \\ \mathbf{A}_{3,1} & 0 & 0 & 0 & \mathbf{A}_{1,1}^{m2} & \mathbf{A}_{2,1}^{m2} & 0 \end{bmatrix} \tag{4.29}$$

$$\mathbf{x}_2 = \begin{Bmatrix} \mathbf{e} & \mathbf{k}_s^{m1} & \mathbf{k}_i^{m1} & \mathbf{F}_c^{m1} & \mathbf{k}_s^{m2} & \mathbf{k}_i^{m2} & \mathbf{F}_c^{m2} \end{Bmatrix}^T \tag{4.30}$$

$$\mathbf{B}_2(\omega) = \begin{Bmatrix} \mathbf{B}_{1,0}^{m1} & \mathbf{B}_{1,1}^{m1} & \mathbf{B}_{1,0}^{m2} & \mathbf{B}_{1,1}^{m2} \end{Bmatrix}^T \tag{4.31}$$

Subscripts in Equation (4.28) denote the matrix or vector size, which depend upon the number of elements taken in the finite element method formulation. The total number of equations associated with (i = 0) and (i = 1) as well as the number of unknowns to be determined are shown by '*a*' and '*b*', respectively. The subscript '*b*' in the combined unknown vector $\mathbf{x}_2$ depends on the total number of disc unbalances and the number of misaligned AMB parameters with constant forces for both misalignment cases. On substituting the unknown vectors of Equation (4.25), Equation (4.30) can be written in expanded form, as

$$\begin{aligned} \mathbf{x}_2 = \Big\{ & e_1 \quad e_2 \quad \cdots \quad k_{sx1}^{m1} \quad k_{sy1}^{m1} \quad \cdots \quad k_{ix1}^{m1} \quad k_{iy1}^{m1} \quad \cdots \quad f_{11}^{m1} \quad f_{21}^{m1} \quad \cdots \\ & k_{sx1}^{m2} \quad k_{sy1}^{m2} \quad \cdots \quad k_{ix1}^{m2} \quad k_{iy1}^{m2} \quad \cdots \quad f_{11}^{m2} \quad f_{21}^{m2} \quad \cdots \Big\}^T \end{aligned} \tag{4.32}$$

Equation (4.28) is in complex form, hence it can be segregated into the real and imaginary components and written as

$$\left(\mathbf{A}_2^{\mathrm{Re}}(\omega)+\mathrm{j}\mathbf{A}_2^{\mathrm{Im}}(\omega)\right)\left(\mathbf{x}_2^{\mathrm{Re}}+\mathrm{j}\mathbf{x}_2^{\mathrm{Im}}\right)=\left(\mathbf{B}_2^{\mathrm{Re}}(\omega)+\mathrm{j}\mathbf{B}_2^{\mathrm{Im}}(\omega)\right) \tag{4.33}$$

where the subscripts Re and Im represent the real and imaginary components, respectively. Further, the real and imaginary components of this equation can be written separately to obtain all real quantities, as

$$\left\lfloor \mathbf{A}_2^{\mathrm{Re}}(\omega) \quad -\mathbf{A}_2^{\mathrm{Im}}(\omega)\right\rfloor\begin{Bmatrix}\mathbf{x}_2^{\mathrm{Re}}\\ \mathbf{x}_2^{\mathrm{Im}}\end{Bmatrix}=\mathbf{B}_2^{\mathrm{Re}}(\omega) \quad \text{and} \quad \left\lfloor \mathbf{A}_2^{\mathrm{Im}}(\omega) \quad \mathbf{A}_2^{\mathrm{Re}}(\omega)\right\rfloor\begin{Bmatrix}\mathbf{x}_2^{\mathrm{Re}}\\ \mathbf{x}_2^{\mathrm{Im}}\end{Bmatrix}=\mathbf{B}_2^{\mathrm{Im}}(\omega) \tag{4.34}$$

Equation (4.34) can be expressed in the combined form, to get estimation equation for the overall unbalance and misaligned AMB parameters, as

$$\mathbf{A}(\omega)_{(2a\times c)}\,\mathbf{x}_{(c\times 1)}=\mathbf{B}(\omega)_{(2a\times 1)} \tag{4.35}$$

with

$$\mathbf{A}(\omega)=\begin{bmatrix}\mathbf{A}_2^{\mathrm{Re}}(\omega) & -\mathbf{A}_2^{\mathrm{Im}}(\omega)\\ \mathbf{A}_2^{\mathrm{Im}}(\omega) & \mathbf{A}_2^{\mathrm{Re}}(\omega)\end{bmatrix};\quad \mathbf{B}(\omega)=\begin{Bmatrix}\mathbf{B}_2^{\mathrm{Re}}(\omega)\\ \mathbf{B}_2^{\mathrm{Im}}(\omega)\end{Bmatrix} \tag{4.36}$$

$$\begin{aligned}\mathbf{x}=\Big\{ & e_1^{\mathrm{Re}} \quad e_1^{\mathrm{Im}} \quad e_2^{\mathrm{Re}} \quad e_2^{\mathrm{Im}} \quad \cdots \quad k_{sx1}^{m1} \quad k_{sy1}^{m1} \quad \cdots \quad k_{ix1}^{m1} \quad k_{iy1}^{m1} \quad \cdots \quad f_{11}^{m1} \quad f_{21}^{m1} \quad \cdots \\ & k_{sx1}^{m2} \quad k_{sy1}^{m2} \quad \cdots \quad k_{ix1}^{m2} \quad k_{iy1}^{m2} \quad \cdots \quad f_{11}^{m2} \quad f_{21}^{m2} \quad \cdots\Big\}^T\end{aligned} \tag{4.37}$$

where the subscript '*c*' in the unknown vector **x** contain the real and imaginary parts of disc eccentricities and AMB misaligned stiffness parameters along with AMB constant forces for both misalignment cases. Here, $\mathbf{A}(\omega)$ is the regression matrix and $\mathbf{B}(\omega)$ is the vector containing known quantities, respectively. The real and imaginary parts of k^{th} disc eccentricity (with k = 1, 2, …, p) are

$$e_k^{\mathrm{Re}}=e_k\cos(\beta_k);\quad e_k^{\mathrm{Im}}=e_k\sin(\beta_k) \tag{4.38}$$

To solve simultaneous linear system of equations and obtain an exact or optimal solution, the number of unknowns must be either equal to or less than the number of equations. If the number of equations (i.e., number of rows in matrix **A** of Equation (4.35)) are more than unknown terms (**x**), then it is called overdetermined system and solved by the Moore-Penrose inverse technique. In case, Equation (4.35) is underdetermined (i.e., $2a < c$), the rotor-AMB system can be operated with at least two different speeds such that the system is transformed into overdetermined type. Increase in the number of rows of matrix **A** from more sets of displacement and current response measurements due to these different speeds, will result in Equation (4.35) as over-determinate. Moreover, to identify all the unknowns utilizing the Moore-Penrose inverse approach, Equation (4.35) can be further given in matrix form as

$$\mathbf{x} = \left(\mathbf{A}(\omega)^T \mathbf{A}(\omega)\right)^{-1} \mathbf{A}(\omega)^T \mathbf{B}(\omega) \tag{4.39}$$

Equation (4.39) can be used to determine the unknown parameters (i.e., unbalance eccentricities and its phases from real and imaginary parts (i.e., using Equation (4.38)), modified AMB stiffness coefficients, AMB constant forces for both the residual and additional trial misalignment cases) with the knowledge of measured rotor displacement and AMB current responses in the frequency domain for ($i = 0$) and ($i = 1$) and the known rotor model parameters. Better estimation of the unknown faults and AMBs parameters can be achieved by taking the system responses for the range of multiple 'n' number of rotor spin speeds using the below equation.

$$\begin{pmatrix} \mathbf{A}_{(\omega_1)} \\ \mathbf{A}_{(\omega_2)} \\ \vdots \\ \mathbf{A}_{(\omega_n)} \end{pmatrix} \mathbf{x} = \begin{pmatrix} \mathbf{B}_{(\omega_1)} \\ \mathbf{B}_{(\omega_2)} \\ \vdots \\ \mathbf{B}_{(\omega_n)} \end{pmatrix} \tag{4.40}$$

Further, the identified AMBs force-displacement constants (i.e., k_{sx1}^{m1}, k_{sy1}^{m1}, k_{sx2}^{m1}, k_{sy2}^{m1}, …) and force-current constants (i.e., k_{ix1}^{m1}, k_{iy1}^{m1}, k_{ix2}^{m1}, k_{iy2}^{m1}, …) and AMBs force constants (i.e., f_{11}^{m1}, f_{21}^{m1}, f_{12}^{m1}, f_{22}^{m1},…) for the first misalignment level (residual misalignment) as well as AMBs force-displacement constants (i.e., k_{sx1}^{m2}, k_{sy1}^{m2}, k_{sx2}^{m2}, k_{sy2}^{m2}, …) and force-current constants (i.e., k_{ix1}^{m2}, k_{iy1}^{m2}, k_{ix2}^{m2}, k_{iy2}^{m2}, …) and AMBs constant forces (i.e., f_{11}^{m2}, f_{21}^{m2}, f_{12}^{m2}, f_{22}^{m2}, …) for the second level of misalignment (additional known trial misalignment) accommodated in the **x** vector, can be utilized in estimating the amounts of misalignment (i.e., δ_{x1}, δ_{y1}, δ_{x2}, δ_{y2}, …) between the rotor and AMBs axes. Subsequently, the identified AMB coefficients (i.e, k_{sx1}^{m1}, k_{sy1}^{m1}, k_{sx2}^{m1}, k_{sy2}^{m1}, …, k_{ix1}^{m1}, k_{iy1}^{m1}, k_{ix2}^{m1}, k_{iy2}^{m1}, …, k_{sx1}^{m2}, k_{sy1}^{m2}, k_{sx2}^{m2}, k_{sy2}^{m2}, … and k_{ix1}^{m2}, k_{iy1}^{m2}, k_{ix2}^{m2}, k_{iy2}^{m2}, …) for both the misalignment cases and the estimated misalignment amounts (i.e., δ_{x1}, δ_{y1}, δ_{x2}, δ_{y2}, …) can be manipulated to identify the actual force-displacement stiffness (k_{sx1}, k_{sy1}, k_{sx2}, k_{sy2}, …) and force-current stiffness (k_{ix1}, k_{iy1}, k_{ix2}, k_{iy2}, …) coefficients (i.e., for perfectly aligned case) for '*r*' number of AMB, presented in Figure 4.1. The ratio of k_{sxq}^{m1} and k_{sxq}^{m2} of Equations (4.5) and (4.8) will be useful in estimating the misalignment amount δ_{xq}, with the known values of trial misalignment, Δ_{xq} and AMB air gap, s_0. Their ratio can be given as

$$\frac{k_{sxq}^{m1}}{k_{sxq}^{m2}} = \frac{k_{sxq}\left(1-p_{1q}^2\right)^2}{k_{sxq}\left(1-\delta_{1q}^2\right)^2} = \frac{\left\{1-\left(\delta_{1q}+\Delta_{1q}\right)^2\right\}^2}{\left(1-\delta_{1q}^2\right)^2}; \quad \delta_{1q} = \frac{\delta_{xq}}{s_0}; \quad \Delta_{1q} = \frac{\Delta_{xq}}{s_0} \tag{4.41}$$

Similarly, for the known values of Δ_{yq} and s_0, the same Equation (4.41) would be followed to estimate the residual misalignment δ_{yq} by replacing *x* with *y*. Thereafter, Equation (4.5) can be utilized for estimating the actual AMB force-displacement and force-current coefficients (k_{sxq},

k_{syq}, k_{ixq} and k_{iyq}) for q^{th} AMB, with the identified values of modified AMB constants and estimated *x*- and *y*-directional misalignment amounts. Thus, the trial misalignment approach can be utilized in estimating the disc unbalances, AMBs stiffness parameters and their residual misalignments, employing the developed mathematical model based identification algorithm. In the next section, the numerical experiments have been presented to establish the procedures proposed in this section. This will be useful in checking the accuracy and effectiveness of the methodology in a flexible rotor-AMBs system.

4.5 Numerical Experiments and Identification

Figure 4.4 shows the schematic diagram of a multidisc flexible rotor-AMB system in the *x*-*z* plane, used for the FEM modelling simulation purpose. The rotor system is fully levitated on two misaligned AMBs, which consists of a shaft connected with five offset discs and a flexible coupling with negligible mass. The misalignment of the rotor with the supported AMBs (AMB 1 and AMB 2) can be followed from Figure 4.5. Both AMBs are misaligned with the different amounts in the *x*- and *y*-directions, thus this misalignment is the combination of lateral and angular misalignments. AMB 1 and AMB 2 are misaligned from the rotor centre (C) by the amounts of δ_{x1} and δ_{x2} in the *x* direction. Similarly, δ_{y1} and δ_{y2} are the amounts of residual misalignments of AMB 1 and AMB 2 in the *y* directions, respectively. In Figure 4.4, the two discs, i.e. disc 2 and disc 5, are the cores of AMB 1 and AMB 2, respectively. The unbalance faults are assumed to be present in disc 1, disc 3 and disc 4 only, not in AMBs cores. AMB 1 and AMB 2 are anisotropic in nature with different stiffness coefficients. The whole rotor system is modelled with Timoshenko beam theory, in which the gyroscopic effects due to shaft and the proportional shaft damping matrix are taken into account. Although the radius of shaft is very small as compared to the shaft length, but the shaft modelling can done more accurately

with Timoshenko beam theory (TBT), which includes effects of shear deformation and rotary inertia (Nelson, 1980). This violates the assumptions of Euler-Bernoulli beam theory (EBT). For finite element modelling of the flexible rotor-AMB system as shown in Figure 4.4, the rotor shaft is divided into 5 number of one–dimensional finite elements of different lengths. The five number of elements have been taken based on best accuracy in the results. More than 5 number of elements does not affect the results of the analysis. Moreover, it is only needed that the discs, AMBs and coupling positions in the shaft (as shown in Figure 4.4) must be considered as nodes, so that the system responses at those nodes can be utilized in the identification equation for estimation of various parameters. There are four DOFs viz. two linear and two angular displacements at each node in the *x*-*z* and *y*-*z* planes. Active magnetic bearings marked as AMB 1 and AMB 2, are placed at node 2 and node 5, respectively. The first disc, third disc and fourth disc (in which unbalance faults are considered) are placed at the nodes 1, 3 and 4, respectively. The cores of AMBs (i.e., the second disc and fifth disc) are also placed at AMBs nodes.

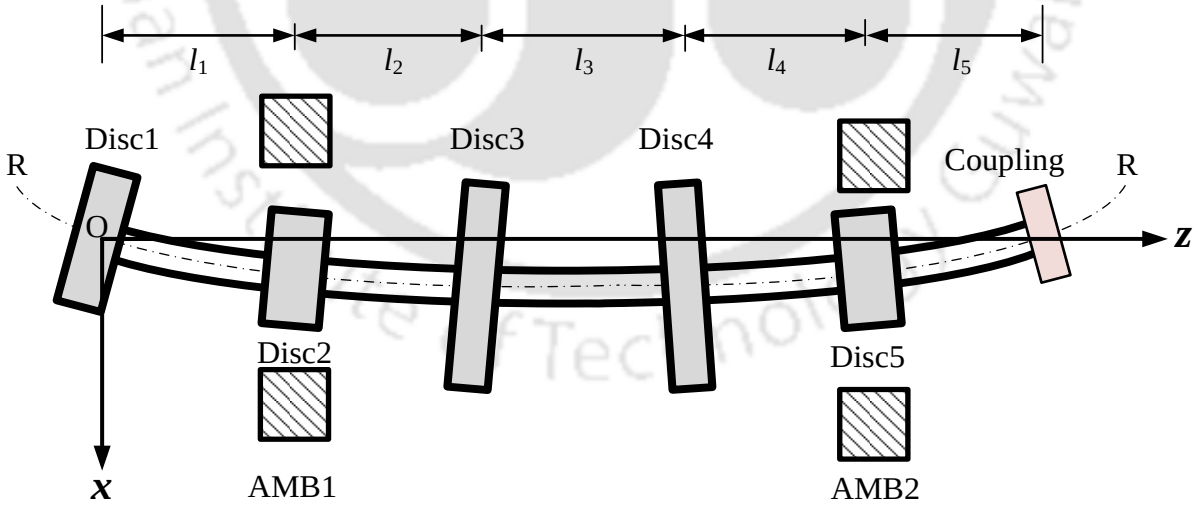

Figure 4.4 A multidisc flexible rotor-AMB system for the numerical simulation in the *x*-*z* plane.

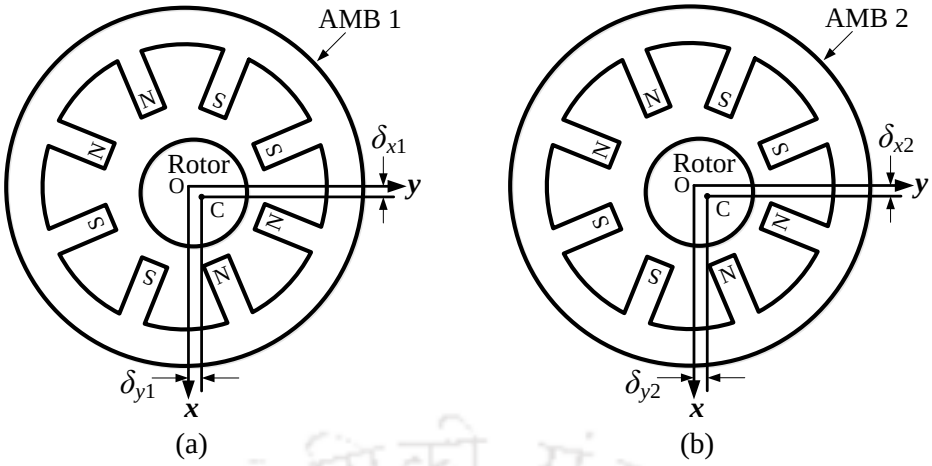

Figure 4.5 Side view of the rotor residually misaligned with AMB in the *x-y* plane (a) AMB 1 location (b) AMB 2 location.

4.5.1 Simulated Responses and Dynamic Effect of Residually Misaligned AMBs

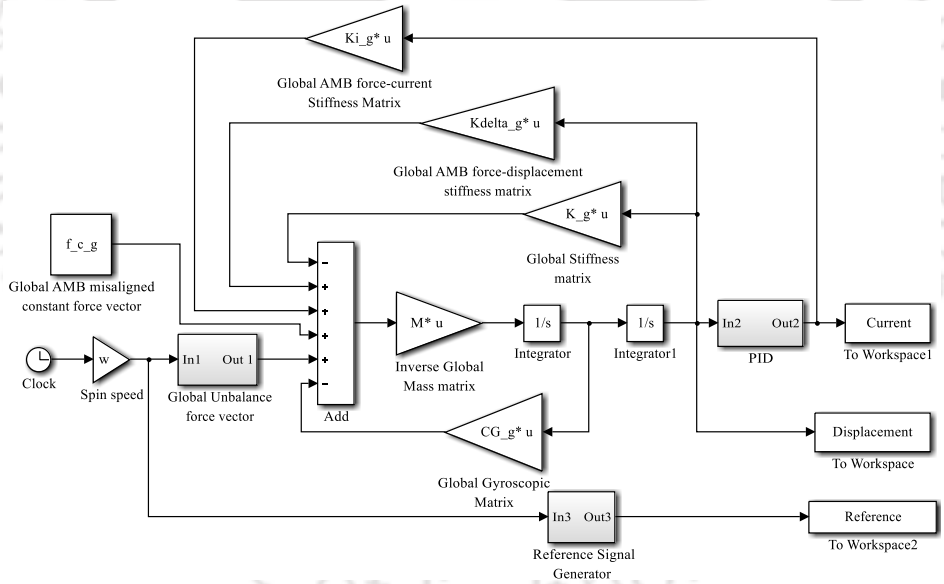

Figure 4.6 Simulink diagram for FEM modelling response generation.

A Simulink model (shown in Figure 4.6) has been built to solve the global equation of motion (i.e., Equation (4.12)) of the unbalanced and misaligned flexible rotor-AMB system in the time domain, for residual and additional trial misalignments. The solutions would give the rotor displacement responses at all nodes and controlling current response at AMB locations for both the cases of AMB misalignment.

Table 4.1 The assumed data of the rotor and unbalance fault for the simulation purpose.

Rotor and unbalance fault parameters	**Assumed values**
Shaft diameter, d and length, l	15.6 mm and 500 mm
Modulus of elasticity of shaft, E	2.1×10^{11} N/m^2
Density of shaft material, ρ	7850 kg/m^3
Disc 1 mass: m_{d1}	0.69 kg
Disc 2 and Disc 3 mass: m_{d2}, m_{d3}	0.85 kg, 1.5 kg
Disc 4 and Disc 5 mass: m_{d4}, m_{d5}	1.5 kg, 0.85 kg
Disc 1, Disc 3, Disc 4 eccentricities: e_1, e_2, e_3	50, 80 and 100 μm
Disc 1, Disc 3, Disc 4 eccentricity phase: β_1, β_2, β_3	10, 30 and 50 deg.
Diametral mass moment of inertia of the disc 1, I_{d1}	4.1×10^{-4} kg-m^2
Diametral mass moment of inertia of the disc 2 and disc 3, I_{d2}, I_{d3}	5.04×10^{-4} and 1.4×10^{-3} kg-m^2
Diametral mass moment of inertia of the disc 4 and disc 5, I_{d4}, I_{d5}	1.4×10^{-3} and 5.04×10^{-4} kg-m^2
Polar mass moment of inertia of the disc 1, I_{p1}	8.2×10^{-4} kg-m^2
Polar mass moment of inertia of the disc 2 and disc 3, I_{p2}, I_{p3}	10.08×10^{-4} and 2.8×10^{-3} kg-m^2
Polar mass moment of inertia of the disc 4 and disc 5, I_{p4}, I_{p5}	2.8×10^{-3} and 10.08×10^{-4} kg-m^2
Distance between each disc, l_1, l_2, l_3, l_4, l_5	70, 130, 120, 110, 70 (in mm)

Table 4.2 The values of properties of AMBs and PID controller.

AMB parameters	**Assumed Values**	**Controller parameters**	**Assumed Values**
AMB 1 force-displacement stiffness in x direction, k_{sx1}	174150 N/m	Proportional, k_P	6000 A/m
AMB 1 force-displacement stiffness in y direction, k_{sy1}	195000 N/m	Derivative, k_D	3 A-s/m
AMB 2 force-displacement stiffness in x direction, k_{sx2}	365710 N/m	Integral, k_I	8000 A/m-s
AMB 2 force-displacement stiffness in y direction, k_{sy2}	383000 N/m	Air gap between rotor and AMB 1, s_0	0.400 mm
AMB 1 force-current stiffness in x direction, k_{ix1}	34.83 N/A	Air gap between rotor and AMB 2, s_0	0.400 mm
AMB 1 force-current stiffness in y direction, k_{iy1}	36.20 N/A	Bias current, i_0	2 A
AMB 2 force-current stiffness in x direction, k_{ix2}	73.14 N/A	Number of poles	8
AMB 2 force-current stiffness in y direction, k_{iy2}	75.40 N/A	Angle between two adjacent poles, α	45 deg

The numerical data of rotor and unbalance fault utilized for the numerical simulation is depicted in Table 4.1. Similarly, Table 4.2 presents the values of AMB and PID controller parameters. The assumed values of residual misalignments (δ_{x1}, δ_{y1}, δ_{x2} and δ_{y2}) and trial misalignments (Δ_{x1}, Δ_{x1}, Δ_{x1} and Δ_{x1}) of AMBs have been taken from Table 3.1. The values of gains of PID controller (i.e., k_P, k_I and k_D) in Table 4.2 have been selected on the basis of tuning from Routh-Hurwitz stability criteria (refer Appendix D), to have a stable vibration and controlling current responses of the flexible rotor-AMB system. For the assumed rotor model and AMB parameters, the first five natural frequencies of the rotor system using the free-free support boundary conditions are 0 Hz, 0 Hz, 53.88 Hz, 113.80 Hz and 178.48 Hz, respectively. The first natural frequency '0 Hz' corresponds to the translational motion in the *x*-direction at node 1, whereas the second natural frequency '0 Hz' corresponds to the rotational motion in the *x*-*z* plane at the same node. The third natural frequency '53.88 Hz' corresponds to the translational motion in the *x*-direction at node 2, whereas the fourth natural frequency '113.8 Hz' corresponds to the rotational motion in the *x*-*z* plane at the same node, i.e., node 2. The fifth natural frequency '178.48 Hz' corresponds to the translational motion in the *x*-direction at node 3. There will be an identical set of natural frequencies for the translational motion in the *y*-direction and the rotational motion in the *y*-*z* plane at the corresponding nodes.

Here, the first two natural frequencies are found to be zero, which represent the translational and rotational rigid body mode shapes of the rotor. The rotor will have rigid body up and down motion corresponding to the translational rigid body mode and it will have rigid body rotation about the centre of gravity for the rotational rigid body mode.

The rotor displacements at all nodes and current responses at both AMB positions have been obtained using a fourth-order Runge-Kutta differential solver with 0.0001 s fixed time step size. The numerical simulation for the flexible rotor-AMB system was undertaken for 5 s using data given in Table 4.1, Table 4.2 and Table 3.1 (only the values of residual and trial

misalignments). To investigate the dynamic influence of AMB residual misalignment in a flexible rotor mounted on active magnetic bearings, the simulated results have been obtained at 120 Hz rotor angular frequency (i.e., rotor spin speed of 753.98 rad/s) for without and with misalignment. Figure 4.7 presents the orbit plots for the generated rotor displacement as well as controlling current output to show the effect of residual misalignment of AMB on the rotor system, at node 2 and node 5 of the shaft. Residual misalignment is the unknown misalignment between the axes of rotor and supported AMBs, which may be created due to initial setting errors, assembling errors and sensor measurement errors, etc. The nodes 2 and 5 are the locations of AMB 1 and AMB 2 in the considered flexible rotor-AMB system. At node 2, the peak values of displacement without and with misalignment are found to be at 2.86×10^{-5} m and 4.20×10^{-5} m, respectively. The absolute maximum values of current are 0.183 A and 0.893 A for without and with misalignment at the same node. Related to AMB perfect alignment at both locations, these responses are observed to be higher for the misalignment state. These increments in the percentage are 46.99% and 388% respectively, for the rotor displacement and AMB current.

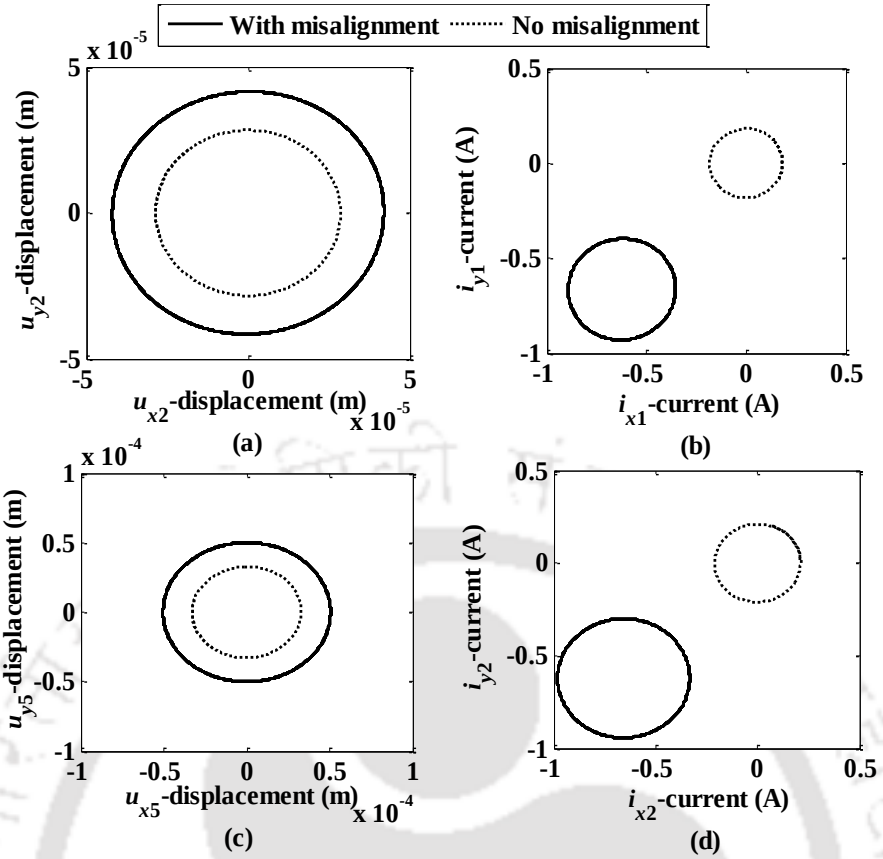

Figure 4.7 Influence of AMB residual misalignment on the rotor system orbital response (a) Rotor displacement at AMB 1 (b) Controlling current at AMB 1 (c) Rotor displacement at AMB 2 (d) Controlling current at AMB 2.

Similarly, for the AMB misalignment state, the absolute peak values of vibration response and current output of PID controller at node 5 are 5.05×10^{-5} m and 0.982 A, respectively. However, the values are only 3.29×10^{-5} m and 0.211 A for the perfectly aligned case. Hence, the displacement and current responses at this node have been enhanced by 53.5% and 365.4% due to severe misalignment fault. Growth in the response magnitudes and more power consumption motivates a researcher to identify quantitatively the residual misalignments between the rotor and AMB. One of important points can be observed from Figure 4.7(b) and 4.7(d) that the current orbit for AMB misalignment condition at nodes 2 and 5 has been moved away from the zero mean positon unlike the perfect alignment state. This is caused due to

constant force of AMB, f_{1q}^{m1} in the *x*- and *y*-directional misaligned AMB force (refer Equation (4.4)), which appears during present formulation of misalignment. This constant force also causes to displace the rotor displacement responses, but these response signals get compensated through the integral gain factor (k_I) of PID controller. The integral factor shifts them to the mean position by introducing a non-zero mean biased controlling currents.

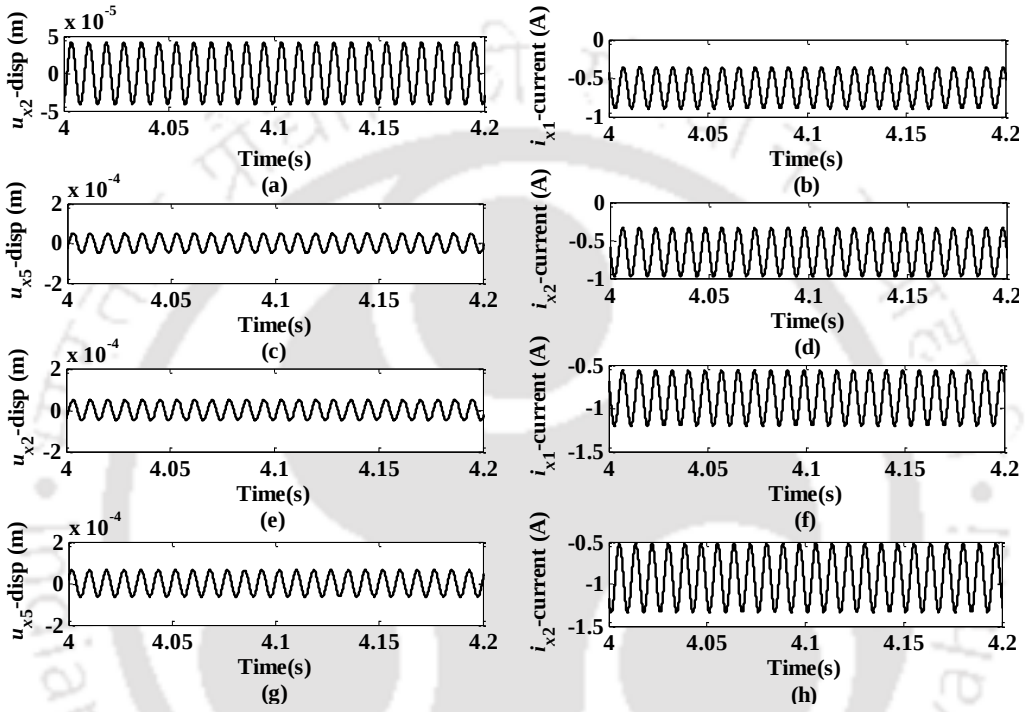

Figure 4.8 System responses in the time domain (a, b) *x*-displacement and current at AMB 1 (c, d) *x*-displacement and current at AMB 2 for residual misalignment case (e, f) *x*-displacement and current at AMB 1 (g, h) *x*-displacement and current at AMB 2 for additional trial misalignment case.

4.5.2 Quantitative Estimation of Unbalance and AMB Misalignment Parameters

For further dynamic vibrational analysis and parameters identification, the rotor displacement and controlling current responses were considered for the time length of 1 s (i.e., time duration from 4 s to 5 s) at various node positions. For the residual and additional trial misalignments, the numerically simulated *x*-directional rotor displacement and current signals in the time domain at node 2 and node 5 are presented in Figure 4.8. These figures have been

plotted at the same rotor angular frequency of 120 Hz. This high-speed for operating AMB-rotor has been arbitrarily selected far away from the first critical speed (i.e., 53.88 Hz) of the rotor system. This is essentially required for measurement related issue near critical speeds. In time domain, the amplitude of displacement responses at AMB 1 and AMB 2 locations are observed to be 4.20×10^{-5} m and 5.05×10^{-5} m, whereas the absolute values of current amplitudes are 0.893 A and 0.982 A, for the residual misalignment case. Apart from this, for the case of additional trial misalignment, the maximum displacement and current values are (5.00×10^{-5} m and 1.203 A) at node 2 and (6.43×10^{-5} m and 1.340 A) at node 5, respectively. From these generated signals data, it can be ascertained that as the misalignment level between the flexible rotor and AMBs increases, there is increment in the displacement and current responses at both AMB locations. The similar pattern would be followed for the displacement signal at all other nodes of the shaft.

Moreover, the time domain data has been converted into frequency domain signals from the fast Fourier transform (FFT) algorithm. FFT function of MATLAB™ is utilized for this purpose. With this approach, the complex values of rotor displacement signals at all nodes (node 1 through node 6) and current signals at only nodes 2 and 5 have been transformed to the frequency domain. For both the conditions of misalignment, the amplitudes and corrected phases using reference signal (refer Appendix C) of FFT processed signals at the nodes where AMBs are residing, are plotted in Figure 4.9.

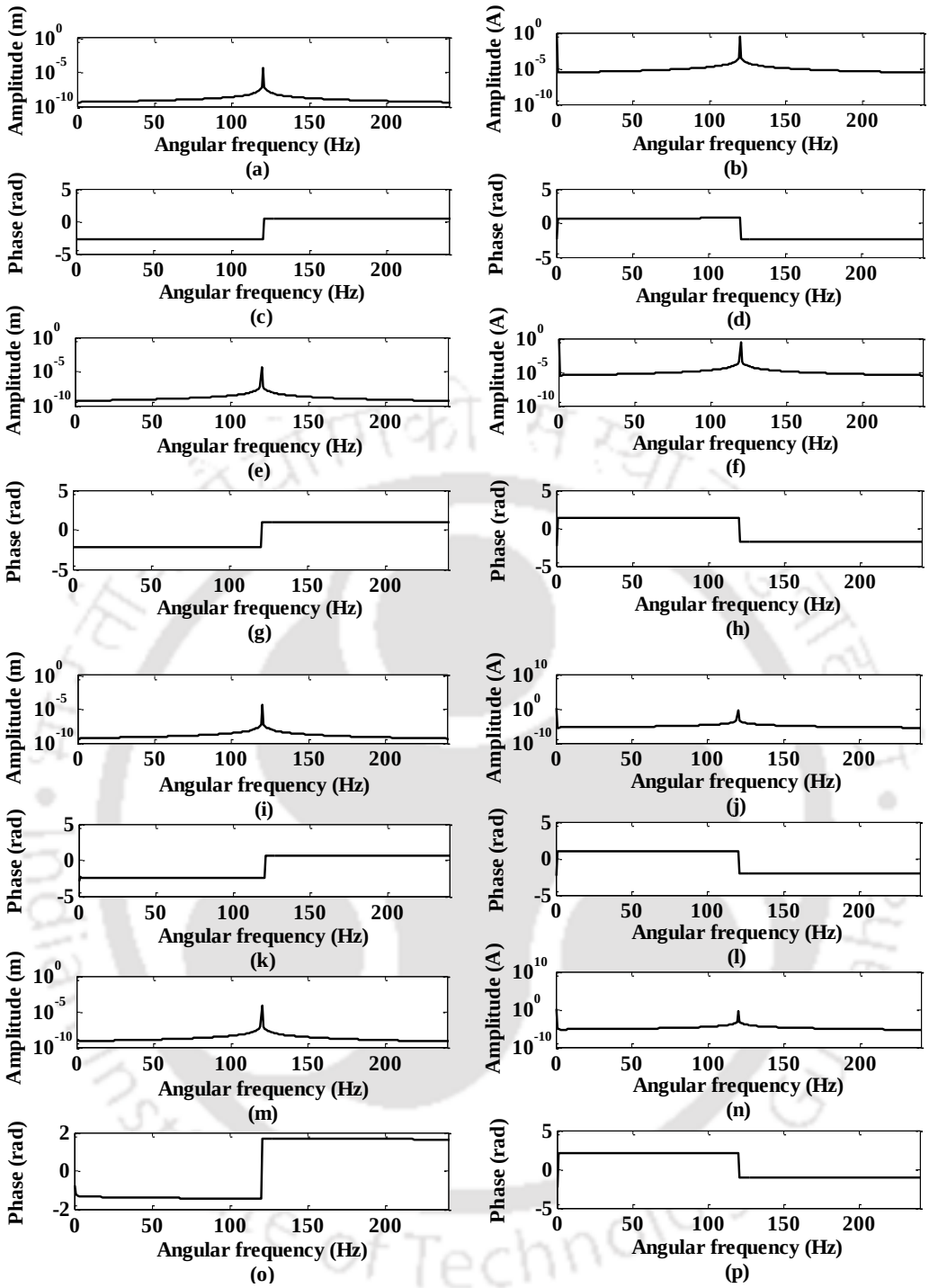

Figure 4.9 FFT processed frequency domain responses (a-d) displacement and current amplitudes as well as corrected phases at node 2 (e-h) displacement and current amplitudes as well as corrected phases at node 5 for residual misalignment case (i-l) displacement and current amplitudes as well as corrected phases at node 2 (m-p) displacement and current amplitudes as well as corrected phases at node 5 for additional trial misalignment case.

Following Figure 4.9 at the rotor angular frequency of 120 Hz, the frequency domain data (i.e., amplitude and corrected phase) of rotor displacement and current signals, for (i = 0, 1) are displayed in Table 4.3. Observations can be made from Table 4.3 that for the residual misalignment condition, the peak values of the frequency domain displacement as well as AMB current signals at nodes 2 and 5 respectively, are 4.18×10^{-5} m and 0.911 A as well as 5.03×10^{-5} m and 0.905 A. However, the frequency domain signals peaks are found to be 4.72×10^{-5} m and 1.271 A as well as 6.53×10^{-5} m and 1.278 A, at node 2 and node 5 for additional trial misalignment case for both (i = 0) and (i = 1). Vibration amplitude values for the additional trial misalignment are also noticed to be higher than the residual misalignment state. Correspondingly, the more power would be consumed for driving the magnetic bearing and levitating the rotor stably during operation, for the case of additional trial misalignment as compared to residual misalignment.

Table 4.3 Rotor displacement and controlling current harmonics obtained from FFT analysed responses at node 2 and node 5 for both residual and additional trial misalignments.

			Displacement (R_i)		Current (I_i)	
Misalignment	Nodes	(i)	Amplitude (m)	Phase (deg)	Amplitude (A)	Phase (deg)
Residual misalignment	Node 2	0	4.21×10^{-10}	-159.68	9.11×10^{-1}	-133.21
		1	4.18×10^{-5}	-159.57	2.68×10^{-1}	40.99
	Node 5	0	5.01×10^{-10}	-123.99	9.05×10^{-1}	-136.59
		1	5.03×10^{-5}	-123.59	3.23×10^{-1}	76.95
Additional trial misalignment	Node 2	0	5.34×10^{-10}	-166.56	12.71×10^{-1}	-133.96
		1	4.72×10^{-5}	-142.04	3.03×10^{-1}	58.50
	Node 5	0	7.72×10^{-10}	-42.55	12.78×10^{-1}	-136.53
		1	6.53×10^{-5}	-83.31	4.19×10^{-1}	117.23

It can also observed from Table 4.3 for both the residual and additional trial misalignment cases that the displacement displayed in this table is of order 10^{-10} m for (i = 0) harmonic. The zero '0' harmonic term is coming into the picture due to the presence of constant

AMB force in the present formulation of force due to misaligned AMB. The order of 10^{-10} m in the displacement is due to the integral factor (k_I) of the PID controller, which shows that the effect of constant AMB force is reduced in the rotor-AMB system.

The real as well as imaginary components of the complex rotor displacement harmonics at all nodes and controlling current harmonics at nodes 2 and 5 are captured from the magnitudes and phases of FFT processed responses, for both the cases of AMB misalignment. Afterwards, these values are given as input in the identification equation (4.35) for estimating the parameters concerned with unbalance, misalignment and AMB stiffness parameters. For the considered flexible rotor-AMB system as shown in Figure 4.4, the number of equations in the regression matrix $\mathbf{A}(\omega)$ are found to be 28 only. However, the number of unknowns in the vector $\mathbf{x}$ is 30, which is greater than the number of equations (commonly known as underdetermined system). These unknown parameters include 6 parameters of unbalance faults (e_1, β_1, e_2, β_2, e_3, β_3), 12 parameters ($k_{sx1}^{m1}, k_{sy1}^{m1}, k_{sx2}^{m1}, k_{sy2}^{m1}, k_{ix1}^{m1}, k_{iy1}^{m1}, k_{ix2}^{m1}, k_{iy2}^{m1}, f_{11}^{m1}, f_{21}^{m1}, f_{12}^{m1}, f_{22}^{m1}$) related to misaligned AMBs for the residual misalignment and other 12 misaligned AMB parameters ($k_{sx1}^{m2}, k_{sy1}^{m2}, k_{sx2}^{m2}, k_{sy2}^{m2}, k_{ix1}^{m2}, k_{iy1}^{m2}, k_{ix2}^{m2}, k_{iy2}^{m2}, f_{11}^{m2}, f_{21}^{m2}, f_{12}^{m2}$ and f_{22}^{m2}) for additional trial misalignment case.

Even though the identification algorithm is undetermined system, it can be made an overdetermined system of linear equations by using multiple rotor speeds. Originally, there are 28 equations and 30 unknowns at a single speed. However, the equations can be increased to 56 with the consideration of the vibration and current harmonics data at another spin speed. Now, the updated size of regression matrix $\mathbf{A}$ is (56×30), with the number of unknowns in the vector $\mathbf{x}$ remain 30 only. Hence, this is the class of overdetermined system. To obtain the solution of this overdetermined system of linear equations, the Moore-Penrose inverse (i.e., Equation (4.39)) has been utilized. This method provides the optimized values of the estimated

system and fault parameters in all cases considered. As such for present case methodology was found to be robust even with the addition of noise in responses. This can be observed further in this section only. For making the identification equation (i.e., Equation (4.35)) overdetermined type, the other high speed chosen to operate the rotor-AMB system in numerical simulation is 130 Hz. For the residual and additional trial misalignments, the real and imaginary components of FFT analysed frequency domain rotor displacement and AMB current signals for (i = 0 and 1), at the angular frequencies of 120 Hz and 130 Hz are the key elements of known **A** matrix and **B** vector for the identification purpose. The two different speeds have been selected in order to apply the identification scheme. These speeds are chosen well above the first critical speed (i.e., 53.88 Hz) of the rotor system to exhibit the shaft flexibility behaviour throughout the operation of AMBs levitated rotor. These speeds are also selected far away from the critical speeds (at least away from the half-power band), since in real practice taking measurements near critical speeds is not feasible due to transients. Therefore, the proposed methodology for estimating system and fault parameters near the critical speed has been avoided which are often associated with transients during measurement of responses.

It is worth mentioning that Figure 4.9 depicts the plots of amplitude and phase of frequency domain displacements and currents with the consideration of material damping of the shaft in the rotor system relying on proportional damping concept (follow $\mathbf{C}^{(e)}$ and **C** matrices in Equations (4.1) and (4.12)). Apart from this, AMB is also providing damping in the system from the PID controller. However, it is also true that in a real system, the sources of damping do exist (e.g. damping in the foundation of AMBs, and damping in other type of bearings when included, e.g. fluid film bearings). Then modelling of such components needs to be considered in the system. Often such damping is difficult to find analytically and using

the present identification procedure such damping (as well as stiffness) parameters can also be estimated along with the present identified parameters.

To mimic the actual rotor vibration and AMB current responses in a rotor system, the random Gaussian noise signals of 1%, 2% and 5% levels have been deliberately added to the numerically simulated responses for both the conditions of AMB misalignment (follow Section 2.5.1 and Appendix E for details in noise and its mathematical model). Further, the real as well as imaginary components of noise added frequency domain signals are used in the identification equation to estimate the several unknown parameters.

Table 4.4 Effect of measurement noise signal and modelling errors on the identified unbalance parameters at the combined angular frequencies of 120 Hz and 130 Hz.

Parameters	**Assumed values**	**Error percentage in identified values with addition of noise and modelling or bias errors**						
		Clean signal	1% noise	1% bias	2% noise	2% bias	5% noise	5% bias
e_1 (μm)	50	-0.08%	0.12%	0.12%	0.33%	0.16%	0.74%	0.25%
β_1 (deg)	10	0.05%	0.08%	0.05%	0.11%	0.06%	0.27%	0.01%
e_2 (μm)	80	0.02%	-0.04%	-0.02%	-0.11%	-0.03%	-0.12%	-0.09%
β_2 (deg)	30	-0.02%	-0.23%	-0.03%	-0.44%	-0.29%	-0.97%	-0.52%
e_3 (μm)	100	0.01%	0.01%	0.02%	-0.05%	-0.08%	-0.13%	-0.13%
β_3 (deg)	50	-0.02%	-0.02%	-0.03%	0.07%	-0.06%	-0.08%	-0.08%

Moreover, the estimation of rotor unbalance and misaligned AMB parameters for residual and additional trial misalignments included in the **x** vector of Equation (4.37) have also been performed for rotor modelling or bias errors (its description is also explored in Section 2.5.1). The random errors of 1%, 2% and 5% are introduced simultaneously in the numerical model parameters such as material density of shaft and disc (ρ), modulus of elasticity

of shaft (E), moment of inertia of disc (I_d). Thus, the shaft mass and stiffness matrices and disc mass matrix discussed in Section 4.3 get modified. With these modified matrices of the system, the displacement and current responses are numerically generated and used in the identification equation (i.e., Equation (4.35)) to estimate the faults and AMB parameters.

Tables 4.4-4.6 depict the percentage deviation in estimated values as compared to the assumed values of unbalance fault parameters (i.e., disc eccentricities and phases), AMBs residual misalignments and actual AMBs stiffness coefficients (force-displacement and force-current constants) for clean signal and up to 5% noise added signals and modelling errors. The estimation results have been obtained considering the displacement and current responses at the rotor angular frequencies of 120 Hz and 130 Hz. For clean signal, the estimated values of unbalance parameters (e_1, β_1, e_2, β_2, e_3, β_3) are found to be very less deviated with respect to the assumed values in Table 4.4. The minimum and maximum absolute values of percentage error in estimation are 0.01% and 0.08% for eccentricities e_3 and e_1, respectively. All three phases (β_1, β_2 and β_3) of unbalance have been estimated with the percentage errors of only 0.05%, -0.02% and -0.02% for the clean signal, respectively. However, the estimated values are slightly get deviated from the assumed ones with the addition of 1%, 2% and 5% noise errors. Overall the absolute values of percentage error in estimating unbalance fault parameters are in the range of 0.01% to 0.97% with addition of different levels of noise error in the generated displacements and current responses at each node. It can also be observed from Table 4.4 that the percentage deviation in the estimated values of almost all the unbalance parameters increases with the increment in the addition of noise error up to 5% level. Similarly, with up to 5% addition of modelling error, any unbalance parameters are not affected severely. The absolute percentage errors in the estimation lie within the range of 0.01% to 0.52% only. Furthermore, the percentage deviation in the estimated values of unbalance parameters from

the corrupted noise signal is also found to be more than the modelling error affected estimations.

Moreover, the estimated values of modified force-displacement AMBs ($k_{sx1}^{m1}, k_{sy1}^{m1}, k_{sx2}^{m1}$, k_{sy2}^{m1}) parameters for without trial misalignment and ($k_{sx1}^{m2}, k_{sy1}^{m2}, k_{sx2}^{m2}, k_{sy2}^{m2}$) for trial misalignment from solving Equation (4.35) along with the known values of user provided misalignment (Δ_{x1}, Δ_{y1}, Δ_{x2}, Δ_{y2}) as displayed in Table 3.1, have been further evaluated using Equation (4.41) to determine quantitatively the amounts of residual misalignments (δ_{x1}, δ_{y1}, δ_{x2}, δ_{y2}). It can be observed from Table 4.5 that even with the addition of highest level of noise signal and rotor modelling errors, the residual misalignments are well estimated with the maximum percentage error of -9.66% (for δ_{y2}) and -6.67% (for δ_{x2}), respectively. The percentage deviation of identified values of δ_{x1} are also found to be in the range of 0.71% to -7.86% for clean, noise added signals and modelling errors. Thus, the estimation process in identifying residual misalignments is found to be quite immune under the effect of modelling errors as well as noise errors.

Table 4.5 Effect of measurement noise signal and modelling errors on the identified AMBs residual misalignments at the combined angular frequencies of 120 Hz and 130 Hz.

Parameters	**Assumed values**	**Error percentage in identified values with addition of noise and modelling or bias errors**						
		Clean signal	1% noise	1% bias	2% noise	2% bias	5% noise	5% bias
δ_{x1} (mm)	0.140	0.71%	-0.71%	0.71%	-3.57%	1.43%	-7.86%	2.86%
δ_{y1} (mm)	0.160	1.25%	-1.88%	2.50%	9.38%	-1.25%	-7.50%	-1.88%
δ_{x2} (mm)	0.150	0.67%	1.33%	-6.00%	1.33%	-6.00%	2.67%	-6.67%
δ_{y2} (mm)	0.145	3.45%	-1.38%	3.45%	-6.90%	4.14%	-9.66%	6.21%

Additionally, the estimation of actual AMB force-displacement (k_{sx1}, k_{sy1}, k_{sx2}, k_{sy2}) and force current coefficients (k_{ix1}, k_{iy1}, k_{ix2}, k_{iy2}) for perfectly aligned case has also been done using the novel trial misalignment approach and the developed identification algorithm. This estimation was not performed in the previous two chapters i.e., Chapters 2 and 3. As these stiffness constants are extremely important and play a vital role in the rotor dynamic vibrational analysis and system stability, thus they should be identified from an AMB integrated rotor system. Following Equation (4.5), the actual force-displacement constants (k_{sx1}, k_{sy1}, k_{sx2}, k_{sy2}) of both AMBs have been identified using the earlier estimated values of ($k_{sx1}^{m1}, k_{sy1}^{m1}, k_{sx2}^{m1}, k_{sy2}^{m1}$) as a solution of Equation (4.35) and the identified values of residual misalignments (δ_{x1}, δ_{y1}, δ_{x2}, δ_{y2}). Similarly, utilizing the same equations, the estimated values of ($k_{sx1}^{m1}, k_{sy1}^{m1}, k_{sx2}^{m1}, k_{sy2}^{m1}$) and (δ_{x1}, δ_{y1}, δ_{x2}, δ_{y2}) have been evaluated to estimate the actual force-current stiffnesses (k_{ix1}, k_{iy1}, k_{ix2}, k_{iy2}) of AMB 1 and AMB 2.

It can be noticed from Table 4.6 that the percentage variation of the identified parameter k_{sx1} lies within the range of -0.05% to 8.41% for clean and noise corrupted signals. The least affected parameter is k_{sx2}, with only percentage error of -3.36 % at 2% noise addition. Comparatively, all the force-displacement coefficients of both AMBs are observed to be less affected than the force-current stiffness constants with the additions of 1%, 2% and 5% noise addition. Besides this, AMBs constants have also been identified excellently with the variations in acceptable range under the effect of modelling errors. Therefore, the developed identification algorithm based on novel trial misalignment approach is observed to be robust and effective in estimating all the identifiable unbalance, misalignment and AMB stiffness parameters, even with the addition of different levels of random Gaussian noise and rotor modelling errors.

Table 4.6 Effect of measurement noise signal and modelling errors on the identified actual AMBs stiffness constants at the combined angular frequencies of 120 Hz and 130 Hz.

Parameters	**Assumed values**	**Error percentage in identified values with addition of noise and modelling or bias errors**						
		Clean signal	1% noise	1% bias	2% noise	2% bias	5% noise	5% bias
k_{sx1} (N/m)	174150	-0.05%	1.96%	0.82%	4.07%	0.29%	8.41%	-0.60%
k_{sy1} (N/m)	195000	-1.85%	4.13%	-2.72%	-23.62%	0.06%	15.97%	0.37%
k_{sx2} (N/m)	365710	-1.31%	-2.25%	6.98%	-3.36%	7.33%	-2.93%	8.37%
k_{sy2} (N/m)	383000	-3.44%	3.14%	-3.47%	7.95%	-3.99%	10.18%	-5.10%
k_{ix1} (N/A)	34.83	12.85%	13.62%	12.88%	16.39%	12.28%	21.04%	11.29%
k_{iy1} (N/A)	36.20	14.08%	18.59%	13.08%	9.11%	16.21%	27.30%	16.49%
k_{ix2} (N/A)	73.14	13.24%	9.87%	21.83%	7.84%	22.76%	7.66%	23.68%
k_{iy2} (N/A)	75.40	10.63%	15.58%	10.62%	20.37%	10.03%	22.51%	8.76%

Although the proposed identification procedure has been applied for two AMBs in this section, the developed methodology can also allow for analysis of rotors with more than two AMBs. This can be followed from the generalized form of the identification equation (i.e., Equation (4.35)), which has been developed for r number of supported AMBs and p number of discs, as shown in Figure 4.1. The unknown vector **x** in Equation (4.35) consists of the several unbalance parameters and multiple modified AMBs force-displacement and force-current stiffness parameters as well as constant force of AMBs due to misalignment. Altogether, it can be stated from this work that the various results of numerical simulation based on the finite element modelled rotor-AMB dynamic analysis and estimation of parameters manifest the accuracy and stability of the developed identification algorithm.

It is also to be noted that the present methodology is based in simulations where linear harmonic analysis is performed and linear harmonic response is assumed. However, in practice the rotor-AMB system is to be designed to have least vibrations in rotor and most of cases such linearity could be justified. However, this is not always the case in rotor systems and nonlinearities do exist. Moreover, if nonlinearity would be considered in the present rotor-AMB system, then the solution of equations of motion for this system can be obtained with the help of Runge-Kutta fourth order method as explained in Desale and Dasre (2013). Further, the FFT analysed responses can be given as input to the developed identification methodology, which can be solved to estimate the system and fault parameters using nonlinear regression analysis (Bates and Watts, 1988).

4.6 Summary

In this chapter, the finite element modelling, dynamic vibrational analysis and identification of a fully levitated flexible rotor with unbalance and misalignment faults have been investigated using active magnetic bearings (AMBs). The combination of lateral and angular misalignments are considered between rotor and AMBs axes. To overcome the practical difficulty in measuring responses, a gyroscopic dynamic reduction scheme has been implemented to eliminate the transverse rotational degrees of freedom from the system model.

A novel idea of trial misalignment approach and identification algorithm (based on utilizing frequency domain displacement and AMBs controlling current signals) have been developed to estimate simultaneously the unbalance and misaligned AMB parameters for residual and additional trial misalignments. These are further employed to determine the unknown residual misalignments. Additionally, the actual force-displacement and force-current stiffness coefficients of AMBs (of anisotropic nature) are also identified, which were not done in the previous chapters.

For demonstrating the proposed novel identification scheme, an unbalanced flexible shaft with multiple discs levitated by multiple misaligned AMBs has been mathematically modelled utilizing finite element method based on Timoshenko beam theory. Equations of motion for each sub-model (shaft, discs and misaligned AMB force model) have been presented individually and further assembled together to obtain a global equation of motion of the rotor-AMB system. The equation of motion has been numerically simulated to obtain the displacement and current responses in the time domain at higher spin speeds. These high speeds were picked above the first critical speed to exhibit flexibility nature of rotor throughout its motion.

Further, the frequency domain responses (obtained from FFT as discussed in Section 2.4.1) were captured at two different spin speeds (it was required for overcoming the ill-conditioning of regression matrix and making the system overdeterminate) and used in the developed identification algorithm to estimate the disc unbalance eccentricities and phases, residual misalignments, the actual force-displacement and force-current stiffnesses of AMBs. Dynamic effect of AMBs misalignment on the rotor displacement and controlling current signals was also presented in this work. More deviations were observed in the system responses for the misaligned case relative to perfectly aligned case. The developed identification algorithm is also found to be effective and robust when tested against different levels of noise errors in responses and modelling errors in the rotor parameters.

The present chapter serves to establish a procedure for flexible rotor-AMB system with greater complexities. However, the technique used for providing known trial misalignments in the system was based on the PTM approach (discussed in Section 2.3.2.2). To overcome the limitations of PTM approach, the next chapter proposes a virtual trial misalignment (VTM) concept based on additional bias current provided at AMB locations. In this approach, the rotor will be shifted with respect to its original position instead of AMB housings by the same trial

misalignment amounts. Apart from this, to make more realistic and generic model, the proximity sensors located at AMB locations for measuring the displacements will also be considered offset with respect to the rotor centre. The linearized form of misaligned AMB force will be derived considering the case of misalignment in sensors. Moreover, the offset amounts of sensors will also be identified using VTM approach in addition to identification of system and faults parameters done in this chapter.

Chapter 5

Finite Element Modelling and Identification in a Misaligned Flexible Rotor-Sensor-AMB System

5.1 Introduction

In the previous chapter, a FEM based model of an unbalanced multidisc flexible rotor supported on multiple misaligned AMBs was presented and analysed by numerically generated time and frequency domain responses. A novel identification algorithm based on trial misalignment concept was developed to estimate the disc unbalance parameters, AMBs residual misalignments and their stiffness constants. The misalignment was considered only between the axes of rotor and AMBs. The physical trial misalignment (PTM) approach (described in Section 2.3.2.2) was utilized to provide known trial misalignments to the actuator housings. The sensors were assumed to be perfectly aligned with respect to the rotor operating axis.

However, in a practical rotor system integrated with AMBs, the sensors can also be misaligned due to initial setting errors, assembling errors, etc. The misalignment in sensors can lead to sending wrong displacement signals to the controller, which will also change the force generated by AMB. This will surely affect the system dynamics. Therefore, it becomes necessary to identify the offset amounts of sensors and then align them to perform effective operations. This chapter presents the finite element modelling, analysis and identification in a magnetically levitated flexible rotor system integrated with multiple misaligned sensors and misaligned AMBs. The force due to misaligned AMBs based on misaligned sensors has been derived for residual and additional trial misalignments.

Moreover, an innovative virtual trial misalignment (VTM) concept has been proposed for providing the trial misalignment to the rotor using additional bias current in AMB. This virtual method for giving the trial misalignment is more reliable and effective than PTM approach, as the method does not need test runs and a precise model of the rotor-sensor-bearing system. The mathematical modelling for the non-contact displacement sensors offset from the rotor centre has been presented and even the offset amounts are identified using this novel approach. Even, the dynamic effect of residual misalignment of sensors and AMBs on the rotor system is also investigated. The VTM based developed identification methodology is able to identify the rotor unbalance, active magnetic bearings (AMBs) residual misalignment, and their displacement and current stiffness parameters. The different levels of the random noise signal as well as rotor modelling errors are also added in the developed VTM based methodology to check its efficacy and sensitiveness in a practical rotor model. The estimation of parameters is also performed in the range of multiple spin speeds. Overall, the work presented in this chapter is quite complex, however, more applicable in smart industries accommodating high speed rotating machineries, such as steam turbines, gas turbines, and aircraft engines, etc. where the high speed rotors can be fully supported by AMBs. This will overcome the performance restrictions of conventional bearings in rotating the rotor at higher speeds and supporting the rotor at high temperatures.

5.2 Misaligned Flexible Rotor-Sensor-AMB System Configuration

Figure 5.1 shows a multidisc flexible rotor system mounted on r number of radial active magnetic bearings (AMBs) and integrated with sensors at different positions in the shaft. This rotor model has been considered to investigate the dynamic behaviour of the system consisting of multiple number of AMBs and sensors (for measuring displacements) as well as for developing the identification methodology derived from VTM strategy. There are p number of rigid discs in the rotor system. Here, the spinning axis of rotor and central axis of flexible shaft

are shown by Oz (straight line) and RR (elastic line), respectively. Misalignment of the rotor with respect to the supported AMBs as well as non-contact eddy current probes is elaborated in the next section. Each AMB is having a stator made up of four-pole pairs. For simplicity, the leakage of magnetic flux, the eddy current loss and core material hysteresis are neglected. Timoshenko beam theory has been used for finite element modelling of the proposed flexible rotor-AMBs system. The mathematical modelling for flexible shaft and rigid discs will follow Equations (4.1) and (4.3), respectively.

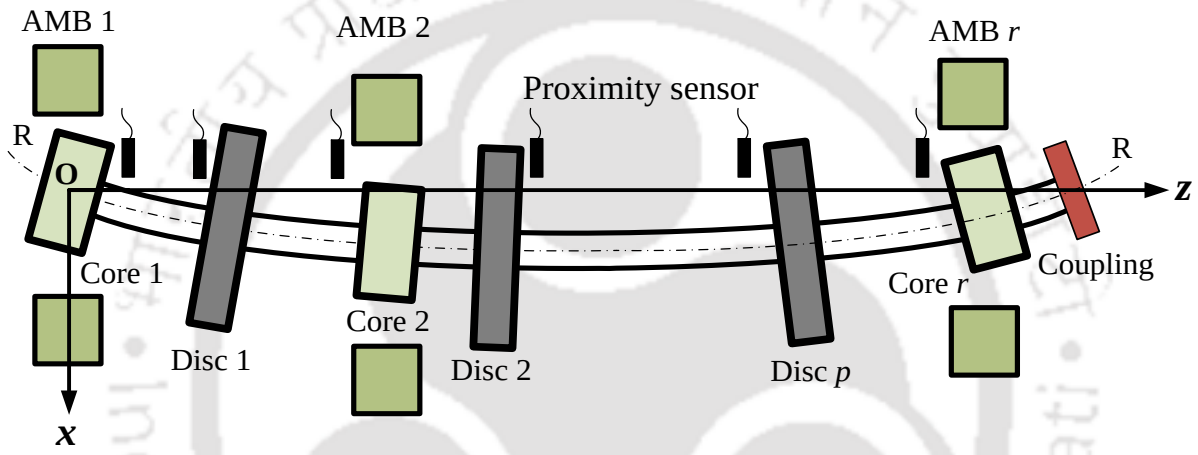

Figure 5.1 A magnetically levitated multidisc flexible rotor-AMBs system accommodated with multiple number of proximity sensors.

5.3 AMB Force sub-model for Residual and Additional Trial Misalignments

In this chapter, there is a misalignment in non-contact proximity sensors along with AMBs misalignment as shown in Figure 5.2. Therefore, the rotor displacement measured by sensors at AMB locations in the vertical and horizontal directions will be different from the case of sensors perfect alignment considered in the previous three chapters. As the force due to misaligned AMB depends on vibration induced displacement, so there will also be change in the force arising from misaligned sensors. This section describes the derivation of misaligned

AMB force (based on displacements captured by misaligned sensors) for residual and additional trial misalignments in the linearized form.

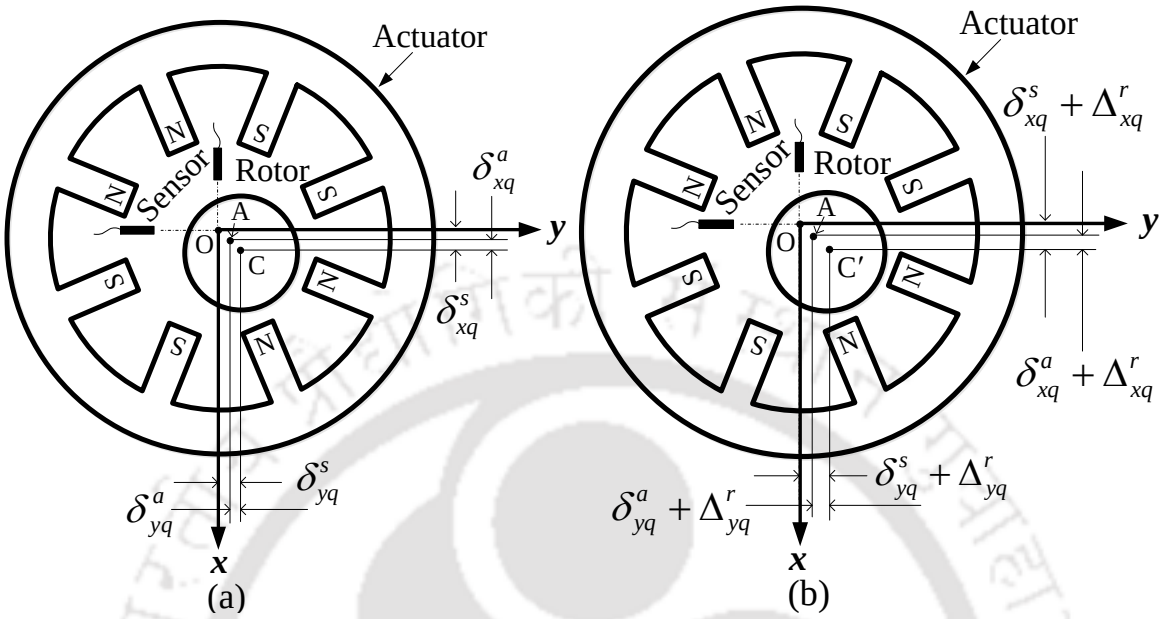

Figure 5.2 Side view representation of rotor, eddy current proximity sensors and eight pole q^{th} AMB actuator in the *xy*-coordinate plane (a) residual misalignment of AMB (δ^a_{xq}, δ^a_{yq}) and sensors (δ^s_{xq}, δ^s_{yq}) with the rotor (b) additional trial misalignment of AMB ($\delta^a_{xq}+\Delta^r_{xq}$, $\delta^a_{yq}+\Delta^r_{yq}$) and sensors ($\delta^s_{xq}+\Delta^r_{xq}$, $\delta^s_{yq}+\Delta^r_{yq}$) with the rotor.

Figure 5.2(a) shows the side view of the rotor misaligned with q^{th} AMB and sensors in the *x*-*y* coordinate plane, by residual amounts (δ^a_{xq}, δ^a_{yq}) and (δ^s_{xq}, δ^s_{yq}). Here, the centre position of proximity sensors, q^{th} AMB actuator (with q = 1, 2, …, r in Figure 5.1) and rotor are represented by O, A and C, respectively. Due to AMB misalignment in the n^{th} direction (where n = 1, 2 shown in Figure 5.3(a)), the air gap between q^{th} AMB stator and rotor is altered. The updated lower as well as upper air gaps in the n^{th} direction are ($s_0-\delta^a_{nq}$) and ($s_0+\delta^a_{nq}$), respectively. On substituting these modified air gaps in Equation (2.2), the AMB force acting in the n^{th} direction, for the case of *residual misalignment* can be written as

$$f_{nq}^{m1} = k_q \left\{ \frac{\left(i_0 + i_{nq}^{m1}\right)^2}{\left(s_0 - \delta_{nq}^a - u_{nq}^{m1}\right)^2} - \frac{\left(i_0 - i_{nq}^{m1}\right)^2}{\left(s_0 + \delta_{nq}^a + u_{nq}^{m1}\right)^2} \right\}; \quad n = 1,\ 2 \tag{5.1}$$

The term u_{nq}^{m1} is the rotor displacement measured by the residually misaligned q^{th} sensors at the positions 'n' (with n = 1, 2) in Figure 5.3(a). Figure 5.3(a) presents the side view of rotor and vertically as well as horizontally placed sensors when there is no trial misalignment given to the rotor. Only, there is residual misalignment between shaft centre and sensors centre.

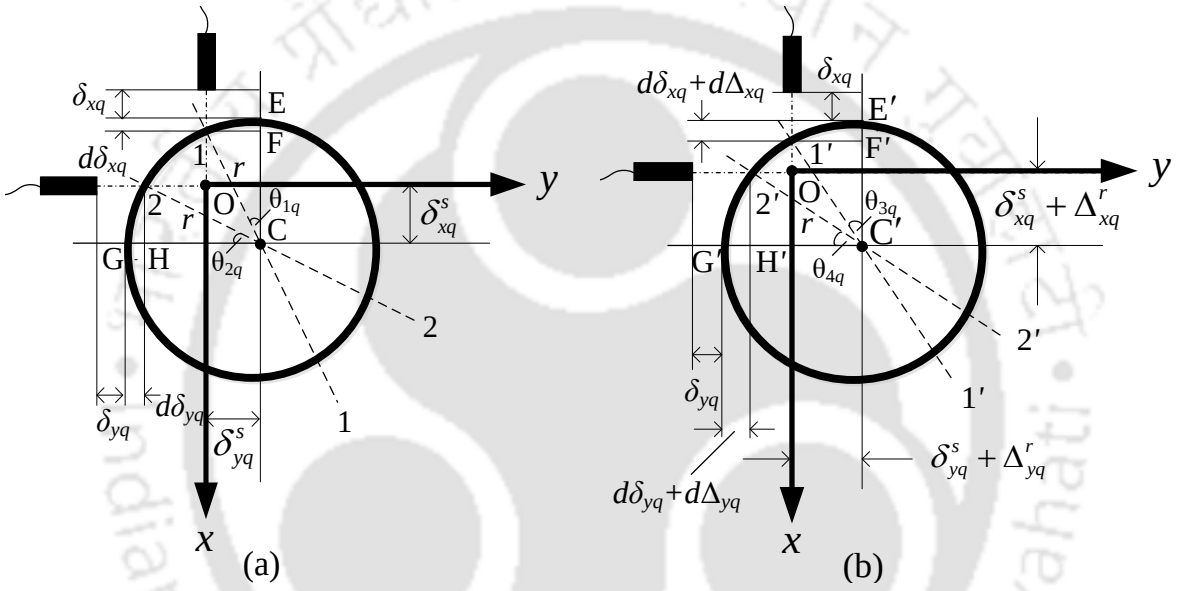

Figure 5.3 Cross-section diagram of the rotor with misaligned sensors present at q^{th} AMB location (a) residual misalignment ($\delta_{xq}^s, \delta_{yq}^s$) (b) additional trial misalignment ($\delta_{xq}^s + \Delta_{xq}^r$, $\delta_{yq}^s + \Delta_{yq}^r$).

In Figure 5.3(a), the points 1 and 2 are the points located at the shaft for which the displacements are measured by vertically and horizontally placed offset proximity sensors, respectively. Points O and C are the sensors centre and shaft centre, respectively. Points E and G are the uppermost and extreme front side points on the shaft without trial misalignment. Point F represents for the intersecting point of vertical line (passing through point E) and horizontal line (passing through point 1). Similarly, the intersection point of vertical line

(passing through point 2) and horizontal line (passing through point G) is shown by point H. Lines 1 and 2 are, respectively, the inclined lines passing through points 1 and 2. The angles θ_{1q} and θ_{2q} are the angles made by lines 1 and 2 with vertical line passing through point E and horizontal line passing through point G, respectively.

Further, upon simplifying Equation (5.1) based on the assumption that the vibration induced displacement is less than the nominal lower and upper air gaps between the rotor and AMB stator i.e., $u_{nq}^{m1} \ll (s_0 - \delta_{nq}^a)$ and $u_{nq}^{m1} \ll (s_0 + \delta_{nq}^a)$ as well as neglecting the higher order non-linear terms, i.e., $(u_{nq}^{m1})^2, (i_{nq}^{m1})^2$, $u_{nq}^{m1}(i_{nq}^{m1})^2$ and $i_{nq}^{m1}u_{nq}^{m1}$, the linearized form of Equation (5.1) is given as

$$f_{nq}^{m1} = k_{snq}^{m1} u_{nq}^{m1} + k_{inq}^{m1} i_{nq}^{m1} + f_{cnq}^{m1} \tag{5.2}$$

with

$$k_{snq}^{m1} = \frac{k_{snq}}{\left(1-\delta_{nq}^2\right)^2};\ k_{inq}^{m1} = \frac{k_{inq}\left(1+\delta_{nq}^2\right)}{\left(1-\delta_{nq}^2\right)^2};\ f_{cnq}^{m1} = \frac{f_q \delta_{nq}}{\left(1-\delta_{nq}^2\right)^2};\ f_q = \frac{4k_q i_0^2}{s_0^2};\ \delta_{nq} = \frac{\delta_{nq}^a}{s_0} \tag{5.3}$$

Although the expression for misaligned AMB force in case of misalignment in sensors (i.e., Equation (5.2)) looks similar to Equation (4.4) considering perfectly aligned sensors, but the constant stiffness terms k_{snq}^{m1} and k_{inq}^{m1} (with n = 1, 2) are slightly different from the terms available in Equation (4.4). These terms will be depending upon the AMBs stiffness coefficients in both the x-and y-directions, which is well explained below.

For (n = 1) and (n = 2), Equation (5.2) can be written as

$$f_{1q}^{m1} = k_{s1q}^{m1} u_{1q}^{m1} + k_{i1q}^{m1} i_{1q}^{m1} + f_{c1q}^{m1}; \qquad f_{2q}^{m1} = k_{s2q}^{m1} u_{2q}^{m1} + k_{i2q}^{m1} i_{2q}^{m1} + f_{c2q}^{m1} \tag{5.4}$$

Using Figure 5.3(a), the misaligned AMB force in the x- and y-directions are written as

$$f_{xq}^{m1} = f_{1q}^{m1}\cos\theta_{1q} + f_{2q}^{m1}\sin\theta_{2q}; \qquad f_{yq}^{m1} = f_{1q}^{m1}\sin\theta_{1q} + f_{2q}^{m1}\cos\theta_{2q} \tag{5.5}$$

After substituting Equation (5.4), the vector form of Equation (5.5) can be given as

$$\begin{Bmatrix} f_{xq}^{m1} \\ f_{yq}^{m1} \end{Bmatrix} = \begin{bmatrix} \cos\theta_{1q} & \sin\theta_{2q} \\ \sin\theta_{1q} & \cos\theta_{2q} \end{bmatrix} \begin{Bmatrix} f_{1q}^{m1} \\ f_{2q}^{m1} \end{Bmatrix} = [S] \begin{Bmatrix} f_{1q}^{m1} \\ f_{2q}^{m1} \end{Bmatrix} = [S] \begin{Bmatrix} k_{s1q}^{m1} u_{1q}^{m1} + k_{i1q}^{m1} i_{1q}^{m1} + f_{c1q}^{m1} \\ k_{s2q}^{m1} u_{2q}^{m1} + k_{i2q}^{m1} i_{2q}^{m1} + f_{c2q}^{m1} \end{Bmatrix} \tag{5.6}$$

where [*S*] is the transformation matrix.

Equation (5.6) can be expressed in the expanded form as

$$\begin{Bmatrix} f_{xq}^{m1} \\ f_{yq}^{m1} \end{Bmatrix} = [S] \begin{bmatrix} k_{s1q}^{m1} & 0 \\ 0 & k_{s2q}^{m1} \end{bmatrix} \begin{Bmatrix} u_{1q}^{m1} \\ u_{2q}^{m1} \end{Bmatrix} + [S] \begin{bmatrix} k_{i1q}^{m1} & 0 \\ 0 & k_{i2q}^{m1} \end{bmatrix} \begin{Bmatrix} i_{1q}^{m1} \\ i_{2q}^{m1} \end{Bmatrix} + \begin{Bmatrix} f_{cxq}^{m1} \\ f_{cyq}^{m1} \end{Bmatrix} \tag{5.7}$$

with

$$\begin{Bmatrix} f_{cxq}^{m1} \\ f_{cyq}^{m1} \end{Bmatrix} = [S] \begin{Bmatrix} f_{c1q}^{m1} \\ f_{c2q}^{m1} \end{Bmatrix} \tag{5.8}$$

Further, with the help of Figure 5.3(a), the stiffness coefficients of AMB (k_{s1q}^{m1}, k_{s2q}^{m1}, k_{i1q}^{m1} and k_{i2q}^{m1}), AMBs constant forces (f_{c1q}^{m1}, f_{c2q}^{m1}) and the rotor displacements (u_{1q}^{m1}, u_{2q}^{m1}) as well as the controlling currents output (i_{1q}^{m1}, i_{2q}^{m1}) can also be expressed with respect to the Cartesian coordinates *x* and *y*, as

$$k_{s1q}^{m1} = k_{sxq}^{m1}\cos\theta_{1q} + k_{syq}^{m1}\sin\theta_{1q}; \quad k_{s2q}^{m1} = k_{sxq}^{m1}\sin\theta_{2q} + k_{syq}^{m1}\cos\theta_{2q} \tag{5.9}$$

$$k_{i1q}^{m1} = k_{ixq}^{m1}\cos\theta_{1q} + k_{iyq}^{m1}\sin\theta_{1q}; \quad k_{i2q}^{m1} = k_{ixq}^{m1}\sin\theta_{2q} + k_{iyq}^{m1}\cos\theta_{2q} \tag{5.10}$$

$$\begin{Bmatrix} u_{1q}^{m1} \\ u_{2q}^{m1} \end{Bmatrix} = \begin{bmatrix} \cos\theta_{1q} & \sin\theta_{1q} \\ \sin\theta_{2q} & \cos\theta_{2q} \end{bmatrix} \begin{Bmatrix} u_{xq}^{m1} \\ u_{yq}^{m1} \end{Bmatrix} = [R] \begin{Bmatrix} u_{xq}^{m1} \\ u_{yq}^{m1} \end{Bmatrix} \text{ and } \begin{Bmatrix} i_{1q}^{m1} \\ i_{2q}^{m1} \end{Bmatrix} = [R] \begin{Bmatrix} i_{xq}^{m1} \\ i_{yq}^{m1} \end{Bmatrix} \tag{5.11}$$

On substituting Equations (5.9), (5.10) and (5.11) into Equation (5.7) and further simplifying them, we get the compact form of misaligned AMB force vector, as

$$\mathbf{f}_{AMB}^{m1}(t)=\mathbf{K}_{s\theta}^{m1}\boldsymbol{\eta}_{AMB}^{m1}(t)+\mathbf{K}_{i\theta}^{m1}\mathbf{i}_{c}^{m1}(t)+\mathbf{f}_{c}^{m1} \tag{5.12}$$

with

$$\mathbf{f}_{AMB}^{m1}(t)=\begin{Bmatrix} f_{xq}^{m1} \\ f_{yq}^{m1} \end{Bmatrix};\ \boldsymbol{\eta}_{AMB}^{m1}(t)=\begin{Bmatrix} u_{xq}^{m1} \\ u_{yq}^{m1} \end{Bmatrix};\ \mathbf{f}_{c}^{m1}=\begin{Bmatrix} f_{cxq}^{m1} \\ f_{cyq}^{m1} \end{Bmatrix};\ \mathbf{i}_{c}^{m1}(t)=\begin{Bmatrix} i_{xq}^{m1} \\ i_{yq}^{m1} \end{Bmatrix};$$

$$\mathbf{K}_{s\theta q}^{m1}=\begin{bmatrix} \left(a_{1q}k_{sxq}^{m1}+b_{1q}k_{syq}^{m1}\right) & \left(b_{1q}k_{sxq}^{m1}+c_{1q}k_{syq}^{m1}\right) \\ \left(b_{1q}k_{sxq}^{m1}+c_{1q}k_{syq}^{m1}\right) & \left(c_{1q}k_{sxq}^{m1}+d_{1q}k_{syq}^{m1}\right) \end{bmatrix};\ f_{cxq}^{m1}=\frac{f_q\delta_{xq}}{\left(1-\delta_{xq}^2\right)^2};$$

$$\mathbf{K}_{i\theta q}^{m1}=\begin{bmatrix} \left(a_{1q}k_{ixq}^{m1}+b_{1q}k_{iyq}^{m1}\right) & \left(b_{1q}k_{ixq}^{m1}+c_{1q}k_{iyq}^{m1}\right) \\ \left(b_{1q}k_{ixq}^{m1}+c_{1q}k_{iyq}^{m1}\right) & \left(c_{1q}k_{ixq}^{m1}+d_{1q}k_{iyq}^{m1}\right) \end{bmatrix};\ f_{cyq}^{m1}=\frac{f_q\delta_{yq}}{\left(1-\delta_{yq}^2\right)^2}; \tag{5.13}$$

$$a_{1q}=\cos^3\theta_{1q}+\sin^3\theta_{2q};\qquad b_{1q}=\sin\theta_{1q}\cos^2\theta_{1q}+\sin^2\theta_{2q}\cos\theta_{2q};$$

$$c_{1q}=\sin^2\theta_{1q}\cos\theta_{1q}+\cos^2\theta_{2q}\sin\theta_{2q};\qquad d_{1q}=\sin^3\theta_{1q}+\cos^3\theta_{2q}$$

and

$$k_{sxq}^{m1}=\frac{k_{sxq}}{\left(1-\delta_{xq}^2\right)^2};\quad k_{ixq}^{m1}=\frac{k_{ixq}\left(1+\delta_{xq}^2\right)}{\left(1-\delta_{xq}^2\right)^2};\quad k_{syq}^{m1}=\frac{k_{syq}}{\left(1-\delta_{yq}^2\right)^2};\quad k_{iyq}^{m1}=\frac{k_{iyq}\left(1+\delta_{yq}^2\right)}{\left(1-\delta_{yq}^2\right)^2}; \tag{5.14}$$

$$\delta_{xq}=\frac{\delta_{xq}^a}{s_0};\ \delta_{yq}=\frac{\delta_{yq}^a}{s_0}$$

It can be observed from Equation (5.13) that the stiffness matrices (both the force-displacement and force-current) for misaligned AMB (with consideration of misalignment in sensors) are the function of angles θ_{1q} and θ_{2q} as well as depend upon the *x*- and *y*-directional stiffness coefficients. This is quite different from Equation (4.10) in the misaligned AMB force without offset in sensors.

Similarly, for the case of *additional trial misalignment* (follow Figure 5.2(b), in which the known trial misalignment is additionally given to the rotor to add over residual misalignment of AMBs and sensors), the force vector due to AMB can be written as

$$\mathbf{f}_{AMB}^{m2}(t)=\mathbf{K}_{s\theta}^{m2}\boldsymbol{\eta}_{AMB}^{m2}(t)+\mathbf{K}_{i\theta}^{m2}\mathbf{i}_{c}^{m2}(t)+\mathbf{f}_{c}^{m2} \tag{5.15}$$

The details of matrix and vector terms $\mathbf{K}_{s\theta}^{m2}$, $\mathbf{K}_{i\theta}^{m2}$ and $\mathbf{f}_{c}^{m2}$, etc., in Equation (5.15) would follow Equation (5.13) by replacing *m*1 with *m*2, the constants (a_{1q}, b_{1q}, c_{1q}, d_{1q}) with (a_{2q}, b_{2q}, c_{2q},

d_{2q}) and the angles (θ_{1q}, θ_{2q}) with (θ_{3q}, θ_{4q}). In Figure 5.3(b), the prime symbol given to all variables (already defined for residual case in Figure 5.3(a)) represent for additional trial misalignment case. The mathematical strategy utilized in finding out these angles is well explored in Section 5.4. For this misalignment case, the *x*- and *y*-directional stiffness constants of AMB as well as the constant force vectors are given as

$$\begin{aligned} &k_{sxq}^{m2}=\frac{k_{sxq}}{\left(1-p_{xq}^2\right)^2};\ k_{ixq}^{m2}=\frac{k_{ixq}\left(1+p_{xq}^2\right)}{\left(1-p_{xq}^2\right)^2};\ k_{syq}^{m2}=\frac{k_{syq}}{\left(1-p_{yq}^2\right)^2};\ k_{iyq}^{m2}=\frac{k_{iyq}\left(1+p_{yq}^2\right)}{\left(1-p_{yq}^2\right)^2};\\ &p_{xq}=\frac{p_{xq}^{ar}}{s_0}=\frac{\left(\delta_{xq}^{a}+\Delta_{xq}^{r}\right)}{s_0};\ p_{yq}=\frac{p_{yq}^{ar}}{s_0}=\frac{\left(\delta_{yq}^{a}+\Delta_{yq}^{r}\right)}{s_0};\ f_{cxq}^{m2}=\frac{f_q p_{xq}}{\left(1-p_{xq}^2\right)^2};\ f_{cyq}^{m2}=\frac{f_q p_{yq}}{\left(1-p_{yq}^2\right)^2} \end{aligned} \tag{5.16}$$

In the *vector form*, the misaligned AMB force for the residual and additional trial misalignments can be expressed as

$$\mathbf{f}_{AMB}^{mis}\left(t\right)=\mathbf{K}_{s\theta}^{mis}\boldsymbol{\eta}_{AMB}^{mis}\left(t\right)+\mathbf{K}_{i\theta}^{mis}\mathbf{i}_{c}^{mis}\left(t\right)+\mathbf{f}_{c}^{mis} \tag{5.17}$$

The expression for controlling current vector for the PID controller in the case of misalignment in AMB and sensors can be written as

$$\mathbf{i}_{c}^{mis}\left(t\right)=-\begin{bmatrix} k_P & 0 & k_I & 0 & k_D & 0 \\ 0 & k_P & 0 & k_I & 0 & k_D \end{bmatrix}\left\{u_x^{mis} \quad u_y^{mis} \quad \int u_x^{mis}\mathrm{d}t \quad \int u_y^{mis}\mathrm{d}t \quad \dot{u}_x^{mis} \quad \dot{u}_y^{mis}\right\}^T \tag{5.18}$$

Equation (5.18) is consistent with Equation (4.11). The superscript *mis* in Equations (5.17) and (5.18) denotes as *m*1 and *m*2, respectively, for the residual and additional (trial) misalignments. The force-displacement and current stiffness matrices are shown by $\mathbf{K}_{s\theta}^{mis}$ and $\mathbf{K}_{i\theta}^{mis}$, whereas $\mathbf{f}_{c}^{mis}$ is the constant force vector for the misaligned AMB. At q^{th} AMB location, the displacement and controlling current vectors are symbolized, respectively, by $\boldsymbol{\eta}_{AMB}^{mis}$ and $\mathbf{i}_{c}^{mis}$. Herein, the transpose of displacement vector in Equation (5.18) is represented by *T* superscript. The novel concept of virtual trial misalignment (VTM) for providing additional (trial) misalignment in the rotor-sensor-AMB system is briefly explained in the next section.

5.3.1 Virtual Trial Misalignment (VTM) approach

To provide known trial misalignments between the rotor and AMBs axes, an innovative *virtual trial misalignment* (VTM) concept is proposed. The VTM approach is utilized to obtain the values of trial misalignments so that it will be helpful in quantitative estimation of AMBs residual misalignments through the developed model based identification algorithm. Compared to the physical trial misalignment method, this virtual method does not need test runs and a precise model of the rotor-bearing system. Moreover, the assembling and disassembling of the rotor-AMB set up for providing physical trial misalignments by means of nut and bolt arrangement, thin aluminium sheets, etc., consume more time, which will be also avoided from the novel VTM method. In this approach, the trial misalignments (Δ_{xq}^{r} and Δ_{yq}^{r}) between the axes of rotor and AMB as well as sensors (refer Figure 5.2(b)) are created virtually in the vertical as well as horizontal directions. This is done by shifting the rotor with respect to AMB's current position, through additional bias current supplied to AMB along with the controlling current. To obtain the values of trial misalignments at q^{th} AMB location, the additional magnetic forces (f_{Txq} and f_{Tyq}) based on bias currents are introduced at the position of AMB. These magnetic excitation forces acting as virtual trial misalignment forces, are generated along with AMBs controlling forces. These *x*- and *y*-directional trial magnetic forces at q^{th} AMB position are given as

$$f_{Txq} = k_{ixq}^{T} i_{Txq}; \quad f_{Tyq} = k_{iyq}^{T} i_{Tyq} \tag{5.19}$$

with

$$k_{ixq}^{T} = \frac{4k_q\left(i_0 + i_{Txq}\right)}{s_0^2}; \quad k_{iyq}^{T} = \frac{4k_q\left(i_0 + i_{Tyq}\right)}{s_0^2} \tag{5.20}$$

where the *x*- and *y*-directional force-current factors of AMB after providing additional bias currents (i_{Txq} and i_{Tyq}) for creating trial misalignments are represented by k_{ixq}^{T} and k_{iyq}^{T}, respectively. Further, the amount of trial misalignments from the VTM approach can be obtained by equating Equation (5.19) with the trial misaligned AMB constant forces, as

$$f_{Txq} = k_{ixq}^{T} i_{Txq} = \frac{f_q \Delta_{xq}}{\left(1-\Delta_{xq}^2\right)^2};\ f_{Tyq} = k_{iyq}^{T} i_{Tyq} = \frac{f_q \Delta_{yq}}{\left(1-\Delta_{yq}^2\right)^2};\ f_q = \frac{4k_q i_0^2}{s_0^2}; \Delta_{xq} = \frac{\Delta_{xq}^r}{s_0};\ \Delta_{yq} = \frac{\Delta_{yq}^r}{s_0} \quad (5.21)$$

On substituting the force-current stiffness terms of Equation (5.20) into Equation (5.21) and further cancelling out the common terms ($4k_q / s_0^2$) on both sides, we get

$$i_{Txq}^2 + i_0 i_{Txq} + \frac{i_0^2 \Delta_{xq}}{\left(1-\Delta_{xq}^2\right)^2} = 0; \qquad i_{Tyq}^2 + i_0 i_{Tyq} + \frac{i_0^2 \Delta_{yq}}{\left(1-\Delta_{yq}^2\right)^2} = 0 \quad (5.22)$$

Equation (5.22) represents the relations between the *x*- and *y*-directional additional bias currents and the trial misalignments between rotor and AMB axes through the concept of virtual trial misalignment (VTM). Therefore, with the known values of the bias current (i_0), nominal air gap (s_0) and the user supplied additional bias currents (i_{Txq} and i_{Tyq}) for shifting the rotor with respect to AMB's current position in both the *x*- and *y*-directions, the *trial misalignments* (Δ_{xq}^r and Δ_{yq}^r) can be calculated using Equation (5.22). These trial misalignment amounts are similar to the physical trial misalignments given to active magnetic bearing housing in both the vertical and horizontal directions, as described in Section 2.3.3.2.

5.4 Misaligned Sensor sub-model for Residual and Additional Trial Misalignments

In this section, the mathematical procedure followed in determining the angles (θ_{1q}, θ_{2q}, θ_{3q} and θ_{4q}) for the residual and additional trial misalignments of sensors (refer Figure (5.4)) has been

explained. This section also discusses about the approach taken in obtaining the amount of residual misalignment of sensors (δ_{xq}^{s} , δ_{yq}^{s}), as depicted in Figure 5.3(a).

From Figures 5.3(a) and 5.3(b) for the residual and additional trial misalignments of sensors with the rotor, we have the following relationships

$$\overline{\mathrm{EC}} = \overline{\mathrm{EF}} + \overline{\mathrm{FC}} \Rightarrow r = d\delta_{xq} + r\cos\theta_{1q} \Rightarrow d\delta_{xq} = r\left(1-\cos\theta_{1q}\right) \tag{5.23}$$

$$\overline{\mathrm{GC}} = \overline{\mathrm{GH}} + \overline{\mathrm{HC}} \Rightarrow r = d\delta_{yq} + r\cos\theta_{2q} \Rightarrow d\delta_{yq} = r\left(1-\cos\theta_{2q}\right) \tag{5.24}$$

$$\sin\theta_{1q} = \frac{\delta_{yq}^{s}}{r}; \quad \sin\theta_{2q} = \frac{\delta_{xq}^{s}}{r} \tag{5.25}$$

$$\overline{\mathrm{E'C'}} = \overline{\mathrm{E'F'}} + \overline{\mathrm{F'C'}} \Rightarrow r = \left(d\delta_{xq} + d\Delta_{xq}\right) + r\cos\theta_{3q} \Rightarrow \left(d\delta_{xq} + d\Delta_{xq}\right) = r\left(1-\cos\theta_{3q}\right) \tag{5.26}$$

$$\begin{aligned} \overline{\mathrm{G'C'}} = \overline{\mathrm{G'H'}} + \overline{\mathrm{H'C'}} &\Rightarrow r = \left(d\delta_{yq} + d\Delta_{yq}\right) + r\cos\theta_{4q} \\ &\Rightarrow \left(d\delta_{yq} + d\Delta_{yq}\right) = r\left(1-\cos\theta_{4q}\right) \end{aligned} \tag{5.27}$$

$$\sin\theta_{3q} = \frac{\delta_{yq}^{s} + \Delta_{yq}^{r}}{r}; \quad \sin\theta_{4q} = \frac{\delta_{xq}^{s} + \Delta_{xq}^{r}}{r} \tag{5.28}$$

where the denominator r is the radius of the shaft.

Subtracting Equations (5.26) and (5.27) from Equations (5.23) and (5.24), respectively, we get

$$\cos\theta_{1q} - \cos\theta_{3q} = \frac{d\Delta_{xq}}{r} \quad \text{and} \quad \cos\theta_{2q} - \cos\theta_{4q} = \frac{d\Delta_{yq}}{r} \tag{5.29}$$

Similarly, on subtracting Equation (5.28) from Equation (5.25), we get

$$\sin\theta_{3q} - \sin\theta_{1q} = \frac{\Delta_{yq}^{r}}{r} \quad \text{and} \quad \sin\theta_{4q} - \sin\theta_{2q} = \frac{\Delta_{xq}^{r}}{r} \tag{5.30}$$

For the residually misaligned state of sensors as depicted in Figure 5.3(a), the x- and y-directional gap between sensors and rotor would be (δ_{xq} + $d\delta_{xq}$) and (δ_{yq} + $d\delta_{yq}$), respectively, which are the known quantities set by a user for measuring the rotor vibration. In the similar

way, the gap between rotor and additionally misaligned sensors ($\delta_{xq} + d\delta_{xq} + d\Delta_{xq}$) and ($\delta_{yq} + d\delta_{yq} + d\Delta_{yq}$) in the *x*- and *y*-directions (follow Figure 5.3(b)) are also known quantities. Therefore, on subtracting the air gaps for additional trial misalignment and residual misalignment of sensors would give the amounts $d\Delta_{xq}$ and $d\Delta_{yq}$, respectively. The virtual trial misalignments of the rotor provided additionally to the system in the *x*- and *y*-directions (Δ_{xq}^{r} and Δ_{yq}^{r}) are also known terms (it is well discussed in Section 5.3.1). Hence, on solving Equations (5.29) and (5.30), the values of the angles θ_{1q} and θ_{2q} can be obtained as

$$\begin{aligned}\theta_{1q} &= \tan^{-1}\left(\frac{d\Delta_{xq}}{\Delta_{yq}^{r}}\right) - \sin^{-1}\left\{\frac{\left(d\Delta_{xq}\right)^2 + \left(\Delta_{yq}^{r}\right)^2}{2r^2}\right\} \\ \theta_{2q} &= \tan^{-1}\left(\frac{d\Delta_{yq}}{\Delta_{xq}^{r}}\right) - \sin^{-1}\left\{\frac{\left(d\Delta_{yq}\right)^2 + \left(\Delta_{xq}^{r}\right)^2}{2r^2}\right\}\end{aligned} \tag{5.31}$$

Afterwards, on substituting Equation (5.31) into Equation (5.29), the angles θ_{3q} and θ_{4q} can be evaluated. Moreover, the *x*- and *y*-directional residual misalignment of sensors (δ_{xq}^{s} , δ_{yq}^{s}) can also be identified using Equation (5.25) with the known values of angles θ_{1q} and θ_{2q},. Therefore, the proposed novel virtual trial misalignment (VTM) concept can be utilized in determining the residual misalignment of sensors.

5.5 Equation of Motion and Identification Equation of the Overall Rotor-Sensor-AMB system

With the proper assembly of flexible shaft sub-model, rigid disc sub-model, residual unbalance force sub-model, misaligned AMB force sub-model, the overall equation of motion of flexible rotor-sensor-AMB can be expressed as

$$\mathbf{M}\ddot{\boldsymbol{\eta}}^{mis} + \left(\mathbf{C} - \omega\mathbf{G}\right)\dot{\boldsymbol{\eta}}^{mis} + \mathbf{K}\boldsymbol{\eta}^{mis} = \mathbf{f}_{unb} + \mathbf{f}_{AMB}^{mis} \tag{5.32}$$

Here, **M**, **C**, **G** and **K** are the globally assembled form of mass, damping, gyroscopic and stiffness matrices, respectively. The spin speed of the rotor is denoted by ω, whereas $\boldsymbol{\eta}^{mis}$ is the global displacement vector of the rotor. The global vectors representing for the residual unbalance force and AMB force arising from misalignment are symbolized, respectively, with $\mathbf{f}_{unb}$ and $\mathbf{f}_{AMB}^{mis}$. The solution of Equation (5.32) is obtained after the application of boundary conditions, which includes the rotor displacement at all nodes in the shaft and controlling current at the AMBs nodes.

The procedure for developing identification algorithm using gyroscopic dynamic condensation scheme remains same as elaborated in Sections 4.3.5 and 4.4, with different elements in the known regression matrix **A** (ω). Elements in the matrix **A** (ω) for this chapter also consist the constant known terms (a_{1q}, b_{1q}, c_{1q}, d_{1q}) and (a_{2q}, b_{2q}, c_{2q}, d_{2q}), which are appearing due to present formulation for the misaligned (residual and additional trial misalignments) sensors at AMB locations (follow Equation (5.13) for the case of residual misalignment). Hence, in consistency with Equation (4.35), the identification equation for estimation of the rotor unbalance parameters (eccentricities and phases) and misaligned AMB stiffness parameters as well as constants forces due to the residual and additional misalignments for the considered rotor-sensors-AMBs system (refer Figure 5.1) can be given as

$$\mathbf{A}(\omega)_{(2a\times c)}\,\mathbf{x}_{(c\times 1)} = \mathbf{B}(\omega)_{(2a\times 1)} \tag{5.33}$$

with

$$\mathbf{A}(\omega) = \begin{bmatrix} \mathbf{A}_2^{\mathrm{Re}}(\omega) & -\mathbf{A}_2^{\mathrm{Im}}(\omega) \\ \mathbf{A}_2^{\mathrm{Im}}(\omega) & \mathbf{A}_2^{\mathrm{Re}}(\omega) \end{bmatrix}; \quad \mathbf{B}(\omega) = \begin{Bmatrix} \mathbf{B}_2^{\mathrm{Re}}(\omega) \\ \mathbf{B}_2^{\mathrm{Im}}(\omega) \end{Bmatrix} \tag{5.34}$$

$$\mathbf{x} = \left\{ e_1^{\mathrm{Re}} \quad e_1^{\mathrm{Im}} \quad e_2^{\mathrm{Re}} \quad e_2^{\mathrm{Im}} \quad \cdots \quad k_{sx1}^{m1} \quad k_{sy1}^{m1} \quad \cdots \quad k_{ix1}^{m1} \quad k_{iy1}^{m1} \quad \cdots \quad f_{11}^{m1} \quad f_{21}^{m1} \quad \cdots \right.$$
$$\left. k_{sx1}^{m2} \quad k_{sy1}^{m2} \quad \cdots \quad k_{ix1}^{m2} \quad k_{iy1}^{m2} \quad \cdots \quad f_{11}^{m2} \quad f_{21}^{m2} \quad \cdots \right\}^T \tag{5.35}$$

where $\mathbf{A}(\omega)$ and $\mathbf{B}(\omega)$ are the regression matrix and the vector comprising of known model quantities, respectively. The vector **x** is the unknown vector which includes the real and imaginary parts of disc eccentricities and stiffness parameters as well as constant forces of misaligned AMBs for both the residual and additional trial misalignments. The subscripts represent the size of the matrix or the vector. For k^{th} (with k = 1, 2, …, p) rigid disc, the real e_k^{Re} and imaginary e_k^{Im} parts of disc eccentricity are $e_k \cos(\beta_k)$ and $e_k \sin(\beta_k)$, respectively. Here, the term β_k is the phase of k^{th} disc unbalance. The exact or optimal solution of Equation (5.33) can be obtained if the number of equations is equal to or more than number of unknowns. The system is said to be overdetermined type of linear equations when the condition ($2a > c$) is satisfied. In case, the linear equation (i.e., Equation (5.33)) is underdetermined type ($2a < c$) at one spin speed, then it has to be made overdetermined system by taking the displacement and current responses for at least two different speeds and increasing the size of regression matrix $\mathbf{A}(\omega)$ and known vector $\mathbf{B}(\omega)$. In general, the least-squares based method i.e., Moore-Penrose inverse is used for solving such overdetermined system to obtain the optimal values of unknown parameters comprised in the vector **x** of Equation (5.33). Based on the Moore-Penrose inverse technique, the solution can be achieved as

$$\mathbf{x} = \left(\mathbf{A}(\omega)^T \mathbf{A}(\omega) \right)^{-1} \mathbf{A}(\omega)^T \mathbf{B}(\omega) \tag{5.36}$$

Moreover, to exhibit the sensitiveness and robustness of the proposed VTM based identification scheme, the parameters associated with unbalance and misalignment faults as well as AMB stiffness constants can be obtained in the range of multiple 'n' number of spin speeds of the rotor, as

$$\begin{pmatrix} \mathbf{A}_{(\omega_1)} \\ \mathbf{A}_{(\omega_2)} \\ \vdots \\ \mathbf{A}_{(\omega_n)} \end{pmatrix} \mathbf{x} = \begin{pmatrix} \mathbf{B}_{(\omega_1)} \\ \mathbf{B}_{(\omega_2)} \\ \vdots \\ \mathbf{B}_{(\omega_n)} \end{pmatrix} \tag{5.37}$$

After estimating the AMBs force-displacement constants (i.e., k_{sx1}^{m1}, k_{sy1}^{m1}, k_{sx2}^{m1}, k_{sy2}^{m1}, …) and force-current constants (i.e., k_{ix1}^{m1}, k_{iy1}^{m1}, k_{ix2}^{m1}, k_{iy2}^{m1}, …) and AMBs force constants (i.e., f_{11}^{m1}, f_{21}^{m1}, f_{12}^{m1}, f_{22}^{m1}, …) for the residual misalignment as well as AMBs force-displacement constants (i.e., k_{sx1}^{m2}, k_{sy1}^{m2}, k_{sx2}^{m2}, k_{sy2}^{m2}, …) and force-current constants (i.e., k_{ix1}^{m2}, k_{iy1}^{m2}, k_{ix2}^{m2}, k_{iy2}^{m2}, …) and AMBs constant forces (i.e., f_{11}^{m2}, f_{21}^{m2}, f_{12}^{m2}, f_{22}^{m2}, …) linked with the additional known (trial) misalignment, the *x*- and *y*-directional residual misalignments δ_{xq}^{a} and δ_{yq}^{a} of q^{th} AMB can be identified from the ratios of k_{sxq}^{m1} and k_{sxq}^{m2} as well as k_{syq}^{m1} and k_{syq}^{m2} of Equations (5.14) and (5.16) with the known values of nominal air gap s_0 and virtually added trial misalignments (Δ_{xq}^{r}, Δ_{yq}^{r}), as

$$\begin{aligned} &\frac{k_{sxq}^{m1}}{k_{sxq}^{m2}} = \frac{\left\{1-\left(\delta_{xq}+\Delta_{xq}\right)^2\right\}^2}{\left(1-\delta_{xq}^2\right)^2}; \quad \frac{k_{syq}^{m1}}{k_{syq}^{m2}} = \frac{\left\{1-\left(\delta_{yq}+\Delta_{yq}\right)^2\right\}^2}{\left(1-\delta_{yq}^2\right)^2}; \\ &\delta_{xq} = \frac{\delta_{xq}^{a}}{s_0}; \quad \delta_{yq} = \frac{\delta_{yq}^{a}}{s_0}; \quad \Delta_{xq} = \frac{\Delta_{xq}^{r}}{s_0}; \quad \Delta_{yq} = \frac{\Delta_{yq}^{r}}{s_0} \end{aligned} \tag{5.38}$$

Additionally, the actual AMB force-displacement stiffness parameters (k_{sxq}, k_{syq}) and force-current stiffness parameters (k_{ixq}, k_{iyq}) for q^{th} AMB can also be identified from Equation (5.14), with the estimated values of (k_{sxq}^{m1}, k_{syq}^{m1}), (k_{ixq}^{m1}, k_{iyq}^{m1}) and (δ_{xq}^{a}, δ_{yq}^{a}) from the proposed algorithm as well as the known value of air gap, s_0. Figure 5.4 presents the mathematical process flow diagram adopted in developing the model based identification algorithm derived

from the virtual trial misalignment (VTM) innovative approach. For verifying the methodology proposed in this section, the results obtained from numerical simulation are presented and discussed in the next section.

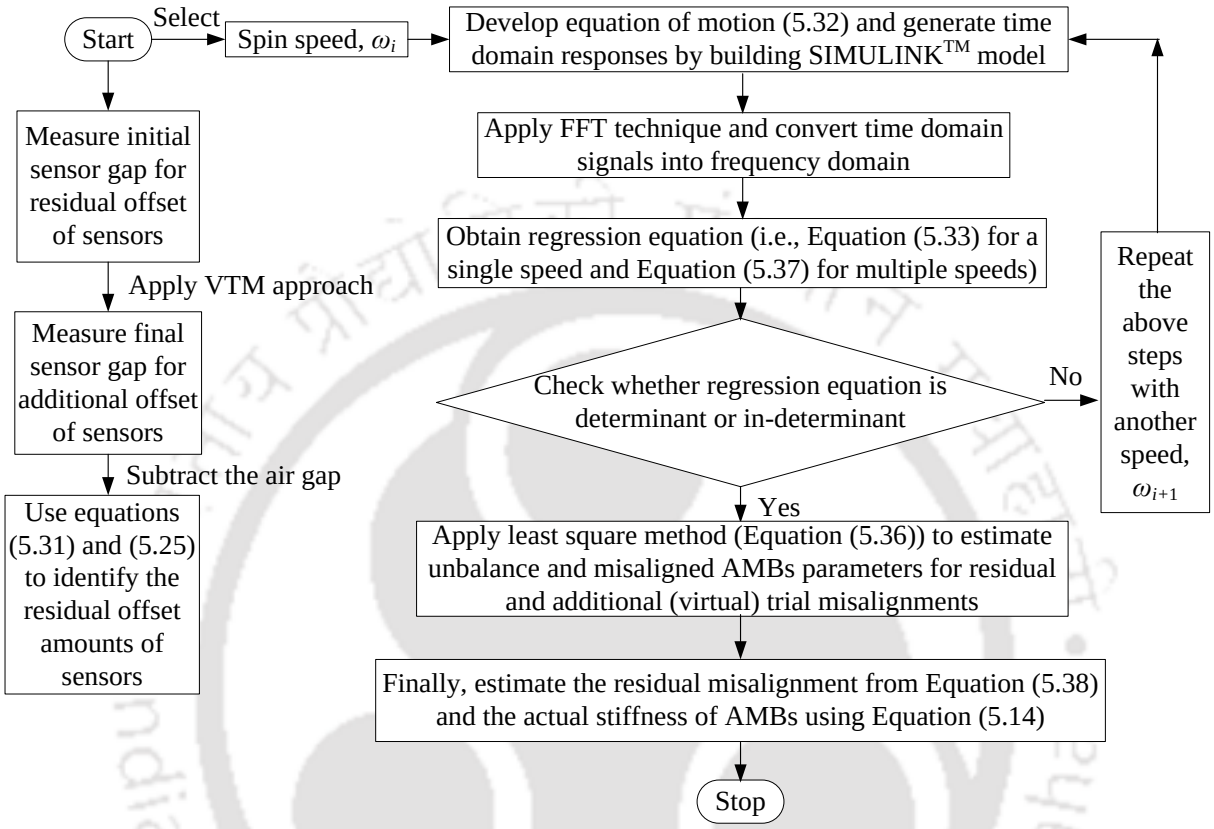

Figure 5.4 Flow diagram for identification of rotor unbalance, sensor and AMB residual misalignments using virtual trial misalignment (VTM) concept.

5.6 Results and Discussion

To explore and test the developed VTM based identification algorithm, a flexible shaft fastened with five discs (in which two are cores of AMBs) mounted on two active magnetic bearings has been considered (depicted in Figure 5.5). Figure 5.5 also shows the positioning of eddy current proximity probes for measuring the shaft displacements at several locations of AMBs and discs. The contactless sensors and supported AMBs are taken to be residually misaligned with respect to the rotor centre, which can be observed from their side view in Figure 5.6. Here,

the amounts (δ_{x1}^{a}, δ_{x2}^{a}) and (δ_{y1}^{a}, δ_{y2}^{a}) are the residual misalignments of AMB 1 and AMB 2 with respect to the rotor in the *x*- and *y*-directions. The *x*- and *y*-directional residual misalignment of sensors (relative to the rotor centre) located at AMB 1 and AMB 2 locations are represented by (δ_{x1}^{s}, δ_{y1}^{s}) and (δ_{x2}^{s}, δ_{y2}^{s}).The values of these misalignments are assumed to be different from each other, which causes AMBs and sensors misalignment as combination of *lateral and angular* misalignments.

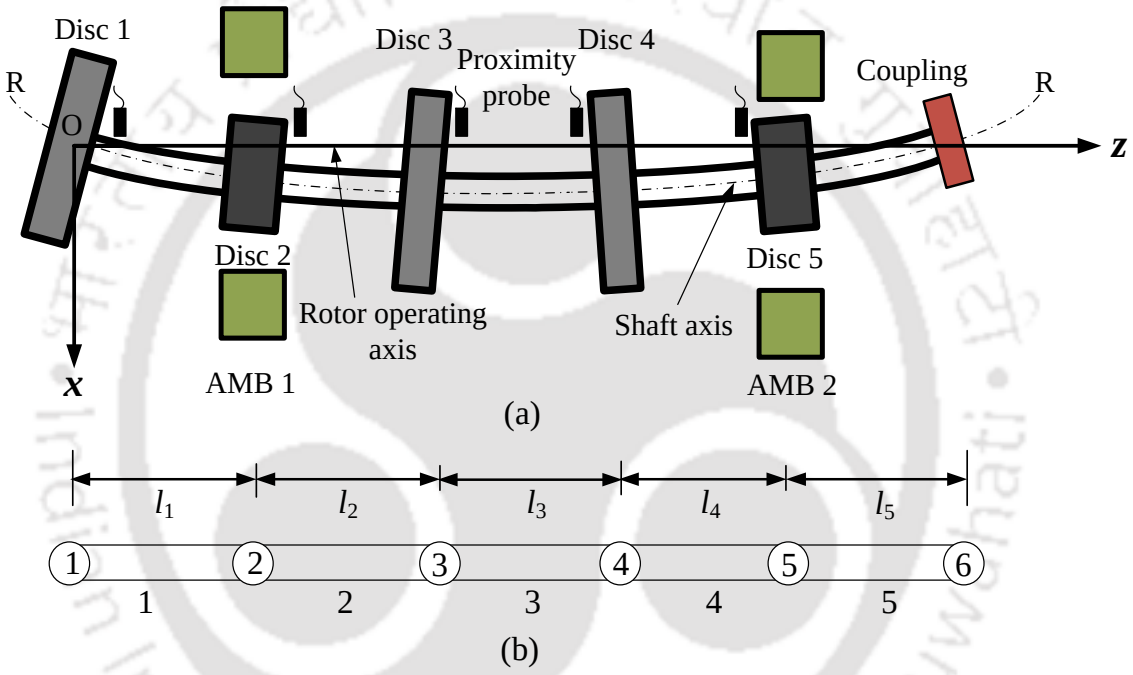

Figure 5.5 (a) A flexible rotor-sensor-AMB system used for the numerical simulation (b) Discretization of the whole rotor model for FEM modelling.

In Figure 5.5, the unbalance fault is assumed to present in the discs 1, 3 and 4 only. For finite element modelling (based on *Timoshenko beam theory*) of the whole rotor-AMB system, the flexible shaft has been divided into five number of one dimensional elements of different lengths (the reason for considering 5 number of shaft elements is explained in Section 4.5). There are four DOFs i.e., two linear and two angular displacements at each node of the shaft element. AMB 1, AMB 2 and their respective cores are present at node 2 and node 5 of the

shaft. The unbalanced discs are available at nodes 1, 3 and 4 of the shaft. Moreover, a flexible coupling of negligible mass used for connecting the rotor with motor shaft, for its driving purpose is placed at the last node i.e., node 6 of the discretised rotor. AMB 1 and AMB 2 are supposed to be *anisotropic* in nature with different values of force-displacement and stiffness coefficients. The *shaft damping* and *shaft gyroscopic* effects are also considered in the finite element modelling of the rotor-sensor-AMB model.

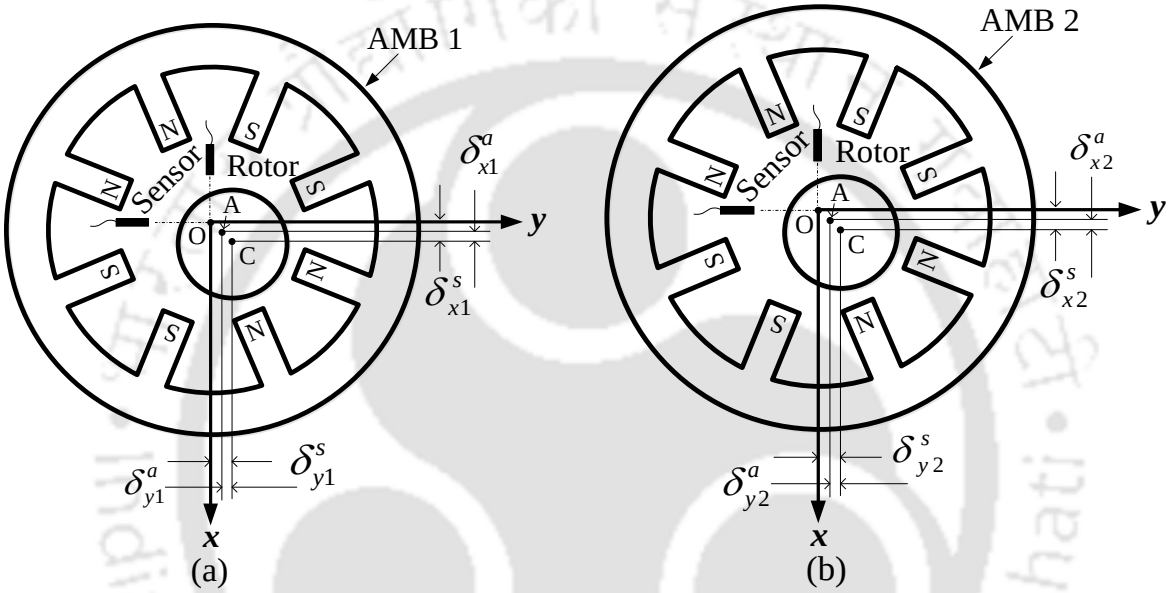

Figure 5.6 Side view of residually misaligned rotor-sensor-AMB system in the *xy*- coordinate plane at (a) AMB 1 location (b) AMB 2 location.

For solving Equation (5.32) and generating the time domain vibrational displacement and current responses of the magnetically levitated rotor-AMB system (integrated with sensors) at all nodes of the shaft, a SIMULINK^{TM} model shown in Figure 4.6 has been utilized. However, it is obvious that there will be change in the elements of global AMB stiffness matrices and constant AMB force vector (due to presence of misalignment in sensors) in Figure 4.5. The assumed values for the rotor and unbalance parameters as well as properties of AMBs and PID controller for the purpose of numerical simulation has been taken from Table 4.1 and Table 4.2. Table 5.1 displays the assumed values of parameters related to AMB residual

misalignments, rotor trial misalignments, additional gaps of sensors and additional bias currents (calculated from Equation (5.22)) required for creating virtual trial misalignments.

Table 5.1 Physical specifications of misaligned rotor-sensor-AMB system.

Parameters related to misaligned rotor-sensor-AMB system	**Values (units)**
Residual misalignment between rotor and AMB 1 in *x*-direction, δ_{x1}^{a}	0.140 mm
Residual misalignment between rotor and AMB 1 in *y*-direction, δ_{y1}^{a}	0.160 mm
Residual misalignment between rotor and AMB 2 in *x*-direction, δ_{x2}^{a}	0.150 mm
Residual misalignment between rotor and AMB 2 in *x*-direction, δ_{y2}^{a}	0.145 mm
Trial misalignment of rotor at AMB 1 location in *x*-direction, Δ_{x1}^{r}	0.100 mm
Trial misalignment of rotor at AMB 1 location in *y*-direction, Δ_{y1}^{r}	0.130 mm
Trial misalignment of rotor at AMB 2 location in *x*-direction, Δ_{x2}^{r}	0.120 mm
Trial misalignment of rotor at AMB 2 location in *y*-direction, Δ_{y2}^{r}	0.110 mm
Additional sensor gap at AMB 1 location in *x*-direction, $d\Delta_{x1}$	0.050 mm
Additional sensor gap at AMB 1 location in *y*-direction, $d\Delta_{y1}$	0.070 mm
Additional sensor gap at AMB 2 location in *x*-direction, $d\Delta_{x2}$	0.060 mm
Additional sensor gap at AMB 2 location in *y*-direction, $d\Delta_{y2}$	0.055 mm
Additional trial bias current at AMB 1 location in *x*-direction, i_{Tx1}	0.462 A
Additional trial bias current at AMB 1 location in *y*-direction, i_{Ty1}	0.620 A
Additional trial bias current at AMB 2 location in *x*-direction, i_{Tx2}	0.565 A
Additional trial bias current at AMB 2 location in *y*-direction, i_{Ty2}	0.512 A

A fourth-order Runge-Kutta ordinary differential equation solver with a fixed step size of 0.00001 s is used for obtaining the displacement and current responses of the system. The simulation was run for 5 s for the numerical analysis purpose. The obtained first five natural frequencies of the system are 0 Hz, 0 Hz, 53.88 Hz (338.6 rad/s), 113.80 Hz (715 rad/s) and 178.48 Hz (1121.4 rad/s), respectively. These frequencies have been acquired from the free-

free support boundary condition. The corresponding first five mode shapes of the proposed rotor-bearing system are shown in Figure 5.7.

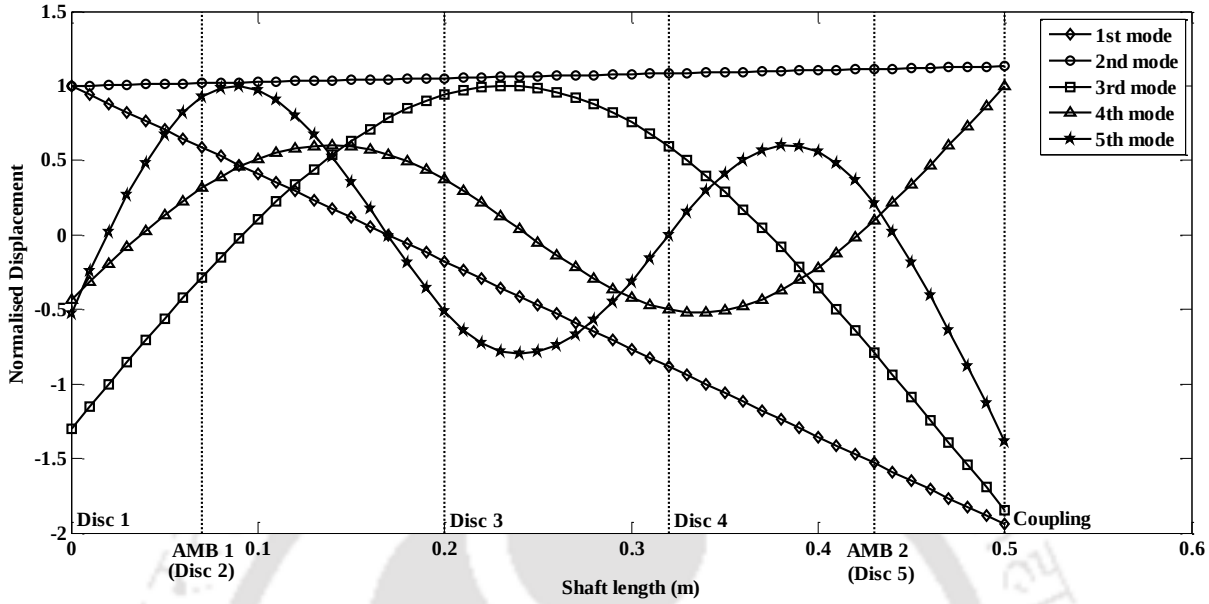

Figure 5.7 First five mode shapes for free-free end support boundary conditions.

It can be observed from Figure 5.7 that the first two mode shapes are straight line which are due to zeroth natural frequencies. These represent for the translational as well as rotational rigid body mode shapes of the rotor. For the translational rigid body mode, the rotor will have rigid body motion in the up and down directions, however it will have rigid body rotation about the centre of gravity for the rotational rigid body mode. Moreover, the Campbell diagram of the considered rotor system has been plotted in Figure 5.8 to present the forward and backward whirling of the rotor. This has been obtained by splitting the natural frequencies due to gyroscopic coupled effects of the discs. The critical speeds of the system for forward whirl are obtained to be 351, 748, 1202 rad/s, whereas for the backward whirl, the critical speeds are 327, 685, 1051 rad/s.

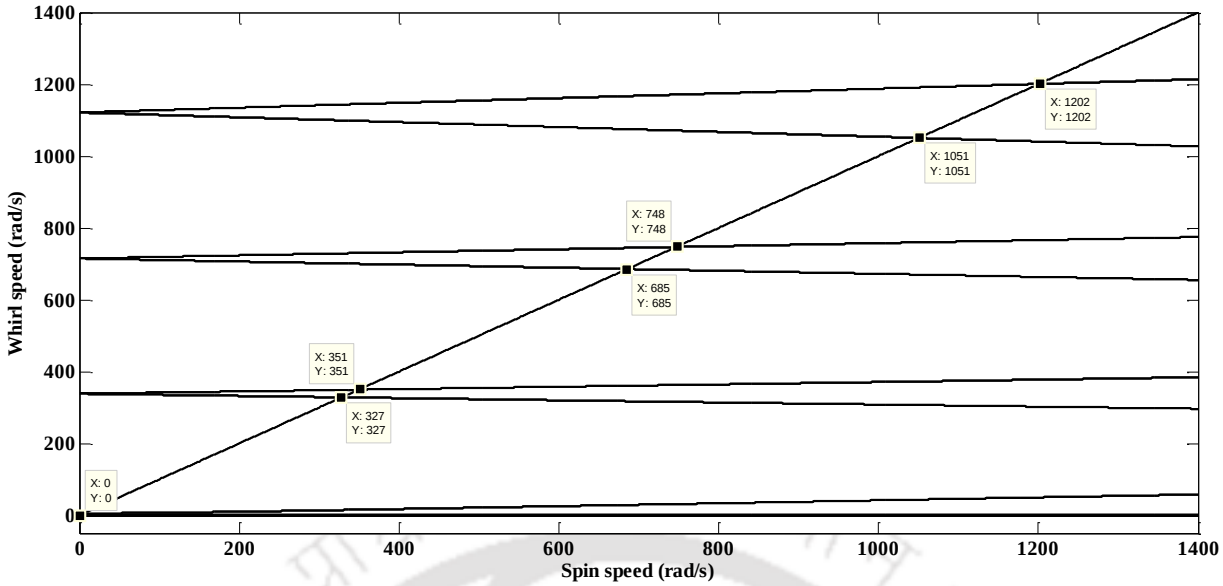

Figure 5.8 Campbell diagram of the proposed rotor system for a spin speed of 0-1400 rad/s representing both the forward and backward whirls.

Table 5.2 Percentage increase in the rotor displacement response (time domain) at AMB locations under the effect of AMB and sensor residual misalignments for 120 Hz angular frequency.

Shaft location	Maximum amplitude in the time domain	AMB and sensor misalignment (1st condition)	AMB misalignment, but no sensor offset (2nd condition)	Perfect alignment state (3rd condition)	Percentage increase in 1st condition (relative to 2nd condition)	Percentage increase in 1st condition (relative to 3rd condition)
Node 2	Displacement (m)	5.63×10^{-5}	4.20×10^{-5}	2.86×10^{-5}	34.05%	96.85%
Node 5	Displacement (m)	7.46×10^{-5}	5.05×10^{-5}	3.29×10^{-5}	47.72%	126.70%

5.6.1 Dynamic Influence of AMB and Sensor Residual Misalignments

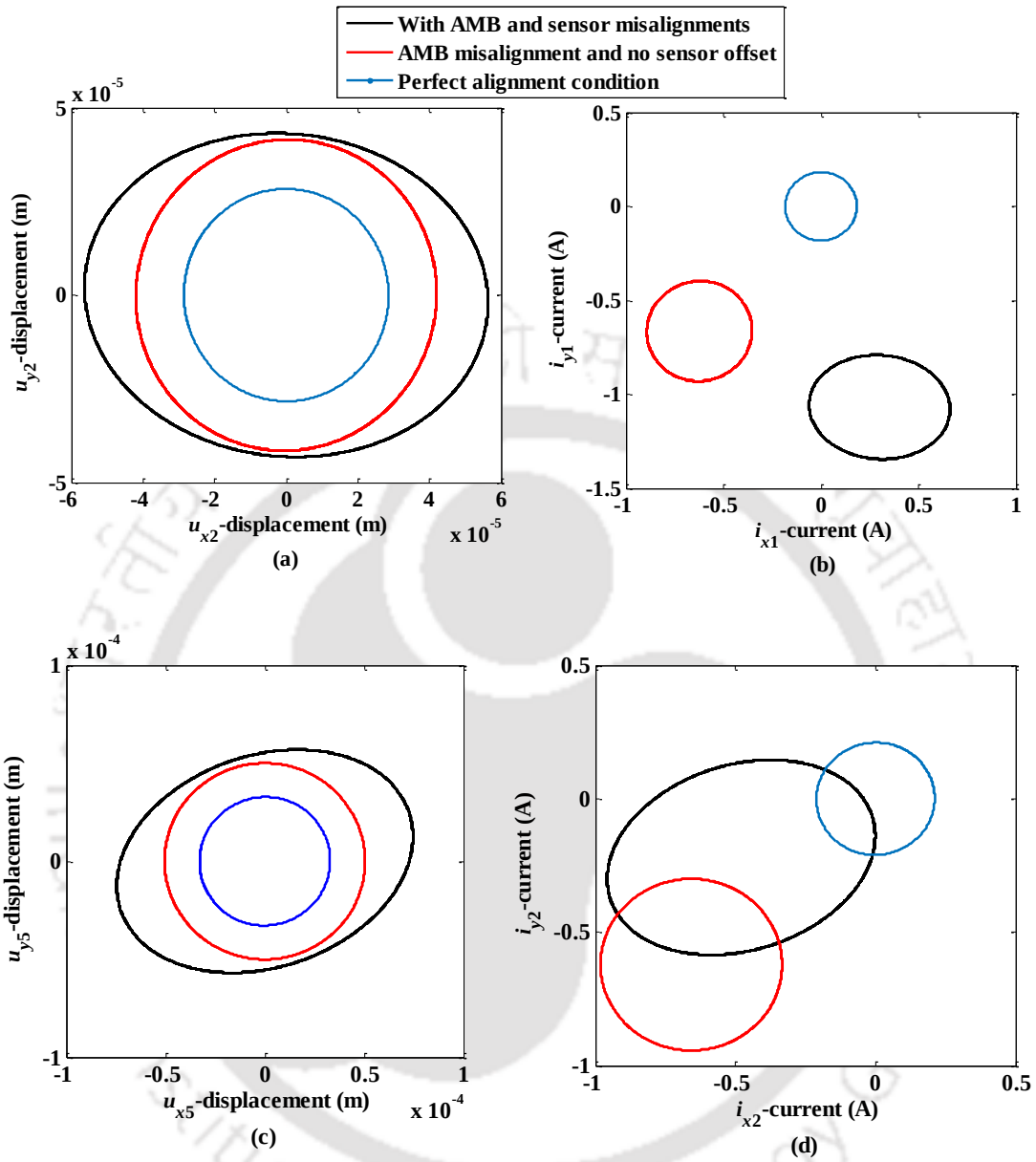

Figure 5.9 Displacement and controlling current orbital responses showing the dynamic influence of AMB and sensor residual misalignments at 120 Hz angular frequency, at (a, b) node 2 (c, d) node 5 locations.

To investigate the dynamic effect of residual misalignments of AMBs and sensors on the rotor system, the displacement and controlling current signals have been generated in the orbit form and compared at the locations of AMBs (i.e., node 2 and node 5), as shown in Figure

5.9. The effect has been explored with three conditions (displayed in Table 5.2). The first condition is considering misalignment in both the AMBs and sensors located at AMBs position. The second is misalignment in AMBs only, but there is no offset in sensors, whereas the perfect alignment of AMBs and sensors with rotor is the third condition. At 120 Hz of rotor angular frequency, the maximum values of rotor displacement for the first, second and third conditions at node 2 are obtained to be 5.63×10^{-5} m, 4.20×10^{-5} m and 2.86×10^{-5} m, respectively. Similarly, at node 5, the peak values of displacement for the three conditions are, respectively, 7.46×10^{-5} m, 5.05×10^{-5} m and 3.29×10^{-5} m. The percentage increase in displacement responses at node 2 and node 5 for the first two conditions are (96.85%, 46.99%) and (126.7%, 53.5%) with respect to perfect alignment condition. However, relative to AMBs misalignment only (i.e., the second condition), the rotor displacement enhances by 34.05% and 47.72% for the residual misalignment of AMBs and sensors as well. Moreover, the orbit size for rotor displacement as well as controlling current signals at nodes 2 and 5 is found to be larger with an increase in misalignment level from the third condition to the first condition. Therefore, it is necessary to identify the amounts of residual misalignments of sensors and AMBs in a magnetically levitated rotor system. This will be beneficial for smooth, efficient and productive operation of rotor-AMB machine in an industry.

It can be observed from Figure 5.9(a-d) that the orbital shapes for the rotor displacement and controlling current responses at both AMB locations (node 2 and node 5) are found to be elliptical in the presence of force due to unbalance and AMBs as well as sensors misalignment faults (i.e., the first condition). This shows that the force coming from the misalignment fault due to combination of parallel and angular misalignments in sensors and AMBs is overshadowing the unbalance force. However, this is not the case for the second and third conditions. The orbit plots for the second condition at 120 Hz angular frequency are also observed to be almost circular, as the unbalance force is more dominating as compared to AMB

misalignment force only (no sensor offset in this case). Further, it is obvious to get circular shape of the plots in the third condition (i.e., perfectly aligned state) as there is only the rotor unbalance force (no misalignment in AMBs and sensors).

Moreover, one of the critical observations can be made from Figure 5.9(b, d) that the controlling current orbits for the first and second misalignment conditions at node 2 and node 5 have been moved away from the zero mean position, unlike the third perfect alignment condition. This has happened due to presence of constant forces (f_{cxq}^{m1}, f_{cyq}^{m1}) in the misaligned AMB force (i.e., Equation (5.12)). These constant forces also cause to displace the rotor displacement responses from the zero mean position, but these response signals get compensated by the integral gain constant (k_I) of the PID controller. This integral constant shifts those to the mean position by introducing a non-zero mean biased controlling currents. It is also worth mentioning that the orbit responses in the rotor displacement and controlling current plots are noticed to be stable although there is some variation with the mean position. Because if a rotor behaves in an unstable manner then the size of the shaft displacement and current orbits would have increased with time, without apparent limit.

5.6.2 Identification of Unbalance, AMB and Sensor Misalignment Parameters

This section describes the time and frequency domain responses as well as identification of unbalance and misalignment faults in a misaligned flexible rotor-sensor-AMB system. For the purpose of estimating simultaneously the system and faults concerned parameters, the displacement and PID output current responses were examined for the time length of 1 s (i.e., from 4 s to 5 s) at each node location of the shaft. The *x*- and *y*-directional displacement and current responses (in the time domain) at AMB 1 and AMB 2 locations are presented in Figure 5.10 and Figure 5.11, respectively, for the residual and additional (trial) misalignments.

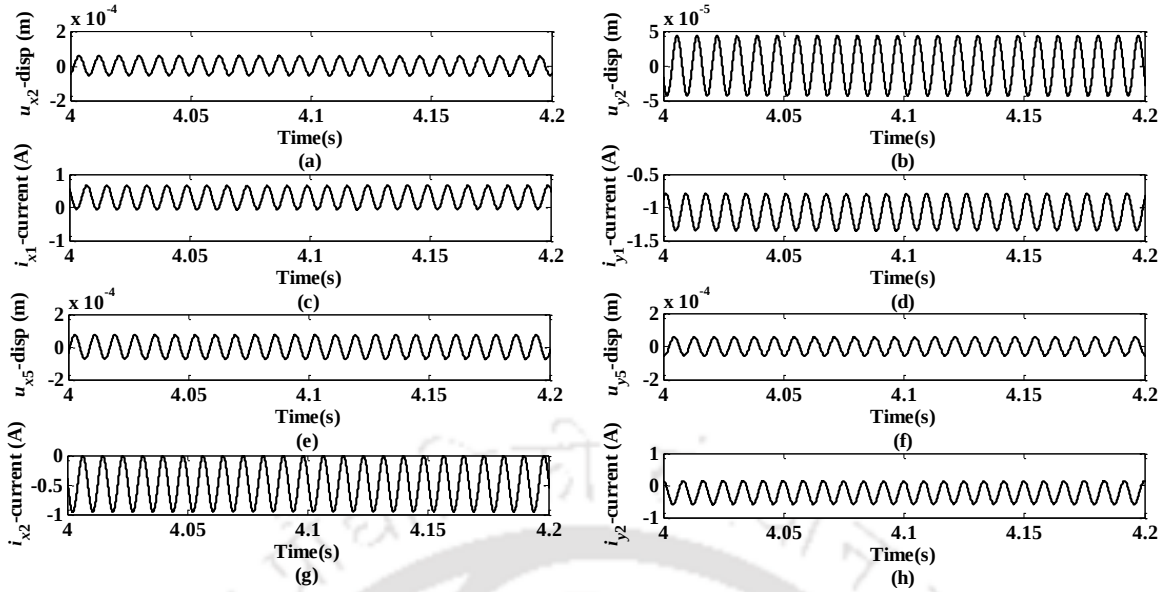

Figure 5.10 Time domain *x*- and *y*-displacement and current responses at 120 Hz angular frequency for residual misalignment at (a-d) node 2 (e-h) node 5 locations.

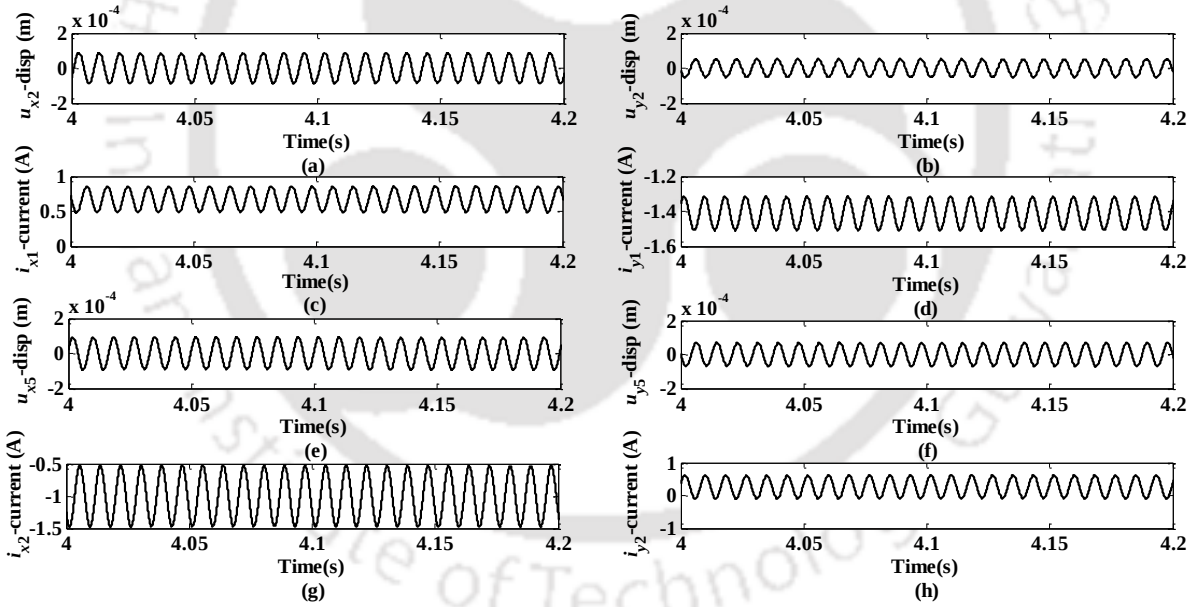

Figure 5.11 Time domain *x*- and *y*-displacement and current responses at 120 Hz angular frequency for additional trial misalignment at (a-d) node 2 (e-h) node 5 locations.

These plots are obtained at the rotor angular frequency of 120 Hz (which is selected far away from first critical speed 53.88 Hz to exhibit the rotor flexibility behaviour and to eliminate the measurement issue close to critical speeds). For the case of residual misalignment of AMBs

and sensors, the peak values of *x*- and *y*-directional displacement response at nodes 2 and 5 are, respectively, obtained to be (5.63×10^{-5} m and 4.33×10^{-5} m) and (7.46×10^{-5} m and 5.69×10^{-5} m), whereas (0.66 A, 1.35 A) and (0.96 A, 0.58 A) are the *x*- and *y*-directional absolute maximum values of current responses at node 2 and node 5 of the shaft. However, the rotor displacements at the same nodes are found to be maximum at (8.70×10^{-5} m and 5.23×10^{-5} m) and (9.18×10^{-5} m and 6.94×10^{-5} m) for the additional (trial) misalignment case (which is combination of residual and rotor trial misalignments) in the *x*- and *y*-directions. Similarly, for the same misalignment case, the absolute maximum values of controlling current responses at node 2 and node 5 are observed to be (0.86 A, 1.51 A) and (1.47 A, 0.62 A), respectively. Hence, it can be remarked from these results that the values of displacement and PID output current responses at AMB locations are higher for the case of additional trial misalignment in comparison to residual misalignment case of sensors and AMBs. The same analysis is perceived for the rotor displacement at other nodes of the shaft element.

Further, FFT function of MATLAB™ is utilized for generating the frequency domain responses from the complex values of time domain signals. The magnitude and corrected phase (follow Appendix C) of frequency domain displacement and current signals at 120 Hz angular frequency, for residual and additional trial misalignments at AMB 1 (node 2) and AMB 2 (node 5) locations are plotted in Figure 5.12 and Figure 5.13. The amplitude and phase of displacement and controlling current responses captured from Figures 5.12 and 5.13 for (i = 0 and 1) are depicted in Table 5.3. The maximum values of rotor displacement and current signals in frequency domain at nodes 2 and 5 are noticed to be (4.98×10^{-5} m, 6.23×10^{-5} m) and (1.10 A, 0.97 A) as well as (6.59×10^{-5} m, 7.85×10^{-5} m) and (1.355 A, 1.338 A) for the residual and additional (trial) misalignment cases, respectively. Thus, the vibration and current amplitude values for the additional trial misalignment are also found to be higher as compared to the residual misalignment case in the frequency domain.

Table 5.3 Amplitude and phase of system responses generated from FFT analysis at both AMB locations.

			Rotor displacement (R_i)		Controlling current (I_i)	
Misalignment	Location	(i)	Amplitude (m)	Phase (deg)	Amplitude (A)	Phase (deg)
Residual misalignment ($m1$)	AMB 1	0	5.39×10^{-10}	-163.87	11.10×10^{-1}	-74.31
		1	4.98×10^{-5}	-157.33	3.19×10^{-1}	43.18
	AMB 2	0	5.61×10^{-10}	-133.61	9.70×10^{-1}	-161.00
		1	6.23×10^{-5}	-116.48	3.74×10^{-1}	84.05
Additional trial misalignment ($m2$)	AMB 1	0	1.91×10^{-9}	138.83	13.55×10^{-1}	-60.22
		1	6.59×10^{-5}	-139.74	3.27×10^{-1}	60.79
	AMB 2	0	2.10×10^{-9}	-57.10	13.38×10^{-1}	-175.50
		1	7.85×10^{-5}	-129.66	4.56×10^{-1}	108.98

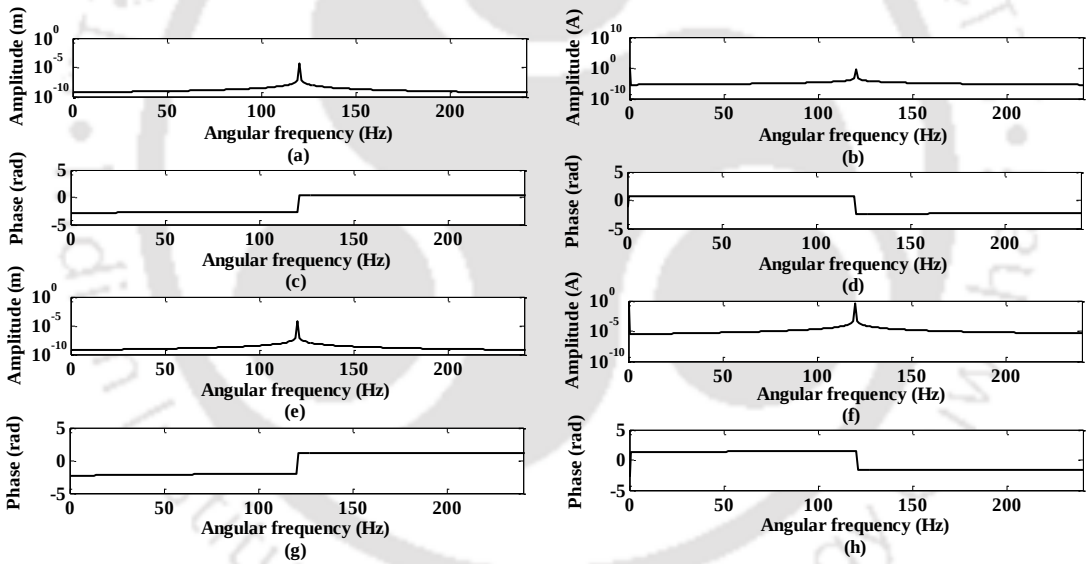

Figure 5.12 FFT based responses at 120 Hz angular frequency for residual misalignment (a-d) amplitude and corrected phase of displacement and controlling current responses at AMB 1 (e-h) amplitude and corrected phase of displacement and controlling current responses at AMB 2.

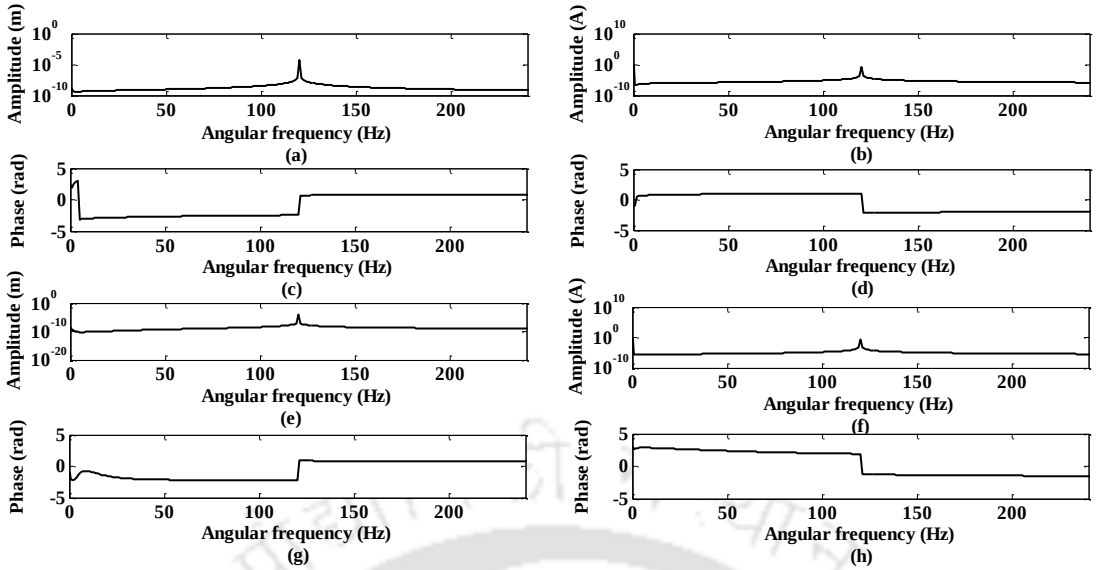

Figure 5.13 FFT based responses at 120 Hz angular frequency for additional trial misalignment (a-d) amplitude and corrected phase of displacement and controlling current responses at AMB 1 (e-h) amplitude and corrected phase of displacement and controlling current responses at AMB 2.

Further, the amplitudes and corrected phases obtained from FFT analysed responses for (i = 0 and 1) are computed to acquire the real as well as imaginary components of displacement at all nodes and current at nodes 2 and 5. Thereafter, these values are utilized in the identification equation (5.33) for identifying the unbalance, AMBs residual misalignment and their stiffness parameters. The number of equations and unknowns for the considered magnetically levitated rotor system (shown in Figure 5.5) is noticed to be 28 and 30, respectively. Here, the number of unknowns is less than the number of equations. Hence, the other angular frequency chosen to operate the rotor system is 130 Hz, which increases the number of rows in known matrix **A** and vector **B** of Equation (5.33) from 28 to 56. This makes the linear system of equations overdeterminate type that is solved using the Moore-Penrose inverse (Equation (5.36)) to obtain the optimal solution. The thirty unknowns in vector **x** of identification equation include 6 unbalance fault parameters (disc eccentricities and phases i.e.,

e_1, β_1, e_2, β_2, e_3, β_3), 24 misaligned AMB 1 and AMB 2 parameters ($k_{sx1}^{m1}, k_{sy1}^{m1}, k_{sx2}^{m1}, k_{sy2}^{m1}, k_{ix1}^{m1}, k_{iy1}^{m1}, k_{ix2}^{m1}, k_{iy2}^{m1}, f_{11}^{m1}, f_{21}^{m1}, f_{12}^{m1}, f_{22}^{m1}, k_{sx1}^{m2}, k_{sy1}^{m2}, k_{sx2}^{m2}, k_{sy2}^{m2}, k_{ix1}^{m2}, k_{iy1}^{m2}, k_{ix2}^{m2}, k_{iy2}^{m2}, f_{11}^{m2}, f_{21}^{m2}, f_{12}^{m2}$ and f_{22}^{m2}) linked with the residual and additional trial misalignments. These unbalance and misaligned AMBs parameters are estimated from the Moore-Penrose inverse. Furthermore, the force-displacement stiffnesses for residual and additional trial misalignments are computed using Equation (5.38) to estimate the AMB residual misalignments (δ_{x1}^{a}, δ_{y1}^{a}, δ_{x2}^{a} and δ_{y2}^{a}) from the known values of rotor virtual trial misalignments (Δ_{x1}^{r}, Δ_{y1}^{r}, Δ_{x2}^{r} and Δ_{y2}^{r}) and AMB air gap (s_0). Additionally, the estimated values of AMB misaligned stiffnesses as well as the residual misalignments are used in Equation (5.14) to estimate the actual force-displacement and force-current stiffness constants (k_{sx1}, k_{sy1}, k_{sx2}, k_{sy2}, k_{ix1}, k_{iy1}, k_{ix2} and k_{iy2}) of AMB 1 and AMB 2 in the *x*- and *y*-directions. The percentage errors in the estimated values relative to the assumed values of disc eccentricities and phases, AMB residual misalignments and their actual stiffness coefficients for clean signal are displayed in Table 5.4. The percentage errors have been achieved by taking the rotor displacement and controlling current responses at the combined angular frequencies of 120 Hz and 130 Hz. Further, the proposed algorithm is tested with addition of noise signal errors (random Gaussian noise) and rotor modelling errors up to 5% level. This has been done to encounter the practical aspects in a real rotor-AMB system. The noise percentage of 1%, 2% and 5% are added individually in the frequency domain simulated responses. Afterwards, these noise corrupted signals are given as input in the identification equation for the estimation purpose. Similarly, the modelling errors of 1%, 2% and 5% are introduced in the assumed values of rotor system and the time domain as well as frequency domain signals are generated. They are utilized in the developed identification algorithm for obtaining the bias error corrupted estimates.

Table 5.4 Sensitivity of estimated unbalance, AMBs residual misalignment and their stiffness parameters with noise signal and rotor modelling errors at the combined angular frequencies of 120 and 130 Hz.

Parameters	Values	Error percentage in estimated values with addition of noise and rotor modelling or bias errors						
		Clean signal	1% noise	1% bias	2% noise	2% bias	5% noise	5% bias
e_1 (μm)	50.00	-0.10%	-0.11%	0.13%	-0.46%	0.17%	1.65%	0.88%
β_1 (deg)	10.00	0.03%	0.04%	0.03%	0.15%	0.04%	0.94%	0.07%
e_2 (μm)	80.00	0.05%	0.16%	0.06%	-0.25%	-0.09%	-1.72%	-1.04%
β_2 (deg)	30.00	-0.01%	-0.36%	-0.01%	-0.73%	-0.04%	-1.01%	-0.28%
e_3 (μm)	100.00	-0.04%	-0.07%	-0.05%	-0.19%	-0.11%	-1.57%	-0.66%
β_3 (deg)	50.00	-0.01%	-0.01%	-0.02%	0.04%	-0.09%	-1.05%	-0.41%
δ^a_{x1} (mm)	0.140	0.95%	-1.23%	1.11%	-2.45%	1.24%	-5.77%	1.91%
δ^a_{y1} (mm)	0.160	1.43%	-2.22%	1.81%	7.97%	-3.53%	-8.44%	-4.36%
δ^a_{x2} (mm)	0.150	1.10%	1.58%	-5.43%	1.33%	-4.88%	3.60%	-8.16%
δ^a_{y2} (mm)	0.145	3.98%	-4.70%	4.39%	-5.86%	5.25%	-7.94%	7.52%
k_{sx1} (N/m)	174150	-0.18%	0.85%	0.76%	3.44%	1.35%	7.81%	-2.96%
k_{sy1} (N/m)	195000	-1.04%	5.42%	-4.37%	-18.05%	2.48%	20.13%	1.87%
k_{sx2} (N/m)	365710	-1.86%	-2.60%	8.05%	-5.91%	6.14%	-9.48%	7.55%
k_{sy2} (N/m)	383000	-4.22%	5.37%	-4.34%	6.88%	-4.73%	12.45%	-8.42%
k_{ix1} (N/A)	34.83	9.37%	10.25%	9.88%	13.85%	12.77%	23.92%	14.01%
k_{iy1} (N/A)	36.20	15.94%	16.87%	16.45%	14.32%	17.90%	25.28%	20.33%
k_{ix2} (N/A)	73.14	16.20%	8.49%	21.26%	9.10%	23.25%	11.39%	24.99%
k_{iy2} (N/A)	75.40	11.19%	13.50%	11.96%	17.21%	12.57%	19.80%	13.58%

Table 5.4 also contains the estimated parameters in the form of error percentage (calculated relative to the assumed values) with the inclusion of noise and modelling errors. Under the impact of these introduced errors, the least influenced parameters are the unbalance fault parameters. They get deviated from the assumed ones only by -1.72% and -1.04% for the highest level of 5% noise and bias errors, respectively. The residual misalignments of AMB 1 and AMB 2 have also been identified with highest deviations of -8.44% and -8.16%, respectively, for 5% level of noise signal and modelling errors. The residual amounts δ_{y1}^{a} and δ_{x2}^{a} are noticed to be mostly affected as compared to estimation from the uncorrupted signal.

It can also be observed from Table 5.4 that the percentage errors in estimates are maximum (i.e., -20.13% and 25.28%) in the force-displacement (k_{sy1}) and force-current (k_{iy1}) stiffnesses of AMB at 5% noise error. Including 5% modelling error, the most affected parameter is k_{ix2} with percentage deviation of 24.99%. Estimated percentage errors in all the AMBs force-displacement and force-current stiffness constants (k_{sx1}, k_{sy1}, k_{sx2}, k_{sy2}, k_{ix1}, k_{iy1}, k_{ix2} and k_{iy2}) are highest with the addition of highest levels of both kinds of measurement signal noise and modelling errors. These are due to the combined errors coming from the identified values of misaligned AMB stiffness parameters (obtained from identification equation (5.33)) and the residual misalignments (δ_{x1}^{a}, δ_{y1}^{a}, δ_{x2}^{a} and δ_{y2}^{a}). Moreover, it is noticeable from Table 5.4 that for almost all the estimated parameters, the estimates are mostly influenced from noise error in comparison to the modelling error.

Moreover, the identification of unbalance and misalignment faults as well as the stiffness constants of AMBs in the considered rotor-AMB system have also been performed with the combined sets of two different rotor angular frequencies. This has been done for testing the robustness and performance of the proposed quantitative based identification technique. Moreover, the estimation has yielded better results with the inclusion of more number of

equations by adding rows corresponding to various speeds in regression matrices, as enunciated in Equation (5.37). For the sensitivity analysis of results with varying modelling error and measurement noise, the range of the first angular frequency chosen is 105 Hz to 141 Hz, and the second angular frequency range is 115 Hz to 151 Hz in discrete steps of 3 Hz. All the selected speeds in the first and second speed ranges are also kept well above half-power band of the first critical speed (i.e., 53.88 Hz) for exhibiting the shaft flexibility behaviour throughout the rotor operation and to avoid transients during measurement of responses close to the critical speed. The effect of addition of various levels of signal noise and modelling errors in estimation of disc unbalance parameters, AMBs residual misalignments and the actual force-displacement and current stiffness constants of AMB 1 and AMB 2 are shown in Figure 5.14. It can be observed from Figure 5.14 that the deviation of the estimated unbalance parameters are found to be same as for the combination of two (single) speeds case (i.e., 120 Hz and 130 Hz). The residual misalignments and AMB parameters at 5% rotor modelling or bias error and 5% noise signal error are also observed to be highest for almost all parameters. Within the selected range of angular frequencies, the minimum and maximum percentage deviations in AMB residual misalignments, are, respectively, 1.11% and -7.03%, for the amounts δ_{x1} and δ_{x2}. However, the parameter k_{sx1} has registered least and highest influence of the noise error with the variations of 0.85% and 5.94%. The percentage errors in almost all the identified parameters is found to be more with the addition of increasing values of random Gaussian noise and rotor modelling errors. Moreover, out of all these estimated parameters, the most vulnerable parameter is k_{iy1} at 5% noise corrupted signal for both the single and range of multiple speeds cases. It can also be seen from Figure 5.14 that cumulative data of responses with the usage of multiple spin speeds is likely to minimize the estimation error in the identification even due to different effects of noise and bias errors. Hence, the identification technique relying on VTM concept is providing good estimates even with the addition of noise

signal and modelling errors for the single as well as combined two different speeds range of the flexible rotor mounted on active magnetic bearings.

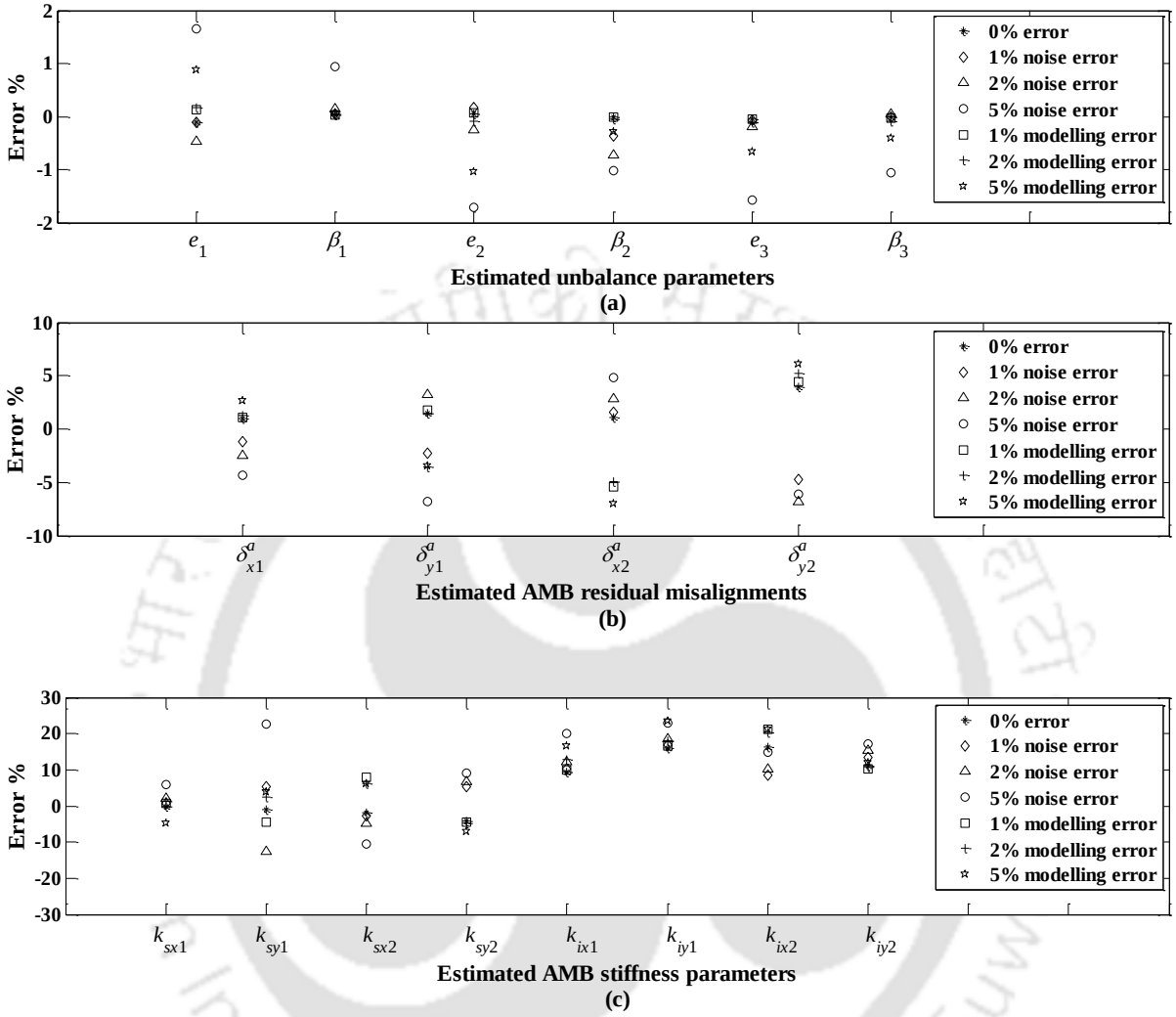

Figure 5.14 Percentage deviation for the combined two speeds range of (105 Hz to 141 Hz) and (115 Hz to 151 Hz) with clean as well as noise and modelling errors added signal (a) estimated unbalance parameters (b) estimated AMB residual misalignments (c) estimated AMB stiffness parameters.

Further, the misalignment of AMB has been also identified at different spin speeds of the shaft for clean signal and noise as well as modelling errors corrupted signals. For the sensitivity analysis of the identified misalignment amounts with different levels of measurement signal noise and modelling errors, the first discrete angular frequencies are

chosen from 105 Hz to 141 Hz in steps of 3 Hz (i.e., 105, 108, 111, 114, 117, 120, 123, 126, 129, 132, 135, 138, 141 Hz) and the second discrete angular frequencies are selected from 115 Hz to 151 Hz in the same steps of 3 Hz (i.e., 115, 118, 121, 124, 127, 130, 133, 136, 139, 142, 145, 148, 151 Hz). The effect of addition of signal noise and modelling errors in the estimation of one of the residual misalignment (i.e., δ_{x1}) of AMB 1 at the discrete mean angular frequencies are shown in Figure 5.15. The minimum and maximum percentage deviations in the estimated residual misalignment, δx1 are 0.54% and -7.93% at the addition of 1% modelling and 5% noise errors, respectively. Moreover, for the clean signal, the estimated value of the residual misalignment is found to be deviated as compared to assumed value only by 0.53%.

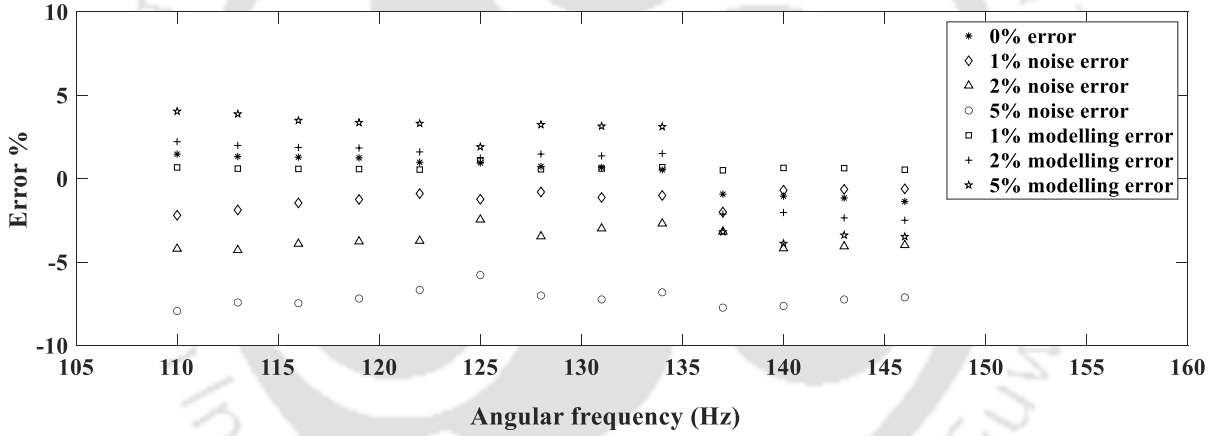

Figure 5.15 Estimated percentage error of residual misalignment of AMB 1 (i.e., δ_{x1}) with the discrete angular frequencies under the influence of noise and modelling errors.

In addition to that, the residual misalignment of sensors at both AMB locations in the *x*- and *y*-directions ($\delta_{x1}^s, \delta_{y1}^s, \delta_{x2}^s$ and δ_{y2}^s as shown in Figure 5.6) are also identified using Equations (5.31) and (5.25) as well as the known values of additional gap of sensors and rotor trial misalignments (follow Table 5.1). Table 5.5 displays the identified values of sensors residual misalignments. The brief procedure for identifying sensor misalignment is explained in Section 5.4 and Figure 5.4.

Table 5.5 Identified values of sensors residual misalignments.

Parameters related to misaligned sensors	**Identified values**
Residual misalignment of sensor in *x*- direction at AMB 1 location, δ_{x1}^{s}	4.50×10^{-3} m
Residual misalignment of sensor in *y*- direction at AMB 1 location, δ_{y1}^{s}	2.80×10^{-3} m
Residual misalignment of sensor in *x*- direction at AMB 2 location, δ_{x2}^{s}	3.20×10^{-3} m
Residual misalignment of sensor in *y*-direction at AMB 2 location, δ_{y2}^{s}	3.70×10^{-3} m

These known values of sensors residual misalignments will help a user to first align the sensor stands for measuring the displacement responses and then operate the rotor at desired speed. From the above discussed results, the salient remark can be made that the novelty of the present work is in the proposed VTM approach and identification methodology. This method has been significantly favourable in identification of unbalance, sensors and AMBs residual misalignment and their stiffness parameters in a flexible rotor-sensor-AMB system.

5.7 Summary

A virtual trial misalignment (VTM) approach and identification algorithm have been proposed in this chapter for the quantitative estimation of rotor unbalance, AMBs residual misalignment and their force-displacement and force-current stiffness parameters in a magnetically levitated rotor-AMB system. The VTM approach has also been utilized in the identification of residual misalignment of sensors located at AMB locations for measuring the displacement responses. The trial (virtual) misalignment to the rotor is given through additional bias currents supplied to AMB along with the controlling current. This innovative concept for providing trial misalignment in addition to residual misalignment is quite reliable and time saving as compared to physical trial misalignment.

For testing this novel identification scheme, a multidisc flexible rotor misaligned with multiple supported AMBs are considered and modelled using finite element method. The linearized form of AMB force for the sensors and AMBs misalignment case is obtained. Modelling for the misaligned sensors at AMB locations for the residual and additional trial misalignments has been well explained. Dynamic effect of residual misalignment of sensors and AMBs on the rotor system is also explored considering three conditions (i.e., the first condition is both AMB and sensor are residually misaligned, the second is only AMB residual misalignment but no sensor offset and the last is perfectly aligned condition). The rotor displacement and controlling current responses are found to be increased with increase in the misalignment level from the third condition to first condition. Further, the frequency domain responses are utilized in identification algorithm for estimating the rotor system and fault parameters. Moreover, the developed algorithm based on VTM concept is also observed to be effective and robust even with the addition of different levels of noise signal and rotor modelling errors as well as in multiple range of spin speeds.

The formulation, analysis and identification presented in this chapter are for a single rotor supported by multiple AMBs. However, this can be extended for more practical dual rotor and turbogenerator (TG) systems. The identification procedure derived from VTM approach has been developed to estimate unbalance on every disc and displacement as well as current stiffness constants of each supported AMB. This makes possible the multiplane balancing of the rotor apart from the identification of AMBs misalignment in the system. This is a significant contribution towards aligning and balancing of the magnetically levitated rotor system.

The mathematical formulations for analysis and identification developed in Chapters 4 and 5 are for multi-AMBs rotor system but simulation is for two AMBs only. This has been done for checking the stability and verification of accuracy of the developed procedure. The robustness and constancy of the identification algorithm can be justified from the presented

numerical results on dynamic influence of misalignment and estimation of parameters in presence of noise signal errors and rotor modelling errors. A summary of the work executed in Chapters 2 through 5 with different models and assumptions, increase in complexity in analysis and identification, are presented in the next chapter. Scopes of future work based on insights acquired from the present work are also described with probable suggestions.

Chapter 6

Conclusions and Scope for Future Work

6.1 Summary of the Present Work

In the present study, an analytical work has been executed to develop a model based identification algorithm derived from a novel trial misalignment approach (physical and virtual trial misalignments) for quantitatively identifying the rotor unbalance and AMB misalignment parameters. This approach is aligned with the idea of trial unbalance in the rotor balancing. The force-displacement and force-current stiffness coefficients of AMB are also estimated. In addition to that, the virtual trial misalignment (VTM) concept has been successfully employed in the identification of offset of misaligned sensors available at AMB locations. The force due to misaligned AMBs has been derived for the case of perfect alignment in sensors as well as misalignment in sensors. The dynamic influence of residual misalignments of AMBs and sensors on the rotor performance has also been investigated. The present identification methodology relies upon the frequency domain rotor displacements and AMB controlling currents. The frequency domain signals have been obtained by solving the equations of motion of the various rotor-AMB models and transforming the generated time domain responses using FFT technique. Moreover, the identification algorithm has been developed and accomplished in such a way that it can be applied to practical rotating machineries integrated with active magnetic bearings. The works carried out in the present dissertation are summarized as follows:

1. An identification methodology has been proposed for a 2-DOFs rigid rotor model mounted on two parallel misaligned (isotropic and identical in nature) AMBs. This fairly simple model serves the purpose of benchmarking various procedures, which is used further in the next rotor-AMB models addressing greater complexities. The linearized form of misaligned AMB force has been obtained based on assumptions of

small induced vibrations in comparison to air gap between rotor and AMB stator. The physical trial misalignment (PTM) method to provide additional (known) misalignments between rotor and AMBs axes has been elaborated with respect to actuator housings. Equations of motion of the rotor-AMB model has been derived with the inclusion of inertia force, unbalance force and misaligned AMB force. The procedures for developing frequency based identification algorithm have also been given in details. Through the numerical simulation, the time and frequency domain responses are obtained and utilized in the developed methodology for identification of the unbalance and AMB misalignment parameters. Dynamic effect of AMB misalignment with less and more amounts is also explored. The more details on noise and modelling errors have been provided here. Further, to mimic the practical rotor-AMB model, the proposed algorithm is also tested against the noisy responses and addition of bias errors in the range of multiple spin speeds.

2. In order to avoid the major assumptions in the previous model and keeping in mind the practical applicability, the next model is presented with incorporation of more complexities. This model has included two offset discs and their gyroscopic effects due to tilting motion, which requires to analysis the system as 4-DOFs. Instead of parallel misalignment and identical nature of AMBs, the combination of lateral and angular misalignments as well as different nature of both AMBs have been considered in the rigid rotor model. The mathematical procedures described in 2-DOFs model have been employed for developing the identification equation. To overcome the ill-conditioning of this equation and convert the linear equations of system from underdetermined to overdetermined type, the FFT based responses has been captured for two different speeds and utilized in the regression equation having more number of rows. The Moore-

Penrose inverse method is used to obtain the optimum solution of identification equation consisting of unbalance parameters (eccentricities and phases for both discs), misaligned AMBs parameters and their residual misalignments.

3. The rotor model considered in previous two models have been shown to exhibit rigid behaviour by numerically operating the rotor below the first flexible critical speed of the system. However, this is not the case with more realistic and applicable rotor system. Therefore, the third model consists of a magnetically levitated flexible rotor system fastened with multiple discs and associated with aligned proximity sensors. The spin speeds for the analysis and identification are chosen above the first flexible critical speed to show flexibility nature of shaft during operation. Moreover, the supported AMBs are considered to anisotropic and different in nature. The well-established finite element method with Timoshenko beam elements is utilized for exploring the mathematical model of the flexible rotor-AMB system. Since the rotational displacements pose practical difficulty of accurate measurements, so the gyroscopic dynamic reduction scheme is implemented to eliminate rotational displacements in identification equation. Displacement and current responses obtained at various nodes in the shaft are analysed further to study the dynamic nature of the system for residual and additional trial misalignments as well as to obtain system and faults parameters from the proposed frequency based algorithm.

4. In the previous rigid rotor and FEM based flexible rotor models, the non-contact eddy current sensors placed near AMBs were considered in perfect alignment with the rotor centre. Nevertheless, in real practice, the sensors can also suffer by some degree of misalignment from the required original position due to initial setting errors, system

assembly errors, manufacturing errors, etc. From this point of view, the next model considers misalignment in the sensors and supported AMBs with respect to the centre position of rotor. Hence, the misaligned AMB force has been obtained in the linearized form in the presence of sensors offset. Mathematical modelling of the misaligned sensors is also presented through their residual and additional trial misalignment conditions. Moreover, an innovative virtual trial misalignment approach has been proposed for providing known trial misalignment to the rotor through additional bias current in AMB. This VTM approach is more reliable and time saving than PTM approach. Dynamic effect of AMBs and sensors residual misalignments on the displacement and controlling current responses are also explored and discussed in details. The proposed identification algorithm is able to estimate the rotor unbalance parameters, AMB misalignment parameters as well as their actual stiffness constants. Additionally, the offset amounts of sensors are determined using VTM approach.

6.2 Conclusions from the Present Work

The following are the major conclusions from present work:

- A novel concept of trial misalignment approach and identification methodology have been successfully developed and explored in magnetically levitated rotor systems to identify simultaneously the rotor unbalance fault and residual misalignments of supported AMBs.
- The linearized form of force due to misaligned AMBs has been obtained for the case of perfect alignment of sensors as well as misalignment of sensors. This force is found to consist of one constant force term along with modified force-displacement and force-

current stiffness parameters. This constant force at AMB location causes more vibration in the system and increases the power consumption in AMB.

- To provide additional (known) trial misalignment in the rotor-AMB system, the two different approaches, i.e. physical trial misalignment (PTM) and virtual trial misalignment (VTM) have been proposed. The second approach is found to be more effective and reliable than PTM approach, as this concept does not require hard labour, perfect and precise model of the system components as well as consume less time.
- The displacement and controlling current responses in the time domain have been obtained from solving the EOMs of the rotor-AMB systems. These responses in the orbit forms are investigated to analyse the dynamic influence of AMBs and sensors residual misalignment on the rotor performance. It is found that the vibration level in the rotor and the requirement of AMB controlling current is more in the misaligned condition of the system as compared to the perfectly aligned case.
- While analysis of the current orbit plots in the misaligned state of the rotor-sensors-AMBs system, it is observed that these orbits have been moved away from the zero mean position, unlike the perfect alignment state. This is caused due to an extra constant force developed in the present formulation of misaligned AMB force. This force also causes to shift the displacement signal, but the integral part of PID controller (k_I) compensates the displacement signal and bring it to the mean position by generating a biased controlling current, having a non-zero mean.
- Moreover, with the consideration of AMBs and sensors residual misalignment, the orbit plots for displacement and controlling current responses are found to be elliptical in shape. It is mainly from overshadowing nature of force arising from the sensors and AMBs misalignment fault on the unbalance force.

- FFT analysis is performed to obtain the frequency dependent responses with their magnitude and phase, from the numerically generated time domain signals. These frequency domain responses (displacement and current) are also noticed to be more for the higher level of AMBs misalignment without and with offset in sensors.
- Utilizing the FFT responses into the proposed identification algorithm, the stiffness coefficients of AMBs (force-displacement and force-current) have been successfully estimated along with the identified unbalance and AMBs residual misalignment parameters, for the clean signals and also by adding various levels of noise signal and rotor modelling errors. More deviations are observed in the estimated AMB stiffness constants relative to their assumed values. This is due to the combined errors resulting from errors in the identified residual misalignments and misaligned AMB parameters. However, all the parameters were identified within the acceptable range.
- Even for checking the performance of identification procedure, the estimation of parameters has also been done within the range of multiple spin speeds of the rotor. For this case also, the developed methodology is found to be effective and robust.
- Additionally, the offset amounts of proximity probes located at AMB locations for measuring rotor displacement responses are also identified using the virtual trial misalignment (VTM) approach. This has been accomplished with the help of subtracted air gaps between rotor and sensors as well as the known values of rotor trial misalignments. The subtraction of the air gaps include final gaps (i.e., for additional offset condition of sensors after providing trial misalignments to the rotor) and initial gaps of sensors (i.e., for residual offset condition of sensors arising from initial setting errors, assembly errors, etc.).

6.2 Main Contribution of the Present Work

Major contributions from the present research work are as follows:

- The developed methodology derived from novel trial misalignment concept is quite helpful in identifying simultaneously the two kinds of severe faults, i.e. the rotor unbalance and the supported bearing (AMBs) residual misalignments. Along with the vibrational signatures of the faults and their effects on the rotor system, the present work is able to provide quantitative information of the faults. Besides that, the identification algorithm is also beneficial in estimating the force-displacement and force-current stiffness constants of AMBs.
- The proposed virtual trial misalignment (VTM) approach using additional bias current at AMB locations is a user-friendly technique, which can reduce the physical efforts for providing known (trial) misalignment in the rotor-AMBs system.
- Moreover, the VTM approach is also able to explore the effect of sensors misalignment and estimate their offset amounts through innovative mathematical modelling of sensors for residual and additional trial misalignments.

6.4 Limitations and scopes of future work

Limitations of the present work and scopes for further research are as follows

- The rotor can have discrete unbalances at disc locations, distributed unbalances along the length of the shaft or a combination of both is also possible. But, in the considered rotor-AMB models, the shaft residual unbalances are neglected based on the assumption that the unbalances in the rotor are distributed to the discrete discs in different magnitudes and at different orientations. However, the identification

algorithm can be developed effectively for multiplane balancing of the physical rotor-AMBs system with consideration of shaft distributed unbalances.

- The present rotor systems include only the shaft material damping and damping force resulting from the PID controller of AMB. However, in a real system, the damping force also comes from AMBs foundation and the foundation of whole rotor system, which have been neglected in the present analysis. Hence, the damping force arising from whole rotor-AMBs foundation (and damping in other type of bearings when included, e.g. fluid film bearings) can also be considered, mathematically modelled and identified by developing an estimation methodology. This can estimate the stiffness as well as damping parameters along with the presently identified system and faults parameters.
- The present work is based on assumptions of linear harmonic analysis and linear response, which can be justified for less vibrations in rotor-AMBs system. However, in real systems, the vibrations can also be high in magnitude due to various faults. Therefore, the identification methodology can be developed for nonlinear flexible rotor-AMB model for estimation of various system and fault parameters. For this, the solution of the non-linear EOMs can be obtained using Runge-Kutta fourth order technique as discussed in Desale and Dasre (2013). Further, the developed identification equation can be solved with the help of non-linear regression analysis (Bates and Watts, 1988) to estimate the parameters.
- The modelling, analysis and identification has been performed for a single rotor system integrated with AMBs, not for a coupled rotor system. Thus, the proposed analytical work can be extended for more practical magnetically levitated dual rotor and turbogenerator systems with consideration of coupling misalignment along with the existing AMBs and sensors misalignment.

- The estimation procedure and analysis have been presented considering two critical faults only, i.e. unbalance in rotor and misalignment in AMBs as well as sensors. However, this can extended for a rotor-AMB system affected simultaneously from several faults such as crack in shaft, shaft bow and rub, coupling misalignment, etc. along with the considered faults.
- The present research work is analytical in nature and the results are based on numerical simulation. Therefore, the laboratory experimentation can be performed to study the effect of AMBs and sensors misalignment on the rotor displacement and AMB controlling current responses in a rotor system levitated by misaligned (parallel and angular) active magnetic bearings.
- Identification of unbalance parameters, AMBs and sensors residual misalignments as well as AMBs stiffness constants using PTM and VTM approaches can be done experimentally for 2 DOFs, 4 DOFs and multi DOFs rotor system. Further, the experimental results can be validated with the numerically obtained estimations.

APPENDICES

Appendix A. Timoshenko Beam model

A.1 Translational mass matrix

$$\mathbf{M}_T = \mathbf{M}_{T_0} + \Phi\mathbf{M}_{T_1} + \Phi^2\mathbf{M}_{T_2} \tag{A.1}$$

where

$$\mathbf{M}_{T_0} = \frac{\rho Al}{420(1+\Phi)^2}\begin{bmatrix} 156 & & & & & & & \\ 0 & 156 & & & \text{Sym} & & & \\ 0 & -22l & 4l^2 & & & & & \\ 22l & 0 & 0 & 4l^2 & & & & \\ 54 & 0 & 0 & 13l & 156 & & & \\ 0 & 54 & -13l & 0 & 0 & 156 & & \\ 0 & 13l & -3l^2 & 0 & 0 & 22l & 4l^2 & \\ -13l & 0 & 0 & -3l^2 & -22l & 0 & 0 & 4l^2 \end{bmatrix}; \tag{A.2}$$

$$\mathbf{M}_{T_1} = \frac{\rho Al}{420(1+\Phi)^2}\begin{bmatrix} 294 & & & & & & & \\ 0 & 294 & & & \text{Sym} & & & \\ 0 & -38.5l & 7l^2 & & & & & \\ 38.5l & 0 & 0 & 7l^2 & & & & \\ 126 & 0 & 0 & 31.5l & 294 & & & \\ 0 & 126 & -31.5l & 0 & 0 & 294 & & \\ 0 & 31.5l & -7l^2 & 0 & 0 & 38.5l & 7l^2 & \\ -31.5l & 0 & 0 & -7l^2 & -38.5l & 0 & 0 & 7l^2 \end{bmatrix}; \tag{A.3}$$

$$\mathbf{M}_{T_2} = \frac{\rho Al}{420(1+\Phi)^2}\begin{bmatrix} 294 & & & & & & & \\ 0 & 294 & & & \text{Sym} & & & \\ 0 & -38.5l & 7l^2 & & & & & \\ 38.5l & 0 & 0 & 7l^2 & & & & \\ 126 & 0 & 0 & 31.5l & 294 & & & \\ 0 & 126 & -31.5l & 0 & 0 & 294 & & \\ 0 & 31.5l & -7l^2 & 0 & 0 & 38.5l & 7l^2 & \\ -31.5l & 0 & 0 & -7l^2 & -38.5l & 0 & 0 & 7l^2 \end{bmatrix} \tag{A.4}$$

with the constant Φ is

$$\Phi = \frac{12EI}{k_{sc}GAl^2}$$

where E and G are the modulus of elasticity and modulus of rigidity of shaft material, respectively. The length, area and moment of inertia of the shaft element are represented by l, A and I, respectively. The shear correction factor is represented by k_{sc}.

A.2 Rotational mass matrix

$$\mathbf{M}_R = \mathbf{M}_{R_0} + \Phi\mathbf{M}_{R_1} + \Phi^2\mathbf{M}_{R_2} \tag{A.5}$$

where

$$\mathbf{M}_{R_0} = \frac{\rho Al}{(1+\Phi)^2}\begin{bmatrix} 6/5 & & & & & & & \\ 0 & 6/5 & & & \text{Sym} & & & \\ 0 & -1/10 & 2l/15 & & & & & \\ 1/10 & 0 & 0 & 2l/15 & & & & \\ -6/5 & 0 & 0 & -1/10 & 6/5 & & & \\ 0 & -6/5 & 1/10 & 0 & 0 & 6/5 & & \\ 0 & -1/10 & -l/30 & 0 & 0 & 1/10 & 2l/15 & \\ 1/10 & 0 & 0 & -l/30 & -1/10 & 0 & 0 & 2l/15 \end{bmatrix}; \tag{A.6}$$

$$\mathbf{M}_{R_1} = \frac{\rho Al}{(1+\Phi)^2}\begin{bmatrix} 0 & & & & & & & \\ 0 & 0 & & & \text{Sym} & & & \\ 0 & 1/2 & l/6 & & & & & \\ -1/2 & 0 & 0 & l/6 & & & & \\ 0 & 0 & 0 & 1/2 & 0 & & & \\ 0 & 0 & -1/2 & 0 & 0 & 0 & & \\ 0 & 1/2 & -l/6 & 0 & 0 & -1/2 & l/6 & \\ -1/2 & 0 & 0 & -l/6 & 1/2 & 0 & 0 & l/6 \end{bmatrix}; \tag{A.7}$$

$$\mathbf{M}_{R_2} = \frac{\rho A l}{(1+\Phi)^2}\begin{bmatrix} 0 & & & & & & & \\ 0 & 0 & & & \text{Sym} & & & \\ 0 & 0 & l/3 & & & & & \\ 0 & 0 & 0 & l/3 & & & & \\ 0 & 0 & 0 & 0 & 0 & & & \\ 0 & 0 & 0 & 0 & 0 & 0 & & \\ 0 & 0 & l/6 & 0 & 0 & 0 & l/3 & \\ 0 & 0 & 0 & l/6 & 0 & 0 & 0 & l/3 \end{bmatrix} \tag{A.8}$$

A.3 Stiffness matrix

$$\mathbf{K} = \mathbf{K}_0 + \Phi\mathbf{K}_1 \tag{A.9}$$

where

$$\mathbf{K}_0 = \frac{EI}{(1+\Phi)l^3}\begin{bmatrix} 12 & & & & & & & \\ 0 & 12 & & & \text{Sym} & & & \\ 0 & -6l & 4l^2 & & & & & \\ 6l & 0 & 0 & 4l^2 & & & & \\ -12 & 0 & 0 & -6l & 12 & & & \\ 0 & -12 & 6l & 0 & 0 & 12 & & \\ 0 & -6l & 2l^2 & 0 & 0 & 6l & 4l^2 & \\ 6l & 0 & 0 & 2l^2 & -6l & 0 & 0 & 4l^2 \end{bmatrix}; \tag{A.10}$$

$$\mathbf{K}_1 = \frac{EI}{(1+\Phi)l^3}\begin{bmatrix} 0 & & & & & & & \\ 0 & 0 & & & \text{Sym} & & & \\ 0 & 0 & l^2 & & & & & \\ 0 & 0 & 0 & l^2 & & & & \\ 0 & 0 & 0 & 0 & 0 & & & \\ 0 & 0 & 0 & 0 & 0 & 0 & & \\ 0 & 0 & -l^2 & 0 & 0 & 0 & l^2 & \\ 0 & 0 & 0 & -l^2 & 0 & 0 & 0 & l^2 \end{bmatrix} \tag{A.11}$$

A.4 Gyroscopic matrix

$$\mathbf{G} = \mathbf{G}_0 + \Phi\mathbf{G}_1 + \Phi^2\mathbf{G}_2 \tag{A.12}$$

where

$$\mathbf{G}_0 = \frac{\rho A r^2}{60(1+\Phi)^2 l}\begin{bmatrix} 0 & & & & & & & \\ 36 & 0 & & & \text{Skew sym} & & & \\ -3l & 0 & 0 & & & & & \\ 0 & -3l & 4l^2 & 0 & & & & \\ 0 & 36 & -3l & 0 & 0 & & & \\ -36 & 0 & 0 & -3l & 36 & 0 & & \\ -3l & 0 & 0 & l^2 & 3l & 0 & 0 & \\ 0 & -3l & -l^2 & 0 & 0 & 3l & 4l^2 & 0 \end{bmatrix}; \quad \text{(A.13)}$$

$$\mathbf{G}_1 = \frac{\rho A r^2}{60(1+\Phi)^2 l}\begin{bmatrix} 0 & & & & & & & \\ 0 & 0 & & & \text{Skew sym} & & & \\ 15l & 0 & 0 & & & & & \\ 0 & 15l & 5l^2 & 0 & & & & \\ 0 & 0 & 15l & 0 & 0 & & & \\ 0 & 0 & 0 & 15l & 0 & 0 & & \\ 15l & 0 & 0 & 5l^2 & 0 & 0 & 0 & \\ 0 & 15l & -5l^2 & 0 & -15l & 5l^2 & 5l^2 & 0 \end{bmatrix}; \quad \text{(A.14)}$$

$$\mathbf{G}_2 = \frac{\rho A r^2}{60(1+\Phi)^2 l}\begin{bmatrix} 0 & & & & & & & \\ 0 & 0 & & & \text{Skew sym} & & & \\ 0 & 0 & 0 & & & & & \\ 0 & 0 & 10l^2 & 0 & & & & \\ 0 & 0 & 0 & 0 & 0 & & & \\ 0 & 0 & 0 & 0 & 0 & 0 & & \\ 0 & 0 & 0 & -5l^2 & 0 & 0 & 0 & \\ 0 & 0 & 5l^2 & 0 & 0 & 0 & 10l^2 & 0 \end{bmatrix} \quad \text{(A.15)}$$

A.5 Rigid disc model

Mass matrix

$$\mathbf{M}_d = \begin{bmatrix} m & 0 & 0 & 0 \\ 0 & m & 0 & 0 \\ 0 & 0 & I_d & 0 \\ 0 & 0 & 0 & I_d \end{bmatrix}; \quad \text{(A.16)}$$

Gyroscopic matrix

$$\mathbf{G}_d = \begin{bmatrix} 0 & 0 & 0 & 0 \\ 0 & 0 & 0 & 0 \\ 0 & 0 & 0 & -I_p \\ 0 & 0 & I_p & 0 \end{bmatrix}; \tag{A.17}$$

Displacement vector

$$\boldsymbol{\eta}_d = \begin{Bmatrix} u_x & u_y & \varphi_y & \varphi_x \end{Bmatrix}^T \tag{A.18}$$

Appendix B. Proportional Damping

The shaft damping matrix can be expressed as a combination of elemental shaft mass and stiffness matrices (Clough and Penzien, 1993) using the Rayleigh damping factors (a_0 and a_1), given as

$$\mathbf{C}^{(e)} = a_0\mathbf{M}^{(e)} + a_1\mathbf{K}^{(e)} \tag{B.1}$$

where the factors a_0 and a_1 are obtained from the relation of damping ratio ζ and natural frequency ω_{nf}. The expression for calculating a_0 and a_1 are written as

$$\begin{Bmatrix} a_0 \\ a_1 \end{Bmatrix} = 2\frac{\omega_{nf_m}\omega_{nf_n}}{\omega_{nf_n}^2 - \omega_{nf_m}^2}\begin{bmatrix} \omega_{nf_n} & -\omega_{nf_m} \\ -1/\omega_{nf_n} & 1/\omega_{nf_m} \end{bmatrix}\begin{Bmatrix} \zeta_m \\ \zeta_n \end{Bmatrix} \tag{B.2}$$

where the damping ratios ζ_m and ζ_n are associated with two specific known system fundamental and highest natural frequencies of interest ω_{nf_m} and ω_{nf_n}.

Appendix C. Reference Signal and Phase Compensation Concept

On account of the linear property of fast Fourier transform (FFT), the magnitude of responses remains same but the phases are changed, in the conversion process of the time domain signal into the frequency domain. Hence, for acquiring the correct phase of the responses in the

frequency domain, a reference signal is associated with the FFT analysed signal. This reference signal is usually measured by an eddy current proximity sensor fastened near the motor shaft. It provides a reference for measuring of phases for the rotor displacement R_i and controlling current I_i signals relative to a fixed orientation mark at the shaft. The complex reference signal (Singh and Tiwari, 2015) utilized for the phase correction method takes the form as

$$s_c(t) = \cos(i\omega t) + \mathrm{j}\sin(i\omega t) \tag{C.1}$$

The time domain reference signal from Eqn. (C.1) can be expressed in frequency domain using FFT technique as

$$s_c(t) \xrightarrow{FFT} |s_i| \angle \phi_i(\omega) \tag{C.2}$$

where the magnitude and phase of reference signal are represented by $|s_i|$ and $\phi_i(\omega)$, respectively. With the phase compensation, the shaft displacement and current responses of the system can be expressed as

$$\begin{cases} R_i = |R_i| \angle (\theta_i - \phi_i) \\ I_i = |I_i| \angle (\psi_i - \phi_i) \end{cases} \tag{C.3}$$

Here, $|R_i|$ and $|I_i|$ are the magnitudes of displacement and current signals. The phases of these signals obtained from the FFT analysis are represented by θ_i and ψ_i.

Appendix D. Routh-Hurwitz stability criteria

The tuning of PID controller to have a stable rotor-AMB system throughout the operation of the rotor, has been done based on the Routh-Hurwitz stability criteria (Tiwari, 2017). These conditions are given as:

$$m > 0, \quad k_D > 0, \quad k_I > 0, \quad k_P > \frac{1}{k_i k_s k_{sn}} \left(\frac{m k_I}{k_D} + k_a \right) \tag{D.1}$$

where k_s and k_{sn} are the amplifier gain and sensor gain, respectively. m is the whole rotor mass and the proportional, integral and derivative gains of PID controller are shown by k_P, k_I and k_D. The force-displacement and force-current stiffness coefficients of AMB are represented by k_a and k_i, respectively.

Appendix E. Random Gaussian Noise

The mathematical model (Tiwari and Chougale, 2014) used for the random Gaussian noise addition in the numerically obtained signals is explained as follows:

Let the response signal of the multidisc rotor-AMB system is represented by A_i (with i = 1, 2,…,n) where n depicts the number of frequency domain rotor response data points. The response signal A_i represents for both the displacement and controller output current signals. Further, the Gaussian random noise signal R_i (with i = 1, 2,…,n) are generated from the normal distribution concept based on the size of A_i. Addition of one percent random noise to the response signal obtained from the numerical simulation, has been done using the below equation:

$$B_i = A_i + 0.01 \times A_i \times R_i; \qquad -0.5 \le R_i \le 0.5 \tag{E.1}$$

where B_i represents the response signal in which one percent (1%) random noise is added. Similarly, the random Gaussian noise of 2% and 5% has been added to the displacement and current response signal, for simulating the actual measurement conditions.

Appendix F. Regression Matrix 'A' and Known Vector 'b'

Rows of regression matrix **A** is given as:

$$A(1,28)=\left\{0,0,0,0,-R^{m1}_{01,\mathrm{Re}},0,0,0,-I^{m1}_{01,\mathrm{Re}},0,0,0,-1,0,0,0,0,0,0,0,0,0,0,0,0,0,0,0\right\}$$
$$A(2,28)=\left\{0,0,0,0,0,-R^{m1}_{01,\mathrm{Im}},0,0,0,-I^{m1}_{01,\mathrm{Im}},0,0,0,-1,0,0,0,0,0,0,0,0,0,0,0,0,0,0\right\}$$
$$A(3,28)=\left\{0,0,0,0,0,0,-R^{m1}_{02,\mathrm{Re}},0,0,0,-I^{m1}_{02,\mathrm{Re}},0,0,0,-1,0,0,0,0,0,0,0,0,0,0,0,0,0\right\}$$
$$A(4,28)=\left\{0,0,0,0,0,0,0,-R^{m1}_{02,\mathrm{Im}},0,0,0,-I^{m1}_{02,\mathrm{Im}},0,0,0,-1,0,0,0,0,0,0,0,0,0,0,0,0\right\}$$
$$A(5,28)=\left\{0,0,0,0,0,0,0,0,0,0,0,0,0,0,0,-R^{m2}_{01,\mathrm{Re}},0,0,0,-I^{m2}_{01,\mathrm{Re}},0,0,0,-1,0,0,0\right\}$$
$$A(6,28)=\left\{0,0,0,0,0,0,0,0,0,0,0,0,0,0,0,0,-R^{m2}_{01,\mathrm{Im}},0,0,0,-I^{m2}_{01,\mathrm{Im}},0,0,0,-1,0,0\right\}$$
$$A(7,28)=\left\{0,0,0,0,0,0,0,0,0,0,0,0,0,0,0,0,0,-R^{m2}_{02,\mathrm{Re}},0,0,0,-I^{m2}_{02,\mathrm{Re}},0,0,0,-1,0\right\}$$
$$A(8,28)=\left\{0,0,0,0,0,0,0,0,0,0,0,0,0,0,0,0,0,0,-R^{m2}_{02,\mathrm{Im}},0,0,0,-I^{m2}_{02,\mathrm{Im}},0,0,0,-1\right\}$$

$$A(9,28)=\left\{-m_{d1}\omega^2\left(\bar{a}_2+\bar{l}_1\right),-m_{d2}\omega^2\left(\bar{a}_2-\bar{l}_2\right),0,0,-R^{m1}_{11,\mathrm{Re}},0,0,0,-I^{m1}_{11,\mathrm{Re}},0,0,0,0,0,0,0,0,0,0,0,0,0,0,0,0,0,0\right\}$$
$$A(10,28)=\left\{0,0,-m_{d1}\omega^2\left(\bar{a}_2+\bar{l}_1\right),-m_{d2}\omega^2\left(\bar{a}_2-\bar{l}_2\right),0,-R^{m1}_{11,\mathrm{Im}},0,0,0,-I^{m1}_{11,\mathrm{Im}},0,0,0,0,0,0,0,0,0,0,0,0,0,0,0,0,0,0\right\}$$
$$A(11,28)=\left\{-m_{d1}\omega^2\left(\bar{a}_1-\bar{l}_1\right),-m_{d2}\omega^2\left(\bar{a}_1+\bar{l}_2\right),0,0,0,0,-R^{m1}_{12,\mathrm{Re}},0,0,0,-I^{m1}_{12,\mathrm{Re}},0,0,0,0,0,0,0,0,0,0,0,0,0,0,0,0,0\right\}$$
$$A(12,28)=\left\{0,0,-m_{d1}\omega^2\left(\bar{a}_1-\bar{l}_1\right),-m_{d2}\omega^2\left(\bar{a}_1+\bar{l}_2\right),0,0,0,-R^{m1}_{12,\mathrm{Im}},0,0,0,-I^{m1}_{12,\mathrm{Im}},0,0,0,0,0,0,0,0,0,0,0,0,0,0,0,0\right\}$$
$$A(13,28)=\left\{-m_{d1}\omega^2\left(\bar{a}_2+\bar{l}_1\right),-m_{d2}\omega^2\left(\bar{a}_2-\bar{l}_2\right),0,0,0,0,0,0,0,0,0,0,0,0,0,0,-R^{m2}_{11,\mathrm{Re}},0,0,0,-I^{m2}_{11,\mathrm{Re}},0,0,0,0,0,0\right\}$$
$$A(14,28)=\left\{0,0,-m_{d1}\omega^2\left(\bar{a}_2+\bar{l}_1\right),-m_{d2}\omega^2\left(\bar{a}_2-\bar{l}_2\right),0,0,0,0,0,0,0,0,0,0,0,0,-R^{m2}_{11,\mathrm{Im}},0,0,0,-I^{m2}_{11,\mathrm{Im}},0,0,0,0,0,0\right\}$$
$$A(15,28)=\left\{-m_{d1}\omega^2\left(\bar{a}_1-\bar{l}_1\right),-m_{d2}\omega^2\left(\bar{a}_1+\bar{l}_2\right),0,0,0,0,0,0,0,0,0,0,0,0,0,-R^{m2}_{12,\mathrm{Re}},0,0,0,-I^{m2}_{12,\mathrm{Re}},0,0,0,0,0\right\}$$
$$A(16,28)=\left\{0,0,-m_{d1}\omega^2\left(\bar{a}_1-\bar{l}_1\right),-m_{d2}\omega^2\left(\bar{a}_1+\bar{l}_2\right),0,0,0,0,0,0,0,0,0,0,0,0,0,-R^{m2}_{12,\mathrm{Im}},0,0,0,-I^{m2}_{12,\mathrm{Im}},0,0,0,0\right\}$$

The known vector **b** is given as:

$$\mathbf{b}=\begin{Bmatrix}0\\0\\0\\0\\\left(m\bar{a}_2^2+i_d-i_p\right)\omega^2R^{m1}_{11,\mathrm{Re}}+\left(m\bar{a}_1\bar{a}_2-i_d+i_p\right)\omega^2R^{m1}_{12,\mathrm{Re}}\\\left(m\bar{a}_2^2+i_d+i_p\right)\omega^2R^{m1}_{11,\mathrm{Im}}+\left(m\bar{a}_1\bar{a}_2-i_d-i_p\right)\omega^2R^{m1}_{12,\mathrm{Im}}\\\left(m\bar{a}_1\bar{a}_2-i_d+i_p\right)\omega^2R^{m1}_{11,\mathrm{Re}}+\left(m\bar{a}_1^2+i_d-i_p\right)\omega^2R^{m1}_{12,\mathrm{Re}}\\\left(m\bar{a}_1\bar{a}_2-i_d-i_p\right)\omega^2R^{m1}_{11,\mathrm{Im}}+\left(m\bar{a}_1^2+i_d+i_p\right)\omega^2R^{m1}_{12,\mathrm{Im}}\\0\\0\\0\\0\\\left(m\bar{a}_2^2+i_d-i_p\right)\omega^2R^{m2}_{11,\mathrm{Re}}+\left(m\bar{a}_1\bar{a}_2-i_d+i_p\right)\omega^2R^{m2}_{12,\mathrm{Re}}\\\left(m\bar{a}_2^2+i_d+i_p\right)\omega^2R^{m2}_{11,\mathrm{Im}}+\left(m\bar{a}_1\bar{a}_2-i_d-i_p\right)\omega^2R^{m2}_{12,\mathrm{Im}}\\\left(m\bar{a}_1\bar{a}_2-i_d+i_p\right)\omega^2R^{m2}_{11,\mathrm{Re}}+\left(m\bar{a}_1^2+i_d-i_p\right)\omega^2R^{m2}_{12,\mathrm{Re}}\\\left(m\bar{a}_1\bar{a}_2-i_d-i_p\right)\omega^2R^{m2}_{11,\mathrm{Im}}+\left(m\bar{a}_1^2+i_d+i_p\right)\omega^2R^{m2}_{12,\mathrm{Im}}\end{Bmatrix}$$

References

Adams R, Cawley P, Pye C and Stone B (1978) A vibration technique for non-destructively assessing the integrity of structures. *Journal of Mechanical Engineering Science* 20: 93-100.

Aenis M, Knopf E and Nordmann R. (2002) Active magnetic bearings for the identification and fault diagnosis in turbomachinery. *Mechatronics* 12: 1011-1021.

Al-Hussain K. (2003) Dynamic stability of two rigid rotors connected by a flexible coupling with angular misalignment. *Journal of Sound and Vibration* 266: 217-234.

Al-Hussain K and Redmond I. (2002) Dynamic response of two rotors connected by rigid mechanical coupling with parallel misalignment. *Journal of Sound and Vibration* 249: 483-498.

Bachschmid N and Pennacchi P. (2003) Accuracy of fault detection in real rotating machinery using model based diagnostic techniques. *JSME International Journal Series C Mechanical Systems, Machine Elements and Manufacturing* 46: 1026-1034.

Bachschmid N, Pennacchi P and Vania A. (2002) Identification of multiple faults in rotor systems. *Journal of Sound and Vibration* 254: 327-366.

Banks H, Inman D, Leo D and Wang Y (1996) An experimentally validated damage detection theory in smart structures. *Journal of Sound and Vibration* 191: 859-880.

Bates DM and Watts DG. (1988) *Nonlinear Regression Analysis and its Applications*: Wiley New York.

Beltran-Carbajal F, Silva-Navarro G and Arias-Montiel M. (2013) Active Unbalance Control of Rotor Systems Using On-Line Algebraic Identification Methods. *Asian Journal of Control* 15: 1627-1637.

Bishop R and Gladwell G. (1959) The vibration and balancing of an unbalanced flexible rotor. *Journal of Mechanical Engineering Science* 1: 66-77.

Bogue R. (2013) Sensors for condition monitoring: a review of technologies and applications. *Sensor Review*.

Bouaziz S, Messaoud NB, Mataar M, et al. (2011) A theoretical model for analyzing the dynamic behavior of a misaligned rotor with active magnetic bearings. *Mechatronics* 21: 899-907.

Brunet M. (1989) Practical applications of the active magnetic bearings to the industrial world. *Magnetic Bearings.* Springer, 225-244.

Cawley P and Adams RD. (1979) The location of defects in structures from measurements of natural frequencies. *The Journal of Strain Analysis for Engineering Design* 14: 49-57.

Chatzisavvas I and Dohnal F. (2015) Unbalance identification using the least angle regression technique. *Mechanical Systems and Signal Processing* 50: 706-717.

Choi D, Kim H and Cho M. (2008) Iterative method for dynamic condensation combined with substructuring scheme. *Journal of Sound and Vibration* 317: 199-218.

Choy F, Liang R and Xu P. (1995) Fault identification of beams on elastic foundation. *Computers and Geotechnics* 17: 157-176.

Clark DJ, Jansen MJ and Montague GT. (2004) An overview of magnetic bearing technology for gas turbine engines. *NASA/TM-2004-213177.* USA.

Clough R and Penzien J. (1993) Dynamics of structures. New York: McGraw Hill.

Das A, Nighil M, Dutt J and Irretier H (2008) Vibration control and stability analysis of rotor-shaft system with electromagnetic exciters. *Mechanism and Machine Theory* 43: 1295-1316.

De Queiroz M. (2009) An active identification method of rotor unbalance parameters. *Journal of Vibration and Control* 15: 1365-1374.

Desale B and Dasre N. (2013) Numerical solution of the system of six coupled nonlinear ODEs by Runge-Kutta fourth order method. *Applied Mathematical Sciences* 7: 287-305.

Dewell D and Mitchell L. (1984) Detection of a misaligned disk coupling using spectrum analysis. *Journal of Vibration, Acoustics, Stress, and Reliability in Design* 106: 9-16.

Dharmaraju N, Tiwari R and Talukdar S. (2005) Development of a novel hybrid reduction scheme for identification of an open crack model in a beam. *Mechanical Systems and Signal Processing* 19: 633-657.

Doebling SW, Farrar CR and Prime MB. (1998) A summary review of vibration-based damage identification methods. *Shock and Vibration Digest* 30: 91-105.

Drechslen J. (1980) Processing surplus information in computer aided balancing of large flexible rotors. *Internation Conference on Vibrations in Rotating Machinery.* Cambridge, UK, 65-70.

Edwards S, Lees A and Friswell M. (2000) Experimental identification of excitation and support parameters of a flexible rotor-bearings-foundation system from a single run-down. *Journal of Sound and Vibration* 232: 963-992.

Edwards S, Lees AW and Friswell MI. (1998) Fault diagnosis of rotating machinery. *Shock and Vibration Digest* 30: 4-13.

El-Mongy HH and Younes YK. (2017) Vibration analysis of a multi-fault transient rotor passing through sub-critical resonances. *Journal of Vibration and Control* 24: 2986-3009.

Flack R, Rooke J, Bielk J and Gunter E (1982) Comparison of the unbalance responses of Jeffcott rotors with shaft bow and shaft runout. *Journal of Mechanical Design* 104: 318-328.

Friswell M, Garvey S and Penny J. (1995) Model reduction using dynamic and iterated IRS techniques. *Journal of Sound and Vibration* 186: 311-323.

Friswell M and Mottershead JE. (1995) *Finite Element Model Updating in Structural Dynamics*: Springer Science & Business Media.

Friswell M, Penny J and Garvey S. (2001) Model reduction for structures with damping and gyroscopic effects. *Proceedings of the International Seminar on Modal Analysis.* KU Leuven; 1998, 1151-1158.

Gibbons C. (1976) Coupling misalignment forces. *Proceedings of the 5th Turbomachinery Symposium.* Texas A&M University. Gas Turbine Laboratories.

Gnielka P. (1983) Modal balancing of flexible rotors without test runs: an experimental investigation. *Journal of Sound and Vibration* 90: 157-172.

Guyan RJ. (1965) Reduction of stiffness and mass matrices. *AIAA journal* 3: 380-380.

Heng A, Zhang S, Tan AC and Mathew J (2009) Rotating machinery prognostics: State of the art, challenges and opportunities. *Mechanical Systems and Signal Processing* 23: 724-739.

Hill J and Baines N. (1988) Application of an expert system to rotating machinery health monitoring. *Proceedings of the Institution of Mechanical Engineers-Vibrations in Rotating Machinery.* 449-454.

Hori Y and Uematsu R. (1980) Influence of misalignment of support journal bearings on stability of a multi-rotor system. *Tribology International* 13: 249-252.

Isermann R. (1984) Process fault detection based on modeling and estimation methods—A survey. *Automatica* 20: 387-404.

Isermann R. (2005) Model-based fault-detection and diagnosis–status and applications. *Annual Reviews in Control* 29: 71-85.

Isermann R and Balle P. (1997) Trends in the application of model-based fault detection and diagnosis of technical processes. *Control Engineering Practice* 5: 709-719.

Jain J and Kundra T. (2004) Model based online diagnosis of unbalance and transverse fatigue crack in rotor systems. *Mechanics Research Communications* 31: 557-568.

Jalan A and Mohanty A. (2013) Model Based Fault Identification of Unbalance and Misalignment Simultaneously Present in a Rotor System. *Advances in Vibration Engineering* 12: 23-32.

Jalan A and Mohanty A. (2009) Model based fault diagnosis of a rotor–bearing system for misalignment and unbalance under steady-state condition. *Journal of Sound and Vibration* 327: 604-622.

Jang J and Khonsari M. (2019) Performance and characterization of dynamically-loaded engine bearings with provision for misalignment. *Tribology International* 130: 387-399.

Jang JY and Khonsari MM. (2015) On the characteristics of misaligned journal bearings. *Lubricants* 3: 27-53.

Jardine AK, Lin D and Banjevic D. (2006) A review on machinery diagnostics and prognostics implementing condition-based maintenance. *Mechanical Systems and Signal Processing* 20: 1483-1510.

Jayaswal P, Wadhwani A and Mulchandani K. (2008) Machine fault signature analysis. *International Journal of Rotating Machinery* 2008.

Jing J and Meng G. (2009) A novel method for multi-fault diagnosis of rotor system. *Mechanism and Machine Theory* 44: 697-709.

Jung Y-K, Qu Z-Q and Jung D-S. (2004) Structural dynamic condensation method with an iterative scheme. *KSCE Journal of Civil Engineering* 8: 205-211.

Karthikeyan M and Tiwari R. (2010) Detection, localization, and sizing of a structural flaw in a beam based on forced response measurements–An experimental investigation. *Mechanism and Machine Theory* 45: 584-600.

Kasarda M. (2000) An overview of active magnetic bearing technology and applications. *Shock and Vibration Digest, 2000* 32: 91-99.

Kasarda M, Allaire P, Humphris R and Barrett E (1990) A magnetic damper for first-mode vibration reduction in multimass flexible rotors. *Journal of Engineering for Gas turbines and Power* 112: 463-469.

Kim K-J and Lee C-W. (2003) Identification of dynamic stiffness of squeeze film damper using active magnetic bearing system as an exciter. *International Sympositum on Stability Control of Rotating Machinery*. The 2nd International Symposium on Stability Control of Rotating Machinery …, 667-677.

Krodkiewski J, Ding J and Zhang N. (1994) Identification of unbalance change using a non-linear mathematical model for multi-bearing rotor systems. *Journal of Sound and Vibration* 169: 685-698.

Kumar A and Kumar R. (2020) Development of LDA based indicator for the detection of unbalance and misalignment at different shaft speeds. *Experimental Techniques* 44: 217-229.

Kuppa SK and Lal M. (2019) Dual flexible rotor system with active magnetic bearings for unbalance and coupling misalignment faults analysis. *Sādhanā* 44: 188.

Kuppa SK and Lal M. (2020) Dynamic behaviour analysis of coupled rotor active magnetic bearing system in the supercritical frequency range. *Mechanism and Machine Theory*: 103915.

Lal M. (2020) Modeling and estimation of speed dependent bearing and coupling misalignment faults in a turbine generator system. *Mechanical Systems and Signal Processing* 151: 107365.

Lal M and Tiwari R. (2012) Multi-fault identification in simple rotor-bearing-coupling systems based on forced response measurements. *Mechanism and Machine Theory* 51: 87-109.

Lal M and Tiwari R. (2013) Quantification of multiple fault parameters in flexible turbo-generator systems with incomplete rundown vibration data. *Mechanical Systems and Signal Processing* 41: 546-563.

Lal M and Tiwari R. (2018) Experimental identification of shaft misalignment in a turbo-generator system. *Sādhanā* 43: 80.

Lee K-C, Jeong Y-H, Koo D-H and Ahan H-J (2006) Development of a radial active magnetic bearing for high speed turbo-machinery motors. *2006 SICE-ICASE International Joint Conference.* IEEE, 1543-1548.

Lee Y-S and Lee C-W. (1999) Modelling and vibration analysis of misaligned rotor-ball bearing systems. *Journal of Sound and Vibration* 224: 17-32.

Lees A. (2007) Misalignment in rigidly coupled rotors. *Journal of Sound and Vibration* 305: 261-271.

Lees A and Friswell M. (1997) The evaluation of rotor imbalance in flexibly mounted machines. *Journal of Sound and Vibration* 208: 671-683.

Lees A, Sinha J and Friswell M. (2009) Model-based identification of rotating machines. *Mechanical Systems and Signal Processing* 23: 1884-1893.

Lei Y, Lin J, He Z and Zuo M. (2013) A review on empirical mode decomposition in fault diagnosis of rotating machinery. *Mechanical Systems and Signal Processing* 35: 108-126.

Li C, Xu M, Guo S, Wang Y and Wang R. (2009) Model-based degree estimation of unbalance and misalignment in flexible coupling-rotor system. *Chinese Journal of Mechanical Engineering*: 550.

Li HW, Yu WT, Fan YP and Liu SQ. (2012) Influence of Retainer Bearing Misalignment on the Performance of Active Magnetic Bearing. *Advanced Materials Research.* Trans Tech Publ, 141-146.

Longxiang CDX. (2009) Influence of Machining Error on the Performance of Active Magnetic Bearing. *Journal of Mechanical Engineering* 6.

Lu L, Yan J and de Silva CW. (2015) Dominant feature selection for the fault diagnosis of rotary machines using modified genetic algorithm and empirical mode decomposition. *Journal of Sound and Vibration* 344: 464-483.

Markert R, Platz R and Seidler M. (2001) Model based fault identification in rotor systems by least squares fitting. *International Journal of Rotating Machinery* 7: 311-321.

Menshikov Y. (2013) Identification of Rotor Unbalance as Inverse Problem of Measurement. *Advances in Pure Mathematics* 2013.

Messaoud NB, BOUAZIZ S, Fakhfakh T and Haddar M (2011) Dynamic behavior of active magnetic bearings in presence of angular misalignment defect. *International Journal of Applied Mechanics* 3: 491-505.

Miao F, Zhao R, Wang X and Jia L (2020) A new fault feature extraction method for rotating machinery based on multiple sensors. *Sensors* 20: 1713.

Mogal S and Lalwani D. (2015) Experimental investigation of unbalance and misalignment in rotor bearing system using order analysis. *Journal of Measurements in Engineering* 3: 114-122.

Morton P. (1985) Modal balancing of flexible shafts without trial weights. *Proceedings of the institution of mechanical engineers, Part C: Journal of Mechanical Engineering Science* 199: 71-78.

Nejadpak A and Yang CX. (2017) Misalignment and unbalance faults detection and identification using KNN analysis. *Proceedings of CANCAM 2017*: 1-4.

Nelson H. (1980) A finite rotating shaft element using Timoshenko beam theory. *Journal of Mechanical Design* 102: 793-803.

Nonami K. (1989) Vibration and control of flexible rotor supported by magnetic bearings. *Magnetic Bearings.* Springer, 177-186.

Nordmann R and Aenis M. (2004) Fault diagnosis in a centrifugal pump using active magnetic bearings. *International Journal of Rotating Machinery* 10: 183-191.

O'Callahan J. (1989) A procedure for an improved reduced system (IRS) model. *Proceedings of 7th IMAC, Las Vegas, NV., 1989*.

Patel TH and Darpe AK. (2008) Vibration response of a cracked rotor in presence of rotor–stator rub. *Journal of Sound and Vibration* 317: 841-865.

Patel TH and Darpe AK. (2009) Experimental investigations on vibration response of misaligned rotors. *Mechanical Systems and Signal Processing* 23: 2236-2252.

Paz M. (1984) Dynamic condensation. *AIAA journal* 22: 724-727.

Pennacchi P, Bachschmid N and Vania A. (2006a) A model-based identification method of transverse cracks in rotating shafts suitable for industrial machines. *Mechanical Systems and Signal Processing* 20: 2112-2147.

Pennacchi P, Bachschmid N, Vania A, Zanetta G and Gregori L (2006b) Use of modal representation for the supporting structure in model-based fault identification of large rotating machinery: part 1—theoretical remarks. *Mechanical Systems and Signal Processing* 20: 662-681.

Pennacchi P and Vania A. (2005) Diagnosis and model based identification of a coupling misalignment. *Shock and Vibration* 12: 293-308.

Pennacchi P, Vania A, Chatterton S, Nistor I, Voinis P, Ricci R and Borghesani P (2013) Unbalance identification in large steam turbo-generator unit using a model-based method. *International Design Engineering Technical Conferences and Computers and Information in Engineering Conference.* American Society of Mechanical Engineers, V008T013A053.

Prabhakar S, Sekhar A and Mohanty A. (2001) Vibration analysis of a misaligned rotor—coupling—bearing system passing through the critical speed. *Proceedings of the Institution of Mechanical Engineers, Part C: Journal of Mechanical Engineering Science* 215: 1417-1428.

Prabhakar S, Sekhar A and Mohanty A. (2002) Crack versus coupling misalignment in a transient rotor system. *Journal of Sound and Vibration* 256: 773-786.

Prasad V and Tiwari R. (2018) Identification of Speed-Dependent Active Magnetic Bearing Parameters and Rotor Balancing in High-Speed Rotor Systems. *Journal of Dynamic Systems, Measurement, and Control* 141: 041013.

Randall RB. (2011) *Vibration-based Condition Monitoring: Industrial, Aerospace and Automotive Applications,* USA: John Wiley & Sons.

Ranjan G and Tiwari R. (2019) Application of active magnetic bearings for in situ flexible rotor residual balancing using a novel generalized influence coefficient method. *Inverse Problems in Science and Engineering* 27: 943-968.

Ranjan G and Tiwari R. (2020) On-Site High-Speed Balancing of Flexible Rotor-Bearing System Using Virtual Trial Unbalances at Slow Run. *International Journal of Mechanical Sciences*: 105786.

Rao AS and Sekhar A. (1996) Vibration analysis of rotor-coupling-bearing system with misaligned shafts. *ASME 1996 International Gas Turbine and Aeroengine Congress and Exhibition.* American Society of Mechanical Engineers, V005T014A001-V005T014A001.

Rao J. (1996) *Rotor Dynamics,* New Delhi: New Age International.

Roy DK and Tiwari R. (2019a) Development of identification procedure for the internal and external damping in a cracked rotor system undergoing forward and backward whirls. *Archive of Mechanical Engineering* 66: 133-152.

Roy DK and Tiwari R. (2019b) Experimental identification of rotating and stationary damping in a cracked rotor system with an offset disc. *Archive of Mechanical Engineering*: 447-474.

Roy DK and Tiwari R. (2020a) Estimation of the internal and external damping from the forward and backward spectrum of a rotor with a fatigue crack. *Propulsion and Power Research* 9: 62-74.

Roy DK and Tiwari R. (2020b) Experimental Identification of Internal and External Damping in a Rotor System with a Fatigue-Crack Using Full Spectrum. *Experimental Techniques*: 1-20.

Rytter A. (1993) Vibrational based Inspection of Civil Engineering Structures. *Ph.D. Dissertation, Department of Building Technology and Structural Engineering.* Aalborg University, Denmark.

Sabnavis G, Kirk RG, Kasarda M and Quinn DD (2004) Cracked shaft detection and diagnostics: a literature review. *Shock and Vibration Digest* 36: 287.

Sarmah N and Tiwari R. (2019) Dynamic analysis and identification of multiple fault parameters in a cracked rotor system equipped with active magnetic bearings: a physical model based approach. *Inverse Problems in Science and Engineering* 28: 1-32.

Sarmah N and Tiwari R. (2020) Analysis and identification of the additive and multiplicative fault parameters in a cracked-bowed-unbalanced rotor system integrated with an auxiliary active magnetic bearing. *Mechanism and Machine Theory* 146: 103744.

Sawalhi N, Ganeriwala S and Tóth M. (2019) Parallel misalignment modeling and coupling bending stiffness measurement of a rotor-bearing system. *Applied Acoustics* 144: 124-141.

Schweitzer G. (2002) Active magnetic bearings-chances and limitations. *6th International Conference on Rotor Dynamics.* Citeseer, 1-14.

Schweitzer G and Maslen EH. (2009) *Magnetic Bearings: Theory, Design, and Application to Rotating Machinery*: Springer Berlin.

Sekhar A and Prabhu B. (1995) Effects of coupling misalignment on vibrations of rotating machinery. *Journal of Sound and Vibration* 185: 655-671.

Sekhar A and Sreenivasa Rao A. (1996) Crack versus misalignment in rotor-coupling bearing system. *Machine vibration* 5: 179-188.

Shari A, Ali AA and Almudhaffer M. (2019) Combination of FFT & ICA methods for faults analysis of rotating machine. *Proceedings of the International Conference on Information and Communication Technology*. ACM, 196-202.

Shih Y-P and Lee A-C. (1997) Identification of the unbalance distribution in flexible rotors. *International Journal of Mechanical Sciences* 39: 841-857.

Shrivastava A and Mohanty AR. (2019) Identification of unbalance in a rotor system using a joint input-state estimation technique. *Journal of Sound and Vibration* 442: 414-427.

Shrivastava A and Mohanty AR. (2020) Identification of unbalance in a rotor-bearing system using Kalman filter–based input estimation technique. *Journal of Vibration and Control* 26: 1081-1091.

Singh M and Suarez L. (1992) Dynamic condensation with synthesis of substructure eigenproperties. *Journal of Sound and Vibration* 159: 139-155.

Singh S and Tiwari R. (2015) Model-based fatigue crack identification in rotors integrated with active magnetic bearings. *Journal of Vibration and Control* 23: 980-1000.

Singh S and Tiwari R. (2016) Model-based switching-crack identification in a Jeffcott rotor with an offset disk integrated with an active magnetic bearing. *Journal of Dynamic Systems, Measurement, and Control* 138: 031006.

Singh S and Tiwari R. (2018) Model based identification of crack and bearing dynamic parameters in flexible rotor systems supported with an auxiliary active magnetic bearing. *Mechanism and Machine Theory* 122: 292-307.

Sinha JK. (2002) Health monitoring techniques for rotating machinery. *Ph.D. Dissertation.* University of Wales, Swansea.

Sinha JK, Friswell M and Lees A. (2002) The identification of the unbalance and the foundation model of a flexible rotating machine from a single run-down. *Mechanical Systems and Signal Processing* 16: 255-271.

Sinha JK, Lees A and Friswell M. (2004) Estimating unbalance and misalignment of a flexible rotating machine from a single run-down. *Journal of Sound and Vibration* 272: 967-989.

Srinivas R S, Tiwari R and Babu CK. (2020) Modeling, Analysis, and Identification of Parallel and Angular Misalignments in a Coupled Rotor-Bearing-Active Magnetic Bearing System. *Journal of Dynamic Systems, Measurement, and Control* 143.

Srinivas RS, Tiwari R and Kannababu C. (2018) Application of active magnetic bearings in flexible rotordynamic systems–A state-of-the-art review. *Mechanical Systems and Signal Processing* 106: 537-572.

Srinivas RS, Tiwari R and Kannababu C. (2019) Model based analysis and identification of multiple fault parameters in coupled rotor systems with offset discs in the presence of angular misalignment and integrated with an active magnetic bearing. *Journal of Sound and Vibration* 450: 109-140.

Sudhakar G and Sekhar A. (2011) Identification of unbalance in a rotor bearing system. *Journal of Sound and Vibration* 330: 2299-2313.

Tahir MM, Hussain A, Badshah S, et al. (2016) Classification of unbalance and misalignment faults in rotor using multi-axis time domain features. *2016 International Conference on Emerging Technologies (ICET).* IEEE, 1-4.

Tiwari R. (2005) Conditioning of regression matrices for simultaneous estimation of the residual unbalance and bearing dynamic parameters. *Mechanical Systems and Signal Processing* 19: 1082-1095.

Tiwari R. (2017) *Rotor Systems: Analysis and Identification*, Boca Raton: CRC Press.

Tiwari R and Chakravarthy V. (2006) Simultaneous identification of residual unbalances and bearing dynamic parameters from impulse responses of rotor–bearing systems. *Mechanical Systems and Signal Processing* 20: 1590-1614.

Tiwari R and Chougale A. (2014) Identification of bearing dynamic parameters and unbalance states in a flexible rotor system fully levitated on active magnetic bearings. *Mechatronics* 24: 274-286.

Tiwari R and Dharmaraju N. (2006) Development of a condensation scheme for transverse rotational degrees of freedom elimination in identification of beam crack parameters. *Mechanical Systems and Signal Processing* 20: 2148-2170.

Tsai N-C, King Y-H and Lee R-M. (2009) Fault diagnosis for magnetic bearing systems. *Mechanical Systems and Signal Processing* 23: 1339-1351.

Vania A and Pennacchi P. (2004) Experimental and theoretical application of fault identification measures of accuracy in rotating machine diagnostics. *Mechanical Systems and Signal Processing* 18: 329-352.

Verma AK, Sarangi S and Kolekar M. (2014) Experimental investigation of misalignment effects on rotor shaft vibration and on stator current signature. *Journal of Failure Analysis and Prevention* 14: 125-138.

Wang H and Gong J. (2019) Dynamic analysis of coupling misalignment and unbalance coupled faults. *Journal of Low Frequency Noise, Vibration and Active Control* 38: 363-376.

Wang L, Xiong X and Xu H. (2017) Non-contact electromagnetic exciter design with linear control method. *Chinese Journal of Mechanical Engineering* 30: 135-143.

Wang N and Jiang D. (2018) Vibration response characteristics of a dual-rotor with unbalance-misalignment coupling faults: theoretical analysis and experimental study. *Mechanism and Machine Theory* 125: 207-219.

Xia Y and Lin R. (2004) A new iterative order reduction (IOR) method for eigensolutions of large structures. *International Journal for Numerical Methods in Engineering* 59: 153-172.

Xu M and Marangoni R. (1994a) Vibration analysis of a motor-flexible coupling-rotor system subject to misalignment and unbalance, part I: theoretical model and analysis. *Journal of Sound and Vibration* 176: 663-679.

Xu M and Marangoni R. (1994b) Vibration analysis of a motor-flexible coupling-rotor system subject to misalignment and unbalance, part II: experimental validation. *Journal of Sound and Vibration* 176: 681-691.

Xu Y, Di L, Zhou J and Guo Q. (2016) Active magnetic bearings used as exciters for rolling element bearing outer race defect diagnosis. *ISA Transactions* 61: 221-228.

Xu Y, Zhou J, Di L and Zhao C (2017) Active magnetic bearings dynamic parameters identification from experimental rotor unbalance response. *Mechanical Systems and Signal Processing* 83: 228-240.

Yao J, Liu L, Yang F, Scarpa F and Gao J. (2018) Identification and optimization of unbalance parameters in rotor-bearing systems. *Journal of Sound and Vibration* 431: 54-69.

Zhang Y. (2018) A brief review of condition monitoring techniques for gas turbines. *Power Engineer*: 15-21.

Zhao W, Hua C, Wang D, and Dong D. (2020) Fault Diagnosis of Shaft Misalignment and Crack in Rotor System Based on MI-CNN. *Proceedings of the 13th International Conference on Damage Assessment of Structures.* Springer, 529-540.

Zhou S and Shi J. (2001) Active balancing and vibration control of rotating machinery: a survey. *Shock and Vibration Digest* 33: 361-371.

List of Publications from the Present Work

Journals:

1. P. Kumar and R. Tiwari (2020), Development of a Novel Approach for Quantitative Estimation of Unbalance and Misalignment in a Rigid Rotor System Levitated by Active Magnetic Bearings, *Iranian Journal of Science and Technology, Transactions of Mechanical Engineering*, Springer. DOI: 10.1007/s40997-020-00364-7.

2. P. Kumar and R. Tiwari (2020), Dynamic Analysis and Identification of Unbalance and Misalignment in a Rigid Rotor with Two Offset Discs Levitated by Active Magnetic Bearings: A Novel Trial Misalignment Approach, *Propulsion and Power Research*, Elsevier. DOI: 10.1016/j.jppr.2020.06.003.

3. P. Kumar and R. Tiwari (2020), Finite Element Modelling, Analysis and Identification using Novel Trial Misalignment Approach in an Unbalanced and Misaligned Flexible Rotor System Levitated by Active Magnetic Bearings, *Mechanical Systems and Signal Processing*, Elsevier. DOI: 10.1016/j.ymssp.2020.107454.

4. R. Tiwari and P. Kumar (2021), An Innovative Virtual Trial Misalignment Approach for Identification of Unbalance, Sensor and Active Magnetic Bearing Misalignment along with its Stiffness Parameters in a Magnetically Levitated Flexible Rotor System, *Mechanical Systems and Signal Processing*, Elsevier (Provisionally accepted).

Conferences:

1. P. Kumar and R. Tiwari; "Dynamic Response Analysis of an Unbalanced and Misaligned Rotor Supported on Active Magnetic Bearings and Touchdown Bearings";

Sixth National Symposium on Rotor Dynamics; 2-3rd July; (NSRD-2019); CSIR-National Aerospace Laboratories, Bangalore, India.

2. P. Kumar and R. Tiwari; "A Numerical Study to Analyze the Effect of Unbalance and Misalignment Fault Parameters in a Rigid Rotor Levitated by Active Magnetic Bearings"; Sixth Biennial Gas Turbine India Conference; 5-6th December; (ASME GT India-2019); Indian Institute of Technology Madras, Chennai, India. DOI: 10.1115/GTINDIA2019-2384.

3. P. Kumar and R. Tiwari; “Effects of Unbalance and AMB misalignment in a Rigid Rotor with an Offset Disc Levitated by Active Magnetic Bearings: A Numerical Investigation”; 12th International Conference on Vibrations in Rotating Machinery, Institution of Mechanical Engineers; 14-15th October 2020; (VIRM-12); Liverpool, United Kingdom.

4. P. Kumar and R. Tiwari; “Modelling, Analysis and Identification in a Magnetically Levitated Rotor System Integrated with Misaligned Sensors and Active Magnetic Bearings using Virtual Trial Misalignment Approach”; 16th International Conference on Vibration Engineering and Technology of Machinery, 16-18th December 2021; (VETOMAC-XVI); B. M. S. College of Engineering, Bangalore, India (Paper submitted).

Book Chapters:

1. P. Kumar and R. Tiwari; "Dynamic Response Analysis of an Unbalanced and Misaligned Rotor Supported on Active Magnetic Bearings and Touchdown Bearings"; Proceedings of the 6th National Symposium on Rotor Dynamics, pp. 407-418, 2020, Lecture Notes in Mechanical Engineering, Springer.

2. P. Kumar and R. Tiwari; “Effects of Unbalance and AMB misalignment in a Rigid Rotor with an Offset Disc Levitated by Active Magnetic Bearings: A Numerical Investigation”; 12th International Conference on Vibrations in Rotating Machinery, pp. 151-168, 2020, Taylor and Francis Group, CRC Press, London.